HOKKAIDO UNIVERSITY

Title	Advances in predictive modeling for bacterial behaviors from food processing to human consumption: application to quantitative microbial risk assessment
Author(s)	安部, 大樹
Degree Grantor	北海道大学
Degree Name	博士(農学)
Dissertation Number	甲第14803号
Issue Date	2022-03-24
DOI	https://doi.org/10.14943/doctoral.k14803
Doc URL	https://hdl.handle.net/2115/88846
Type	doctoral thesis
File Information	Abe_Hiroki.pdf



Hokkaido University Collection of Scholarly and Academic Papers : HUSCAP

Advances in predictive modeling for bacterial behaviors from food processing to human consumption: application to quantitative microbial risk assessment

（食品加工から喫食に至る過程における細菌挙動の予測モデリング：定量的微生物リスク評価への応用）

Hokkaido University
Graduate School of Agriculture
Frontiers in Production Science
Doctor Studies

Hiroki Abe

Acknowledgements

The support of many people has allowed me to complete my PhD project. First, I expressed my gratitude to my supervisor Professor Shigenobu Koseki for his excellent supervision during my PhD. Millions of his supports, encouragements, in depth knowledge, and positive feedbacks have helped me accomplish my PhD study. And I have passed my gratitude Assistant Professor Kento Koyama. Almost all my PhD research were with him. I appreciated many supports of Professor Shuso Kawamura. Furthermore, I gratefully appreciated Professor Marcel Zwietering, Associate Professor Heidy den Besten, and Dr. Alberto Garre of Wageningen University and Research, who had accepted me as a visiting PhD student for one year from October 2020 to September 2021. Their supports have encouraged me, and the many experiences at Wageningen were my treasure. Many students helped me during my PhD course, Mr. Kohei Takeoka, Mr. Yuto Fuchisawa, Ms. Satoko Hiura, Mr. Shinya Doto, and many laboratory members of Hokkaido University and Wageningen University. Finally, I gave special thanks to my family, Ms. Shione Furugoori, Ms. Yumi Aiba, other friends, and all the people who have supported me.

The work of Chapter 5 and 6 was supported by JSPS KAKENHI Grant-in-Aid for Japan Society for the Promotion of Science Fellows, Grant number 20J11550); Chapter 7 was supported by the following overseas research under the Japan Society for the Promotion of Science.

Table of Contents

Page

Acknowledgements ····· **i**

Table of Contents ····· **ii**

List of Tables ····· **ix**

List of Figures ····· **x**

List of publications ····· **xxi**

Chapter 1 General Introduction 1

1.1. Risks of food poisoning and foodborne illness 1

1.2. Changes in microbial foodborne illness risk during food chains 1

1.3. Hazard Analysis and Critical Control Point, and Quantitative Microbial Risk Assessment 2

1.4. Predictive microbiology for risk assessment 3

1.5. Goal of this study 4

1.5. References 4

Chapter 2 Probabilistic predictive approach for *Salmonella enterica* lethality by iso-thermal heating 6

2. 1. Introduction 6

2.2. Materials and Methods 8

2.2.1. Bacterial strain and culture conditions 8

2.2.2. Thermal treatment for analyzing changes in survival probability 9

2.2.3. Thermal treatment for analyzing conventional survival kinetics *10*

2.2.4. Modelling survival probability *11*

2.2.5. Analysis of S. enterica Oranienburg survival kinetics data *15*

2.3. Results 16

2.3.1. Probabilistic evaluation of S. enterica Oranienburg survival during heating *16*

2.3.2. Survival kinetics of S. enterica Oranienburg *23*

2.3.3. Comparison of the probability of death estimated by stochastic and deterministic models *24*

2. 4. Discussion 25

2. 5. References 28

Chapter 3 Stochastic predictive simulation for *Bacillus simplex* spore inactivation behaviors by iso-thermal heating 32

3.1. Introduction 32

3.2. Material and Methods 35

3.2.1. Bacterial strain and sporulation conditions *35*

3.2.2 Thermal treatment for analyzing survival kinetics *36*

3.2.3 Fitting parameters of Weibullian distributions to kinetic data *37*

3.2.4 Procedure for computer simulation of survival spore counts *38*

3.2.5 Procedure for computer simulation of the survival probability of bacterial spore populations *40*

3.2.5 Thermal treatment for validation of the sporular inactivation simulation *41*

3.3. Results 42

3.3.1 Sporular survival kinetics and fitting parameters of the Weibullian model 42

3.3.2 Comparison of viable spore numbers between simulation and observed values ... 43

3.4. Discussion 53

3.5 References 59

Chapter 4 Stochastic and dynamic predictive simulation for inactivation behaviors of *Bacillus simplex* spore by non-isothermal heating 62

4.1 Introduction 62

4.2 Materials and Methods 65

4.2.1. Sample and experimental description 65

4.2.2. Estimation of Weibull parameter uncertainty & thermotolerance heterogeneity with Bootstrap methods 68

4.2.3. Numerical estimation for true randomness variability in bacterial behavior during non-isothermal conditions with stochastic model 72

4.2.4. Second-order Monte Carlo simulation procedure 76

4.3 Results and Discussion 77

4.3.1. Distribution of Weibullian parameters derived from the bootstrap 77

4.3.2. Validation of dynamic stochastic model using second-order Monte Carlo simulation 82

4.3.3. Evaluation of the validity of the second-order Monte Carlo simulation 85

4.3.4. Potential of adaptation for other bacterial behavior description 86

4.3.5. Limitations of the developed modelling procedure 88

4.3.6. Conclusions and future perspectives *89*

4.4 References 90

Chapter 5 Predictive model for invading behaviors of *Campylobacter jejuni* into human intestinal cells 94

5.1. Introduction 94

5.2. Materials and methods 96

5.2.1. Cell strain and culture conditions *96*

5.2.2. Bacterial strain and culture conditions *97*

5.2.3. Invading cell count assay *97*

5.2.4. Data analysis and Bayesian modeling condition *98*

5.3. Results 99

5.3.1. Behaviors of invading C. jejuni count into Caco-2 cells *99*

5.3.2. Bayesian inference for model parameters for invading C. jejuni *105*

5.4. Discussion 112

5.4.1. Advantages of the present model *112*

5.4.2. Limitations of the present model *114*

5.4.3. How to use the information obtained from the cell invasion model *115*

5.4.4. Conclusions *117*

5.5. References 118

Chapter 6 Development of dose-response model for *Campylobacter jejuni* based on human digestive systems 121

6.1. Introduction 121

6.2. Materials and methods 124

6.2.1. Modeling for postprandial gastric pH change among younger and elder individuals 124

6.2.2. Pathogen survival in stomach with between- and within-strain variability 125

6.2.3. Bacterial transfer to the small intestine 126

6.2.4. Bacterial invasion in intestinal cells 127

6.2.5. Retention time in the small intestine 127

6.2.6. Invasion probability in human tissues 127

6.2.7. Computation 128

6.3. Results 128

6.3.1. Defining the key events of campylobacteriosis infection 128

6.3.2. Gastric bacterial reduction 130

6.3.3. Bacterial transfer to the small intestine 134

6.3.4. Retention time in the small intestine 136

6.3.5. Probability of infection in human intestinal cells 138

6.3.6. Sensitivity analysis of the framework for estimating invasion probability 139

6.4. Discussion 141

6.5. References 146

6.6. Supplementary materials 150

Chapter 7 Elucidation of relevant factors to foodborne listeriosis on pasteurized milk from quantitative microbial risk assessment 155

7.1. Introduction 155

7.2. Materials and methods 157

7.2.1. Thermotolerance model for Listeria monocytogenes in milks from metadata based on Bayesian inference 157

7.2.2. Growth model for Listeria monocytogenes in milks based on Bayesian inference 158

7.2.3. Food-chain calculation frame & conditions 159

7.2.4. Illness occurrence from illness probability per one serving 172

7.2.5. Sensitivity analysis for elucidating the relevance factors to listeriosis 172

7.2.6. Scenario analysis for different thermal condition target 172

7.3. Results 173

7.3.1. Bayesian model fitting 173

7.3.2. Illness cases and expected value of illness probability 173

7.3.3. The change of pathogen concentration during food chain 177

7.3.4. L. monocytogenes dose per one pasteurized milk serve 178

7.3.5. Distribution of deltas of pathogen concentration 180

7.3.6. Sensitivity analysis of each factor to pathogen log concentration at eating & illness occurrence 183

7.3.7. Uniqueness in time-temperature condition 185

7.3.8. Uniqueness in pathogen characteristics 188

7.3.9. Scenario analysis for thermal condition target 188

7.4. Discussion 189

7.5. References 197

7.6. Supplementary materials 199

Chapter 8 General Discussion 202

8.1. Advantages and perspective of this study 202

8.2. Further perspectives of predictive microbiology and QMRA 203

8.3. Summary 205

8.4. References 207

List of Tables

Table Page

2-1 The parameter and RMSE of the fitted Gamma distribution ····· 18

3-1. Accuracy of simulated variabilities in survival spore counts when $n_{inactivation}$ is 10^4 replicates ····· 52

3-2. Accuracy of simulated survival probabilities of spore population when $n_{inactivation}$ is 10^6 replicates ····· 53

3-3. Statics of goodness-of-fit test of fitted Poisson distributions to variability in survival spore counts ····· 57

5-1 Parameter values and R-hat values of the estimated model of each isolate ····· 108

5-2 Accuracy of each isolation model in test validation. ····· 112

6-1. Details of components in the constructed key events dose-response model ····· 130

7-1 Variables used in the QMRA simulation ····· 164

7-2 Conditions in the illness cases ····· 174

7-3 Results of scenario analysis ····· 189

List of Figures

Figure Page

1-1. The schematics of pathogen concentration changes during the food chain (Farm to Consumption). ····· 2

2-1. An example of heating protocol even at experimental temperature: 600 s heating at 60°C, 450 s heating at 62°C, 300 s heating at 64°C, and 210 s heating at 66°C by thermal cycler. Preheating of 30 s at 25°C to standardize the initial temperature across trials. After heating process, the 96-PCR microplates were immediately chilled at 4ºC. ···· 10

2-2. Schematic illustration of the stochastic procedure for estimating survival probability. Upper and lower figures represent survival probability: equation (2-2) with cumulative gamma distribution and frequency of total reduction time with gamma distribution, respectively. Red and blue lines indicate heating time with a bacterial population survival probability of 0.5 and 10^{-6}, respectively. The time with a probability of 0.5 represents the average of the distribution, and the time with a probability 10^{-6} is that at which the risk of bacterial survival can be disregarded. ····· 14

2-3. Schematic illustration of the deterministic procedure for estimating survival probability by first-order kinetics. The survival probability of the bacterial population estimated by the deterministic procedure was derived from Eq. 2-7. As in Figure 2-1, red and blue lines indicate heating time with a bacterial population survival probability of 0.5 and 10^{-6}, respectively. ····· 16

2-4. Change in the probability of 60 bacterial populations each with nearly 1 × 10n cells

where n = 1 (○), 2 (□), 3 (△), 4 (+), 5 (×), heated at 60°C (a), 62°C (b), 64°C (c) and 66°C (d) in TSB. The five different lines show the best fit of a cumulative gamma distribution of nearly 1 × 10n cells (n = 1, 2, 3, 4, 5) at each heating temperature. The highest and lowest RMSE was 0.069 and 0.004, respectively. ····· 19

2-5. Relationship between mean (a) and variance (b) of the best fit of a cumulative gamma distribution; inserted cells were heated at 60°C (○), 62°C (□), 64°C (+), and 66°C (×) in TSB. The lines show the linear regression lines (a) heated at each temperature; the highest and lowest R^2 value was 0.99 and 0.88. Fourth-order regression curves are shown (b) that describe the heterogeneity in variance of total reduction time. ····· 20

2-6. Kinetics of *S. enterica* Oranienburg survival from an initial concentration of 10^9 CFU/ml heated at 60°C (a), 62°C (b), 64°C (c), and 66°C (d) in TSB. Error bars indicate standard deviations. Each point with error bar is the mean of two or three values, and each point without an error bar is a single value. No colonies were detected at the time indicated by an asterisk (*). A small shoulder reduction was observed by heating 60°C (a) and linear reductions were observed by heating at 62°C (b), 64°C (c), and 66°C (d). Lines show the linear regression of kinetic changes in surviving cell counts, and yield *D* values at each heating temperature in TSB. R^2 value at 60°C is 0.97, 62°C, and 64°C were 0.99 and 66°C was 1.00. ····· 22

2-7. Probability contour lines indicating total inactivation heating time of various cell numbers and survival probability of bacterial population at specific levels of inactivation (0.5 and 10^{-6}), as predicted using stochastic and kinetic model heated at 60°C (a), 62°C (b), 64°C (c), and 66°C (d). This figure enabled us to draw two comparisons between stochastic-0.5 (bold solid line) and kinetic-0.5 (bold dash line)

predicted heating time, and between stochastic-10^{-6} (solid line) and kinetic-10^{-6} (dashed line) predicted heating time. ····· 23

3-1. An example of heating protocol: 300 s heating at 94°C by thermal cycler. Preheating of 30 s at 25°C to standardize the initial temperature across trials. After heating process, the 96-PCR microplates were immediately chilled at 4ºC. the red dotted lines show the standard deviation of the temperature of all 60 wells used for heating.····· 37

3-2. Survival kinetics of *B. simplex* spore population of N_0 of 10^5 CFU heated at 94 °C in 0.3 M phosphate buffer (a_w = 0.98). Error bars indicate standard deviations. Each point with an error bar represents the mean of two or three values. No colonies were detected at the time indicated by an asterisk (*). Lines show the Fitted Weibull model of kinetic changes in surviving spore counts. Fitted parameters of b and n for the Weibullian model were 1.54 × 10^{-3} (p = 0.089, where p indicates the significance level of fitting) and 1.40 (p = 4.67 × 10^{-6}), respectively, with an RMSE of 0.13.····· 43

3-3. Monte Carlo simulation results (100 simulations) for thermal inactivation of *B. simplex* with initial counts of 1 × 10^n cells, where n = 1 (purple), 2 (orange), 3 (green), 4 (blue), and 5 (red), based on fitted Weibull distributions (black lines) for individual cell inactivation times. ····· 45

3-4. Change in the observed heterogeneity of viable spore count (red points) of 60 bacterial populations each representing nearly 1 × 10^n cells, where n = 1, 2, 3, 4, and 5, heated at 94 °C in 0.3 M phosphate buffer (a_w = 0.98) for a particular heating time. The lines show the results of 100 Monte Carlo simulations (black lines) in each condition.···· 47

3-5. Change in the observed survival probability of 60 bacterial populations (colored circles) each representing nearly 1 × 10^n cells, where n = 1 (purple), 2 (orange), 3 (green), 4

(blue), and 5 (red), heated at 94 °C in 0.3 M phosphate buffer (a_w = 0.98). The colored lines show Monte Carlo simulation results (100 simulations) of equivalent bacterial populations. ····· 48

3-6. Change in the simulated heterogeneity of viable spore count of 10^6 simulations each representing nearly 1×10^n cells, where n = 1, 2, 3, 4, and 5, heated at 94 °C in 0.3 M phosphate buffer (a_w = 0.98) for a particular heating time. The red points show the observed results of viable spore count of 60 bacterial populations in each condition. 49

3-7. Change in the simulated survival probability of 10^6 simulations (colored lines) each representing nearly 1×10^n cells, where n = 1 (purple), 2 (orange), 3 (green), 4 (blue), and 5 (red), heated at 94 °C in 0.3 M phosphate buffer (a_w = 0.98). The colored circles show the observed results of 60 bacterial populations of equivalent cell number. ···· 50

4-1. Example of heating protocol using thermal cycler. (A): Temperature profiles of inactivation trials for model fitting dataset. 80 min heating at 80°C (red), 35 min heating at 85°C (green), and 18 min heating at 90°C (blue). Preheating is conducted for 30 s at 25°C to standardize the initial temperature across trials. (B): Temperature profiles of inactivation trials for model validation dataset. Slow come-up (blue), bumpy (green) and waving (red) temperature profiles. Following the heating process, the 96-PCR microplates are immediately chilled at 4ºC. ····· 67

4-2. Schematic of the bootstrapping procedure. The bootstrapping was conducted using 1,000 replicates of both the Weibullian parameter distributions and the secondary models for each parameter, with the uncertainty of each parameter considered based on 1,000 replicates of the resampled surviving cell ratio. ····· 69

4-3. Schematic of the Markov Chain Monte Carlo (MCMC) procedure. The proposed

stochastic explanation describes bacteria death or continued survival based on the pure death process in the branch of modelling biological populations. ····· 75

4-4. Survival kinetics of *Bacillus simplex* spores under different temperature conditions, (A): 80ºC, (B): 85ºC, (C): 90ºC. The points, error bars, and curves indicate, average value of observed survival ratio (three replicates), standard errors of observed survival ratio, and estimated Weibull model curves, respectively, based on 1,000 bootstrap replicates. · 78

4-5. Weibullian parameter distributions under each condition derived from 1,000 bootstrap replicates, and the relationship between the two bootstrapped Weibullian parameters. The gray lines indicate the relationship between the two estimated parameters from bootstrapped secondary model sets. ····· 79

4-6. Changes in $\log_{10}\delta$ and p as functions of heating temperature and pH (data points). (A): $\log_{10}\delta$ against temperature; (B): $\log_{10}\delta$ against pH; (C): p against temperature; (D): p against pH. Error bars indicate standard deviation of the 1,000 estimated Weibullian parameter replicates; lines indicate secondary model (upper left & upper right: Eq. 4-2; bottom left & bottom right: Eq. 4-3) derived from 1,000 bootstrap replicates. ····· 81

4-7 Predictions of second-order Monte Carlo simulation (gray) and dynamic kinetic model (blue) and changes in 10 replicates of observed survival *Bacillus simplex* spore counts (○) under each temperature profile (red curve) of slow come-up heating in pH 6.5: (A), bumpy heating in pH 6.3: (B), and waving in pH 6.4: (C). × represents no colonies were detected. ····· 84

4-8. Comparison of 99% confidence intervals derived from only-bootstrap model (blue region), only-MCMC model (red region), and 2DMC models (gray region) during heating at 85°C in pH-adjusted TSB at pH 5.4. The data points indicate two or three

replicates of observed values. The only-bootstrap model is derived from the dynamic kinetic modeling of 1,000 secondary-model sets using the bootstrap method, while the only-MCMC model is derived from a dynamic stochastic secondary model constructed without application of the bootstrap model. ····· 86

5-1. Differences in the number of invading different strains of *Campylobacter jejuni* (RIMD 0366027) into monolayer-cultured Caco-2 cells (RCB0988). Each symbol and line describe the behaviors of each exposure concentration condition. The exposure concentrations (CFU/mL) of each *C. jejuni* strain were approximately 10^3 (circle), 10^4 (insert triangle), 10^5 (triangle), 10^6 (square), 10^7 (plus), and 10^8 (cross).····· 100

5-2. Differences in the number of invading different strains of *Campylobacter jejuni* (RIMD 0366042) into monolayer-cultured Caco-2 cells (RCB0988). Each symbol and line describe the behaviors of each exposure concentration condition. The exposure concentrations (CFU/mL) of each *C. jejuni* strain were approximately 10^3 (circle), 10^4 (insert triangle), 10^5 (triangle), 10^6 (square), 10^7 (plus), and 10^8 (cross).····· 101

5-3. Differences in the number of invading different strains of *Campylobacter jejuni* (RIMD 0366048) into monolayer-cultured Caco-2 cells (RCB0988). Each symbol and line describe the behaviors of each exposure concentration condition. The exposure concentrations (CFU/mL) of each *C. jejuni* strain were approximately 10^3 (circle), 10^4 (insert triangle), 10^5 (triangle), 10^6 (square), 10^7 (plus), and 10^8 (cross).····· 102

5-4. Differences in invading *Campylobacter jejuni* (RIMD 0366027) ratios into monolayer-cultured Caco-2 cells (RCB0988). Each symbol and line describe the behaviors of each exposure concentration condition as in Fig. 5-1.····· 103

5-5. Differences in invading *Campylobacter jejuni* (RIMD 0366042) ratios into monolayer-

cultured Caco-2 cells (RCB0988). Each symbol and line describe the behaviors of each exposure concentration condition as in Fig. 5-2. ····· 104

5-6. Differences in invading *Campylobacter jejuni* (RIMD 0366048) ratios into monolayer-cultured Caco-2 cells (RCB0988). Each symbol and line describe the behaviors of each exposure concentration condition as in Fig. 5-3. ····· 105

5-7. Characteristics of estimated cell-invading model parameters of each bacterial isolate (RIMD 0366027) by Bayesian regression. Relationship of posterior distribution of parameters $\mathrm{Log}_{10}N_{max}$, $\mathrm{Log}_{10}\mu$, and σ (under the diagonal), corresponding histograms (on the diagonal), and correlation coefficients (over the diagonal). ····· 106

5-8. Characteristics of estimated cell-invading model parameters of each bacterial isolate (RIMD 0366042) by Bayesian regression. Relationship of posterior distribution of parameters $\mathrm{Log}_{10}N_{max}$, $\mathrm{Log}_{10}\mu$, and σ (under the diagonal), corresponding histograms (on the diagonal), and correlation coefficients (over the diagonal). ····· 107

5-9. Characteristics of estimated cell-invading model parameters of each bacterial isolate (RIMD 0366048) by Bayesian regression. Relationship of posterior distribution of parameters $\mathrm{Log}_{10}N_{max}$, $\mathrm{Log}_{10}\mu$, and σ (under the diagonal), corresponding histograms (on the diagonal), and correlation coefficients (over the diagonal). ····· 108

5-10. Estimated (curves and ranges) and observed (point) invading bacterial counts of *C. jejuni* (RIMD 0366027) into monolayered Caco-2 cells at each exposure bacterial concentration. Painted ranges show 60%, 95%, and 99% prediction intervals, in order from the median. ····· 109

5-11. Estimated (curves and ranges) and observed (point) invading bacterial counts of *C. jejuni* (RIMD 0366042) into monolayered Caco-2 cells at each exposure bacterial

concentration. Painted ranges show 60%, 95%, and 99% prediction intervals, in order from the median.····· 110

5-12. Estimated (curves and ranges) and observed (point) invading bacterial counts of *C. jejuni* (RIMD 0366048) into monolayered Caco-2 cells at each exposure bacterial concentration. Painted ranges show 60%, 95%, and 99% prediction intervals, in order from the median.····· 111

5-13. Reported dose-response relationship (Teunis et al., 2005) and relationship between the probability that one or more bacteria of bacterial population invade cells, $P_{p_invading}$ and exposed bacterial counts, $LogN_{Dose}$ of *C. jejuni* (RIMD 0366027, blue; RIMD 0366042, orange; and RIMD 0366048: green). Each colored range indicates the 95% prediction interval derived from the present predictive model of *C. jejuni* invading counts into Caco-2 cells. The reported mean retention time at the small intestine, 7.5 h (Davis et al., 1986; Song et al., 2012), the volume, 319 mL (Schliller et al., 2005), and surface area of small intestine, 32 m^2 (Helander & Fändriks, 2014), were used.····· 117

6-1. Directed acyclic graph of the model parameters and factors. Solid arrows indicate distributions, dashed arrows deterministic functions. The abbreviations and details of components are summarized in Table 6-1.····· 129

6-2. Changes in the observed pH in human stomach after-meal pH data (points) of young (upper; Dressman et al., 1990) and elderly (lower; Russel et al., 1993) people, and the prediction band derived from the exponential model. The estimated parameter traceplots and distributions of Bayesian MCMC in supplementary information (Fig. 6-S2). ····· 132

6-3. Predicted after-meal survival curves (solid curve: median, dash curve and covered range:

90% prediction band) of *C. jejuni* in the stomach of young (upper) and elderly (lower) people derived from a predictive model for *C. jejuni* reduction in gastric juice (Koyama et al., 2021). ····· 133

6-4. Reported retention ratio (**a**; point; Hellström et al., 2006) & predicted cumulative gamma distributions (**a** and **b**; solid curve: median, dash curve and covered range: 95% prediction band) for gastric retention time. The estimated parameter traceplots and distributions of Bayesian MCMC in supplementary information (Fig. 6-S3). ····· 135

6-5. Calculated transferred survival ratio (solid curve: median, dash curve and covered range: 90% prediction band) in intestine under each condition (**a**: young and liquid food, **b**: elderly and liquid food, **c**: young and liquid food, **d**: elderly and solid food). ····· 136

6-6. Reported colonic (large intestine) filling ratio (**a**; points; Read et al., 1986) and predicted cumulative (**a**) and density (**b**) gamma distribution for the time for food to move from the small intestine to the large intestine after a meal (solid curve: median, dash curve and covered range: 95% prediction band). The estimated parameter traceplots and distributions of Bayesian MCMC in supplementary information (Fig. 6-S4). ····· 137

6-7. Predicted infection probability (solid curve: median, dash curve and covered range: 60% and 95% prediction band) of *C. jejuni* (total of all three strains) under each condition (Same position as Fig. 6-5) and the reported ill probability of milk outbreak for children (8-13 years old) with milk (square; Teunis et al., 2005). ····· 139

6-8. Spearman's ranked correlation coefficients of parameter and computable factors against the predicted infection probability. Factors located at the upper position of this figure have a stronger relevance to infection probability. ····· 141

7-1. The comparison of listeria concentration changes in whole scenario and illness occurred

scenario. The prediction band (upper figure; Max-Min: light blue; 99%: blue; median: solid blue line) of the change in listeria concentration in milk during the simulated food chains, and the concentration change in case of illness occurrence (upper figure; 61 orange lines; spaghetti plot). The boxplot of the initial contamination level (log CFU/mL) and the changing ratio (log CFU/CFU) by storages and pasteurisation in whole scenario (lower; black boxplot) and illness occurred scenario (lower; orange boxplot). The prediction range and box plot were based on only the situation of the milk contaminated. ····· 178

7-2. The distribution of the estimated *L. monocytogenes* dose from pasteurised milk (blue distribution) and its location in scenarios with illness (orange bar above；barcode chart). The scale and x-axis grid of the above orange barcode chart is same as that of the below blue distribution of Log dose of contaminated dose scenario. The contaminated dose scenario was the 0.04% of whole scenario: the doses of the 99.96% of whole simulated scenario were zero. ····· 180

7-3. The distributions of the estimated pathogen behaviour (blue distribution) of *L. monocytogenes* in raw milk and its location in scenarios with illness (orange bars; A: initial contamination level; B: growth ratio on farm storage; C: reduction ratio by pasteurisation; D: growth ratio on distributing storage; E: growth ratio on retail storage; F: growth ratio on domestic storage). The scale and x-axis grid of the above orange barcode chart is same as that of the below blue distribution. All of distributions depend on only the contaminated situations in each stage. ····· 182

7-4. The Spearman's correlation coefficients of the impact of stochastic variable factors on the final contamination levels of *L. monocytogenes* at the moment of consumption (upper figure) and on the illness occurrence (lower figure). The error bars indicate the

standard deviation of ten times of the correlation estimations. Factors with stronger correlation coefficients are located at the top. ····· 184

7-5. The distributions of the pasteurization temperature: A and time: B (blue distribution) and its location in scenarios with illness (orange bars). The scale and x-axis grid of the above orange barcode chart is same as that of the below blue distribution. ····· 186

7-6. The distributions of the domestic storage temperature: A and the time: B (blue distribution) and its location in scenarios with illness (orange bars). The scale and x-axis grid of the above orange barcode chart is same as that of the below blue distribution. ····· 187

7-7. The distributions (blue) of the Log D deviation from the medians at each heating temperature: A, the √μ deviation during domestic storage: B, the one cell illness probability of dose-response model: C, and its location in scenarios with illness (orange bars). The scale and x-axis grid of the above orange barcode chart is same as that of the below blue distribution. ····· 188

7-8. The distribution (blue) of the post pasteurization time (sum of the storage time of distributing, retail and domestic), and its location in scenarios with illness (orange bars). The scale and x-axis grid of the above orange barcode chart is same as that of the below blue distribution. ····· 195

List of publications

1. **Abe H**, Koyama K, Kawamura S, Koseki S. Stochastic evaluation of Salmonella enterica lethality during thermal inactivation. International Journal of Food Microbiology, Elsevier, Volume 285, pp129–135, 2018

2. **Abe H**, Koyama K, Kawamura S, Koseki S. Stochastic modeling of variability in survival behavior of Bacillus simplex spore population during isothermal inactivation at the single cell level using a Monte Carlo simulation. Journal of Food Microbiology, Elsevier, Volume 82, pp436–444, 2019

3. **Abe H**, Koyama K, Takeoka T, Doto S, Koseki S. Describing the Individual Spore Variability and the Parameter Uncertainty in Bacterial Survival Kinetics Model by Using Second-Order Monte Carlo Simulation. Frontiers in Microbiology, Frontiers Media S.A., Volume 11, pp1–14, 2020

4. **Abe H**, Koyama K, Koseki S. Modeling Invasion of *Campylobacter jejuni* into Human Small Intestinal Epithelial-Like Cells by Bayesian Inference. Applied and Environmental Microbiology, American Society for Microbiology, Volume 87, 1, 2021

5. **Abe H**, Takeoka K, Fuchisawa Y, Koyama K, Koseki S. A New Dose-Response Model for Estimating the Infection Probability of *Campylobacter jejuni* Based on the Key Events Dose-Response Framework. Applied and Environmental Microbiology, American Society for Microbiology, Volume 87, 20, 2021

Chapter 1 General Introduction

1.1. Risks of food poisoning and foodborne illness

Foodborne illnesses are one of the most common health risk. There are three types of foodborne hazard: physical, chemical, and biological. Biological hazards are the most frequent, with 350 million cases of foodborne biological illness occurring on the planet annually (WHO, 2015). The biological hazards derived from foodborne pathogenic bacteria are more difficult to manage than the other two types of hazards because of self-amplification, time required for detection, and heterogeneity due to individual cells. In recent years, food production and distribution networks have expanded and become more complex on a global scale, and food hygiene management has become more important than ever before. Quantification and objectivity of risk of foodborne illnesses in each food are essential for smooth and efficient international trade and distribution of foods.

1.2. Changes in microbial foodborne illness risk during food chains

Microbial risks on foodborne illness change depending on the environment to which the food is exposed. Primary products are harvested at farms, fishing grounds, etc., then processed, distributed, preserved, and consumed by people. This flow of foods from farm to consumption is called a food chain. Almost all foods are contaminated by some kinds of microorganism when they are harvested. As shown in Figure 1-1, the number of microorganisms in foods generally increase from farm to pre-processing stage, and then reduce with processing such as thermal processing or low pH treatment etc. Microorganisms survived in processing grow during transportation and storage in retail stores and homes. The number of microbial cells changes through the food chain can cause foodborne illness and food spoilage. The minimum numbers and/or concentration of microorganisms in foods that

does not cause foodborne illness when consumed is called the Food Safety Objective: FSO (FAO/WHO, 2021). Understanding and controlling microbial changes in food chain will enable to ensure food safety certainly.

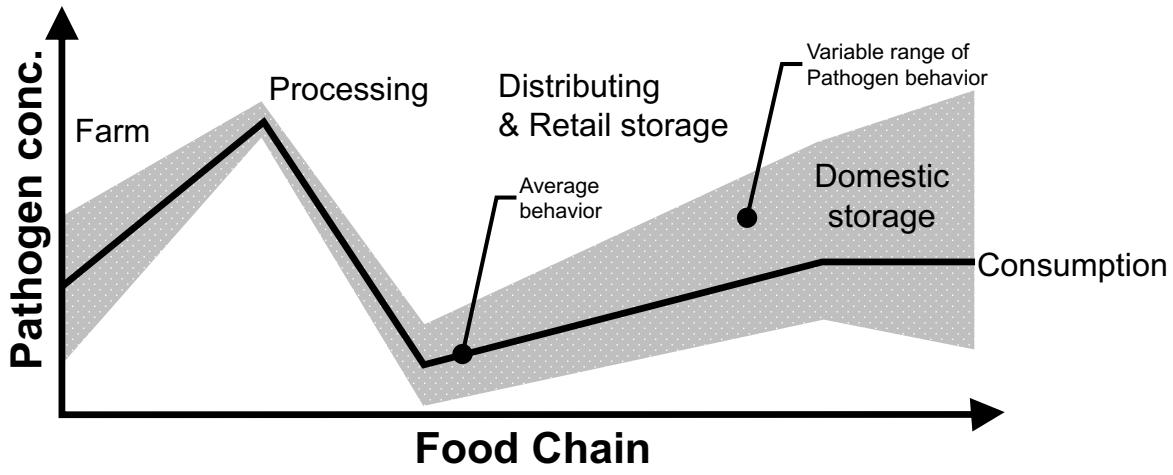


Fig. 1-1. The schematics of pathogen concentration changes during the food chain (Farm to Consumption).

1.3. Hazard Analysis and Critical Control Point, and Quantitative Microbial Risk Assessment

In recent decades, Hazard Analysis Critical Control Point (HACCP) system has been proposed to establish international standards for food safety. HACCP is a management system in which food safety is addressed by analyzing and controlling biological, chemical, and physical hazards from raw material production, procurement and handling, to manufacturing, distribution and consumption of the finished product (U.S. FDA, 2018). HACCP promotes food hygiene management among producers and protects the health and safety of consumers. Quantitative microbial risk assessment (QMRA) is often conducted for HACCP to quantify risk of foodborne illness induced by pathogenic microorganisms in food. QMRA combines existing literature and surveillance databases with computational techniques to yield models that predict public health outcomes (Dennis, Buchanan, & Miller,

2002). QMRA consists of combination of following four procedures: hazard identification, hazard characterization, exposure assessment, and risk characterization. A probabilistic approach is performed (Nauta, 2002) in QMRA, and the probabilistic approach for QMRA is to consider heterogeneity coming from processing and storage conditions and bacterial individuality. This heterogeneity can be divided into two types that are uncertainty and variability, and it has been proposed that risk assessment should take into account the heterogeneity derived from both types. In this context, “uncertainty” represents the lack of perfect knowledge of a parameter value, which might be reduced by further measurements, whereas “variability” represents the true randomness or heterogeneity of the population or environments, which are a consequence of the physical system and irreducible through additional measurements (Nauta, 2000). The probabilistic approach to risk assessment allows for more realistic estimates than the deterministic estimates based on a single estimate.

1.4. Predictive microbiology for risk assessment

Predictive microbiology can be applied to estimate growth or inactivation behavior of microorganisms in QMRA. Predictive microbiology takes the approach to explain the response of microorganisms to environmental factors (e.g., temperature, pH, water activity) using mathematical models (Ross et al., 1994). It is useful for HACCP and QMRA because it explains various behavior of bacteria using mathematical models. In particular, the mathematical model of growth and inactivation behavior is useful for the exposure assessment in QMRA which evaluate changes in pathogen numbers during processing, distribution, and storage; the prediction models for probability of infection or illness (dose-response models) play an important role for risk characterization in QMRA. However, since most of the predictive models are deterministic predictions of the average bacterial behavior (Fig. 1-1; solid line), most conventional models are insufficient for application to QMRA,

which requires a probabilistic prediction approach. In a realistic situation, the environmental conditions, the pathogen characteristics and behavior are variable (Fig. 1-1; colored range). Therefore, probabilistic or stochastic predictive models are indispensable for the application to QMRA.

1.5. Goal of this study

The goal of this study was to develop advanced predictive models and analysis procedures that can be applied to QMRA. In Chapters 2, 3, and 4, these studies developed probabilistic and stochastic models for the variability in the behavior of bacterial populations and bacterial spore populations during thermal inactivation, based on the inactivation of individual bacterial cell. In Chapters 5 and 6, these studies estimated the reduction and migration of pathogenic bacteria (*Campylobacter jejuni)* in a human digestive system and developed a model to predict the infection probability. In Chapter 7, this study developed analytical methods for elucidation of relevant factors on food chain to the occurrence of foodborne illness using QMRA of listeriosis on pasteurized milk. This PhD project as a whole aimed at contributing to advancement for more realistic QMRA throughout the food chain.

1.5. References

Dennis, S. B., Buchanan, R. L., & Miller, A. J. 2002. Microbial Risk Assessment: Achievements and Future Challenges, 1–5.

Food and Agriculture Organization of the United Nations/ World Health Organization, Agriculture Organization of the United Nations. (2021). Microbiological risk assessment: guidance for food. Food and Agriculture Organization of the United Nations/ World Health Organization/Agriculture Organization of the United Nations, 1–288.

Nauta, M.J., 2000. Separation of uncertainty and variability in quantitative microbial risk assessment models. International Journal of Food Microbiology 57, 9–18. doi:10.1016/S0168-1605(00)00225-7

Nauta, M.J., 2002. Modelling bacterial growth in quantitative microbiological risk assessment: Is it possible? Int. J. Food Microbiol. 73, 297–304.

Ross, T., McMeekin, T.A., 1994. Predictive microbiology 23, 241–264. doi:10.1016/0168-

1605(94)90155-4
U.S. Food and Drug Administration, 2018. https://www.fda.gov/food/guidance-regulation-food-and-dietary-supplements/hazard-analysis-critical-control-point-haccp (accessed December 14th, 2021)
World Health Organization. (2015). *WHO ESTIMATES OF THE GLOBAL BURDEN OF FOODBORNE DISEASES* (pp. 1–265).

Chapter 2 Probabilistic predictive approach for *Salmonella enterica* lethality by iso-thermal heating

2. 1. Introduction

Thermal inactivation processes for assuring microbiological food safety must meet certain criteria. To this end, the food industry relies on kinetic or deterministic models to describe temporal changes in the number of surviving bacteria in foods (e.g. log-linear model, Weibull model and other semi-logarithmic survival curves). The traditional concept of microbial inactivation kinetics is based on a study dating back nearly a century that estimated the thermal end point (Bigelow and Esty, 1920), which has long been the standard for safe food production.

Although it is necessary to correctly describe thermal death behaviour to establish the appropriate heating temperatures and times for microbial inactivation, there are some problems with the deterministic approach. One is that it relies on point estimates or single values such as the mean or average of a dataset to generate a single risk estimate value (Cassin and Paoli, 1998) that disregards the variability and uncertainty of biological phenomena (Membré et al., 2006). In this context, 'uncertainty' represents the lack of perfect knowledge of the parameter value, which may be reduced by further measurements. 'Variability', on the other hand, represents a true heterogeneity of the population that is a consequence of the physical system and irreducible by additional measurements (Nauta, 2000). The former reflects the true heterogeneity of a population, which is a characteristic of the physical system and is irreducible, while the latter arises from the lack of perfect knowledge of a parameter value and can be minimised by additional measurements (Nauta, 2002). Thermal death in a bacterial population is a phenomenon that exhibits greater heterogeneity for lower bacterial counts (Aspridou and Koutsoumanis, 2015). Another

problem with deterministic models is that they estimate survival probability from decimal reduction kinetics of bacterial counts. Conventional thermal death time calculations assume that once a certain level of reduction has been achieved, the probability of actual survival is so low that it can be discounted. However, the deterministic methodology does not accurately describe survival probability, because the reduction levels do not reflect actual bacterial numbers obtained in an experiment. Moreover, thermal death time is typically estimated by extrapolation of a linearized isothermal semi-logarithmic survival curve, yielding an overestimate of the true time needed reach a reduction in number when isothermal survival curves have a downward concavity, and an underestimate when the curves indicate tailing (Peleg, 2006). For these reasons, deterministic methodology cannot achieve accurate quantitative microbial risk assessment (QMRA) of contaminating bacteria in foods.

A probabilistic approach using a more highly developed mathematical methodology than point estimate-based deterministic models makes QMRA improve (Thompson and Graham, 1996). It has been suggested that probability distributions be used to describe both uncertainty and variability for quantitative risk assessment (Thompson and Graham, 2008; Vose, 1998). Recent studies support a bacterial inactivation model derived from a stochastic approach using Monte Carlo simulation (Aspridou and Koutsoumanis, 2015; Marks et al., 1998; Membré et al., 2006), while others advocate applying Monte Carlo simulation to bacterial growth (Cassin and Paoli, 1998; Nauta, 2001). Although the heterogeneity in total reduction time of bacterial populations has been reported (Aspridou and Koutsoumanis, 2015; Koyama et al., 2017), few studies (Koyama et al., 2017) have described changes in the observed survival probability of bacterial populations with a cumulative probability distribution. However, this would enable prediction of actual bacterial lethality and could explain the variability in total reduction time of bacterial populations upon thermal

inactivation. The survival probability distribution could also be used in QMRA to establish appropriate thermal conditions for minimizing negative impact in foods.

In this study, we developed a stochastic model for estimating the survival probability of bacterial populations by taking into account the heterogeneity in total reduction time. We investigated the relationship between initial cell counts and bacterial survival at various temperatures. Changes in total reduction probability over time were described as a probability distribution based on the reliability theory, which considers the probability of failure by describing variability with probability distribution. Based on the probabilistic evaluation, we estimated heating time for different survival probabilities (P = 0.5 and 10^{-6}) of a bacterial population. A probability of 0.5 is the average value described by a deterministic model (Cassin and Paoli, 1998), while 10^{-6} is the probability that the risk can be ignored (Bigelow and Esty, 1920) at a given initial cell number. We verified whether the model supported the conventional deterministic heating time of thermal inactivation, and compared the stochastically predicted heating time with the value derived from first-order kinetics of the change in the number of surviving cells.

2.2. Materials and Methods

2.2.1. Bacterial strain and culture conditions

Salmonella enterica Oranienburg derived from a food-borne illness originating from smoked squid in the Aomori prefecture of Japan in 1999 was used in this study as a representative highly thermotolerant vegetative bacterial strain. The cause of the food poisoning accident is management mistake that the temperature of the drying process should have been set at 45ºC-50ºC but it was 40°C-45°C in which the isolates can growth(Itoh, 2001; Hiroshi et al., 2007). A stock culture of the strain was stored frozen in 10% glycerol at −80°C; the strain was activated by incubating once at 37°C for 24 h on tryptic soy agar (TSA;

Merck, Darmstadt, Germany) and twice at 37°C for 24 h in tryptic soy broth (TSB; Merck). The 24-h culture of *S. enterica* Oranienburg was centrifuged at 3000 × *g* for 10 min; the cells were washed with TSB and centrifuged again under the same conditions. For the stochastic approach, harvested cells were washed with TSB and diluted in TSB to obtain cell concentrations of 10^n CFU/ml (where n = 2, 3, 4, 5, 6) by serial dilution. Diluted cultures were stored at 4°C for the duration of the experiment. There is no concern of proliferation at 4 ° C from the results of pre-experiment, but since heat resistance may change by cold insulation, there are cases where cold insulation is up to 4 hours. For the deterministic approach, cells were resuspended in TSB (10^9 CFU/ml), and initial bacterial counts were determined on TSA plates after culturing at 37°C for 24 h.

2.2.2. Thermal treatment for analyzing changes in survival probability

Aliquots of diluted culture (100 µl) were dispensed into the wells of a 96-well PCR microplate to obtain cell concentrations of 10^n CFU/ml in each well (where n = 1–5). The microplates were heated at 60°C, 62°C, 64°C, and 66°C on a T100 Thermal Cycler (Bio-Rad, Hercules, CA, USA) after 30 s of preheating at 25°C to standardize the initial temperature across trials as shown in Fig. 2-1. The total duration of the trials depended on the initial counts and heating temperature. In total, we analyzed 15 samples at each heating temperature. The time intervals of 15 samples at each temperature were determined to reflect the rate of changes in the survival probability of *S. enterica* Oranienburg preliminary measured. The microplates were cooled by 4°C immediately after heating and then incubated at 37°C for 24 h to evaluate the reduction in the bacterial population based on examination of turbidity by naked eye. We assume that the recovery of all damaged bacteria was measured because there is no significant difference between 24 h incubation and over 72 h incubation as the result of pre-experiments.

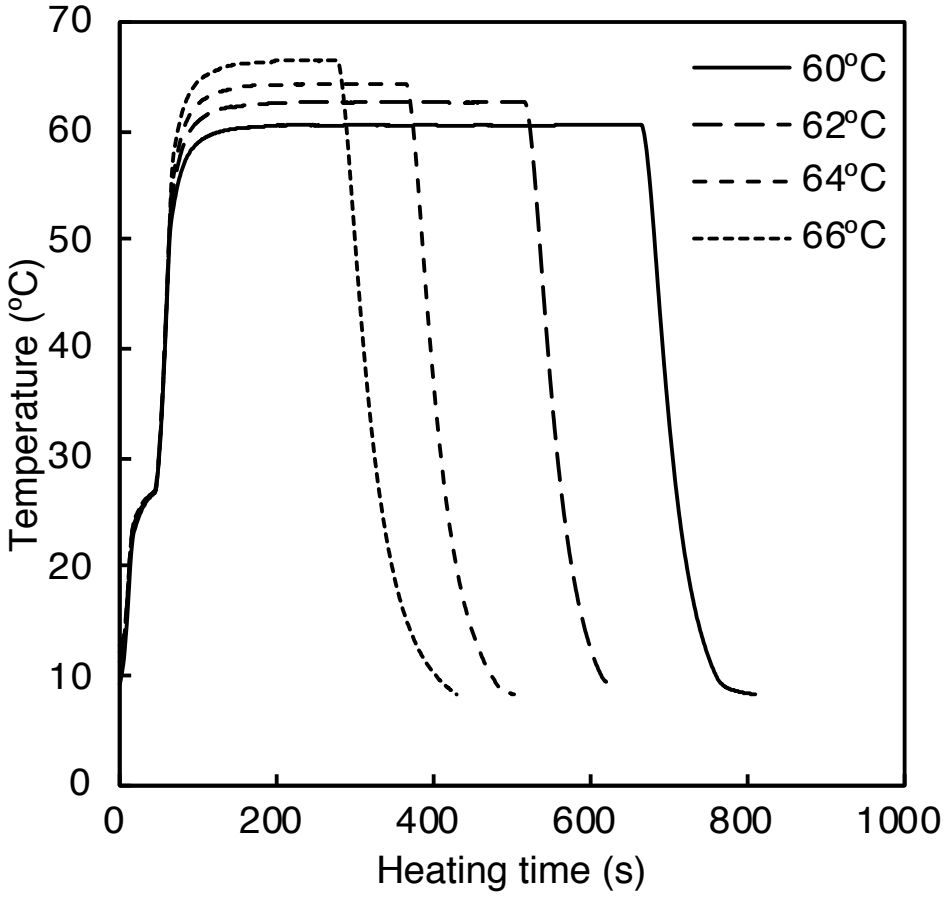


Fig. 2-1. An example of heating protocol even at experimental temperature: 600 s heating at 60°C, 450 s heating at 62°C, 300 s heating at 64°C, and 210 s heating at 66°C by thermal cycler. Preheating of 30 s at 25°C to standardize the initial temperature across trials. After heating process, the 96-PCR microplates were immediately chilled at 4°C.

2.2.3. Thermal treatment for analyzing conventional survival kinetics

Aliquots of washed bacterial culture (100 μl) were dispensed into PCR tubes that were heated at 60°C, 62°C, 64°C, and 66°C on a thermal cycler after 30 s of preheating at 25°C to standardize the initial temperature across trials. A total of 10 samples were obtained at each temperature at time intervals required for effective analysis of microbial inactivation kinetics. Serial 10-fold dilutions of sample in 0.1% peptone water were plated on TSA.

Population survival was determined by three replicates of survivors evaluation of incubation at 37°C for 24 h after heating.

2.2.4. Modelling survival probability

The survival probability of bacterial populations was determined from 60 replicates on a microplate according to the following equation (2-1):

$$P_{survival} = 1 - \frac{W_t}{60} \qquad (1\text{-}1)$$

where $P_{survival}$ is the survival probability, and W_t is the turbid well count among the 60 wells of the plate in which temperatures are homogeneously distributed at heating time t.

A cumulative gamma distribution is typically used for lifetime modelling in reliability engineering (Cohen and Whitten, 1988). The description of changes in death probability as a cumulative gamma distribution is related to reliability theory (Barlow, 1998), in which a gamma distribution explains durability. The variability in total reduction time can be described as a gamma distribution. Engineering reliability is defined as the probability of a device effectively carrying out its purpose for a given period of time, during which the device is intended to operate under normal conditions (Barlow, 1998). In this context, the time to failure or risk of failure is generally described as a probability distribution—for example, as a Weibull or gamma distribution. The single cell inactivation follows exponential distribution when the inactivation behaviour is log-linear, because the thermal death curve has a characteristic as a cumulative form of the heat distribution resistance (Peleg, 2006). The cumulative gamma distribution describes the probability of a situation in which frequency of some events following an exponential distribution is more than a specific frequency at given time point. We used the gamma distribution in this study based on the hypothesis that the total reduction of the bacterial population is achieved when thermal inactivation of single cells occurs as many times as the initial cell number. Waiting times until the occurrence of

the event modelled by the Poisson process are gamma-distributed (Bury, 1999). In this study, it was assumed that the total reduction time of the bacterial population is a waiting time because single cell death can be modelled as an exponential distribution, which is a Poisson process when the reduction of bacterial cells follows first-order kinetics.

The survival probability of the bacterial population is the inverse of total inactivation probability; therefore, the survival probability of the bacterial population is described by a cumulative gamma distribution, which was used to approximate the change in total inactivation probability of the bacterial population, according to the following equation (2-2):

$$P_{survival} = 1 - \frac{1}{\Gamma_{(\alpha)}}\gamma_{(\alpha,\beta t)} \qquad (1\text{-}2)$$

where $P_{survival}$ is the survival probability of bacterial population at arbitrary heating time t; α is the shape parameter; β is the rate parameter of gamma distribution; $\Gamma_{(\alpha)}$ is the gamma function: $\Gamma_{(\alpha)} = \int_0^\infty e^{-u}u^{\alpha-1}\,du$; and $\gamma_{(\alpha,\beta t)}$ is the lower incomplete gamma function: $\gamma_{(\alpha,\beta t)} = \sum_{k=0}^{\infty}\frac{(\beta t)^{\alpha+k}e^{-\beta t}}{\alpha(\alpha+1)\ldots(\alpha+k)}$. We assumed that single cell death events followed an exponential distribution since the decline in the ratio of surviving cells is log-linear because the proportion of inactivated bacteria: $\overline{N}_{(t)}$ is described as the same type of equation with cumulative exponential distribution: $\overline{N}_{(t)} = 1 - e^{-k_{(T)}t}$. The experimentally obtained stochastic data were fitted with equation (2-2) using a non-linear least squares approach.

To determine the characteristics of the fitted gamma distribution, we calculated the mean and variance using equation (2-3) and (1-4):

$$E_{(T)} = \frac{\alpha}{\beta} \qquad (1\text{-}3)$$

$$Var_{(T)} = \frac{\alpha}{\beta^2} \qquad (1\text{-}4)$$

where $E_{(T)}$ is the mean and $Var_{(T)}$ is the variance of the fitted gamma distribution (Scheaffer et al., 2010). The obtained mean and the variance were fitted by a polynomial equation, and

the gamma distribution of arbitrary initial cell counts was estimated at each heating temperature. Since the deterministic model is based on point estimates, the model describes the mean of the bacterial dataset (Cassin and Paoli, 1998). Additionally, the heating time with a survival probability of 0.5 describes the mean total reduction time from the standpoint of probabilistic theory. Mean total reduction times were compared to evaluate the relationship between stochastic and deterministic approaches. Finally, heating times required for an arbitrary log-cycle reduction with survival probabilities of 0.5 (average) and 10^{-6} (sterile level of objective bacteria) derived from estimated gamma distributions (Fig. 2-2) were drawn as contour plots.

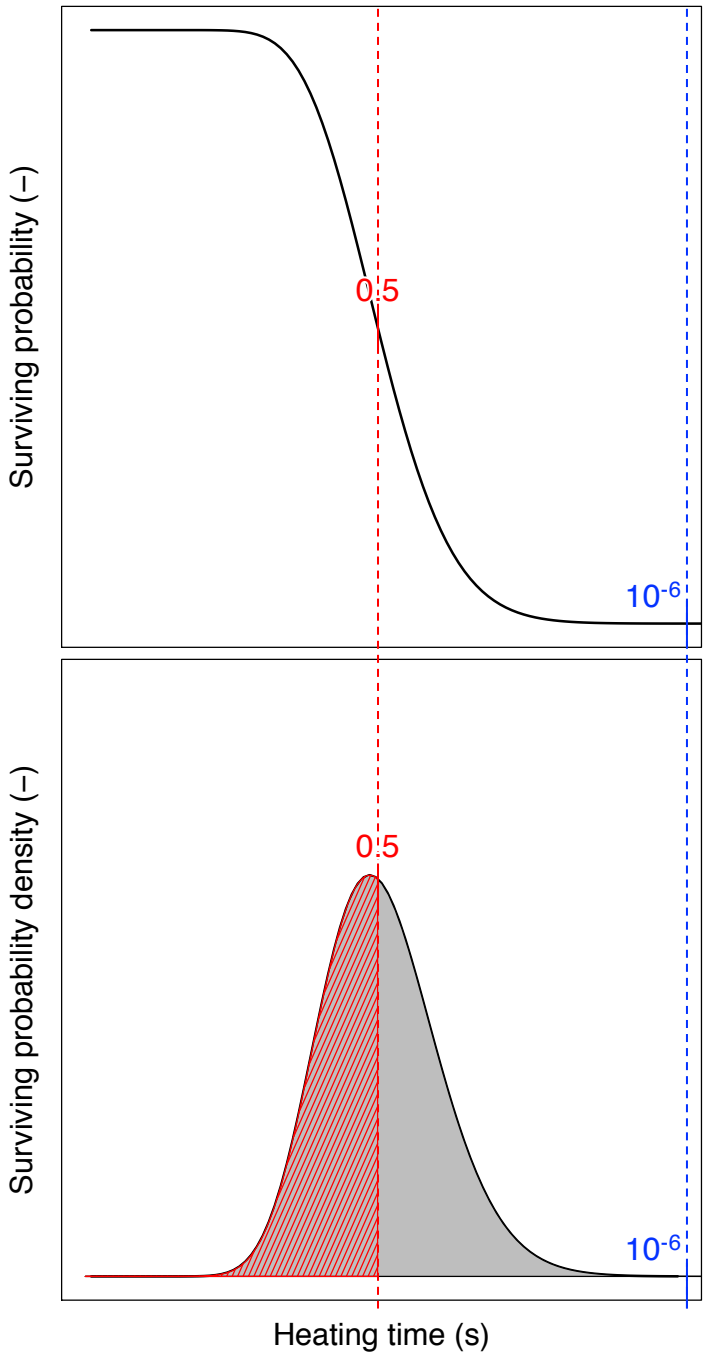


Fig. 2-2. Schematic illustration of the stochastic procedure for estimating survival probability. Upper and lower figures represent survival probability: equation (2-2) with cumulative gamma distribution and frequency of total reduction time with gamma distribution, respectively. Red and blue lines indicate heating time with a bacterial population survival probability of 0.5 and 10^{-6}, respectively. The time with a probability of 0.5 represents the average of

the distribution, and the time with a probability 10^{-6} is that at which the risk of bacterial survival can be disregarded.

2.2.5. Analysis of S. enterica Oranienburg survival kinetics data

Isothermal survival curves of target cells follow first-order inactivation kinetics:

$$N_{(t)} = N_0 e^{-k_{(T)}t} \qquad (1\text{-}5)$$

where $N_{(t)}$ and N_0 are the instantaneous and initial numbers of organisms, respectively; $k_{(T)}$ is the exponential rate constant for temperature-dependent inactivation; and t is inactivation time (Brul et al., 2007). Data obtained from kinetic experiments were described by linear least squares according to equation (2-6):

$$\log_{10} \frac{N_{(t)}}{N_0} = -\frac{t}{D} \qquad (1\text{-}6)$$

where D is the decimal reduction time which is also temperature-dependent parameter (D value).

Probability of a non-sterile unit (PNSU), which it cannot describe survival probability but survival counts, was adopted as a deterministic approach to estimate the survival probability of the objective bacterial population. The concept of PNSU (Fig. 2-3) is used to describe the ratio of the probability of a single microorganism surviving in a specific number of units such as cans or packages (Pflug, 2003) after the sterilisation process. For example, a single viable bacterial cell surviving in 10^9 containers of food after heating yields a PNSU of 10^{-9}. PNSU was calculated at each heating temperature as the survival probability of the bacterial population according to equation (2-7):

$$P_{PNSU} = N_0 10^{-\frac{t}{D}} \qquad (1\text{-}7)$$

where P_{PNSU} is the probability of a non-sterile unit ($P_{PNSU} \leq 1$) and N_0 is the initial number of bacteria in a well when $N_0 10^{-\frac{t}{D}} \leq 1$. Finally, heating times with probabilities of 0.5 and

10^{-6} estimated from the PNSU at each heating temperature were drawn as deterministic probability contour lines.

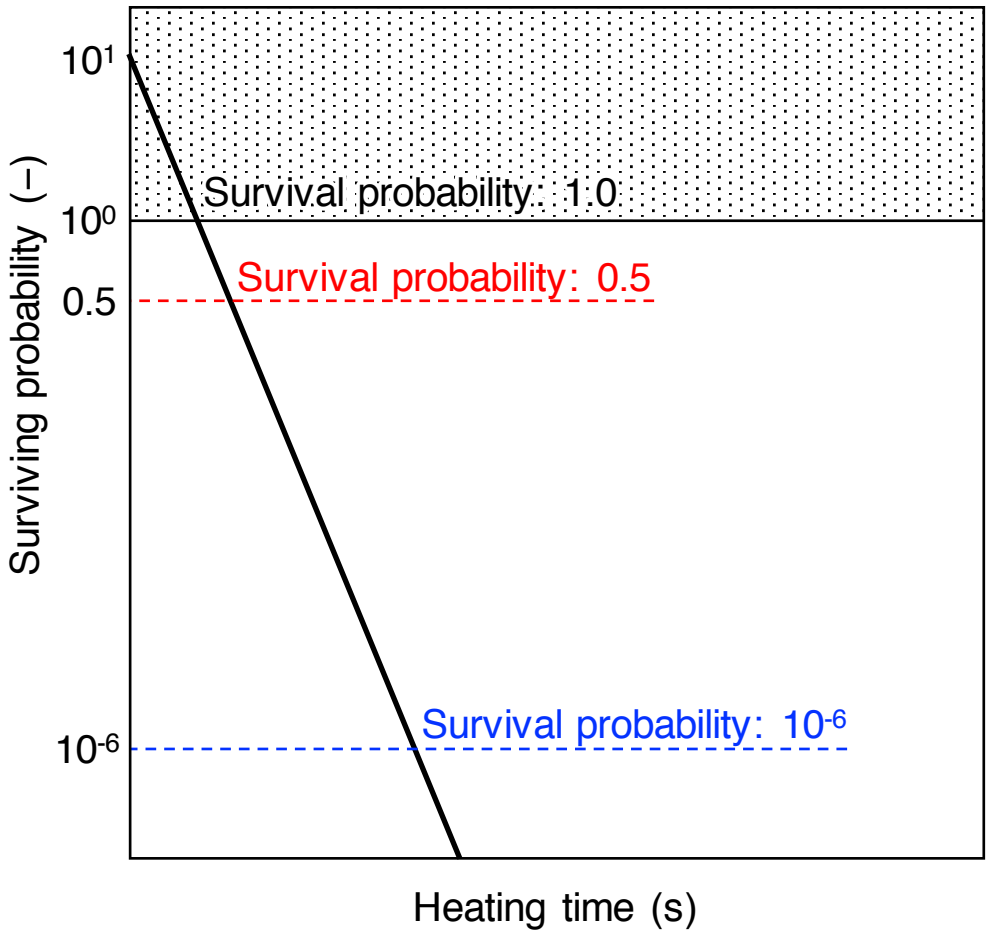


Fig. 2-3. Schematic illustration of the deterministic procedure for estimating survival probability by first-order kinetics. The survival probability of the bacterial population estimated by the deterministic procedure was derived from equation (2-7). As in Figure 2-1, red and blue lines indicate heating time with a bacterial population survival probability of 0.5 and 10^{-6}, respectively.

2.3. Results

2.3.1. Probabilistic evaluation of S. enterica Oranienburg survival during heating

We determined the survival probability of 60 bacterial population replicates at each sampling time point under each heating temperature. Changes in the survival probability of a bacterial population over time at each temperature were fitted by a cumulative gamma

distribution using equation (2-2); the distribution described the changes irrespective of heating temperature or initial cell counts (Fig. 2-4). The fitted parameters and root mean square error (RMSE) as an indicator of the goodness-of-fit are shown in Table 2-1. RMSE values ranged from 0.004 to 0.069 and adjusted R^2 was very close to 1 ($0.92 <$ adjusted $R^2 <$ 1.00), indicating that the fitted gamma distributions accurately described changes in the survival probability. The mean of the fitted Gamma distribution (Eq. 3) was described as a linear function of initial cell numbers ($0.88 <$ adjusted $R^2 < 0.99$, $6.1\times10^3 <$ RMSE $< 7.4\times10^4$; Fig. 2-5a). According to the fitted parameters, the mean of total reduction time was longer at lower heating temperatures. In contrast, although the variances of the fitted gamma distribution were scattered and were unrelated to initial cell counts, they tended to increase at higher heating temperatures (Fig. 2-5b).

Table 2-1 The parameter and RMSE of the fitted Gamma distribution

Temperature (ºC)	Initial counts (logCFU)	Fitted parameter		Adjusted R^2 (-)	RMSE (-)
		SHAPE (-)	RATE (/s)		
60	0.9	16	0.029	0.98	0.049
	1.8	242	0.331	1.00	0.017
	2.9	501	0.581	1.00	0.009
	3.8	1199	1.180	1.00	0.008
	4.9	81	0.067	1.00	0.026
62	0.7	15	0.072	0.99	0.027
	1.7	98	0.293	0.98	0.069
	2.9	187	0.323	1.00	0.004
	3.9	208	0.334	1.00	0.020
	4.9	124	0.163	0.99	0.063
64	0.7	16	0.148	1.00	0.020
	1.7	30	0.229	0.99	0.036
	2.8	59	0.362	0.96	0.021
	3.8	218	1.022	1.00	0.025
	4.8	175	0.516	1.00	0.019
66	0.7	32	0.913	1.00	0.021
	1.8	84	1.181	0.99	0.048
	2.8	124	1.387	0.92	0.027
	3.8	111	1.059	0.99	0.039
	4.8	83	0.558	0.99	0.052

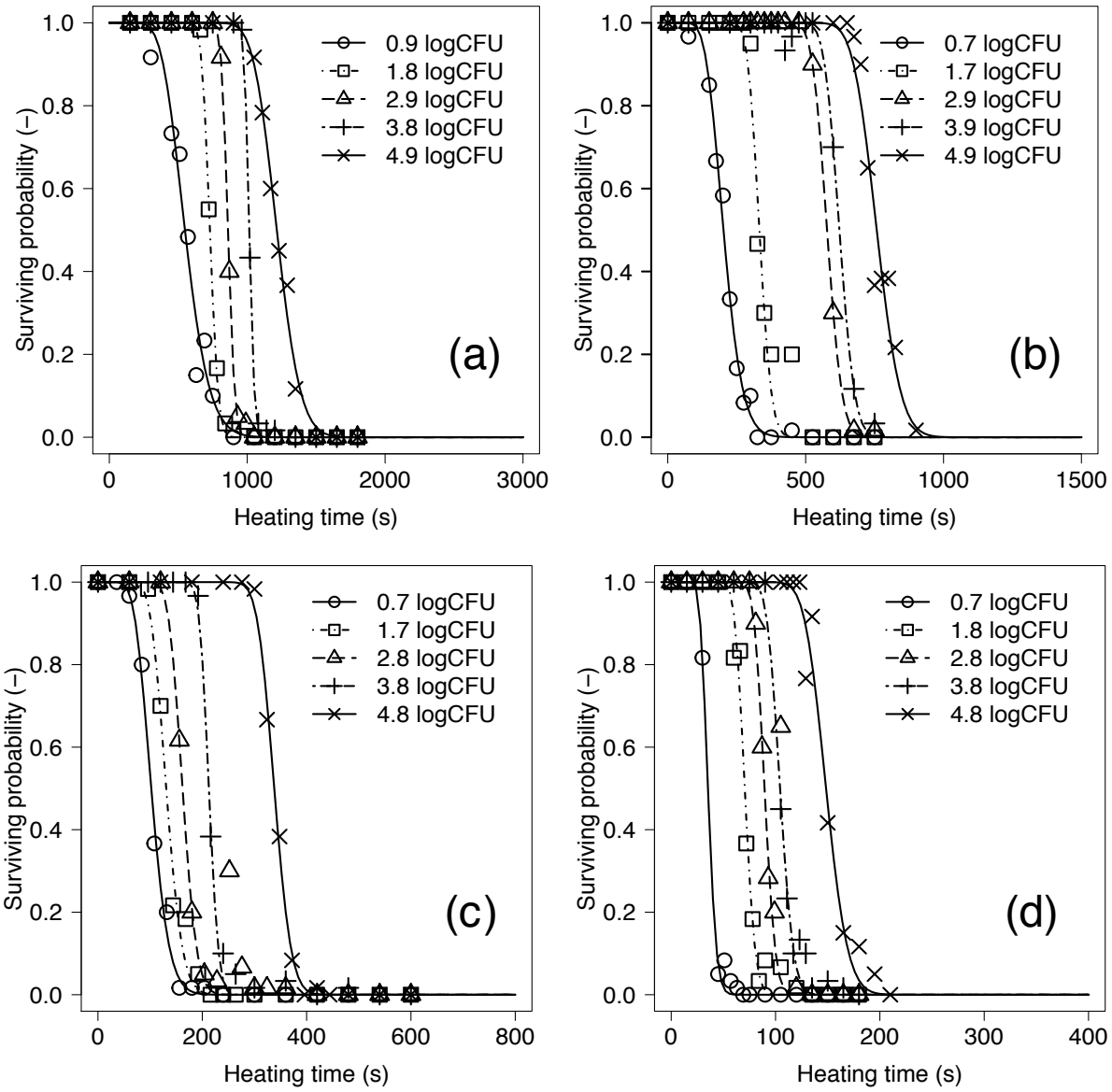


Fig. 2-4. Change in the probability of 60 bacterial populations each with nearly 1×10^n cells where n = 1 (○), 2 (□), 3 (△), 4 (+), 5 (×), heated at 60°C (a), 62°C (b), 64°C (c) and 66°C (d) in TSB. The five different lines show the best fit of a cumulative gamma distribution of nearly 1×10^n cells (n = 1, 2, 3, 4, 5) at each heating temperature. The highest and lowest RMSE was 0.069 and 0.004, respectively.

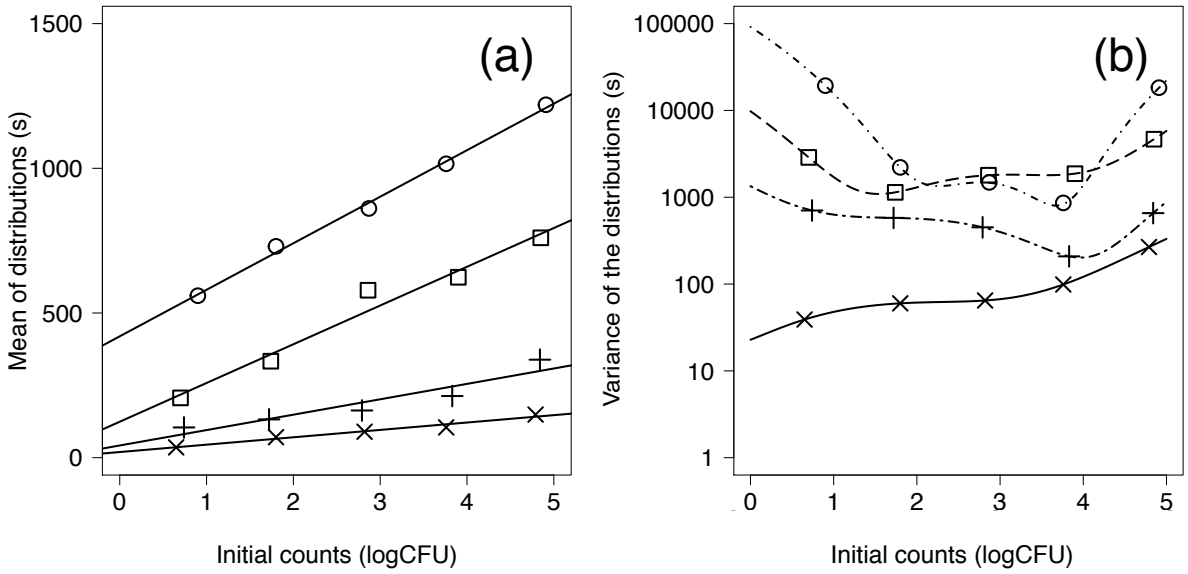


Fig. 2-5. Relationship between mean (a) and variance (b) of the best fit of a cumulative gamma distribution; inserted cells were heated at 60°C (○), 62°C (□), 64°C (+), and 66°C (×) in TSB. The lines show the linear regression lines (a) heated at each temperature; the highest and lowest R^2 value was 0.99 and 0.88. Fourth-order regression curves are shown (b) that describe the heterogeneity in variance of total reduction time.

To summarize the death probability with respect to the initial number of cells, we described the death probability of the bacterial population as an interface (Fig. 2-6). The target number of cells was described as a negative value of the initial number of cells (Figs. 2-6 and 2-7). The death probability contour line for the log-linear model exhibited a linear relationship between time and the targeted initial cell reduction (Fig. 2-6). In contrast, the death probability contour line for the downward or upward concavity cases did not exhibit a linear relationship between time and the targeted initial cell reduction (Fig. 2-6). The trend in the contour line of the death probability had the same curvature as the inactivation kinetics (Figs. 2-1 and 2-6). We compared the death probability of the bacterial population calculated via inactivation kinetics with that given by the stochastic model developed in this study. The contour line of the death probability was almost congruent with the inactivation kinetics

calculation (Fig. 2-7). This indicates that the death probability of the bacterial population can be estimated from the kinetic model, as in Fig. 2-2. The best fit parameters for the 3.4 $\log_{10}$CFU/ml level are b = 0.064 and n = 0.970, which give an RMSE of 0.172, and those for the 2.3 $\log_{10}$CFU/ml level are b = 0.087 and n = 0.914, which give an RMSE of 0.151. The validation results are shown in Fig. 2-8. The observed data (●) are broadly consistent with the simulation results in the regions where a number of survivors are expected. Instances of no survivors after six trials (×) mostly occur after the simulations have finished, when no survivors are expected. Thus, our simulation model can describe the variability in the inactivation behavior of the population.

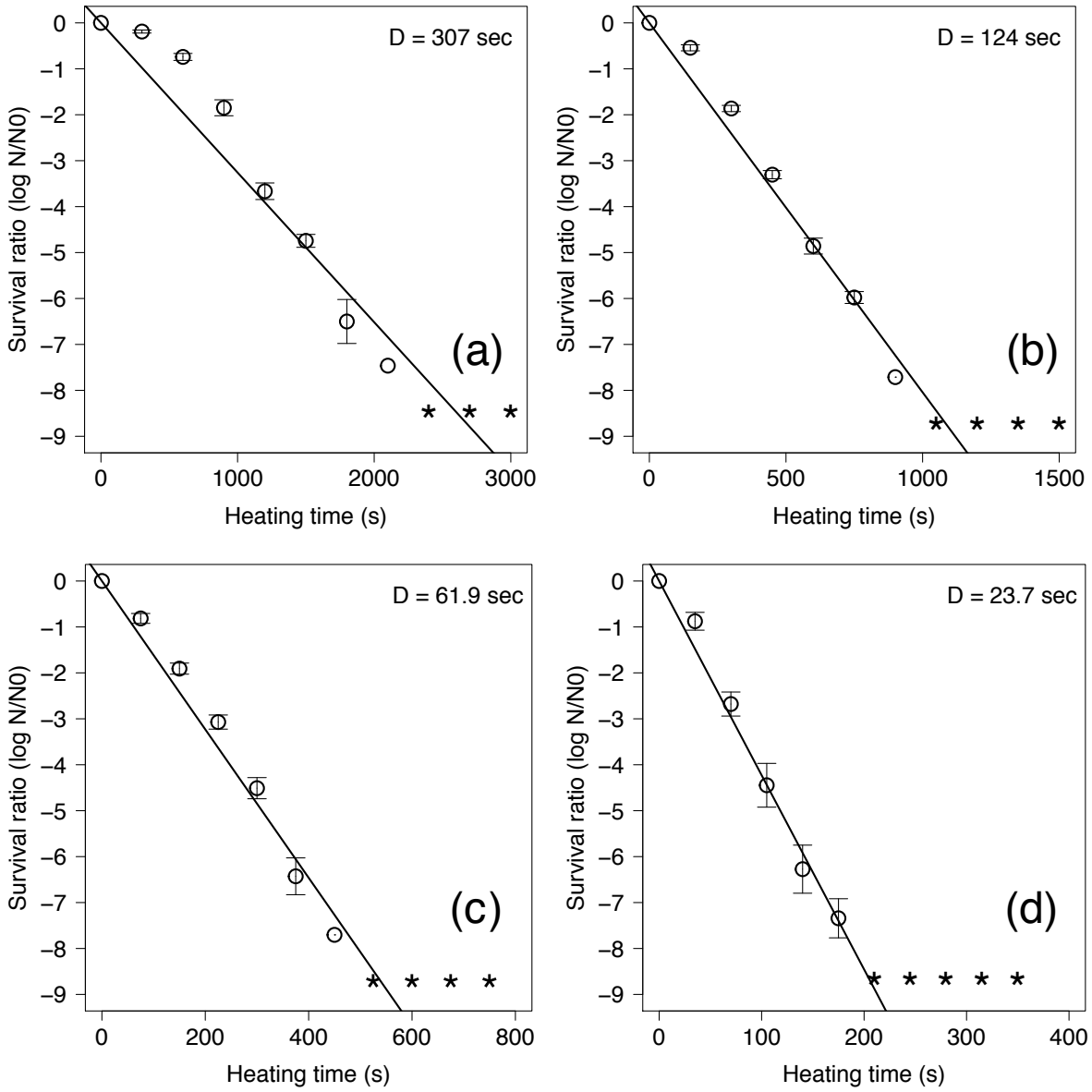


Fig. 2-6. Kinetics of *S. enterica* Oranienburg survival from an initial concentration of 10^9 CFU/ml heated at 60°C (a), 62°C (b), 64°C (c), and 66°C (d) in TSB. Error bars indicate standard deviations. Each point with error bar is the mean of two or three values, and each point without an error bar is a single value. No colonies were detected at the time indicated by an asterisk (*). A small shoulder reduction was observed by heating 60°C (a) and linear reductions were observed by heating at 62°C (b), 64°C (c), and 66°C (d). Lines show the linear regression of kinetic changes in surviving cell counts, and yield *D* values at each heating temperature in TSB. R^2 value at 60°C is 0.97, 62°C, and 64°C were 0.99 and 66°C was 1.00.

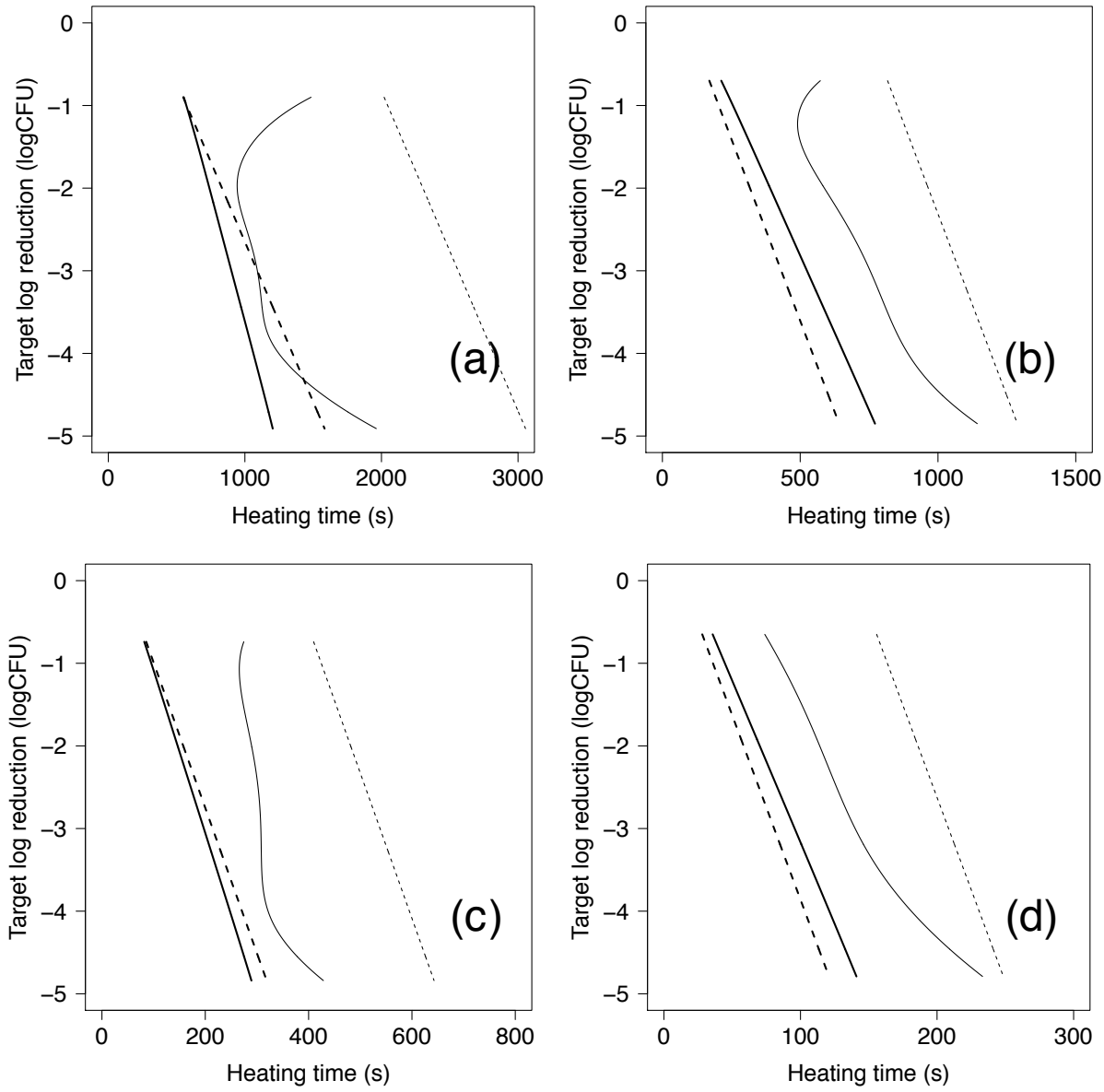


Fig. 2-7. Probability contour lines indicating total inactivation heating time of various cell numbers and survival probability of bacterial population at specific levels of inactivation (0.5 and 10^{-6}), as predicted using stochastic and kinetic model heated at 60°C (a), 62°C (b), 64°C (c), and 66°C (d). This figure enabled us to draw two comparisons between stochastic-0.5 (bold solid line) and kinetic-0.5 (bold dash line) predicted heating time, and between stochastic-10^{-6} (solid line) and kinetic-10^{-6} (dashed line) predicted heating time.

2.3.2. Survival kinetics of S. enterica Oranienburg

Surviving cell counts of three bacterial population replicates were determined at each heating temperature. Changes in the surviving cell ratio at each temperature were described

by first-order kinetics (Eq. 6) (0.97 < adjusted-R^2 <0.99, 0.76 < RMSE < 2.0; Fig. 2-6) and the *D*-value at each heating temperature was determined (Fig. 2-6). Changes in the surviving cell ratio were larger at higher heating temperatures.

2.3.3. Comparison of the probability of death estimated by stochastic and deterministic models

We estimated the heating time required for an arbitrary log-cycle reduction with specific survival probabilities (0.5 and 10^{-6}) using both the probabilistic and kinetic approaches; these were drawn as contour plots for each heating temperature (Fig. 2-7).

There was a significant difference in the predicted heating times between survival probabilities of 0.5 and 10^{-6} determined by the two calculation methods. In particular, heating times calculated according to the deterministic model showed much larger differences in survival probability. By comparison, the required heating times derived from the stochastic calculation showed small differences between survival probabilities of 0.5 and 10^{-6}. Required heating times with a survival probability of 10^{-6} (solid line) were twisted out of shape in the low and high log-cycle reductions, whereas those with a survival probability of 0.5 (bold solid line) were linear (Fig. 2-7). The stochastic prediction with a survival probability of 0.5 was similar to the deterministic prediction, while the prediction with a probability of 10^{-6} differed significantly.

2. 4. Discussion

Our results indicate that changes in the survival probability of the bacterial population can be described by a cumulative gamma distribution (Fig. 2-4). Total reduction times were gamma-distributed in accordance with reliability theory, in which the time to failure or risk of failure is described as a probability distribution. Therefore, the theory of reliability engineering which essentially describes the probability enables an accurate or support estimation of the probability that one or more bacterial cells remain alive after the thermal inactivation process, as compared to the deterministic estimation which essentially describes the bacterial counts.

The reason why the total reduction time can vary is that there is variability in bacterial reduction. If there is no variability, the bacterial population should annihilate simultaneously by heating at every iteration. However, in practice there are variations in the total reduction time. It can be the evidence that the bacterial reduction has variability. And, in this study, the heterogeneity in the total reduction time of bacterial population was described with the gamma distribution. It can be said that the gamma distribution capable of expressing the variation of the total reduction time of the bacterial population expresses the variability of bacterial reduction during thermal inactivation. On the other hand, both the deterministic procedure and the probabilistic procedure used in this study do not take into account the variation of fitting parameters (i.e. uncertainty). Therefore, in order to represent uncertainty, it is necessary to use a distribution that is expected to follow parameters by Bayesian statistics.

Recent studies have reported stochastic models describing bacterial inactivation behavior. In particular, it has been proposed that the survival curve is a cumulative distribution of heat resistance (Couvert et al., 2005; Fernandez et al., 1999; Peleg, 2006). Since the survival curve reflects the ratio of surviving bacterial counts at a given heating

time, the inactivation kinetics describe the probability distribution of single cell inactivation times (Peleg, 2006). The heterogeneity of total reduction times of a bacterial population has been described by Monte Carlo simulation (Aspridou and Koutsoumanis, 2015); however, few studies have investigated the actual variability in total reduction time (Koyama et al., 2017; Koseki et al., 2009; McKellar et al., 2002). The inactivation model based on the survival/death interface (Koseki et al., 2009; McKellar et al., 2002) assumed that the heterogeneity of total reduction times follows a binomial distribution. However, the Weibull or gamma distribution is generally used to describe lifespan or durability (Cohen and Whitten, 1988). In the present study, an improved methodological and analytical procedure for estimating the heterogeneity of total reduction time of a bacterial population during thermal inactivation was developed as an alternative to the conventional methodology for estimating the time required for thermal death.

The results of stochastic modelling highlighted the limitations of conventional methods for estimating microbial thermal death kinetics. This was evident by comparing heating times estimated by stochastic and deterministic approaches. The stochastic and deterministic (first-order kinetics) models were similar in that the change in estimated heating time—that is, the change in mean total reduction time over time—with a survival probability of 0.5 was linear. Thus, heating times with a survival probability of 0.5 estimated by the stochastic and deterministic methods were described by linear model. However, the models differed in two respects: the first is that heating time with survival probability of 10^{-6} was much shorter when estimated by the stochastic as compared to the deterministic procedure; and the second is that heating time with survival probability of 10^{-6} estimated by the stochastic procedure was represented by twisted curve. The first point shows that thermal death time estimated by deterministic models is an overestimate in terms of linear kinetics as well as downward kinetics, especially downward concavity (e.g. heating at 60ºC), which is

supposed overestimate (Peleg, 2006). Regarding the second point, there appeared to be insufficient resolution in the heating time with a survival probability of 10^{-6} that was estimated by the stochastic procedure, making the estimate unreliable. The distortion of contours caused by insufficient resolution could be reduced by including more than the 60 replicates used in the present study. Our results suggest that thermal death time derived from a conventional deterministic procedure will be longer than the actual time required. Moreover, it is possible that 60 replicates may be inadequate for accurately estimating heating time with a survival probability of 10^{-6}, for which the risk of bacterial survival can be ignored.

A stochastic procedure with a high resolution is necessary for accurately estimating heating time with an extremely low survival probability such as 10^{-6}. Although more replicates (e.g., $\geq 10^6$) would yield a higher resolution, this may not be realistic. One solution to this problem is to apply a Monte Carlo simulation to estimate total reduction time (Aspridou and Koutsoumanis, 2015), which allowed a description of bacterial population decline until all of the cells were dead. By assuming the kinetics as a cumulative distribution of single cell inactivation times, the simulation can be derived from bacterial inactivation kinetics data. Using a Monte Carlo simulation could overcome the shortcomings of the procedure proposed in this study (the small number of replicates) since numerous replicates can be easily generated in silico, although it may not always completely simulate the actual phenomenon.

The stochastic procedure limited the degradation of food quality during thermal inactivation, as evidenced by the fact that estimated thermal death time was shorter by the stochastic as compared to the kinetic procedure. Thermal processing at a high temperature or heating for a long period induces chemical and physical reactions in foods that reduce product quality (Awuah et al., 2007; Fellows, 2009; Ling et al., 2015) while achieving the

commercial standard for sterility. The demand for processed foods goes beyond the fundamental requirements of safety and shelf life, and more emphasis is being placed on comprehensively labelled, high-quality, value-added foods with convenient end use (Awuah et al., 2007). It is therefore important to establish appropriate inactivation conditions to reduce the risk of spoilage and/or foodborne disease, while assuring a long shelf life and minimizing negative impacts on food quality.

The stochastic modelling procedure describes the heterogeneity of total reduction time using a gamma distribution that is based on reliability engineering as an alternative to the conventional D-value based on thermal death kinetics estimation method. Reliability engineering can enable appropriate risk analysis. According to the stochastic modelling procedure, reducing heating time can minimize the degradation of food quality during thermal inactivation. In conclusion, a mathematical model for total reduction time with a probability distribution is necessary to determine optimal heating conditions based on the concept of reliability theory.

2. 5. References

Aspridou, Z., Koutsoumanis, K.P., 2015. Individual cell heterogeneity as variability source in population dynamics of microbial inactivation. Food Microbiol. 45, 216–221. doi:10.1016/j.fm.2014.04.008

Awuah, G.B., Ramaswamy, H.S., Economides, A., 2007. Thermal processing and quality: Principles and overview. Chemical Engineering and Processing: Process Intensification 46, 584–602. doi:10.1016/j.cep.2006.08.004

Barlow, R.E., 1998. Engineering Reliability. Society for Industrial and Applied Mathematics. doi:10.1137/1.9780898719758.fm

Bigelow, W.D., Esty, J.R., 1920. The thermal death point in relation to time of typical thermophilic organisms. J. Infect. Dis. 27, 602–617. doi:10.2307/30082406

Brul, S., Gerwen, S., Van, Zwietering, M., 2007. Modelling Microorganisms in Food. Woodhead Publishing in Food Science Technology and Nutrition. Woodhead Publishing, Sawston, UK.

Bury, K., 1999. Statistical Distributions in Engineering. Cambridge University Press. doi:10.1017/CBO9781139175081

Cassin, M.H., Paoli, G.M., 1998. Simulation modeling for microbial risk assessment. J. Food Prot. 61, 1560–1566. doi:10.1046/j.1365-2672.2000.01059.x/full

Cohen, A.C., Whitten, B.J., 1988. Parameter Estimation in Reliability and Life Span Models. CRC Press, Boca Raton, FL, USA.

Couvert, O., Gaillard, S.P., Savy, N., Mafart, P., Leguérinel, I., 2005. Survival curves of heated bacterial spores: effect of environmental factors on Weibull parameters. Int. J. Food Microbiol. 101, 73–81. doi:10.1016/j.ijfoodmicro.2004.10.048

Fellows, P.J., 2009. Food Processing Technology: Principles and Practice, 3rd ed. Elsevier, Amsterdam, Netherlands.

Fernández, A., Salmerón, C., Fernández, P.S., Martínez, A., 1999. Application of a frequency distribution model to describe the thermal inactivation of two strains of *Bacillus cereus*. Trends Food Sci. Technol. 10, 158–162. doi:10.1016/S0924-2244(99)00037-0

Hiroshi, N., Ritsuko, O., Hideaki, K., 2007. A Rare Outbreak of Food Poisoning Caused by *Salmonella enterica* serovar. Oranienburg . The Journal of the Japanese Association for Infectious Diseases. 81, 242–248. doi:10.11150/kansenshogakuzasshi1970.81.242

Itoh, T., 2001. The challenges of food safety for microbiological foodborne diseases. Journal of Urban Living and Health Association. 45, 3–13. doi:10.11468/seikatsueisei1957.45.3

Koseki, S., Matsubara, M., Yamamoto, K., 2009. Prediction of a required log reduction with probability for *Enterobacter sakazakii* during high-pressure processing, using a survival/death interface model. Appl. Environ. Microbiol. 75, 1885–1891. doi:10.1128/AEM.02283-08

Koyama, K., Hokunan, H., Hasegawa, M., Kawamura, S., Koseki, S., 2017. Estimation of the probability of bacterial population survival: Development of a probability model to describe the variability in time to inactivation of *Salmonella enterica*. Food Microbiology 68, 121–128. doi:10.1016/j.fm.2017.07.007

Ling, B., Tang, J., Kong, F., Mitcham, E.J., Wang, S., 2015. Kinetics of food quality changes during thermal processing: a Review. Food Bioprocess. Technol. 8, 343–358. doi:10.1007/s11947-014-1398-3

Marks, H.M., Coleman, M.E., Lin, C.T.J., Roberts, T., 1998. Topics in microbial risk assessment: dynamic flow tree process. Risk Anal. 18, 309–328. doi:10.1111/j.1539-6924.1998.tb01298.x

McKellar, R.C., Lu, X., Delaquis, P.J., 2002. A probability model describing the interface between survival and death of *Escherichia coli* O157:H7 in a mayonnaise model system. Food Microbiol. 19, 235–247. doi:10.1006/fmic.2001.0449

Membré, J.M., Amézquita, A., Bassett, J., Giavedoni, P., Blackburn, C. de W., Gorris, L.G.M., 2006. A probabilistic modeling approach in thermal inactivation: estimation of postprocess *Bacillus cereus* spore prevalence and concentration. J. Food Prot. 69, 118–129.

Nauta, M.J., 2000. Separation of uncertainty and variability in quantitative microbial risk assessment models. International Journal of Food Microbiology 57, 9–18. doi:10.1016/S0168-1605(00)00225-7

Nauta, M.J., 2001. A modular process risk model structure for quantitative microbiological risk assessment and its application in an exposure assessment of *Bacillus cereus* in a REPFED. Rijksinstituut voor Volksgezondheid en Milieu RIVM.

Nauta, M.J., 2002. Modelling bacterial growth in quantitative microbiological risk assessment: is it possible? Int. J. Food Microbiol. 73, 297–304. doi:10.1016/S0168-1605(01)00664-X

Peleg, M., 2006. Advanced Quantitative Microbiology for Foods and Biosystems. CRC Press, Boca Raton, FL, USA.

Pflug, I.J., 2003. Microbiology and Engineering of Sterilization Processes. Environmental Sterilization Laboratory.

Scheaffer, R., Mulekar, M., McClave, J., 2010. Probability and Statistics for Engineers. Cengage Learning, Boston, MA, USA.

Thompson, K.M., Graham, J.D., 2008. Going beyond the single number: Using probabilistic risk assessment to improve risk management. Hum. Ecol. Risk. Assess. 2, 1008–1034. doi:10.1080/10807039609383660

Vose, D.J., 1998. The application of quantitative risk assessment to microbial food safety. J. Food Prot. 61, 640–648. http://dx.doi.org/10.4315/0362-028X-61.5.640. doi:10.4315/0362-028X-61.5.640

Chapter 3 Stochastic predictive simulation for Bacillus simplex spore inactivation behaviors by iso-thermal heating

3.1. Introduction

Mathematical models have been used for predicting various bacterial behaviors in foods to ensure microbiological food safety. The first study on bacterial death kinetics during thermal inactivation was reported nearly a century ago (Bigelow and Esty, 1920). However, the generally used log-linear model, which is based on *D*-value (decimal reduction time), leads to overestimation or underestimation of thermal death time (Peleg, 2006). In addition, recent consumer demand for processed foods goes beyond the fundamental requirements of safety and longer shelf life. More emphasis is being placed on informatively labeled, high-quality, value-added foods for their convenience (Awuah et al., 2007). Conversely, thermal processing at a high temperature or heating for a long period induces chemical and physical reactions in foods that reduce product quality (Awuah et al., 2007; Fellows, 2009; Ling et al., 2015). Accordingly, the microbial inactivation process should be minimized. In order to correspond to consumer demands, mathematical models will be indispensable to provide more accurate description of the microbial behavior during inactivation.

Thermal inactivation kinetics of bacterial spores comprises a well-studied branch in predictive microbiology, having been extensively analyzed in order to ensure the safety of foods requiring sterilization for storage at ambient temperature such as canned food, retort foods, and soft drinks. Alternatively, in recent years, food products that are pasteurized and stored at chilled temperatures are increasingly produced to retain quality characteristics such as original color, scent, and taste in accordance with consumer demand. Notably, in these processed food products, microorganisms that can grow even in chilled temperatures represent a critical factor for determining product shelf life. However, there have been few

reports related to psychrophilic bacterial spores control although control of such they play an important role in relatively low temperature processing conditions that enable inactivation only of vegetative cells.

Almost all mathematical models describing change in bacterial counts comprise kinetic models (deterministic models), although various mathematical models (log-linear or non-log-linear models) have been used to describe the death behavior during bacterial inactivation. However, the deterministic predictive model disregards the variability and uncertainty of bacterial phenomena (Membré et al., 2006). In this context, “uncertainty” represents the lack of perfect knowledge of the parameter value, which may be reduced by further measurements. In comparison, “variability” represents the true heterogeneity of the population that is a consequence of the physical system and irreducible by additional measurements (Nauta, 2000). In the context of the guidance of quantitative microbial risk assessment applied at the European and international level for food safety management, the importance of variability of biological and natural phenomena is widely recognized (FAO/WHO, 2008). Deterministic inactivation models providing point estimation are generally recognized as being unable to achieve satisfactory food safety management (Couvert et al., 2010); (Koutsoumanis and Angelidis, 2007) because these models do not take into account heterogeneity in the resistance of individual cells to a lethal stress (Casolari, 1988).

Few clues are available in the literature to tackle the individual cell heterogeneity of heat resistance. According to them, one fact is that the kinetic data models have a characteristic of providing a cumulative form of the distribution of heat resistance of individual cells (Peleg, 2006). In addition, a study has been performed to evaluate and describe the individual cell heterogeneity as a source of variability in population dynamics of microbial inactivation via Monte Carlo simulation (Aspridou and Koutsoumanis, 2015).

These investigators reported the existence of variability in the total reduction times of a bacterial population during inactivation processing such that the coefficient of variation of total reduction time increases as the initial bacterial count decreases. Generally, Monte Carlo simulation sometimes sets the number of iterations to a hundred or a thousand, in some cases a million in order to obtain more detailed answers. Therefore, a million experiment iterations must be done for strict validation of this simulation. However, it is difficult to validate the result derived from the Monte Carlo simulation because the number of iterations for the validation experiment must be huge. Alternatively, if the validity of the simulation was demonstrated in relatively small iteration (60 replicates in this paper), it would be possible to represent the variation of bacterial death behavior from conventional kinetic data-sets and describe the death behavior of bacteria in greater detail.

Accordingly, the goal of this study was to illustrate and describe the variability in bacterial population behavior during thermal processing as a probability distribution based on individual cell heterogeneity with regard to heat resistance. To achieve this goal, we aimed to calculate the survival probability of the spore population (i.e., the probability that at least one bacterial spore survives) and describe the distribution of the number of viable bacterial spores using computer simulation based on the property that the kinetic model represents the cumulative distribution of the death time of individual cells. In this study, the Weibull model is used as one of the most general kinetic models for bacterial reduction. Furthermore, we aimed to compare and verify the computer-derived results of Monte Carlo simulation based on the kinetic model with actual experimental observed values of bacterial spore survival probability and viable numbers. Such a simulation approach may contribute to the improvement of food quality through risk-based processing designs and the enhancement of the accuracy of risk assessment models.

3.2. Material and Methods

3.2.1. Bacterial strain and sporulation conditions

The bacterium *Bacillus simplex*, a psychrophilic spore forming bacteria originating from pasteurized milk (Kobayashi et al., 2016), was acquired from Hokkaido Research Organization (Japan). The stock culture was maintained at −80 °C in 10% peptone water (Merck, Darmstadt, Germany) with glycerol, consisting of peptone from casein (1 g/L), NaCl (0.5 g/L), KH_2PO_4 (0.15 g/L), $Na_2HPO_4•12H_2O$ (0.9 g/L), and glycerol (100 g/L). The strain was activated by incubating once at 30 °C for 24 h on Nutrient Agar (Eiken, Tokyo, Japan) containing peptone (10 g/L), meat extract (5 g/L), and NaCl (5 g/L), and once at 30 °C for 24 h in 200% Nutrient Broth (Merck) with NaCl containing peptone from meat (10 g/L), meat extract (6 g/L), and NaCl (5 g/L). *B. simplex* spores were produced on Spo8-agar (Faille et al., 2007; Helmond et al., 2017) comprised of Nutrient Broth (8 g/L; Merck), $MgSO_4•7H_2O$ (0.51 g/L), KCl (0.97g/L), $CaCl_2•2H_2O$ (0.2 g/L), $MnCl_2•4H_2O$ (3 mg/L), $FeSO_4•7H_2O$ (55 mg/L), and agar (12 g/L). Activated bacterial suspension (5 mL) was centrifuged (3000 × *g*, 10 min) and condensed to 1 mL of suspension. Subsequently, 10 plates of Spo8-agar were inoculated with 100 µL of condensed suspension and incubated at 30 °C in an incubator. The spores were harvested after 6 days of incubation or when 85% of the spores were released from mother cells as observed by phase contrast microscopy. Plates were flooded with 5 mL of sterile distilled water, scraped with a bacteria spreader to loosen the spores from the agar, and spore suspensions obtained from the plates were pooled in a sterile centrifuge tube then washed and condensed by centrifugation (3000 × *g*, 10 min, 4 °C) with cold sterile distilled water. The condensed suspension was heated at 80 °C for 10 min, then immediately cooled at 4 °C with iced water. This resulted in spore crops of 1×10^{10} colony forming units (CFU)/mL of *B. simplex*; the spores were stored at 4 °C until use. The sporular suspension was used prior to heat resistance changes (within 2 months).

3.2.2 Thermal treatment for analyzing survival kinetics

The harvested *B. simplex* spores were heated by heating method based on previous studies (Abe et al., 2018) using a thermal cycler and PCR microplate. The spores were diluted by 0.3 M phosphate buffer (a_w = 0.98); aliquots of diluted spore suspension (10 μL) were dispensed into three representative wells of a 96 well polymerase chain reaction microplate (PCR microplate) to obtain cell concentrations of 10^5 CFU/well in each well; aliquots of 10 μL of distilled water were dispensed into other wells. The microplates were heated at 94 °C on a T100 Thermal Cycler (Bio-Rad, Hercules, CA, USA) after 30 s of preheating at 25 °C to standardize the initial temperature across trials. Fig. 3-1 shows the thermal history of spore suspension at 94ºC 300 seconds. Since the standard deviation of the temperature of 60well is small, we can say that there is no variability in the temperature among different wells (Fig. 3-1). The total duration of the trials depended on each temperature at time intervals required for effective analysis of microbial inactivation kinetics. Serial 10-fold dilutions of samples in 0.3 M phosphate buffer were plated on Nutrient Agar. Population survival was determined by incubating three replicates of each microplate at 30 °C for 2 days as previous study (Kobayashi et al., 2016). Furthermore, we confirm in advance that there is no difference in the number of colonies between those cultured for 2 days and those cultured for a longer time at 30ºC.

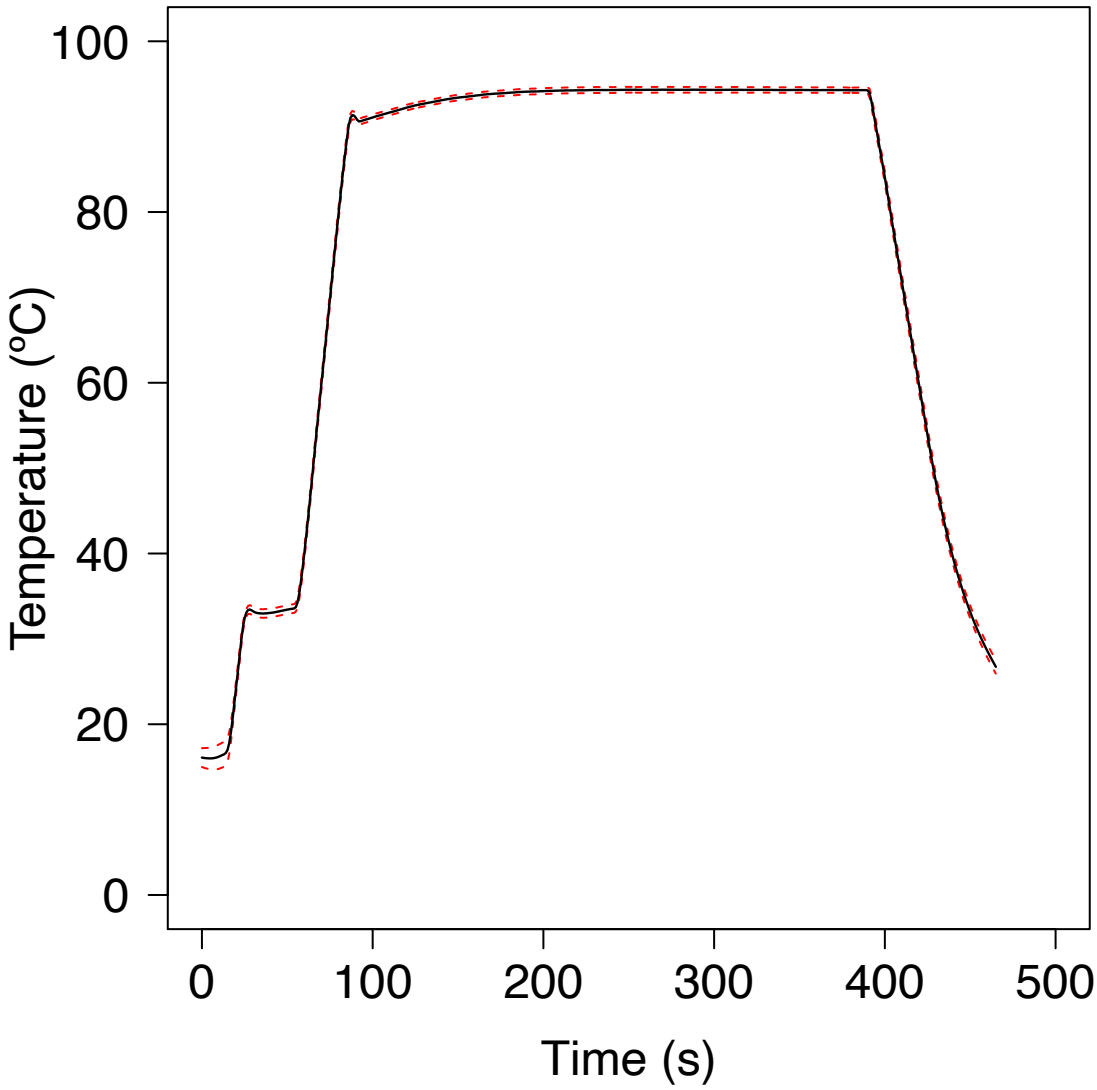


Fig. 3-1. An example of heating protocol: 300 s heating at 94°C by thermal cycler. Preheating of 30 s at 25°C to standardize the initial temperature across trials. After heating process, the 96-PCR microplates were immediately chilled at 4°C. the red dotted lines show the standard deviation of the temperature of all 60 wells used for heating.

3.2.3 Fitting parameters of Weibullian distributions to kinetic data

The parameters of Weibullian distribution were fitted to experimental data. The change of survival spore counts was represented in the form of a survival ratio, $S_{(t)}$, defined as the ratio between the number of survivors after an exposure time t, $N_{(t)}$, and the initial

number, N_0, as $S_{(t)} = N_{(t)}/N_0$. The Weibull model considers that cells and spores in a population have different resistances, with the model just representing the cumulative form of a distribution of lethal agents (Chen, 2007). The frequency (density) form of the Weibull distribution is:

$$\frac{dS}{dt} = b' t^{n-1} \exp\left(-b' t^n\right) \quad (3\text{-}1)$$

and its cumulative

$$S_{(t)} = \exp\left(-b' t^n\right) \quad (3\text{-}2)$$

or

$$\log_e S_{(t)} = -b' t^n \quad (3\text{-}3)$$

where b' and n are parameters of the cumulative Weibull distribution. These parameters are constants from which the mode, mean, variance, and coefficient of skewness of the distribution can be calculated by standard formulas (Peleg, 2006; 1999). In particular, as the 10-base logarithm is commonly used in microbiology; Eq. (3-3) can be written in the form:

$$\log_{10} S_{(t)} = -bt^n \quad (3\text{-}4)$$

where $b' = b(\log_e 10)$ (Chen, 2007; Corradini and Peleg, 2009; Kevin et al., 2005; Mattick et al., 2001; Peleg, 2006; 2000; 1999). Experimental data obtained from kinetic experiments were described by non-linear regression analysis according to Eq. (3-4).

3.2.4 Procedure for computer simulation of survival spore counts

The Weibull distribution was used to predict the inactivation of *B. simplex* spore populations of various initial spore counts N_0 using Monte Carlo simulation basically following previously reported methods (Aspridou and Koutsoumanis, 2015; Koyama et al., 2019). We added a hypothesis of variability in initial cell numbers to the computer simulation

of the previous study and changed the used distribution from a gamma distribution to the Weibull distribution.

At first, the initial spore number of a simulation $N_0^{'}$ was generated as a random number following a Poisson distribution with an average of N_0 (Koyama et al., 2016) as follows:

$$N_0^{'} \sim Poisson(N_0) \quad (3\text{-}5)$$

where $N_0^{'}$ is the initial spore number from the Poisson distribution with parameter N_0.

Secondly, individual sporular inactivation times of $N_0^{'}$ cells were estimated. Whereas a survival curve, $S_{(t)}$, describes the change in the survival ratio, a curve constitutes the cumulative form of a temporal distribution of mortality or destruction by definition (Peleg, 2006). In the present study, the Weibull model: cumulative Weibull distribution was used for the survival curve; i.e., we described the distribution of individual sporular inactivation times using the Weibull distribution. Therefore, the individual sporular inactivation times, IIT_i, could be described with random numbers following the fitted Weibull distribution as follows:

$$IIT_i \sim Weibull(b^{'}, n),\ i = 1, 2, 3, \ldots N_0^{'} \quad (3\text{-}6)$$

where IIT_i is a randomly selected value from the fitted Weibull distribution of individual sporular inactivation times.

Finally, we estimated the survival bacterial counts in the sporular population by simulation. The simulated survival counts at an arbitrary time can be regarded as the number of the IIT_i larger than the arbitrary heating time as follows:

$$SSC = \#A,\ A = \{x \in IIT_i \mid x > t\} \quad (3\text{-}7)$$

where SSC is the simulated survival cell counts at an arbitrary time t and $\#A$ is the number of elements in the individual sporular inactivation times larger than the arbitrary heating time.

This procedure forms one replicate of the inactivation simulation. By repeating the inactivation simulations, the variability in the inactivation behavior of the population could be evaluated; i.e., the survival probability of the sporular population. The R script of one example simulation estimating survival cell counts and the script estimating heterogeneity in the viable spore counts were shown in the Appendix 1 (Since it is a .txt file, copy and paste it to R or R studio and use it.).

3.2.5 Procedure for computer simulation of the survival probability of bacterial spore populations

We estimated the survival probability of sporular populations by repeating the inactivation simulations. The maximum value in the generated individual sporular inactivation times, IIT_i, is the total reduction time of the sporular population, TRT_j, with initial sporular counts of a simulation $N_0^{'}$ as follows:

$$TRT_j = \max(IIT_i), j = 1, 2, 3, \dots, n_{inactivation} \quad (3\text{-}8)$$

where $n_{inactivation}$ is the replication number of the inactivation simulation. From the above, the simulated survival probability of the sporular population at an arbitrary heating time could be described with the number of elements in the total reduction time of the sporular population larger than the arbitrary heating time as follows:

$$P_{(t)_surivival} = \frac{\#\, B}{n_{inactivation}}, B = \{x \in TRT_j \mid x > t\} \quad (3\text{-}9)$$

where $P_{(t)_surivival}$ is the simulated survival probability of the sporular population at an arbitrary heating time t, and $\#\, B$ is the number of elements in the total reduction time of the sporular population larger than the arbitrary heating time. The R script of one example simulation estimating survival probability was shown in Appendix 1 (Since it is a .txt file, copy and paste it to R or R studio and use it.).

3.2.5 Thermal treatment for validation of the sporular inactivation simulation

The variability in total reduction time and the heterogeneity in viable cell counts were measured by heating method based on previous studies (Abe et al., 2018) using a thermal cycler and PCR microplate. Aliquots of spore suspension diluted by 0.3 M phosphate buffer (10 µl) were dispensed into the wells of a 96 well PCR microplate to obtain cell concentrations of 10^n CFU/mL in each well (where n = 1 to 5). The microplates were heated at 94 °C on a T100 Thermal Cycler after 30 s of preheating at 25 °C to standardize the initial temperature across trials. The total duration of the trials depended on the initial counts; in total, we analyzed 18 samples at each initial count. The time intervals of 18 samples at each initial cell count were determined to reflect the rate of changes in the survival probability of *B. simplex* spores. The microplates were cooled to 4 °C immediately after heating. Subsequently, the survival of bacterial spores in each well was assessed by culturing on nutrient agar in 94 well microplates at 30 °C for 2 days. We observed the variability in total reduction time and the heterogeneity in viable counts as the number of bacterial colonies in each well after incubation.

The survival probability of sporular populations was determined from 60 replicates on a microplate according to the following equation (3-10):

$$\bar{P}_{(t)_surivival} = 1 - \frac{W_t}{60} \quad (3\text{-}10)$$

where $\bar{P}_{(t)_surivival}$ is the observed survival probability and W_t is the survival well count among the 60 wells of the plate in which temperatures are homogeneously distributed at heating time t. Furthermore, the viable colony number was counted in the conditions in which there was a well wherein the survival probability was not 1.0.

In the present study, the replicates number of inactivation simulation $n_{inactivation}$ was 60 in order to equal the variability of observed value and that of the simulated value. In

addition, we also conducted two types of simulations with the heterogeneity in viable counts when $n_{inactivation}$ is 10^4 and the variability in total reduction time when $n_{inactivation}$ is 10^6, in order to improve the resolution of the simulated survival probability of bacterial populations. We set $n_{inactivation}$ as 10^6 for the simulated survival probability because the survival of microorganisms can be considered to be negligible when the survival probability is less than 10^{-6} (Bigelow and Esty, 1920). All statistical analyses were conducted with R statistical software (Version 3.5.1 for Mac OS X; http://ww.r-project.org).

3.3. Results

3.3.1 Sporular survival kinetics and fitting parameters of the Weibullian model

The sporular survival kinetics upon heating at 94 °C and the sporular survival curve indicated a downward concavity (Fig. 3-2). Fitted parameters of b and n for the Weibullian model were 1.54×10^{-3} ($p = 0.089$, where p indicates the significance level of fitting) and 1.40 ($p = 4.67 \times 10^{-6}$), respectively. The root mean square error (RMSE) of the fitted model was 0.13.

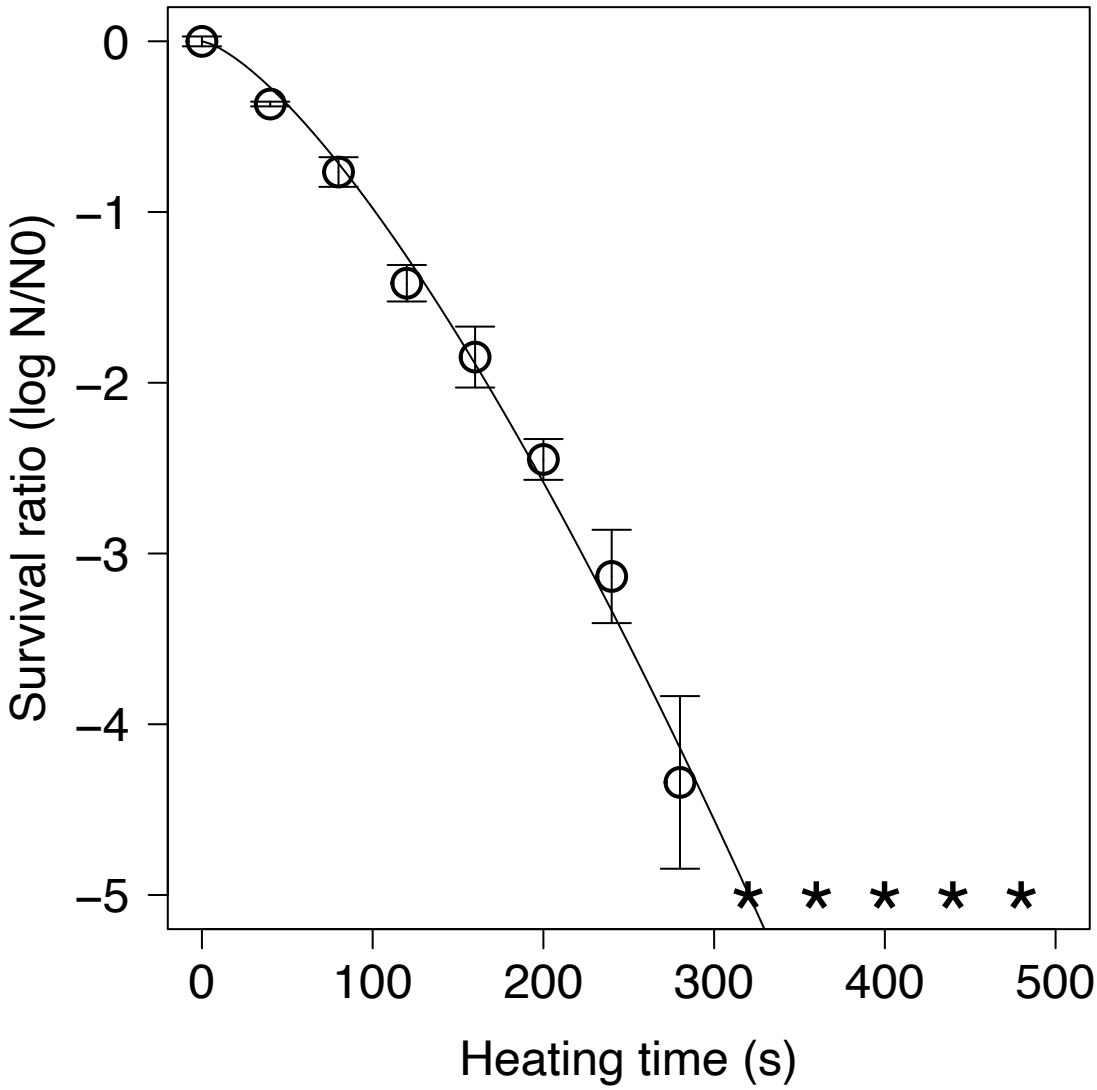


Fig. 3-2. Survival kinetics of *B. simplex* spore population of N_0 of 10^5 CFU heated at 94 °C in 0.3 M phosphate buffer (a_w = 0.98). Error bars indicate standard deviations. Each point with an error bar represents the mean of two or three values. No colonies were detected at the time indicated by an asterisk (*). Lines show the Fitted Weibull model of kinetic changes in surviving spore counts. Fitted parameters of *b* and *n* for the Weibullian model were 1.54×10^{-3} (p = 0.089, where p indicates the significance level of fitting) and 1.40 (p = 4.67×10^{-6}), respectively, with an RMSE of 0.13.

3.3.2 Comparison of viable spore numbers between simulation and observed values

Simulation of sporular inactivation based on the estimated parameters from section 3.3.1 showed the same results in 60 replicates as those of (Aspridou and Koutsoumanis, 2015); i.e., when the number of bacteria was small, the variation in inactivation time until reaching an arbitrary bacterial count become large regardless of initial sporular counts (Fig. 3-3). In addition, our inactivation simulation showed the variability in the initial bacterial counts, resulting from the assumption that the initial sporular counts follow a Poisson distribution. The variability became relatively large in the range below 2 log CFU. Specifically, according to 60 replicates of the simulation model, the variance at the initial bacterial counts 1, 2, 3, 4, 5 log CFU was 3.0×10^{-2}, 2.1×10^{-3}, 2.2×10^{-4}, 2.4×10^{-5}, 1.1×10^{-6} respectively.

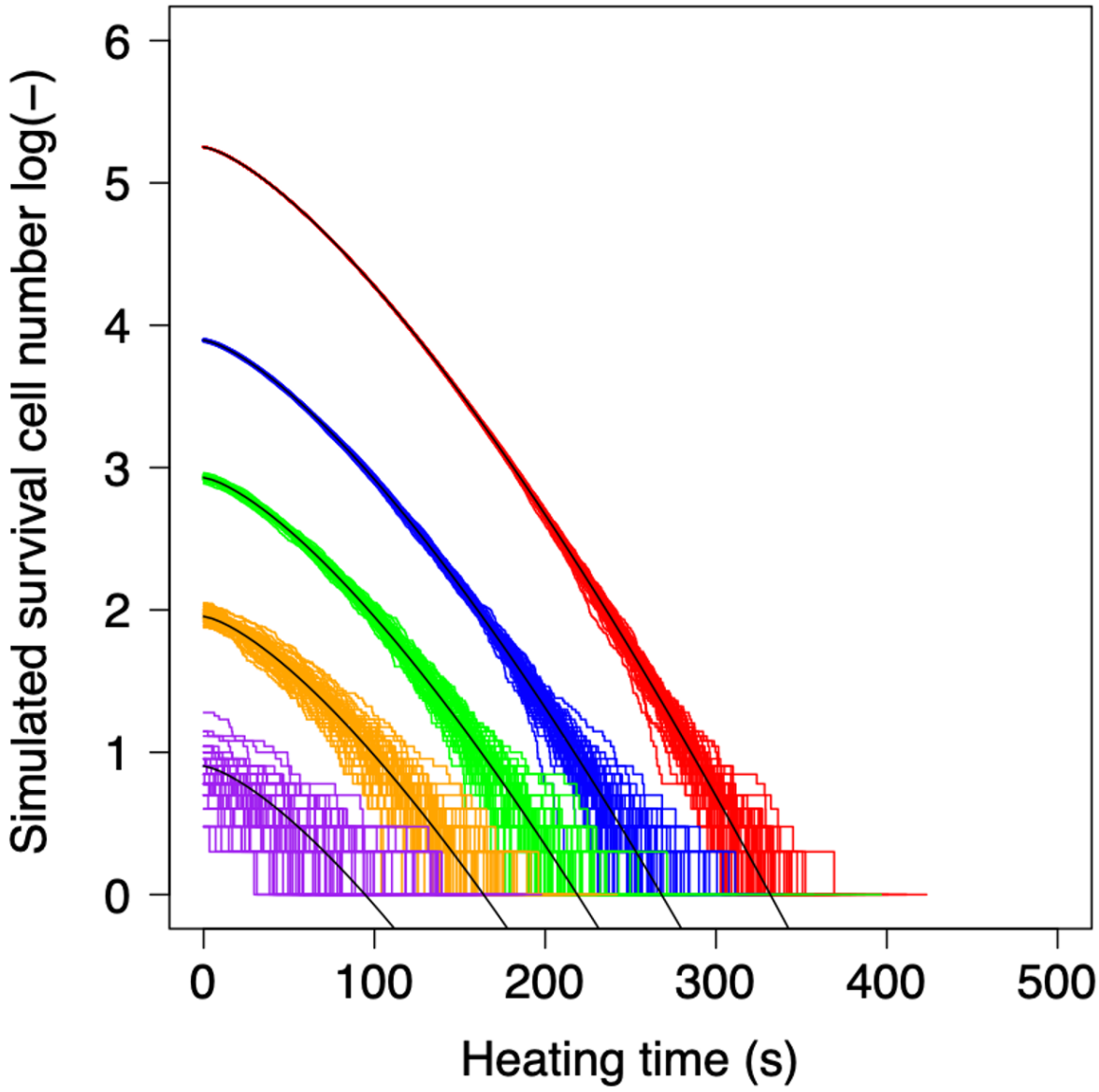


Fig. 3-3. Monte Carlo simulation results (100 simulations) for thermal inactivation of *B. simplex* with initial counts of 1×10^n cells, where n = 1 (purple), 2 (orange), 3 (green), 4 (blue), and 5 (red), based on fitted Weibull distributions (black lines) for individual cell inactivation times.

The points in Fig. 3-4 and 3-6 mean observed values of viable count distribution, and the points in Fig. 3-5 and Fig. 3-7 mean observed values of bacterial spore survival probability. In addition, the points in Fig. 3-4, 3-6, and Fig. 3-5, 3-7 mean simulated value of those lines, respectively. The variabilities in the observed survival cell counts of less than 10 CFU and those of the simulated survival sporular counts derived from simulations of 100

repetitions illustrated strongly similar behavior upon increasing the heating time within each initial sporular count (Fig. 3-4). Furthermore, the observed survival probability of the sporular population and the simulated survival probability derived from 100 replicate simulations also indicated comparable behavior (Fig. 3-5). These results demonstrated that the simulation of inactivation of the sporular population can describe the behavior along with the variability of sporular reduction during thermal inactivation.

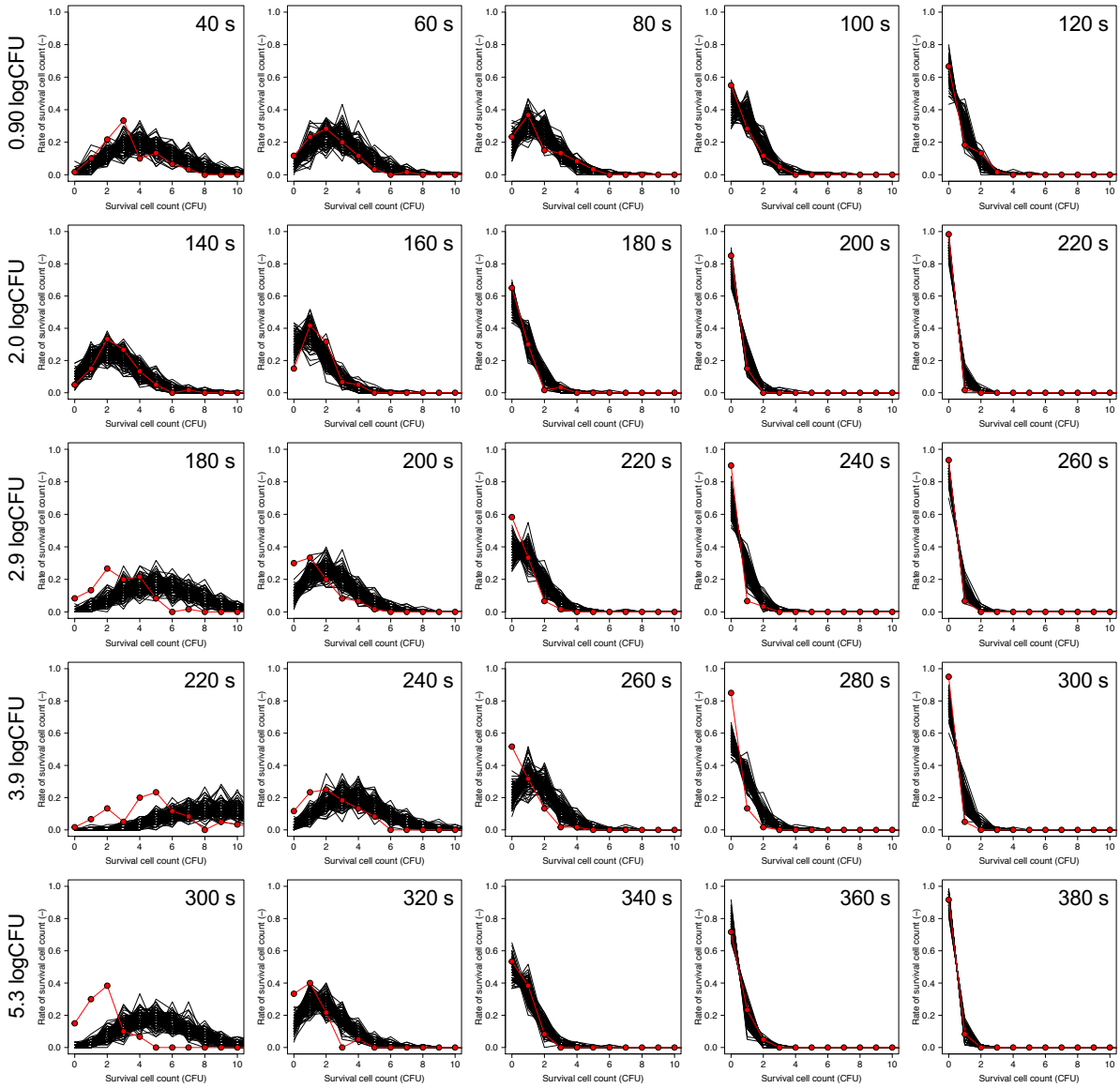


Fig. 3-4. Change in the observed heterogeneity of viable spore count (red points) of 60 bacterial populations each representing nearly 1×10^n cells, where n = 1, 2, 3, 4, and 5, heated at 94 °C in 0.3 M phosphate buffer (a_w = 0.98) for a particular heating time. The lines show the results of 100 Monte Carlo simulations (black lines) in each condition.

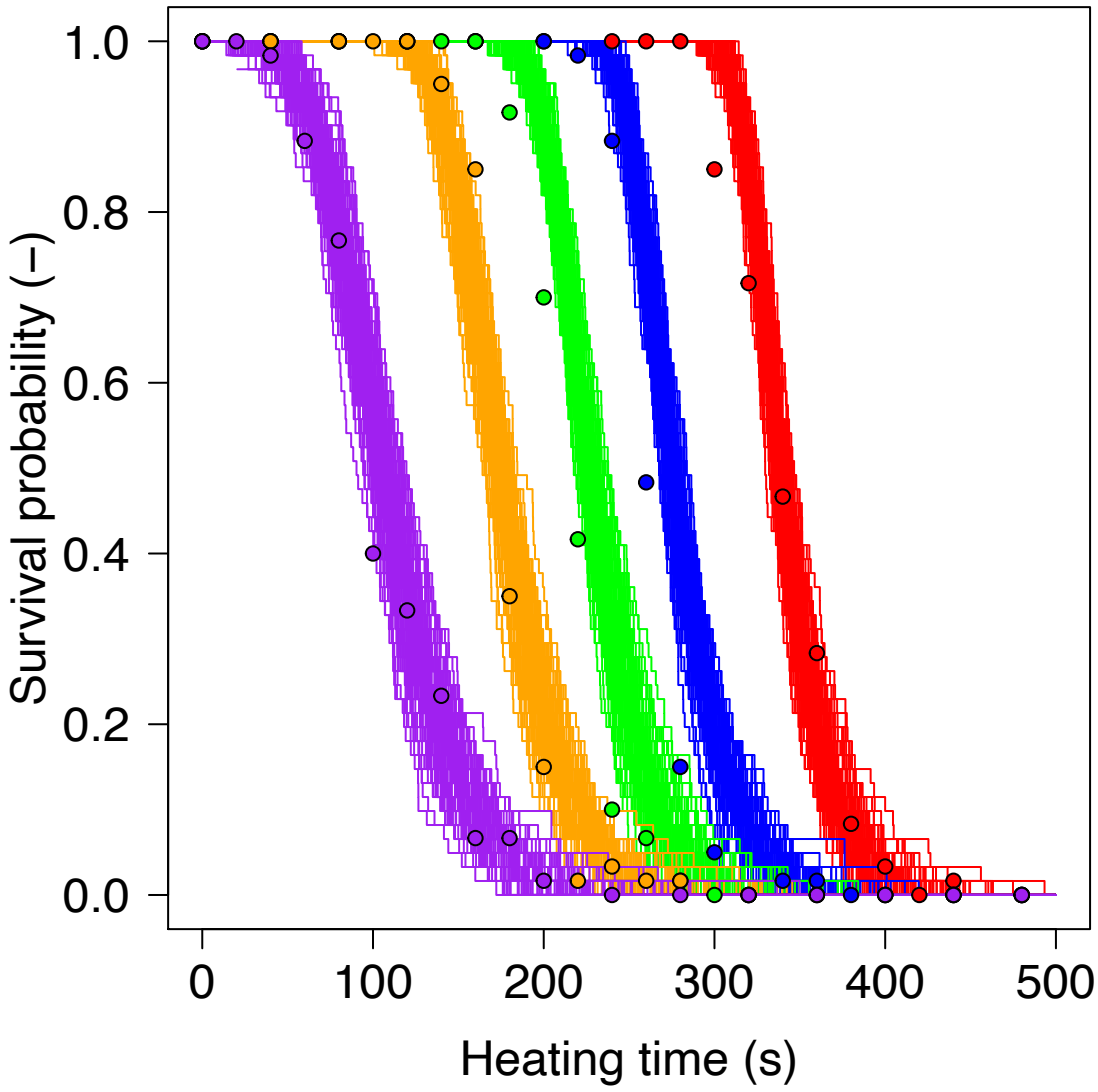


Fig. 3-5. Change in the observed survival probability of 60 bacterial populations (colored circles) each representing nearly 1×10^n cells, where n = 1 (purple), 2 (orange), 3 (green), 4 (blue), and 5 (red), heated at 94 °C in 0.3 M phosphate buffer (a_w = 0.98). The colored lines show Monte Carlo simulation results (100 simulations) of equivalent bacterial populations.

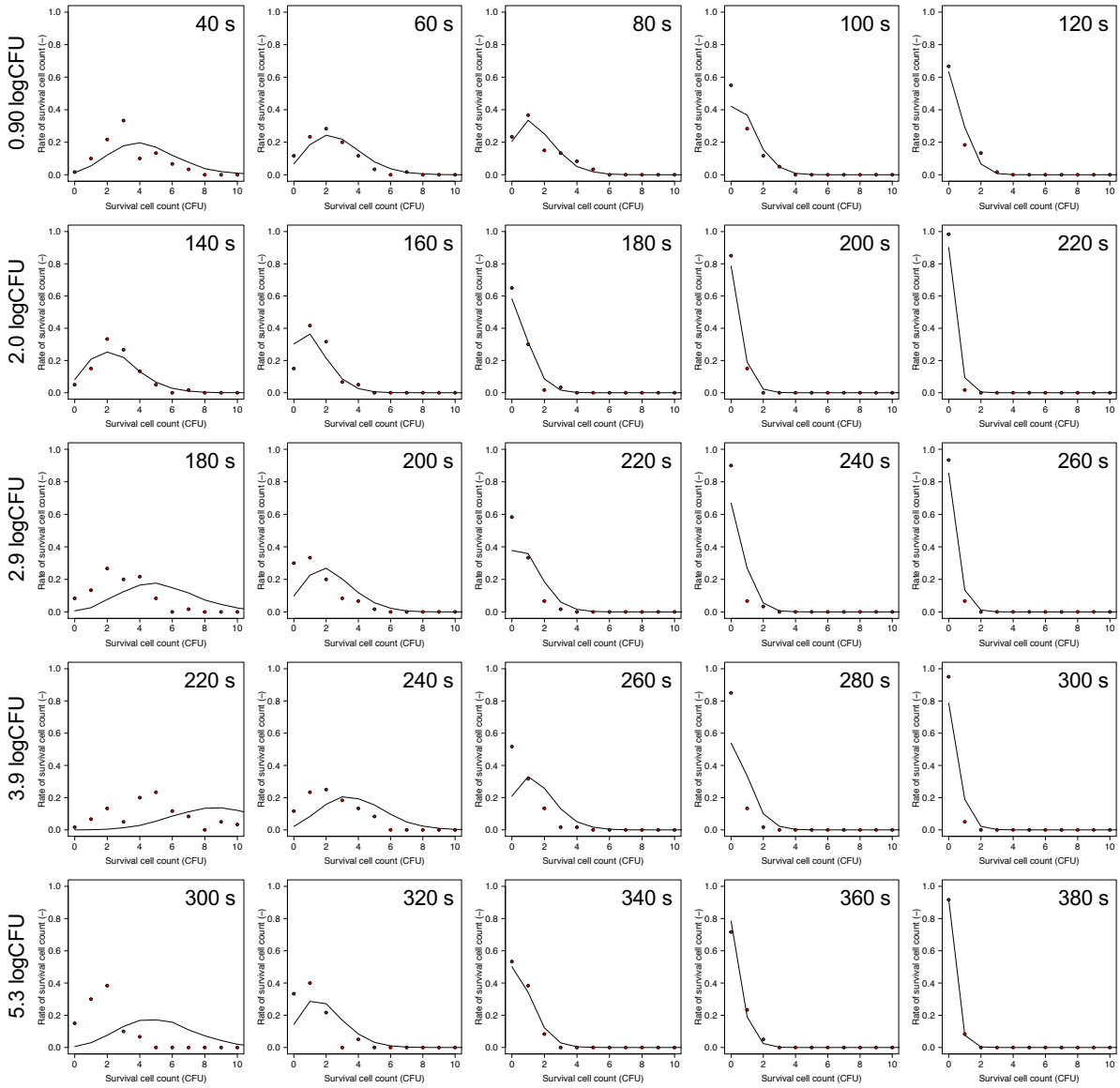


Fig. 3-6. Change in the simulated heterogeneity of viable spore count of 10^6 simulations each representing nearly 1×10^n cells, where n = 1, 2, 3, 4, and 5, heated at 94 °C in 0.3 M phosphate buffer (a_w = 0.98) for a particular heating time. The red points show the observed results of viable spore count of 60 bacterial populations in each condition.

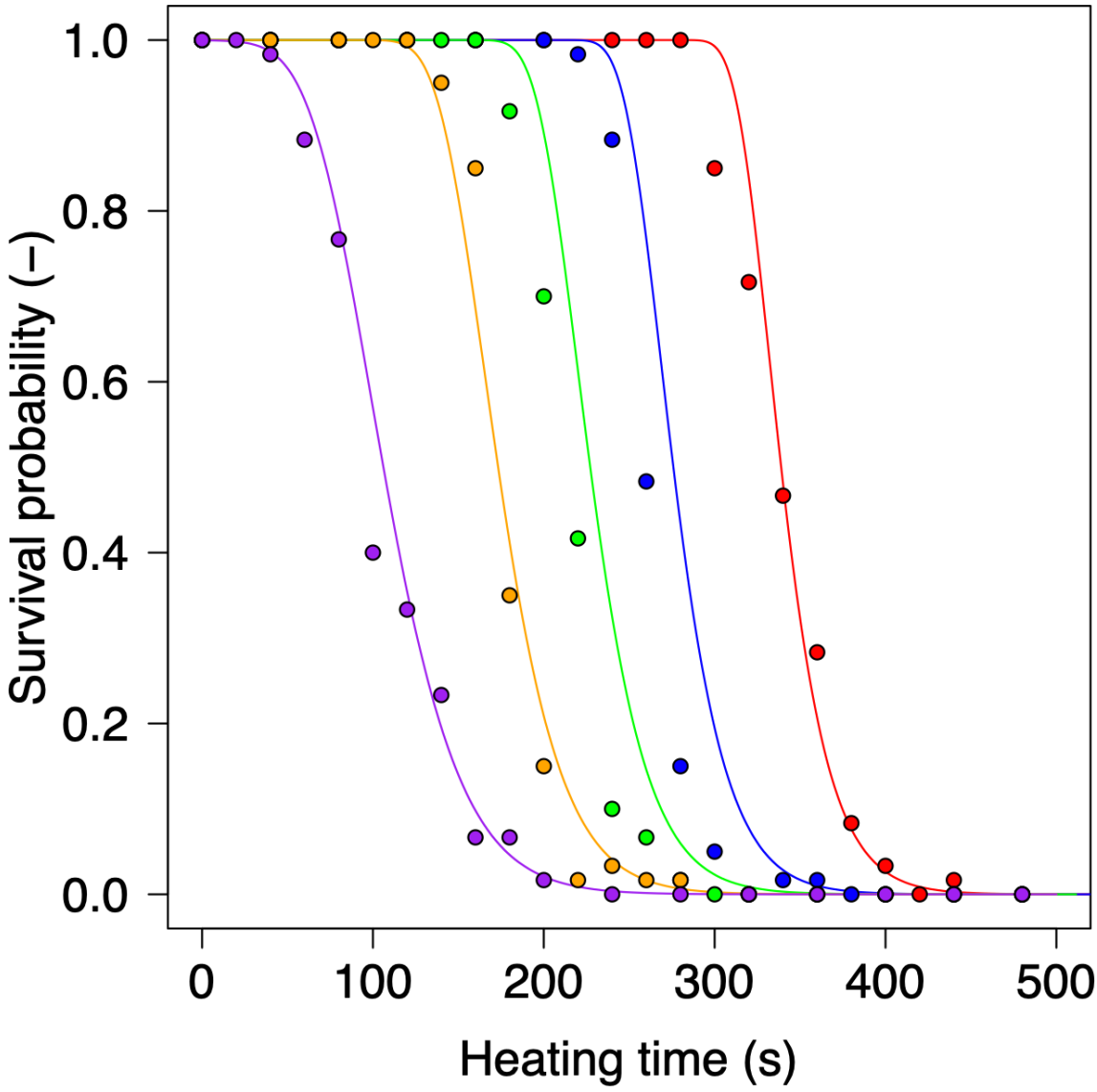


Fig. 3-7. Change in the simulated survival probability of 106 simulations (colored lines) each representing nearly 1 × 10n cells, where n = 1 (purple), 2 (orange), 3 (green), 4 (blue), and 5 (red), heated at 94 °C in 0.3 M phosphate buffer (aw = 0.98). The colored circles show the observed results of 60 bacterial populations of equivalent cell number.

Although the replicates of simulation ($n_{inactivation}$) value was set as 60 in order to equalize the magnitude of the variation in the experimentally observed 60 replicated values in the previous paragraph, the value for replicates of the simulation ($n_{inactivation}$) was set as more than the previous simulations (i.e. Fig. 3-4 and 5) to improve the resolution of the

simulation. The simulated variability in survival spore counts for each condition (initial count: 1–5 log CFU) by 10^4 replicates of simulation is shown in Fig. 3-6 and the accuracy of simulated variability in survival spore counts compared with observed survival probabilities is summarized in Table 3-1. The RMSEs were very small (0.008–0.08) and we confirmed a strong similarity between the observed value and the predicted value by 10^4 replicates of simulation. Furthermore, the estimated survival probability for each initial count (1–5 log CFU) by 10^6 replicates of simulation is shown in Fig. 3-7 and the accuracy of simulated survival probabilities of the spore population compared to observed survival probabilities is shown in Table 3-2. The validity of the prediction by 10^6 replicates of simulation was illustrated as small RMSEs (0.008–0.029). Notably, it is possible to predict survival probability almost continuously without using an approximation as shown in Fig. 3-7 by the simulation of numerous $n_{inactivation}$ values. For example, this method can be used for risk assessment, such as estimating how many defective products will be produced in one year by setting $n_{inactivation}$ to be the number of products produced per year, because $n_{inactivation}$ can be arbitrarily set.

Table 3-1. Accuracy of simulated variabilities in survival spore counts when $n_{inactivation}$ is 10^4 replicates

Initial counts (logCFU)	Heating time (s)	RMSE (-)
0.9	40	0.018
	60	0.008
	80	0.009
	100	0.012
	120	0.010
2.0	140	0.009
	160	0.015
	180	0.008
	200	0.006
	220	0.009
2.9	180	0.026
	200	0.021
	220	0.019
	240	0.024
	260	0.008
3.9	220	0.080
	240	0.081
	260	0.023
	280	0.021
	300	0.020
5.3	300	0.018
	320	0.008
	340	0.009
	360	0.012
	380	0.010

Table 3-2. Accuracy of simulated survival probabilities of spore population when $n_{inactivation}$ is 10^6 replicates

Initial counts (logCFU)	R^2 value (-)	RMSE (-)
0.9	0.99	0.008
2.0	0.99	0.011
2.9	0.96	0.029
3.9	0.95	0.024
5.3	0.99	0.011

Comparing the viable counts between observation and the high-resolution-simulation, we obtained a high accuracy of the Monte Carlo simulation with low RMSE as shown in Table 3-1. However, as shown Fig. 3-6, a difference occurred between the estimated distribution and the observed distribution when the initial bacterial count was large (3 log CFU or more). This represents the same trend as observed in Fig. 3-4. As mentioned above, the present Monte Carlo simulation describes only the variability among two heterogeneities; uncertainty cannot be described by the present Monte Carlo simulation. As shown by the error bar in Fig. 3-2, the measurement data underlying the Weibull model had a large standard deviation when the number of bacteria decreased (−3 log CFU or less). In addition, when the initial number of bacteria increased (≥ 3 log CFU), distribution shifts occurred. As shown in Fig. 3-3, simulation with an initial bacterial count of ≥ 3 log CFU had a strong influence from measured data below −3 log CFU. These findings indicated that the magnitude of the error between the estimated value and the measured value likely comprised the cause of the standard deviation of the measured values of kinetic data. As the number of bacteria decreases, the variability and the uncertainty of measured data increases. It likely causes large uncertainty in kinetic model. For these reasons, we considered this difference in Fig. 3-4 as originating from the uncertainty of the fitted Weibull model.

3.4. Discussion

The validity of the estimation by the present Monte Carlo simulation was demonstrated as shown in Fig. 3-4 to 3-7. The simulation approach was effective to estimate bacterial reduction when bacteria are sterilized or when the number of bacteria is reduced by 100 or less, because small bacterial counts induce greater heterogeneity of inactivation time until an arbitrary number of survivors is reached, as shown Fig. 3.

Although some researchers have developed stochastic models until now, new discoveries of this study compared to all of them are descriptions of simulations of bacterial behavior in the form of probability distributions and verification of the distributions with measured distributions. In the previous studies on simulation (Aspridou and Koutsoumanis, 2015; Corradini et al., 2010; Horowitz et al., 2010; Koyama et al., 2019), they focused on the variability of single cells. However, they did not pay attention to the most important measurement points of this research, such as the heterogeneity in the survival cell counts and the change in the survival probability of bacterial populations. Therefore, it has not been verified in the previous studies how much probability the occurrence of contaminated food products is made by how long heating is done. In addition, Aspridou et al. expressed the death time of individual bacteria as a gamma distribution, which is not general as a model representing the bacterial reduction behavior. The remarkable point of this research is that stochastic results can be derived from a general Weibull model as a model representing bacterial reduction. In the model of Abe et al., the survival probabilities of the bacterial population were estimated by fitting with an approximate probability distribution. The conventional kinetic data cannot be used in the model of Abe et al. The derivation of an appropriate probabilistic result from a general kinetic model is a remarkable point of the present simulation model.

However, this Monte Carlo simulation enabled description of only the variability among the two heterogeneities, because the simulation does not take into account

heterogeneity in parameters (uncertainty). For example, when the initial bacterial count was large (≥3 log CFU), a difference occurred between the estimated value and the observed value under the condition in which the bacteria survive, which likely arose from the uncertainty of the Weibull model as the source of the simulation. In order to carry out a simulation taking uncertainty into consideration, Bayesian statistics or bootstrapping methods should be applied to clarify the distribution that parameters follow; i.e., the parameters of distribution describing single cell inactivation times should be determined by the random number of the distribution that parameters follow. However, the Monte Carlo simulation, which takes only variability but not uncertainty into consideration, successfully described the heterogeneity of bacterial reduction in the present study. This indicates that the degree of uncertainty of the Weibull curve derived in this study is relatively small compared to the variability of bacterial reduction.

It is expected that this simulation will yield similar phenomena with other bacterial reductions and other inactivation methods because *B. simplex* was only used as a model microorganism to clarify the mathematical characteristics of natural randomness (variability); thus, verification using other conditions and organisms is necessary. If validated, the simulation may enable quantitative microbial risk assessment at a single cell level in various bactericidal methods of various bacteria. In particular, this simulation should be valid for risk assessments of specific bacteria that may cause infection or problems upon ingestion of even a small number of cells, such as enterohemorrhagic *Escherichia coli* and *Salmonella* spp., in addition to its efficacy for assessing the deterioration probability of canned or retort food caused by e.g., *Bacillus* spp. or *Clostridium* spp. It may also be used to predict the survival probability of psychrophilic spore-forming bacteria in long-life chilled food. Moreover, although the probability of survival of a bacterial population has been approximately expressed using a gamma distribution in a few prior studies (Abe et al., 2018; Koyama et al.,

2017), in the simulation method from the present study, it was possible to predict survival probability without using approximation.

It has been claimed that the final numbers of survivors after heat treatment exhibit Poisson distributions (Aguirre et al., 2009; Koyama et al., 2016). Using the maximum likelihood estimation method and goodness-of-fit test, we determined whether the heterogeneity of the observed bacterial numbers in the present study also followed the Poisson distribution. As a result, the null hypothesis was not rejected in almost all of the conditions wherein the observed heterogeneity of survivor counts followed Poisson distribution, although the null hypothesis was significantly rejected in some conditions (Table 3-3). Overall, considering the goodness-of-fit test, the final numbers of survivors after heat treatment approximately followed the Poisson distribution.

Table 3-3. Statics of goodness-of-fit test of fitted Poisson distributions to variability in survival spore counts

Initial counts (logCFU)	Heating time (s)	Parameter of Poisson distribution	Chi-squared-statistic	Degree of freedom	Significance probability	Rejection of the null hypothesis
0.9	40	3.2	9.2	6	0.16	
	60	2.1	3.6	5	0.61	
	80	1.6	5.9	4	0.20	
	100	0.7	2.5	2	0.29	
	120	0.5	6.1	2	0.05	*
2.0	140	2.5	8.2	5	0.15	
	160	1.4	7.8	3	0.05	*
	180	0.4	5.3	2	0.07	
	200	0.2	1.4	0	0.00	**
	220	0.0	0.0	0	0.00	**
2.9	180	2.7	8.1	5	0.15	
	200	1.3	2.9	4	0.57	
	220	0.5	0.5	2	0.76	
	240	0.1	4.4	1	0.04	*
	260	0.1	0.3	0	0.00	**
3.9	220	4.7	18.8	9	0.03	*
	240	2.2	4.8	4	0.31	
	260	0.7	1.7	3	0.63	
	280	0.2	0.2	1	0.64	
	300	0.0	0.1	0	0.00	**
5.3	300	1.6	7.8	3	0.05	
	320	1.0	11.4	2	0.00	**
	340	0.5	3.2	1	0.07	
	360	0.3	0.7	1	0.39	
	380	0.1	0.4	0	0.00	**

In the case of adopting conditions in which several bacteria are predicted to survive using a simulation with a priority on food quality, it is necessary to set conditions wherein surviving cells do not proliferate even if they survive. Even if bacteria enter the body, it is critical to establish conditions that will not cause infection or disease onset. In order to realize such outcomes, we argue that the simulation from the present study should be used in

combination with a growth model and a dose-response model. Furthermore, if these latter models are expressed within a stochastic process model, it should be possible to perform comprehensive quantitative microbial risk assessment from production to digestion that predicts whether food poisoning will occur in the consumer throughout the process by which raw materials become food products and are distributed.

Notably, the simulation approach will enable calculation of the survival probability and heterogeneity in the viable cell count from the kinetic parameters estimated from conventional experimental data. In other words, there are possibilities that the results of 60 iterations of experiments can be derived from only three iteration experiments using Monte Carlo simulation. If the developed simulation can be applied to other bacteria as well as *B. simplex*, the numerous existing thermal inactivation data in databases such as ComBase (Baranyi and Tamplin, 2004) will enable simulation of the respective bacterial survival probability and heterogeneity in the viable cell counts although the problem of uncertainty remains. Furthermore, if this simulation procedure can also be applied to thermal in addition to other non-thermal inactivation processes, we should be able to obtain stochastic results from conventional kinetic data in the literature and/or databases. As the developed simulation would realize numerical “visualization” of the microbial risk in foods, modifying the process/inactivation conditions to improve food quality could then be determined by risk-based evaluation.

Although the developed simulation could predict survival probability in the present study, problems still exist for practical use, such as the unevenness of damage to bacteria caused from temperature unevenness. As the bacterial solution used in the present study was very small (as low as 10 μL), temperature unevenness in the bacterial solution was considered to be almost negligible. However, in actual thermal inactivation of food, temperature unevenness owing to heating obviously occurs. Therefore, when simulation

prediction is performed, a temperature-predictable physical model established via heat transfer with a fine mesh will be required. Concurrently, a secondary model of the relationship between temperature and the parameters of the Weibull model will be necessary to predict the bacterial death associated with each mesh.

In conclusion, a Monte Carlo simulation based on kinetic data that explains individual cell heterogeneity could describe the variability of the total reduction time and the change in the survival probability of bacterial populations during thermal inactivation. It was also found that the simulation could describe the heterogeneity in the bacterial survival numbers. The Monte Carlo simulation thus exhibits potential to be applied for quantitative microbial risk assessment, risk management, and risk-based process design of mainly thermal inactivation along with other inactivation methods for various bacteria and foods to enhance food safety.

3.5 References

Abe, H., Koyama, K., Kawamura, S., Koseki, S., 2018. Stochastic evaluation of *Salmonella enterica* lethality during thermal inactivation. International Journal of Food Microbiology 285, 129–135. doi:10.1016/j.ijfoodmicro.2018.08.006

Aguirre, J.S., Pin, C., Rodríguez, M.R., Garcia de Fernando, G.D., 2009. Analysis of the variability in the number of viable bacteria after mild heat treatment of food. Appl. Environ. Microbiol. 75, 6992–6997. doi:10.1128/AEM.00452-09

Aspridou, Z., Koutsoumanis, K.P., 2015. Individual cell heterogeneity as variability source in population dynamics of microbial inactivation. Food Microbiology 45, 216–221. doi:10.1016/j.fm.2014.04.008

Awuah, G.B., Ramaswamy, H.S., Economides, A., 2007. Thermal processing and quality: Principles and overview. Chemical Engineering and Processing: Process Intensification 46, 584–602. doi:10.1016/j.cep.2006.08.004

Baranyi, J., Tamplin, M.L., 2004. ComBase: A Common Database on Microbial Responses to Food Environments†. http://dx.doi.org/10.4315/0362-028X-67.9.1967 67, 1967–1971. doi:10.4315/0362-028X-67.9.1967

Bigelow, W.D., Esty, J.R., 1920. The Thermal Death Point in Relation to Time of Typical Thermophilic Organisms. J Infect Dis 27, 602–617. doi:10.2307/30082406

Casolari, A., 1988. Microbial death. CRC Press.

Chen, H., 2007. Use of linear, Weibull, and log-logistic functions to model pressure inactivation of seven foodborne pathogens in milk. Food Microbiology 24, 197–204. doi:10.1016/j.fm.2006.06.004

Corradini, M.G., NORMAND, M.D., Peleg, M., 2010. Stochastic and Deterministic Model of Microbial Heat Inactivation. Journal of Food Science 75, R59–R70. doi:10.1111/j.1750-3841.2009.01494.x

Corradini, M.G., Peleg, M., 2009. Dynamic model of heat inactivation kinetics for bacterial adaptation. Appl. Environ. Microbiol. 75, 2590–2597. doi:10.1128/AEM.02167-08

Couvert, O., Pinon, A., Bergis, H., Bourdichon, F., Carlin, F., Cornu, M., Denis, C., Besse, N.G., Guillier, L., Jamet, E., Mettler, E., Stahl, V., Thuault, D., Zuliani, V., Augustin, J.C., 2010. Validation of a stochastic modelling approach for Listeria monocytogenes growth in refrigerated foods. International Journal of Food Microbiology 144, 236–242. doi:10.1016/j.ijfoodmicro.2010.09.024

Faille, C., Tauveron, G., Le Gentil-Lelièvre, C., Slomianny, C., 2007. Occurrence of Bacillus cereus Spores with a Damaged Exosporium: Consequences on the Spore Adhesion on Surfaces of Food Processing Lines. Journal of Food Protection 70, 2346–2353. doi:10.4315/0362-028X-70.10.2346

FAO/WHO, 2008. Exposure assessment of microbiological hazards in food. who.int.

Fellows, P.J., 2009. Food Processing Technology: Principles and Practice, 3rd ed. Elsevier.

Helmond, M., Groot, M.N.N., van Bokhorst-van de Veen, H., 2017. Characterization of four Paenibacillus species isolated from pasteurized, chilled ready-to-eat meals. International Journal of Food Microbiology 252, 35–41. doi:10.1016/j.ijfoodmicro.2017.04.008

Horowitz, J., NORMAND, M.D., Corradini, M.G., Peleg, M., 2010. Probabilistic Model of Microbial Cell Growth, Division, and Mortality. Appl. Environ. Microbiol. 76, 230–242. doi:10.1128/AEM.01527-09

Kevin, P.K., Heike, S.P., Helmar, S., 2005. Modelling the thermal inactivation of vegetative microorganisms. Chem. Ing. Tech. 77, 841–852.

Kobayashi, T., Yasokawa, D., Nakagawa, R., Kawakami, M., 2016. Growth Characteristics and Thermal Resistance of Spores of Psychrophilic Bacteria Isolated from Chilled Agricultural Food Products. J. Antibact. Antifung. Agents 44, 509–514.

Koutsoumanis, K., Angelidis, A.S., 2007. Probabilistic modeling approach for evaluating the compliance of ready-to-eat foods with new European Union safety criteria for Listeria monocytogenes. Appl. Environ. Microbiol. 73, 4996–5004. doi:10.1128/AEM.00245-07

Koyama, K., Abe, H., Kawamura, S., Koseki, S., 2019. Stochastic simulation for death probability of bacterial population considering variability in individual cell inactivation time and initial number of cells. International Journal of Food Microbiology 290, 125–131. doi:10.1016/j.ijfoodmicro.2018.10.009

Koyama, K., Hokunan, H., Hasegawa, M., Kawamura, S., Koseki, S., 2017. Estimation of the probability of bacterial population survival: Development of a probability model to describe the variability in time to inactivation of *Salmonella enterica*. Food Microbiology 68, 121–128. doi:10.1016/j.fm.2017.07.007

Koyama, K., Hokunan, H., Hasegawa, M., Kawamura, S., Koseki, S., 2016. Do bacterial cell numbers follow a theoretical Poisson distribution? Comparison of experimentally obtained numbers of single cells with random number generation via computer simulation. Food Microbiology 60, 49–53. doi:10.1016/j.fm.2016.05.019

Ling, B., Tang, J., Kong, F., Mitcham, E.J., Wang, S., 2015. Kinetics of Food Quality Changes During Thermal Processing: a Review. Food Bioprocess Technol 8, 343–358. doi:10.1007/s11947-014-1398-3

Mattick, K.L., Legan, J.D., Humphrey, T.J., Peleg, M., 2001. Calculating *Salmonella* Inactivation in Nonisothermal Heat Treatments from Isothermal Nonlinear Survival Curves. http://dx.doi.org/10.4315/0362-028X-64.5.606 64, 606–613. doi:10.4315/0362-028X-64.5.606

Membré, J.M., Amézquita, A., Bassett, J., Giavedoni, P., de W Blackburn, C., Gorris, L.G.M., 2006. A Probabilistic Modeling Approach in Thermal Inactivation: Estimation of Postprocess Bacillus cereus Spore Prevalence and Concentration. Journal of Food Protection 69, 118–129. doi:10.4315/0362-028X-69.1.118

Nauta, M.J., 2000. Separation of uncertainty and variability in quantitative microbial risk assessment models. International Journal of Food Microbiology 57, 9–18. doi:10.1016/S0168-1605(00)00225-7

Peleg, M., 2006. Advanced Quantitative Microbiology for Foods and Biosystems. CRC Press.

Peleg, M., 2000. Microbial survival curves — the reality of flat “shoulders” and absolute thermal death times. Food Research International 33, 531–538. doi:10.1016/S0963-9969(00)00088-0

Peleg, M., 1999. On calculating sterility in thermal and non-thermal preservation methods. Food Research International 32, 271–278. doi:10.1016/S0963-9969(99)00081-2

Chapter 4 Stochastic and dynamic predictive simulation for inactivation behaviors of *Bacillus simplex* spore by non-isothermal heating

4.1 Introduction

Although thermal inactivation is the most often used procedure for controlling microbial contamination in processed foods, thermal processing at higher temperatures or longer heating times can induce chemical and physical deterioration in foods (Awuah et al., 2007; Fellows, 2009; Ling et al., 2015). The demand for food processing has begun to exceed the fundamental requirements of safety and shelf life, with more emphasis being placed on comprehensively labeled, high-quality, value-added foods that are convenient to consume (Awuah et al., 2007). In line with these goals, the microbial inactivation process in foods should be minimized. While thermal sterilization process is required for shelf-stable foods, milder thermal processing (<100ºC) allowing for higher food quality retention is usually applied to ready-to-eat (RTE) food products intended to be stored under refrigeration. In recent years, many RTE foods, which maintain their quality through relieved long-time thermal inactivation higher than 80 ºC but below 100ºC and storage at refrigeration temperatures, have been introduced. These products are called long-life refrigeration foods. However, some bacterial species are known to grow even at refrigeration temperatures; in particular, spore-forming food spoilage bacteria such as Bacillus simplex can germinate and grow at refrigeration temperatures (below 10ºC) and also have greater heat resistance than vegetative bacterial cells (Kobayashi et al., 2016). Moreover, parts of Bacillus spp. including B. simplex can produce heat-stable toxins similar to cereulide (Taylor et al., 2005). The control of spore-forming bacteria can therefore help ensure food safety and quality of minimally processed RTE foods preserved at refrigeration temperatures.

Appropriate predictions and assessments based on mathematical models is necessary for food safety assurance. Many mathematical models have been used to predict bacterial behavior in foods and ensure food safety through quantitative microbial risk assessment (QMRA). However, one of the most popular models, the log-linear approach based on the D-value (decimal reduction time), can lead to over- or underestimation of the thermal death time (Peleg, 2006). To determine safe minimum processing levels, more accurate mathematical models for describing bacterial behavior during inactivation are needed.

The importance of uncertainty and variability in the evaluation of microbial behavior for QMRA purposes has been increasingly recognized (Besten et al., 2018; FAO/WHO, 2008; Hoornstra and Notermans, 2001; Koutsoumanis and Aspridou, 2017; Membré et al., 2006; Nauta, 2000; Pouillot and Delignette-Muller, 2010) In this context, "uncertainty" represents the lack of perfect knowledge of a parameter value, which might be reduced by further measurements, whereas "variability" represents the true randomness or heterogeneity of the population or environments, which are a consequence of the physical system and irreducible through additional measurements (Nauta, 2000). Because conventional kinetic models do not take into account uncertainty or variability between individual bacterial cells (Besten et al., 2018; Koutsoumanis and Aspridou, 2017), the estimation of bacterial behavior using kinetic modeling is considered insufficient in certain food safety management approaches (Couvert et al., 2010; Koutsoumanis and Angelidis, 2007). To describe variability and uncertainty in predictive modeling, stochastic models with Monte Carlo (MC) simulation using repeated random number simulations have been developed. As variability differs critically from uncertainty, the stochastic model can be roughly divided into sub-models for: 1) expressing variability, 2) expressing uncertainty, and 3) representing both.

Many studies have tried to express the variability of individual-cell inactivation behavior using stochastic process models (Abe et al., 2019; Aspridou and Koutsoumanis,

2015; Koyama et al., 2019b; 2019a). Stochastic processes describe true randomness (true randomness comes even if completely same parameter value) with generating random number following a probability distribution. However, most such models, which describe bacterial reduction behavior at a constant temperature, cannot be adapted to the long come-up times frequently seen in the heating of actual food processings. In this study, it is tried to describe the variability in dead bacterial counts at a momentary dynamic condition during a short time lapse based on an individual bacteria's death or survival model.

Parameter uncertainty has been investigated using bootstrap models to describe variations in bacterial behavior (Quinto et al., 2018; Schaffner, 1994). The bootstrap method (Efron and Tibshirani, 1991) is a resampling technique used to estimate statistics via computer simulation. Bootstrapping describes statistic parameters or values as distribution, and it could enable representing the variation in them caused from the lack of information by random resampling following observed values. In other words, bootstraps have been used to describe parameter uncertainty comes from variation of observed values, in terms of the lack of perfect knowledge of the parameter's value (Nauta, 2000), as probability distributions.

Uncertainty and variability in bacterial behavior can be expressed using second-order Monte Carlo (2DMC) analysis and some researchers have advocated the application of 2DMC to describe both factors (Abe et al., 2019; Cassin and Paoli, 1998; Nauta et al., 2009; Pouillot and Delignette-Muller, 2010; Wu and Tsang, 2004). The separation and combined description of uncertainty and variability play an important role in the valid prediction of bacterial behavior.

The objectives of this study were development and validation of a dynamic 2DMC model constructed by combining calculations of (i) uncertainty in model parameters, (ii) dynamic kinetics, and (iii) variability in individual cell inactivation times. The resulting dynamic model, which includes both uncertainty and variability, can contribute to the

improvement of risk-based process design and the development of accurate risk assessment models.

4.2 Materials and Methods

4.2.1. Sample and experimental description

4.2.1.1. Bacterial strain and sporulation conditions

The bacterial strain used as a model bacterium in this study was a *Bacillus simplex* isolate (isolation number: 2501), a spore-forming bacterial isolate associated with spoilage of refrigerated RTE food and provided by the Japan Canners Association (Tokyo, Japan). A sporulation procedure based on previous study (Kuroda et al., 2019) was applied. The frozen pure bacterial cultures were transferred to tryptic soy agar (TSA; Merck, Darmstadt, Germany) plate and incubated at 37 °C for 5 days, after which an isolated colony of each bacterium was transferred to 5 mL of tryptic soy broth (TSB; Merck, Darmstadt, Germany) in a sterile plastic tube, which was then incubated at 37 °C for 24 h. The cultures were transferred into soil extract agar (2 g/L beef extract, 3 g/L yeast extract, 10 g/L peptone, 5 g/L NaCl, 20 g/L agar, 1 g/L starch, 1 mL/L $MnSO_4$ solution, 250 mL/L soil solution, 750 mL/L pure water) and the inoculated plates were again incubated at 37 °C for 10 days. Following incubation, the bacterial colonies were scratched and collected using a platinum loop and suspended in 2 mL of 1/15 M phosphate buffer. Following confirmation of spore formation using phase contrast microscopy observations, the spores were collected by centrifugation (1,000 × *g* for 10 min at 20 °C). The supernatant was discarded, and the spores were subsequently resuspended in 1/15 M phosphate buffer. This procedure was repeated three times and then the spore solutions were heated to 80 °C for 10 min to remove remaining vegetative cells. The prepared spore suspensions were stored at -80°C and thawed gently (20 min in ice water) as needed.

4.2.1.2. Inactivation trials for model fitting dataset

Bacterial reduction behaviors were experimentally observed using thermally processed *B*. *simplex*. Following the methodology applied in previous studies (Abe et al., 2018; 2019), the harvested *B*. *simplex* spores were heated using a thermal cycler and polymerase chain reaction (PCR) microplates. The *B. simplex* spores were washed by centrifugation and diluted with pH-adjusted TSB (pH:5.4, 5.8, 6.2, 6.6, and 7.0) and aliquots of diluted spore suspension (100 μl) were then dispensed into three representative wells of a 96-well PCR microplate to obtain cell concentrations of 10^6 CFU/well. The temperature profile of the wells was checked beforehand to ensure that there were no temperature differences. Following 30 s of preheating at 25°C to standardize the initial temperature across the trials, the microplates were heated at various temperatures (80, 85, and 90°C) on a MiniAmp Plus Thermal Cycler (Thermo Fisher Scientific, Waltham, Massachusetts, USA). Immediately after heating, the PCR microplates were cooled to 4°C. Fig. 4-1(A) shows examples of the thermal profiles in each one of these processes. The total duration of the trials depended on the temperature at various time intervals. Serial 10-fold dilutions of samples in TSB were plated onto TSA, and population survival was determined after a 24-h warming up of three replicate microplates to 37°C, a culturing condition that was previously confirmed as capable of assuring recovery.

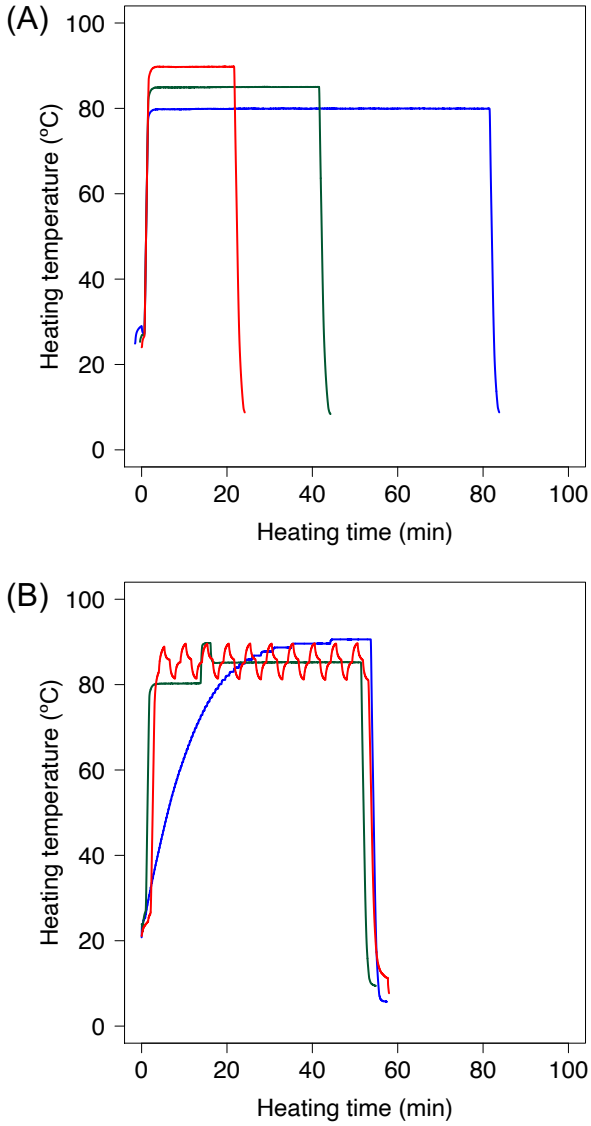


Fig. 4-1. Example of heating protocol using thermal cycler. (A): Temperature profiles of inactivation trials for model fitting dataset. 80 min heating at 80°C (red), 35 min heating at 85°C (green), and 18 min heating at 90°C (blue). Preheating is conducted for 30 s at 25°C to standardize the initial temperature across trials. (B): Temperature profiles of inactivation trials for model validation dataset. Slow come-up (blue), bumpy (green) and waving (red) temperature profiles. Following the heating process, the 96-PCR microplates are immediately chilled at 4°C.

4.2.1.3. Inactivation trials for model validation dataset

As a validation data set, *B. simplex* suspensions of 100 μL, which initial counts were 10^n CFU (n = 2, 3 and 4), were heated with the thermal cycler. Inactivation conditions were performed in three dynamic temperature profiles (slow-come-up, bumpy, and waving temperature profiles; Figure 1b), three pH conditions, and 10 repetitions per each heating time. To compare the simulated and the observed value, maximum RMSE (root mean square error) and minimum RMSE were derived from them.

4.2.2. Estimation of Weibull parameter uncertainty & thermotolerance heterogeneity with Bootstrap methods

4.2.2.1. Resampling viable bacterial ratio data

To obtain parameter distributions of Weibull model, we described the parameter uncertainties and thermotolerance heterogeneity of individual cells using a nonparametric bootstrap. Fig. 4-2 shows a schematic of the overall bootstrapping process applied in this study. To carry out bootstrapping, new samples are recollected from observed data (nonparametric bootstrapping) or from a fitted distribution (parametric bootstrapping). Nonparametric bootstrapping is useful when the distribution of a population is unknown, poorly understood, or when the investigator does not want to use a predefined population distribution; parametric bootstrapping is useful in problems in which some knowledge of the form of the underlying bacteria population is available and for comparison with nonparametric analysis (Quinto et al., 2018). In this study, we applied nonparametric methods to account for the uncertainties in observed values.

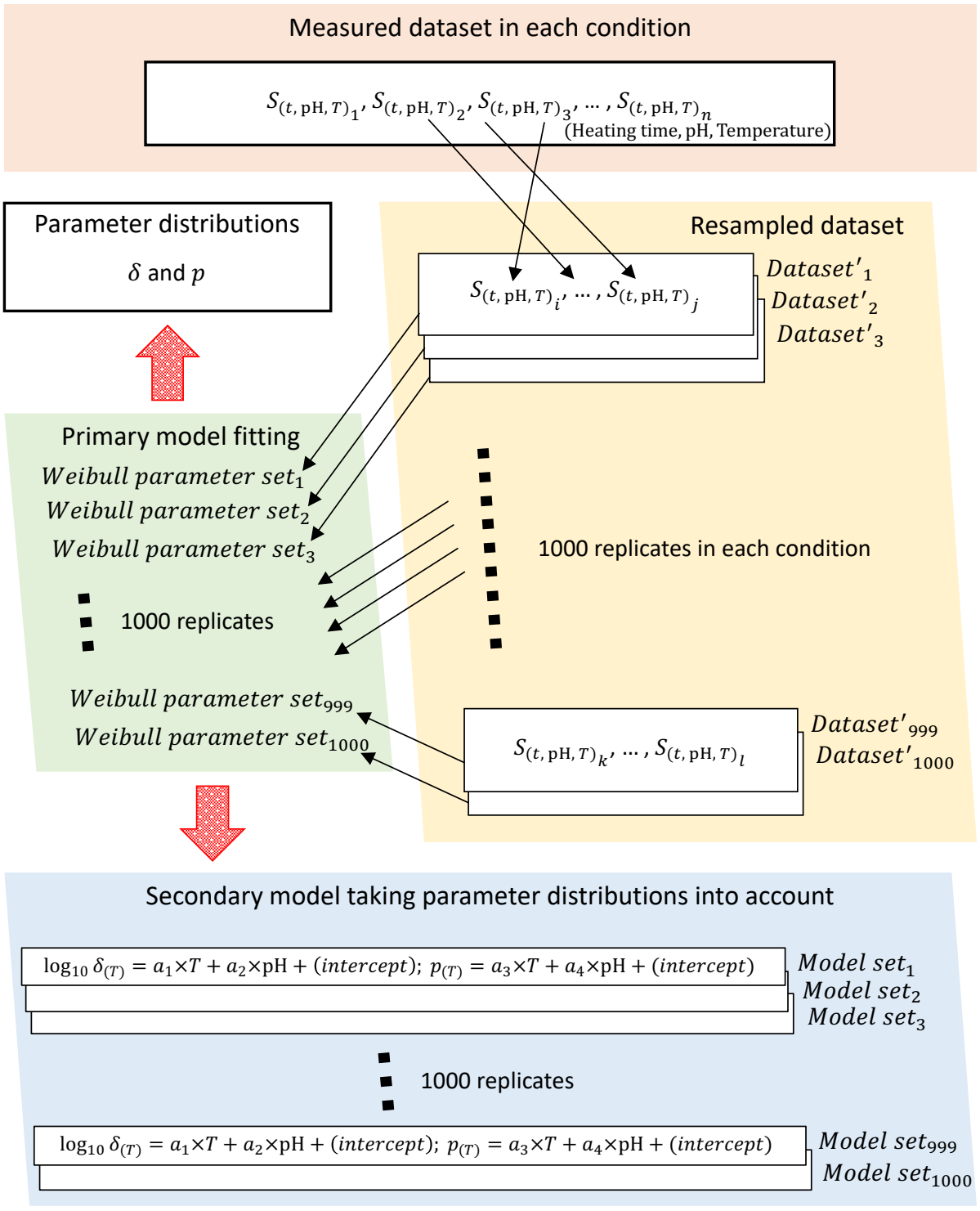


Fig. 4-2. Schematic of the bootstrapping procedure. The bootstrapping was conducted using 1,000 replicates of both the Weibullian parameter distributions and the secondary models for each parameter, with the uncertainty of each parameter considered based on 1,000 replicates of the resampled surviving cell ratio.

Sample sets of 1,000 iterations were resampled with replacement for Weibull fitting to calculate the random variables as Weibull model parameters. The change in surviving bacterial counts was represented in the form of a survival ratio, $S_{(t)}$, defined as the ratio between the number of survivors after exposure time t, $N_{(t)}$, and the initial population, N_0, i.e., $S_{(t)} = N_{(t)}/N_0$. Each condition (heating time, pH, heating temperature) was represented using three repetitions of observed data; in other words, the survival ratio data for three replicates were resampled three times, including duplication, per heating condition. Each set of three samples was randomly selected as resampled data from the set of data observed at all thermal conditions. Each resampled set was used as a replicate bootstrapped dataset, of which a total of 1,000 were generated.

4.2.2.2. Fitting resampled data of survival ratio to Weibull model and secondary models

To perform Weibull fitting of the 1,000 bootstrapped data sets described in the previous section, the parameters of a Weibull model at each temperature were fitted to the respective values at each temperature of the resampled survival ratios derived from the inactivation experiment. The Weibull models were constructed under the assumption that vegetative cells and spores within a population have different resistances:

$$\log_{10} S_{(t)} = -\left(\frac{t}{\delta}\right)^p \quad (4\text{-}1)$$

where δ and p are constant parameters of the Weibull model from which the mode, mean, variance, and coefficient of skewness of the distribution can be calculated (Mattick et al., 2001). The Weibull model is one of the general mathematical models to describe various behaviors of inactivation or reduction (Davey, 1993; Gomez et al., 2005; Koseki et al., 2015; Mafart et al., 2002; Peleg and Normand, 2004; Van Boekel, 2002).

The δ is called the time of the first decimal reduction (time necessary to inactivate a decimal reduction of the microbial population when p parameter is 1.0) and is the so-called scale parameter; n and p parameter is the so-called shape parameter (Gomez et al., 2005). Its

value depends on the shape of the survival curve; $p < 1$ for concave upwards survival curves, $p = 1$ for linear survival curves and $p > 1$ for concave downwards survival curves (Gomez et al., 2005). In this study, δ and p were used to describe the experimental data obtained from the kinetic experiments using non-linear regression analysis (least mean square error) in which 1,000 iterations of the resampled Weibullian parameters were estimated at each pH and temperature.

The parameters of the secondary models were then calculated based on the Weibullian parameters obtained for the primary model, with 1,000 replicates of the secondary model estimated to describe the relationship between pH, temperature, and the primary parameters derived in the preceding section. Based on the results of previous studies, the temperature dependency of the Weibull model parameters δ and p was described using the fitted exponential-type functions $\delta_{(T)}$ and $p_{(T)}$, respectively, where $\delta_{(T)}$ is given as:

$$\log_{10} \delta_{(T)} = a_1 \times T + a_2 \times \mathrm{pH} + (intercept) \quad . (4\text{-}2)$$

This interaction-term-free polynomial equation was initially proposed (Davey, 1993) to describe the combined effect of temperature and pH on the *D*-values of *Clostridium botulinum* spores (Gomez et al., 2005). It has been reported that $p_{(T)}$ varies linearly or is constant at both increasing and decreasing temperatures (Van Boekel, 2002); in a constant case, it can be represented by a linear equation (when the coefficient of temperature and pH is 0). The following linearly expression for $p_{(T)}$ was used in this study:

$$p_{(T)} = a_3 \times T + a_4 \times \mathrm{pH} + (intercept) \quad . (4\text{-}3)$$

The coefficients of the parameters of each of the models were calculated using a multivariate linear least square error regression.

The convergences of parameter distributions were indicated by the Gelman-Rubin convergence statistic ($\hat{R}$-value). The $\hat{R}$-value is generally used for confirming the convergences of parameter distributions in Markov chain Monte Carlo (MCMC) on Bayesian

statistic (Vehtari et al., 2019); it is said that $\hat{R}$-value lower than 1.1 indicates the convergence of the parameter distribution.

4.2.3. Numerical estimation for true randomness variability in bacterial behavior during non-isothermal conditions with stochastic model

4.2.3.1. Numerical calculation of bacterial non-isothermal inactivation for stochastic simulation

To serve as the basis of our dynamic probability model, we created a dynamic kinetic model based on previously developed methodologies (Campanella and Peleg, 2001; Corradini and Peleg, 2009; Peleg et al., 2005). Under fluctuating temperature conditions, a very short time interval was taken into consideration, $[t_i, t_{i+1}]$. The parameters of Weibullian model for inactivation rate during the interval can be assumed as average of the parameters of t_i and t_{i+1} (Peleg, 2006), following:

$$\bar{\delta} = \frac{\delta_{t_i} + \delta_{t_{i+1}}}{2}, \qquad \bar{p} = \frac{p_{t_i} + p_{t_{i+1}}}{2} \quad . (4\text{-}4)$$

The actual heating time is described by transforming Eq. 4-1(Campanella and Peleg, 2001) as follows:

$$t^* = \left[\frac{-\log_{10} S_{t_i}}{\bar{\delta}}\right]^{\frac{1}{\bar{p}}} \quad . (4\text{-}5)$$

Since the parameters are constant values in the intervals, the reduction behavior can be assumed as the isothermal in the interval. Therefore, the survival ratio at t_{i+1}, $S_{t_{i+1}}$,can be described as following Eq. 4-6:

$$\log_{10} S_{t_{i+1}} = -\left(\frac{t^* + \Delta t}{\bar{\delta}}\right)^{\bar{p}} = -\left(\frac{\left[\frac{-\log_{10} S_{t_i}}{\bar{\delta}}\right]^{\frac{1}{\bar{p}}} + \Delta t}{\bar{\delta}}\right)^{\bar{p}} \quad . (4\text{-}6)$$

$$\Delta t = t_{i+1} - t_i$$

Furthermore, the survival counts can be described by transformation of Eq. 4-6 following:

$$N_{t_{i+1}} = N_0 \times 10^{-\left(\frac{t^*+\Delta t}{\bar{\delta}}\right)^{\bar{p}}} \quad . (4\text{-}7)$$

Defining the dead bacterial count over the time interval Δt as

$$N_{dead\ cell_{[t_i,t_{i+1}]}} = N_{(t_i)} - N_{(t_{i+1})} \quad , (4\text{-}8)$$

We assumed these kinetic estimations as average behaviour of stochastic behavior.

4.2.3.2. Stochastic description of variability in viable bacterial counts

In this study, two types of variability were considered, namely the initial cell counts variability and the variability in cell inactivation during short time intervals, and were described by two types of probability distributions. According to previous studies (Abe et al., 2019; Koyama et al., 2016; 2019b), the initial cell counts variability can be described as a Poisson distribution. Therefore, the initial spore number was generated as a random number following a Poisson distribution with an average of $N_{(0)}$, i.e.,

$$N_{(0)} \sim Poisson(\overline{N_0}) \quad , (4\text{-}9)$$

, where $N_{(0)}$ is the simulated initial cell count from a Poisson distribution in which the expected value is $\overline{N_0}$.

Next, we consider the variability in bacterial death counts under heating process during the infinitesimal interval (Fig. 4-3). A model of possible explanation of bacteria death or continued survival (Corradini et al., 2010b) was used. Focusing on individual cells, a cell has a probability of P_m to be inactivated and $1 - P_m$ to remain viable after a short time interval Δt. Assuming that individual bacterial cells (or spores) get inactivated during this short time interval, the probability $p_{(k)}$, i.e. the probability that k cells/spores are inactivated out of $N_{(t)}$ surviving cells/spore, can be expressed as a binomial distribution. The general binomial distribution form is $p_{(k)} = \binom{n}{k} p^k (1-p)^{n-k}$ (Rychlik and Ryden, 2006) and the expected value of the general distribution is calculated as np. Here, the average value of the dead bacterial counts during an interval from t to $t + \Delta t$, $\overline{N_{dead\ cell}}_{[t,t+\Delta t]}$, was assumed as

the kinetic estimation. The binomial distributions are generally used as a probabilistic distribution describing the pure death process in the branch of modelling biological populations (Renshaw, 1993). $\overline{N_{dead\ cell}}_{[t,t+\Delta t]}$ follows a binomial distribution of size $N_{(t)}$ with a probability parameter $\frac{\overline{N_{dead\ cell}}_{[t,t+\Delta t]}}{N_{(t)}}$. Thus, the simulated survival cell counts $N_{(t_{i+1})}$ at exposure time t can be described in terms of $N_{(t)}$ as

$$N_{(t+\Delta t)} \sim N_{(t)} - Binomial(N_{(t)}, \frac{\overline{N_{dead\ cell}}_{[t,t+\Delta t]}}{N_{(t)}}) \quad , (4\text{-}10)$$

where $Binomial(N_{(t)}, \frac{\overline{N_{dead\ cell}}_{[t,t+\Delta t]}}{N_{(t)}})$ is a random number derived from a binomial distribution of size $N_{(t)}$ in which the probability parameter is $\frac{\overline{N_{dead\ cell}}_{[t,t+\Delta t]}}{N_{(t)}}$.

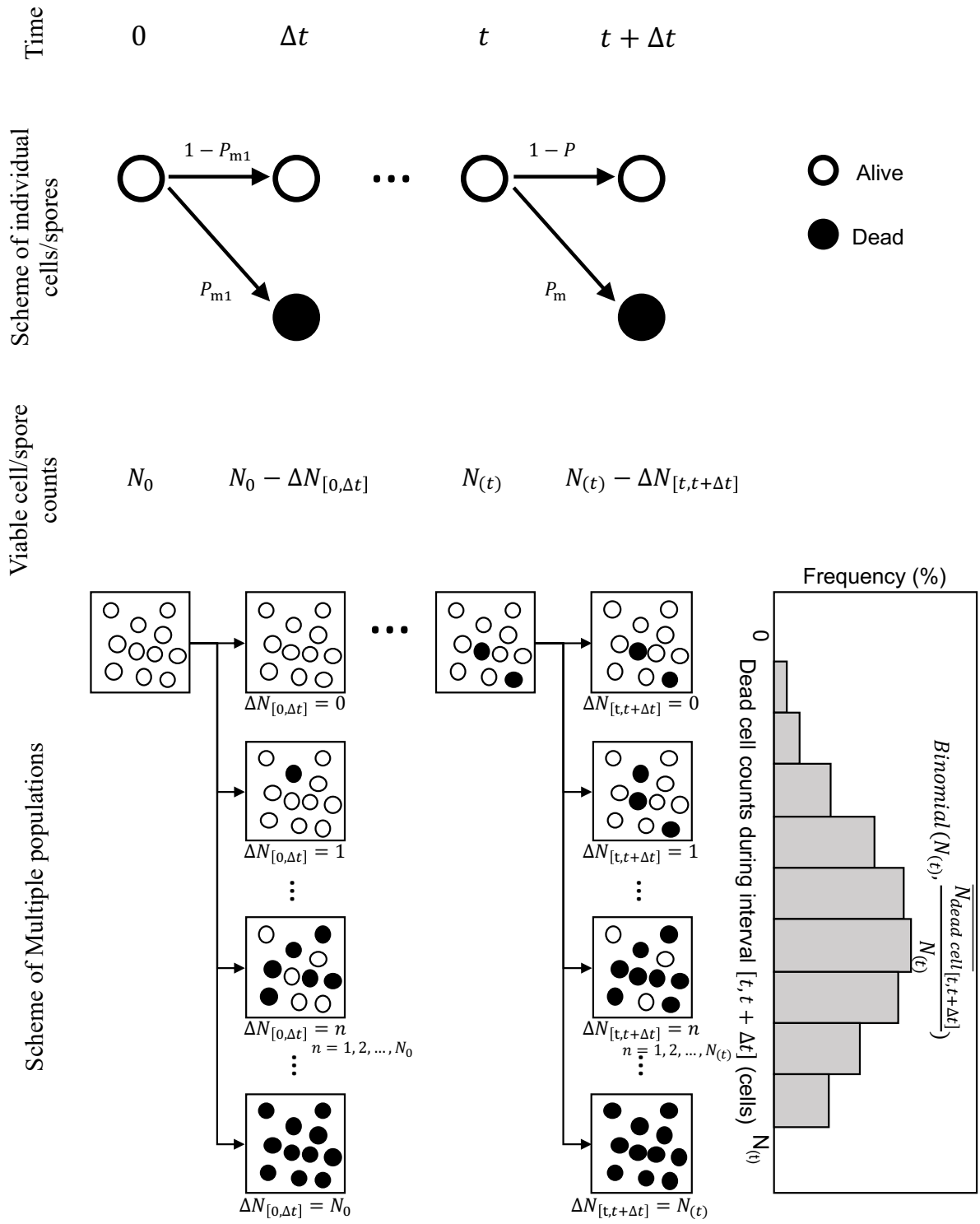


Fig. 4-3. Schematic of the Markov Chain Monte Carlo (MCMC) procedure. The proposed stochastic explanation describes bacteria death or continued survival based on the pure death process in the branch of modelling biological populations.

4.2.4. Second-order Monte Carlo simulation procedure

Three types of randomness were used to describe variability and uncertainty under the proposed bacterial inactivation model. Under the first type, which describes the variability in the initial bacterial count. The second type describes the uncertainty in an estimated parameter derived from the secondary models obtained from the bootstrap. The third type describes true randomness variability in bacterial reduction using Eq. 4-10. Using these approaches, the specific uncertainty in bacterial behavior was simulated as follows:

I. Using the first approach, a simulated initial count, $N_{(0)}$, was generated as a random number derived from the Poisson distribution. (Eq. 4-9):
II. To describe the uncertainty stemming from variation in the observed values, a secondary model set was randomly selected from the model set of 1,000 replicates obtained from the bootstrap.
III. The two Weibull parameters were derived from the secondary model set randomly selected in procedure II and the thermal history, respectively.
IV. Based on the dynamic kinetic model (Eq. 4-8) with III's parameters, the average inactivated spore count , $\overline{N_{dead\ cell}}_{[t,t+\Delta t]}$, during the very short time interval $[t, t+\Delta t]$ (Δt was set as 1 s in this study) was obtained from the derived Weibull parameters and $N_{(t)}$, the surviving cell count at t.
V. From $\overline{N_{dead\ cell}}_{[t,t+\Delta t]}$, a simulated inactivated cell count during the time interval was generated as a random number, $\Delta N_{[t,t+\Delta t]}$, derived from the binomial distribution.
VI. A simulated survival cell count at $t+\Delta t$ was derived from the simulated inactivated cell count during the short time interval and $N_{(t)}$. (Eq. 4-10)
VII. Procedures III–VI were repeated until the thermal treatment had finished or $N_{(t)}$ became zero.

The above series of procedures was repeated 100 times to determine the variance, including variability and one type of uncertainty, in bacterial behavior. The R statistics（Ver. 3.5.1 for Mac OS X）statistical software was used to carry out all statistical analyses.

4.3 Results and Discussion

4.3.1. Distribution of Weibullian parameters derived from the bootstrap

The spore survival kinetics under heating for each condition and the Weibull fitted survival curve based on 1,000 bootstrap replicates are shown together in Fig. 4-4, in which the error bars indicate the standard deviations (from three observations) under the respective conditions. Based on the variation in the estimated Weibullian model, each condition has 1,000 replicates. The estimated Weibull model parameters (i.e., $\log_{10}\delta$ and p) derived from the bootstrap were convergent, since all the $\hat{R}$-values of the parameters were equal to 1.0; they followed empirical distributions (Fig. 4-5), with both decreasing as either the temperature increased, or the pH decreased. These distributions come from the variations in combinations of resampled observed values by the bootstrap. Therefore, it reflects the fitting uncertainty in Weibullian parameters and the thermotolerance variability of individual cells that arise from observations. The variation in p values was larger than that observed in $\log_{10}\delta$. Under some conditions in which the variation in p was particularly large, its distribution had two peaks (Fig. 4-5). These indicate that it is difficult to detect the true one parameter from observed bacterial survival kinetics during thermal inactivation.

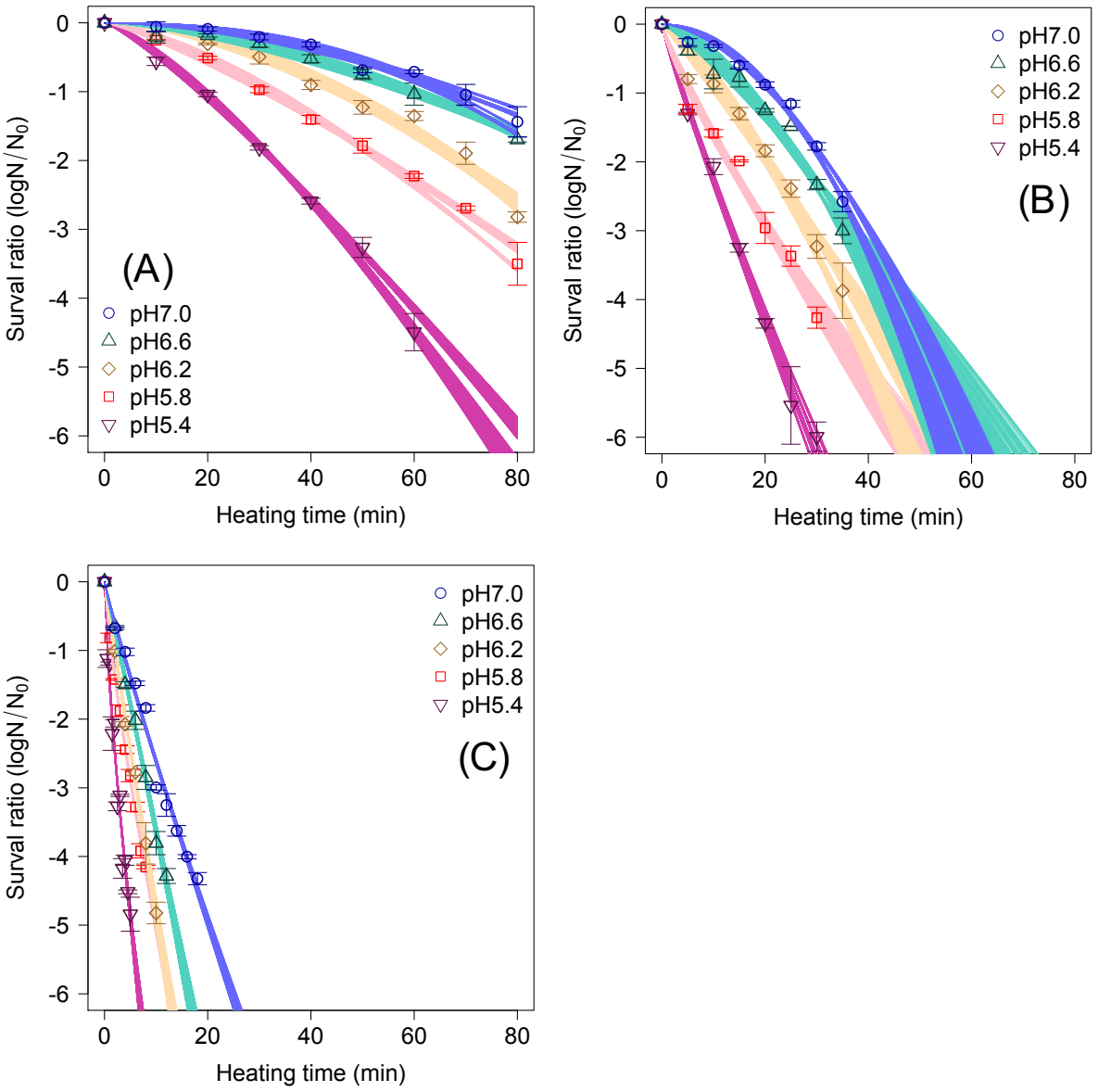


Fig. 4-4. Survival kinetics of *Bacillus simplex* spores under different temperature conditions, (A): 80°C, (B): 85°C, (C): 90°C. The points, error bars, and curves indicate, average value of observed survival ratio (three replicates), standard errors of observed survival ratio, and estimated Weibull model curves, respectively, based on 1,000 bootstrap replicates.

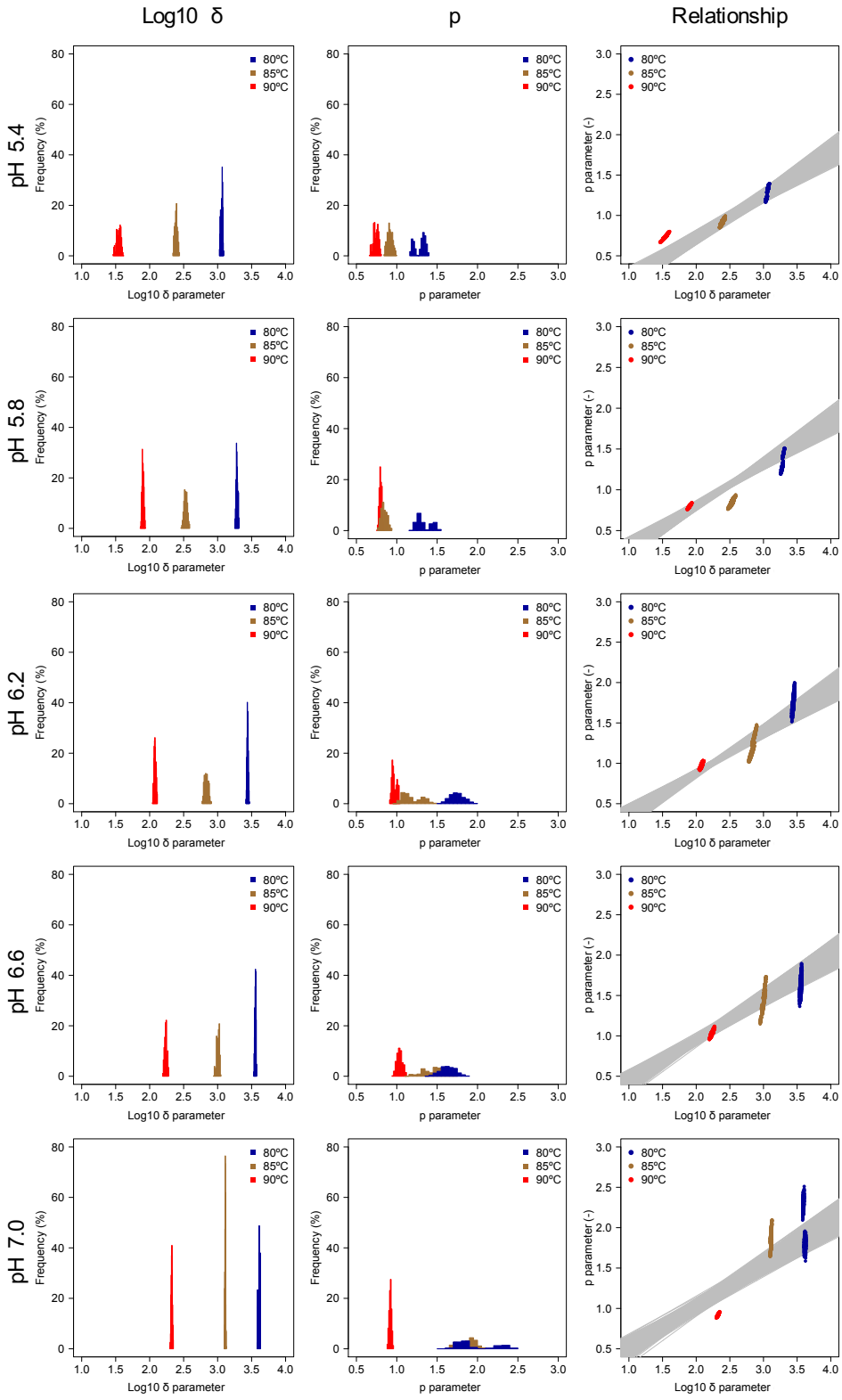


Fig. 4-5. Weibullian parameter distributions under each condition derived from 1,000 bootstrap replicates, and the relationship between the two bootstrapped Weibullian parameters. The gray lines indicate the relationship between the two estimated parameters from bootstrapped secondary model sets.

The secondary model was used to describe the relationship between the bootstrapped parameters and those for pH and temperature (Fig. 4-6). In the figure, the points, error bars, and lines indicate the average values of the bootstrapped parameters, the standard deviations of the bootstrapped parameters, and the 1,000 replicates of the bootstrapped secondary model, respectively. It is seen that the secondary model has confirmed the results of previous studies (Mafart et al., 2002), in which the temperature dependencies of the δ parameter were shown to follow a conventional *D*-value form. The pH dependencies of δ also follow a conventional *D*-value form. Although it has been reported that p parameter does not show any temperature and/or pH dependency in most cases (Van Boekel, 2002), the p parameter values obtained in the present study show a temperature and pH dependency (Fig. 4-6c; 4-6d). Similar to the present study, there are some reports that it was found that p decreased linearly as the temperature rose before reaching a constant level, suggesting that the results for p corresponded to a partially linear regression (Campanella and Peleg, 2001; Gomez et al., 2005).

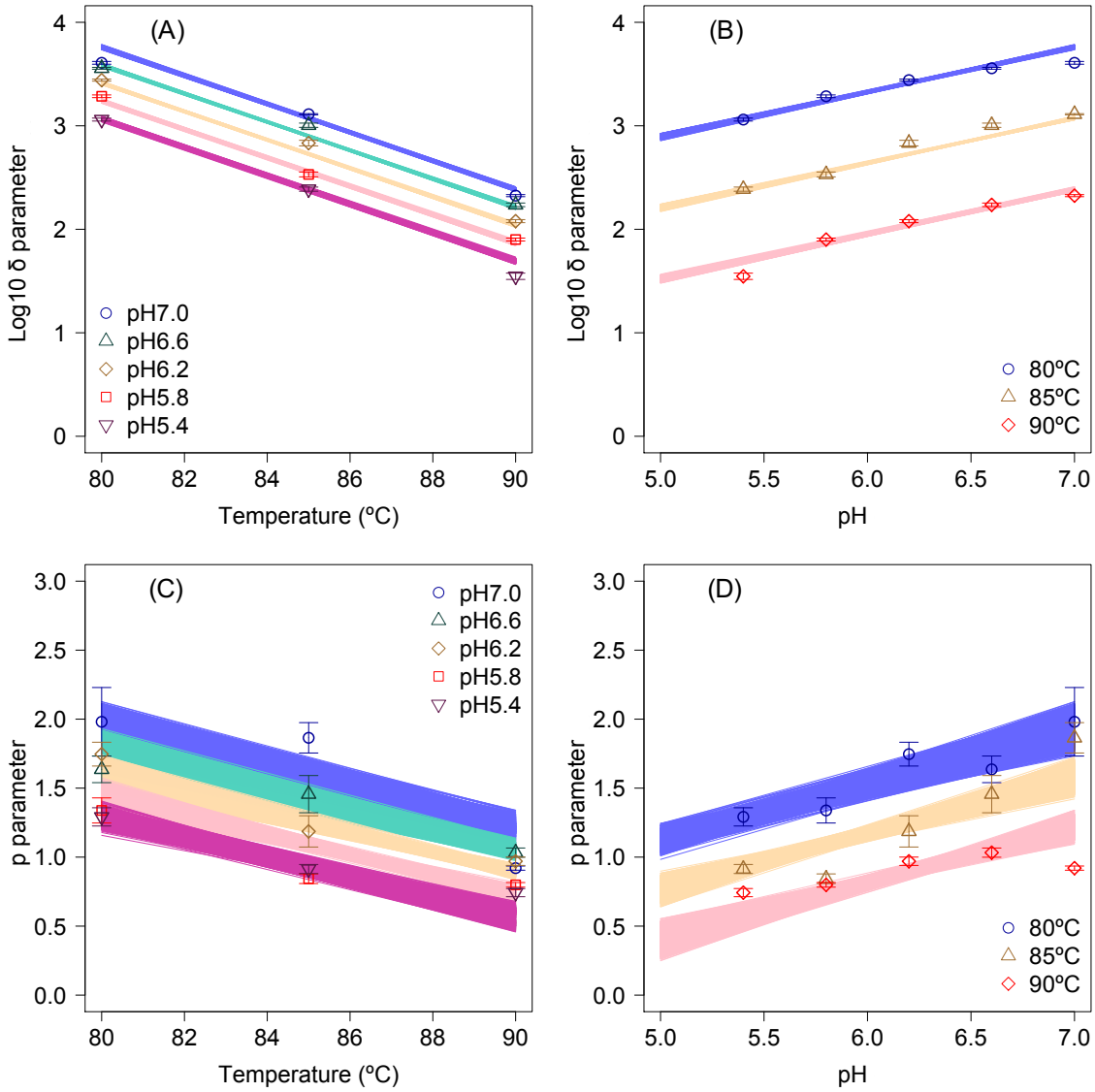


Fig. 4-6. Changes in $\log_{10}\delta$ and p as functions of heating temperature and pH (data points). (A): $\log_{10}\delta$ against temperature; (B): $\log_{10}\delta$ against pH; (C): p against temperature; (D): p against pH. Error bars indicate standard deviation of the 1,000 estimated Weibullian parameter replicates; lines indicate secondary model (upper left & upper right: Eq. 4-2; bottom left & bottom right: Eq. 4-3) derived from 1,000 bootstrap replicates.

Apart from temperature/pH dependency of the parameters (δ and p), there is an interaction between the δ and p parameters, because the shapes depend on the both of parameters (Peleg, 2006). The developed 2DMC model enables to take into account the interaction of both the parameters, because it estimates the Weibull parameters using sets of

secondary models of the corresponding δ and p parameters to resampled datasets. Comparing the fitted parameters' interaction and the estimated parameters' interaction by the bootstrapped secondary model sets, the bootstrapped secondary model sets explain linearly the interaction between δ and p parameter as shown in the right columns of Fig. 4-5.

Comparing the variations in p-parameters and $\log_{10}\delta$ derived from the bootstrapped parameters, the variations in the estimated p-parameter derived from the secondary model using bootstrapping were larger than those of $\log_{10}\delta$, possibly because they arose from small differences such as those between repetitions (Fig. 4-6). These results confirm the difficulty to develop a secondary model of p from only one parameter per condition.

4.3.2. Validation of dynamic stochastic model using second-order Monte Carlo simulation

Simulations based on 1,000 repetitions of the secondary models derived from the nonparametric bootstrap methods were used to model the variation in bacterial reduction behavior, including the variability and uncertainty in the fitting model estimation (Fig. 4-7). In the figure, the temperature profile and dynamical kinetic model predictions based on prior research (Campanella and Peleg, 2001; Peleg and Penchina, 2000) are shown as red and blue lines, respectively, while the gray lines indicate the results of 100 runs of simulated spore counts under non-isothermal inactivation. It is seen that the reduction rate follows the heating temperature, increasing and decreasing as the latter increases and decreases, respectively. Moreover, the predicted survival cell counts can describe the tendency of the observed bacterial behavior ($0.12 < \text{RMSE} < 0.55$). However, there were differences between observed and estimated values in some conditions. As described below, the cause of these discrepancies would be considered to be another factor that cannot be expressed in the 2DMC model. At small bacteria counts, there is a large variation in inactivation times until an arbitrary bacterial count (Fig. 4-7). The variability in the time needed to reduce the surviving

cell count to a specific level is increased in the range below 2 $\log_{10}$ CFU. The kinetic prediction passed through the center of the estimated range of survival spore count derived from the stochastic model, it is suggested that kinetic models tend to describe the average behavior of bacterial heterogeneity. The points in the figure indicate the observed surviving spore counts and are used to validate the 2DMC simulation model. Although the observed values in the region below 2 $\log_{10}$ CFU are within the 2DMC-estimated range, those above 2 $\log_{10}$ CFU are outside of the estimated range.

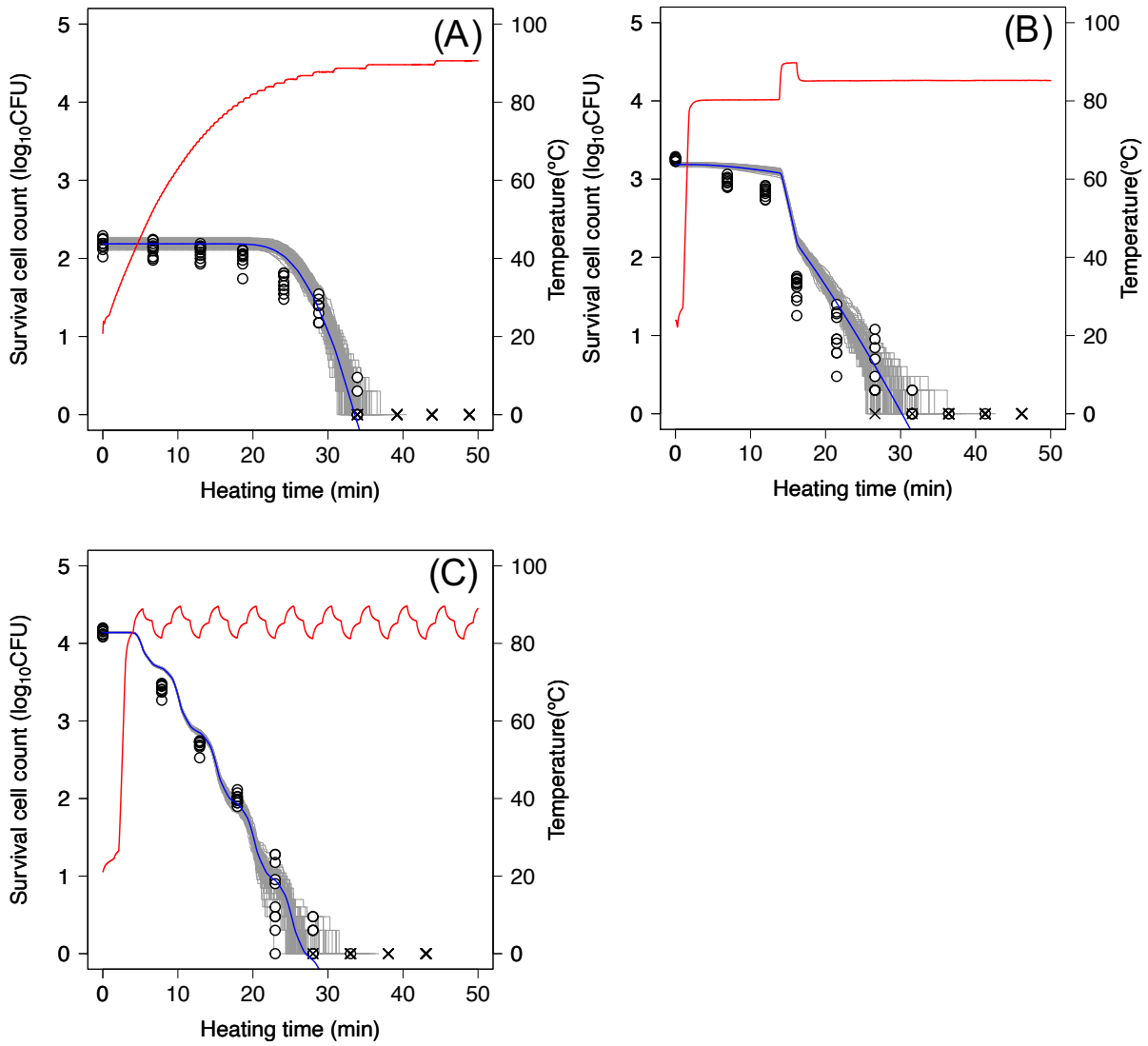


Fig. 4-7 Predictions of second-order Monte Carlo simulation (gray) and dynamic kinetic model (blue) and changes in 10 replicates of observed survival *Bacillus simplex* spore counts (○) under each temperature profile (red curve) of slow come-up heating in pH 6.5: (A), bumpy heating in pH 6.3: (B), and waving in pH 6.4: (C). × represents no colonies were detected.

The 2DMC developed in this study gives the distribution derived from the bootstrap and reflects the stochastic process describing bacterial reduction. In this manner, it describes both the uncertainty in observed value and the variability in bacterial lethality. Although most previous stochastic models describing bacterial behavior were based on only variability (Abe et al., 2019; Aspridou and Koutsoumanis, 2015; Corradini et al., 2010a; Koyama et al.,

2019b) or uncertainty (Schaffner, 1994), some researchers have advocated using models that integrate variability and uncertainty estimation (Abe et al., 2019; Cassin and Paoli, 1998; Nauta, 2000; Pouillot and Delignette-Muller, 2010). In this study, the variations of parameters were described with bootstrap while the randomness of dead cell counts were described with MCMC. The variations of parameters can describe the fitting uncertainty and the heterogeneity in individual cell thermotolerance; the randomness of dead cell counts can describe the true randomness in behaviors of bacteria population with exactly the same properties.

4.3.3. Evaluation of the validity of the second-order Monte Carlo simulation

To further assess the 2DMC approach, we compared it to "only-bootstrap" and "only-MCMC" models, i.e., to a dynamic kinetic model derived from 1,000 secondary model sets using the bootstrap method and a dynamic stochastic model derived from a secondary model without the application of bootstrapping, respectively. Fig. 4-7 shows the 99% confidence intervals for the time required to obtain a specific decrease in the number of surviving cells under a thermal condition (pH 5.4, heating temperature 85ºC) derived from the only-bootstrap (blue region), only-MCMC (red region), and 2DMC models (gray region). We compared the three models in terms of their confidence intervals. At surviving cell counts larger than 2 $\log_{10}$ CFU, the confidence intervals of the 2DMC model matched those of the only-bootstrap model, whereas those of the only-MCMC model were much smaller. At surviving cell counts of less than 2 $\log_{10}$ CFU, the confidence intervals of the 2DMC were larger than those of the other models. Furthermore, the confidence intervals of the 2DMC model corresponded to the variations in the observed values (Fig. 4-8). These results further validate the use of a 2DMC model that describes both uncertainty and variability and suggest that a stochastic model combining multiple Monte Carlo simulations, such as the one used in

this study, can accurately estimate cell reduction behavior that includes both variability and uncertainty.

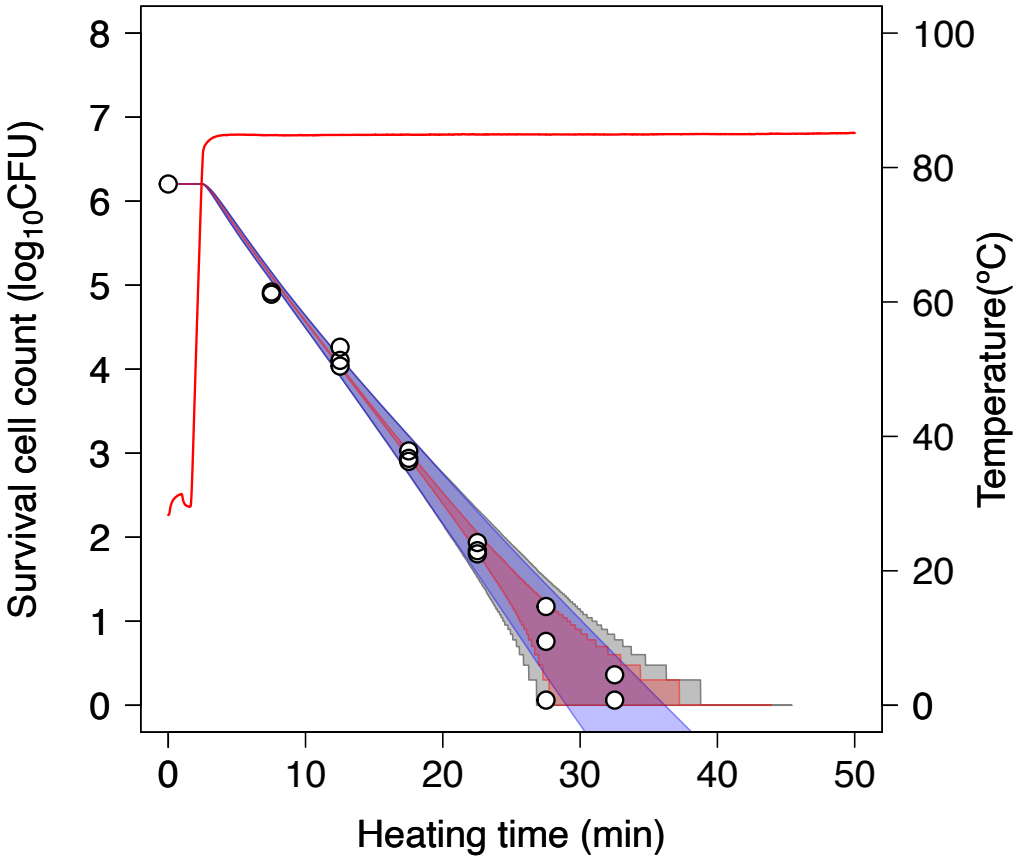


Fig. 4-8. Comparison of 99% confidence intervals derived from only-bootstrap model (blue region), only-MCMC model (red region), and 2DMC models (gray region) during heating at 85°C in pH-adjusted TSB at pH 5.4. The data points indicate two or three replicates of observed values. The only-bootstrap model is derived from the dynamic kinetic modeling of 1,000 secondary-model sets using the bootstrap method, while the only-MCMC model is derived from a dynamic stochastic secondary model constructed without application of the bootstrap model.

4.3.4. Potential of adaptation for other bacterial behavior description

The 2DMC simulation model proposed in the present study (Fig. 4-7) is based on the previously developed Weibullian dynamic models. One of the fundamental formulations used

to develop the 2DMC, Eq. 4-6, is based on the previous kinetic Weibullian dynamic studies (Campanella and Peleg, 2001; Corradini and Peleg, 2009; Peleg and Normand, 2004). The applicability of the Weibullian dynamic kinetic model to other types of bacteria has been demonstrated in the previous studies, with the results of these studies confirming our description of bacterial reduction behavior under non-isothermal heating by an adaptation of conventional kinetic models. In addition to the conventional Weibullian dynamic models mentioned above, the proposed model enables to assess the variation in bacterial count during an actual thermal process. This suggests the possibility of developing a 2DMC model based on a database such as ComBase (Baranyi and Tamplin, 2004) for not only average behaviors but also variabilities and uncertainties of vegetative cells' behaviors as well as spores, although the results would need to be validated. Generalizing the proposed model, the model can also be used to calculate the bacterial or sporular death behaviors including variation in real-time under existing or planned industrial thermal processes.

There is a possibility of application of the Markov property for other dynamic model than thermal inactivation. The proposed 2DMC model performs MC simulation by applying the Markov property, i.e., by using only the current state to predict the next state, with any other information about the past states disregarded (Durrett, 2011). This simulation approach, referred to as MCMC, is generally used for the simulation of stochastic processes with probability densities known up to a constant of proportionality (Geyer, 1992). In this paper, the Markov property is introduced in Eq. 4-10. Unlike the conventional stochastic Weibullian dynamic model (Corradini et al., 2010a), which does not consider the influence of the randomness of instantaneous survival ratio, the proposed stochastic dynamic model takes both $S_{(t)}$ and the instantaneous count of surviving bacteria $N_{(t)}$ into account. From Eq. 4-5, as adapted from previous work (Mattick et al., 2001; Peleg et al., 2005), the randomness of the instantaneous survival ratio depends on the instantaneous values of $S_{(t)}$. Considering the

dependency to instantaneous $S_{(t)}$, it is important to take an idea of the Markov property into account for not only in Weibull models but in any type of reduction model. In addition to reduction behavior, formulations based on the Markov property such as Eq. 4-10 can describe growth behavior because growth behaviors depend on the instantaneous bacterial counts. Thus, by applying MCMC it is possible to create multiple stochastic prediction models even under dynamic environments.

4.3.5. Limitations of the developed modelling procedure

The proposed dynamic model, however, might have some limitations in its ability to predict variations in the reduction behavior of arbitrary bacterial types. The proposed model ignores several factors, including the interactive influence between bacteria and thermal unevenness. As cell (and in this particular case spore) interactions are not taken into account in the developed modelling approach, it is possible that the proposed model cannot be used to predict bacterial population dynamics involving such interactions. As Eq. 4-10 describes change over an infinitesimal interval under any type of bacterial reduction model, it can be applied via Eq. 4-10 to express average bacterial behavior through a kinetic model. In this study, very small (100-μL) bacterial suspensions were tested to avoid uneven temperature conditions across the samples. Under conditions of actual thermal inactivation in food or beverages, however, there will be significant temperature unevenness as a result of heating, which should therefore be taken into account through the use of a temperature-predictive physical model established via the modeling of heat transfer with a fine mesh. By doing so, the problem of kinetic modeling of the interactive dependence among bacteria can be solved.

Another critical limitation with the proposed model is that it cannot completely express uncertainty and variability. The proposed 2DMC method attempts to use the bootstrap method to express uncertainty in the Weibull model parameter estimations,

although it does not account for uncertainty related to experimental procedures (e.g., plate counting), model selection and other sources. The same applies for variability sources not explicitly taken into account in the present modelling approach such as intra-species (i.e. strain-to-strain) variability, other than true randomness and thermotolerance variability within a bacterial strain. The differences seen in Fig. 4-7 between the estimated and observed surviving cell counts in the range above 2 $\log_{10}$ CFU demonstrate its failure to obtain accurate parameter values. This discrepancy arises from various factors in the creation of the primary and secondary models, and the development of a more robust dynamic model requires the selection of a more appropriate combination of these models. The proposed model is based on a conventional kinetic dynamic model, and the use of inappropriate secondary or primary models can therefore result in inappropriate dynamic predictions. In particular, the bootstrap process through which the model estimates the parameter distribution involves the selection of a most suitable value for each iteration via the least square method. However, the standard error of fitting using the least squares method was not considered in this study. In future applications of the proposed method, this could be addressed by resampling the prediction parameters based on a normal distribution with a standard error equivalent to that of the fitting to widen the parameter distribution and obtain a more accurate parameter value. In addition, Bayesian analysis might be useful in describing the uncertainties in the primary parameters. Given that the observed values used for validation will themselves have inherent and unavoidable uncertainties, full validation of the stochastic process model will require a method that can completely account for uncertainty in observed values.

4.3.6. Conclusions and future perspectives

If the problems described above can be overcome, it would be possible to model the heterogeneity of bacterial behavior throughout the entire manufacturing process. A simulation model such as the one described in this study can be used to obtain the survival probability of bacteria populations and a distribution of surviving cell counts (Abe et al., 2019), which would aid in the risk assessment of food processing. Real food manufacturing processes inevitably have many variabilities and uncertainties. Describing all the variabilities and uncertainties using 2DMC or even 3DMC or higher-order simulations to obtain better-detailed assessments of heterogeneities in bacterial behavior will enhance the bacterial food safety in the manufacturing processes. Such models would also make it possible to determine the inactivation conditions of safety-guaranteed foods while better maintaining original food quality.

The results of this study demonstrate the potential of 2DMC simulation to describe bacterial inactivation behavior during non-isothermal inactivation with variability in individual cell heterogeneity and parameter uncertainty both taken into account. Comparison of the results of the 2DMC approach with models looking only at uncertainty or variability further revealed the importance of using a combined model. The 2DMC simulation model developed in this study should be useful in quantitative microbial risk assessment, aiding in the design of risk-based thermal processes for the efficient inactivation of bacterial spores, and ensuring food safety and quality with minimal negative impact on the sensorial attributes of foods.

4.4 References

Abe, H., Koyama, K., Kawamura, S., and Koseki, S. (2018). Stochastic evaluation of *Salmonella enterica* lethality during thermal inactivation. *International Journal of Food Microbiology* 285, 129–135. doi:10.1016/j.ijfoodmicro.2018.08.006.

Abe, H., Koyama, K., Kawamura, S., and Koseki, S. (2019). Stochastic modeling of variability in survival behavior of *Bacillus simplex* spore population during isothermal inactivation at the single cell level using a Monte Carlo simulation. *Food Microbiology*

82, 436–444. doi:10.1016/j.fm.2019.03.005.

Aspridou, Z., and Koutsoumanis, K. P. (2015). Individual cell heterogeneity as variability source in population dynamics of microbial inactivation. *Food Microbiology* 45, 216–221. doi:10.1016/j.fm.2014.04.008.

Awuah, G. B., Ramaswamy, H. S., and Economides, A. (2007). Thermal processing and quality: Principles and overview. *Chemical Engineering and Processing: Process Intensification* 46, 584–602. doi:10.1016/j.cep.2006.08.004.

Baranyi, J., and Tamplin, M. L. (2004). ComBase: A Common Database on Microbial Responses to Food Environments. *Journal of Food Protection* 67, 1967–1971. doi:10.4315/0362-028X-67.9.1967.

Besten, den, H. M. W., Wells-Bennik, M. H. J., and Zwietering, M. H. (2018). Natural Diversity in Heat Resistance of Bacteria and Bacterial Spores: Impact on Food Safety and Quality. *https://doi.org/10.1146/annurev-food-030117-012808* 9, 383–410. doi:10.1146/annurev-food-030117-012808.

Campanella, O. H., and Peleg, M. (2001). Theoretical comparison of a new and the traditional method to calculate Clostridium botulinum survival during thermal inactivation. *Journal of the Science of Food and Agriculture* 81, 1069–1076. doi:10.1002/jsfa.895.

Cassin, M. H., and Paoli, G. M. (1998). *Simulation Modeling for Microbial Risk Assessment*. Journal of Food Protection doi:10.1046/j.1365-2672.2000.01059.x/full.

Corradini, M. G., and Peleg, M. (2009). Dynamic model of heat inactivation kinetics for bacterial adaptation. *Appl. Environ. Microbiol.* 75, 2590–2597. doi:10.1128/AEM.02167-08.

Corradini, M. G., Normand, M. D., and Peleg, M. (2010a). Stochastic and Deterministic Model of Microbial Heat Inactivation. *Journal of Food Science* 75, R59–R70. doi:10.1111/j.1750-3841.2009.01494.x.

Corradini, M. G., Normand, M. D., Eisenberg, M., and Peleg, M. (2010b). Evaluation of a Stochastic Inactivation Model for Heat-Activated Spores of Bacillus spp. *Appl. Environ. Microbiol.* 76, 4402–4412. doi:10.1128/AEM.02976-09.

Couvert, O., Pinon, A., Bergis, H., Bourdichon, F., Carlin, F., Cornu, M., et al. (2010). Validation of a stochastic modelling approach for Listeria monocytogenes growth in refrigerated foods. *International Journal of Food Microbiology* 144, 236–242. doi:10.1016/j.ijfoodmicro.2010.09.024.

Davey, K. R. (1993). Extension of the Generalized Sterilization Chart for Combined Temperature and pH. *LWT - Food Science and Technology* 26, 476–479. doi:10.1006/fstl.1993.1093.

Durrett, R. (2011). *Essentials of Stochastic Processes*. 2nd ed. Cham: Springer doi:10.1007/978-3-319-45614-0.

Efron, B., and Tibshirani, R. (1991). Statistical Data Analysis in the Computer Age. *Science* 253, 390–395. doi:10.1126/science.253.5018.390.

FAO/WHO (2008). Exposure assessment of microbiological hazards in food. who.int.

Fellows, P. J. (2009). Food Processing Technology: Principles and Practice. 3rd ed. Elsevier.

Geyer, C. J. (1992). Practical Markov Chain Monte Carlo. *Statistical Science*. doi:10.2307/2246094.

Gomez, N., Garcia, D., Alvarez, I., Raso, J., and Condon, S. (2005). A model describing the kinetics of inactivation of Lactobacillus plantarum in a buffer system of different pH and in orange and apple juice. *Journal of Food Engineering* 70, 7–14. doi:10.1016/j.jfoodeng.2004.09.007.

Hoornstra, E., and Notermans, S. (2001). Quantitative microbiological risk assessment. *International Journal of Food Microbiology* 66, 21–29. doi:10.1016/S0168-

1605(00)00529-8.

Kobayashi, T., Yasokawa, D., Nakagawa, R., and Kawakami, M. (2016). Growth Characteristics and Thermal Resistance of Spores of Psychrophilic Bacteria Isolated from Chilled Agricultural Food Products. *J. Antibact. Antifung. Agents* 44, 509–514.

Koseki, S., NAKAMURA, N., and SHIINA, T. (2015). Comparison of Desiccation Tolerance among Listeria monocytogenes, Escherichia coli O157:H7, *Salmonella enterica*, and Cronobacter sakazakii in Powdered Infant Formula. *https://doi.org/10.4315/0362-028X.JFP-14-249* 78, 104–110. doi:10.4315/0362-028X.JFP-14-249.

Koutsoumanis, K. P., and Aspridou, Z. (2017). Individual cell heterogeneity in Predictive Food Microbiology: Challenges in predicting a noisy world. *International Journal of Food Microbiology* 240, 3–10. doi:10.1016/j.ijfoodmicro.2016.06.021.

Koutsoumanis, K., and Angelidis, A. S. (2007). Probabilistic modeling approach for evaluating the compliance of ready-to-eat foods with new European Union safety criteria for Listeria monocytogenes. *Appl. Environ. Microbiol.* 73, 4996–5004. doi:10.1128/AEM.00245-07.

Koyama, K., Abe, H., Kawamura, S., and Koseki, S. (2019a). Calculating stochastic inactivation of individual cells in a bacterial population using variability in individual cell inactivation time and initial cell number. *Journal of Theoretical Biology* 469, 172–179. doi:10.1016/j.jtbi.2019.01.042.

Koyama, K., Abe, H., Kawamura, S., and Koseki, S. (2019b). Stochastic simulation for death probability of bacterial population considering variability in individual cell inactivation time and initial number of cells. *International Journal of Food Microbiology* 290, 125–131. doi:10.1016/j.ijfoodmicro.2018.10.009.

Koyama, K., Hokunan, H., Hasegawa, M., Kawamura, S., and Koseki, S. (2016). Do bacterial cell numbers follow a theoretical Poisson distribution? Comparison of experimentally obtained numbers of single cells with random number generation via computer simulation. *Food Microbiology* 60, 49–53. doi:10.1016/j.fm.2016.05.019.

Kuroda, S., Okuda, H., Ishida, W., and Koseki, S. (2019). Modeling growth limits of Bacillus spp. spores by using deep-learning algorithm. *Food Microbiology* 78, 38–45. doi:10.1016/j.fm.2018.09.013.

Ling, B., Tang, J., Kong, F., Mitcham, E. J., and Wang, S. (2015). Kinetics of Food Quality Changes During Thermal Processing: a Review. *Food Bioprocess Technol* 8, 343–358. doi:10.1007/s11947-014-1398-3.

Mafart, P., Couvert, O., Gaillard, S., and Leguerinel, I. (2002). On calculating sterility in thermal preservation methods: application of the Weibull frequency distribution model. *International Journal of Food Microbiology* 72, 107–113. doi:10.1016/S0168-1605(01)00624-9.

Mattick, K. L., Legan, J. D., Humphrey, T. J., and Peleg, M. (2001). Calculating *Salmonella* Inactivation in Nonisothermal Heat Treatments from Isothermal Nonlinear Survival Curves. *http://dx.doi.org/10.4315/0362-028X-64.5.606* 64, 606–613. doi:10.4315/0362-028X-64.5.606.

Membré, J. M., Amézquita, A., Bassett, J., Giavedoni, P., de W Blackburn, C., and Gorris, L. G. M. (2006). A Probabilistic Modeling Approach in Thermal Inactivation: Estimation of Postprocess Bacillus cereus Spore Prevalence and Concentration. *Journal of Food Protection* 69, 118–129. doi:10.4315/0362-028X-69.1.118.

Nauta, M. J. (2000). Separation of uncertainty and variability in quantitative microbial risk assessment models. *International Journal of Food Microbiology* 57, 9–18. doi:10.1016/S0168-1605(00)00225-7.

Nauta, M., Hill, A., Rosenquist, H., Brynestad, S., Fetsch, A., van der Logt, P., et al. (2009). A comparison of risk assessments on Campylobacter in broiler meat. *International*

Journal of Food Microbiology 129, 107–123. doi:10.1016/j.ijfoodmicro.2008.12.001.

Peleg, M. (2006). Advanced Quantitative Microbiology for Foods and Biosystems : Models for Predicting Growth and Inactivation. CRC Press doi:10.1201/9781420005370.

Peleg, M., and Normand, M. D. (2004). Calculating Microbial Survival Parameters and Predicting Survival Curves from Non-Isothermal Inactivation Data. *Crit Rev Food Sci Nutr* 44, 409–418. doi:10.1080/10408690490489297.

Peleg, M., and Penchina, C. M. (2000). Modeling Microbial Survival during Exposure to a Lethal Agent with Varying Intensity. *Crit Rev Food Sci Nutr* 40, 159–172. doi:10.1080/10408690091189301.

Peleg, M., Normand, M. D., and Corradini, M. G. (2005). Generating microbial survival curves during thermal processing in real time. *Journal of Applied Microbiology* 98, 406–417. doi:10.1111/j.1365-2672.2004.02487.x.

Pouillot, R., and Delignette-Muller, M. L. (2010). Evaluating variability and uncertainty separately in microbial quantitative risk assessment using two R packages. *International Journal of Food Microbiology* 142, 330–340. doi:10.1016/j.ijfoodmicro.2010.07.011.

Quinto, E. J., Marin, J. M., Caro, I., Mateo, J., Redondo-del-Rio, M. P., and de-Mateo-Silleras, B. (2018). Bootstrap parametric GB2 and bootstrap nonparametric distributions for studying shiga toxin-producing Escherichia coli strains growth rate variability. *Food Research International*. doi:10.1016/j.foodres.2018.11.045.

Renshaw, E. (1993). Modelling Biological Populations in Space and Time. Cambridge University Press.

Rychlik, I., and Ryden, J. (2006). Probability and Risk Analysis -An Introduction for Engineers. Spriger.

Schaffner, D. W. (1994). Application of a statistical bootstrapping technique to calculate growth rate variance for modelling psychrotrophic pathogen growth. *International Journal of Food Microbiology*.

Taylor, J. M. W., Sutherland, A. D., Aidoo, K. E., and Logan, N. A. (2005). Heat-stable toxin production by strains of Bacillus cereus, Bacillus firmus, Bacillus megaterium, Bacillus simplexand Bacillus licheniformis. *FEMS Microbiol Lett* 242, 313–317. doi:10.1016/j.femsle.2004.11.022.

Van Boekel, M. A. J. S. (2002). On the use of the Weibull model to describe thermal inactivation of microbial vegetative cells. *International Journal of Food Microbiology* 74, 139–159. doi:10.1016/S0168-1605(01)00742-5.

Vehtari, A., Gelman, A., Simpson, D., Carpenter, B., and Bürkner, P.-C. (2019). Rank-normalization, folding, and localization: An improved R-hut for assessing convergence of MCMC. *arxiv.org*.

Wu, F.-C., and Tsang, Y.-P. (2004). Second-order Monte Carlo uncertainty/variability analysis using correlated model parameters: application to salmonid embryo survival risk assessment. *Ecological Modelling* 177, 393–414. doi:10.1016/j.ecolmodel.2004.02.016.

Chapter 5 Predictive model for invading behaviors of *Campylobacter jejuni* into human intestinal cells

5.1. Introduction

Campylobacter jejuni is one of the most common foodborne pathogens worldwide, causing substantial health and economic losses to society. Thus, this food, beverage (Kaakoush, Castaño-Rodríguez, Mitchell, & Man, 2015), and water-borne pathogen has become an important focus of microbial risk assessment (World Health Organization, 2009). Appropriate quantitative risk assessment of *C. jejuni* in foods should be carried out to predict the status of *C. jejuni* infection through foods.

Although dose-response models are important for quantitative microbial risk assessment (Food and Agriculture Organization of the United Nations/ World Health OrganizationWorld Health Organization, 2003), dose-response information on human infection with *C. jejuni* is limited. Only one human feeding study has been reported (Black, Levine, Clements, Hughes, & Blaser, 1988), but only high doses of *C. jejuni* populations were tested, resulting in high infection/illness rates. Although few epidemiological estimation data are available (Teunis et al., 2005) on *C. jejuni* infection caused by unpasteurized milk on farms (Evans, Roberts, Ribeiro, Gardner, & Kembrey, 1996), the relationship between low-dose *C. jejuni* ingestion and the probability of infection is still not fully understood (Medema, Teunis, Havelaar, & Haas, 1996). The most important dose-response relationship for maintaining public health is the relationship of the hazard probability is low, that is when the pathogen dose shows a low.

An alternative approach to assessing low-dose response relationships named as the key events dose-response framework (KEDRF) (Buchanan, Havelaar, Smith, Whiting, & Julien, 2009; Julien, Boobis, Olin, The ILSI Research Foundation Threshold Working Group,

2009) has been proposed based on the mechanism of foodborne pathogen ingestion for causing an infection. The KEDRF is an analytical approach that facilitates the use of currently available data to gain insight into dose-response relationships. For example, the KEDRF approach for *Listeria* has been proposed and involves the following five major and necessary steps, termed as key events: (i) survival of pathogens in the upper gastrointestinal tract, (ii) establishment in the intestine and attachment to and uptake into epithelial cells, (iii) survival and escape from phagosomes in enterocytes and transfer of the pathogen to phagocytes, (iv) transfer of pathogens across the placenta, and (v) pathogen growth leading to fetal morbidity and mortality. Therefore, it is necessary to estimate the microbial behavior at each key event from oral ingestion to illness onset when implementing the KEDRF. A study has also been conducted to determine the dose-response relationship of *Listeria monocytogenes* based on the infection mechanism (Rahman, Munther, Fazil, Ben Smith, & Wu, 2016), and establishment of a mechanism-based dose-response model is becoming more important for clarifying the appropriate dose-response relationship.

Campylobacter spp. including *C. jejuni* invade host human tissues through complex putative mechanisms. *Campylobacter jejuni* reaching the intestinal tract in contaminated food attempts to migrate to upper intestinal epithelial cells because of their chemotaxis motility activated by mucus (Szymanski, King, Haardt, & Armstrong, 1995). The pathogen binds to intestinal cell matrix protein fibronectin by utilizing its putative adhesion or binding factors such as fibronectin-binding outer membrane protein CadF, the autotransporter CapA, the periplasmic binding protein PEB1, and the surface-exposed lipoprotein JlpA (Dasti, Tareen, Lugert, Zautner, & Groß, 2010). Finally, *C. jejuni* enter intestinal cells via a microtubule-dependent and actin filament-independent invasion mechanism (Szymanski et al., 1995). The invasion process enables *C. jejuni* to enter the cell first with its tip followed by its flagellar end (Krause-Gruszczynska et al., 2007). After cell invasion, *C. jejuni* uses a transcytosis

mechanism (transfer of molecules/materials from one side of a cell to another side in membrane-bound vesicles) to migrate to various body tissues and adversely affects vital functions in the host such as intestine, blood vessel, and lymphatic fluid functions by producing cytolethal-distending toxin, which causes inflammation (Man, 2011). Therefore, the pathogenic mechanism of *C. jejuni* involves the aforementioned key event (iii). Quantitative modeling of the cell invasive behavior of *C. jejuni* into intestinal cells is essential for estimating dose-response relationships using the KEDRF.

This study was conducted to experimentally investigate the invasion behavior of *C. jejuni* into intestinal epithelial cells using human colonic carcinoma cells (Caco-2) *in vitro*, which has functional properties characteristic of small bowel enterocytes and been widely used as a model cell for small intestinal epithelial-like cells (Verhoeckx et al., 2015), as one of the Key Events. Furthermore, we developed a mathematical model describing the invasion behavior of *C. jejuni* into Caco-2 cells, which is necessary for constructing a new dose-response model of *C. jejuni* based on the KEDRF concept.

5.2. Materials and methods

5.2.1. Cell strain and culture conditions

Human colonic carcinoma Caco-2 cells (RCB0988) were obtained from the Riken Cell Bank (Tsukuba, Japan).and stored at -80°C in cryopreservation media (Merck, Darmstadt, Germany). The cells were grown at 37°C in Dulbecco's modified Eagle's medium (DMEM; Sigma-Aldrich, St. Louis, MO, USA) supplemented with 10% fetal bovine serum (Gibco, Grand Island, NY, USA), 2 mM L-glutamine (Sigma-Aldrich), 1% non-essential amino acids (Sigma-Aldrich), and penicillin (10,000 U/L)-streptomycin (10 mg/L) antibiotic solution in a humidified atmosphere containing 5% CO_2 and 95% air. The cells were cultured for 12 days with two medium exchanges and passaging once. The cultured cells were plated at a density of 8.2×10^4 cells/well into 96-well tissue culture plates (Techno Plastic Products,

Trasadingen, Switzerland) and grown for 2 days to confluency in the same medium but in the presence of antibiotic solution (penicillin-streptomycin).

5.2.2. Bacterial strain and culture conditions

Three strains of *C. jejuni* (RIMD 0366027, RIMD 0366042, RIMD 0366048) originating from patients and patient feces, was acquired from the Research Institution for Microbial Disease (Osaka, Japan). According to the bacterial strain donor, strain RIMD 0366048 causes Guillain-Barre syndrome. The stock culture was maintained at -80°C in Bolton broth (Oxoid, Basingstoke, UK) containing 10% glycerol. The strain was activated by incubation at 42°C for 48 h on Preston agar under microaerophilic conditions (6–12% O_2, 5–8% CO_2) with Anaero Pack MicroAero (Mitsubishi, Tokyo, Japan) followed by two incubations in Bolton Broth under the same conditions. After three washing and centrifugation steps (3000 ×*g*, 10 min) with the supplemented DMEM without antibiotic solution, the bacteria were resuspended in DMEM and used in the experiments.

5.2.3. Invading cell count assay

Caco-2 cell monolayers in DMEM with supplements were infected with cultured *C. jejuni* at 37°C under microaerophilic conditions (6–12% O_2, 5–8% CO_2). The assays were based on previous research (Szymanski et al., 1995). *C. jejuni* at concentrations of 10^n (n = 4-9) colony-forming units per mL were used. Caco-2 cell monolayers were infected with *C. jejuni* for exposure times (10 s and 1.5, 3.0, 4.5, 6.0, 7.5, 9.0, 10.5, and 12 h). It has been confirmed in advance that there is no remarkable difference in the Caco-2 cells and the *C. jejuni* counts between before and after 12-hours culturing in DMEM. The infected cells were washed three times with Dulbecco's phosphate-buffered saline (DPBS) and then incubated with 100 μg/mL of gentamicin (Wako, Osaka, Japan) in DMEM-FBS at 37°C for 1 h to kill

any extracellular organisms. The cells were washed again with DPBS and treated with 1% Triton X-100 (Sigma) in DPBS at 4°C for 30 min to release intracellular organisms. Dilutions from each well were plated on Preston agar and incubated at 42°C for 48 h on Preston agar under microaerophilic conditions. After incubation, the invading bacterial counts were determined as CFU. We previously determined that Triton X-100 did not inhibit the growth of *C. jejuni*. The results obtained at bacterial concentrations of 10^n (n = 5, 7 and 9) CFU were used for model development; the results at bacterial concentrations of 10^n (n = 4, 6, and 8) CFU were used for model validation.

5.2.4. Data analysis and Bayesian modeling condition

Changes in the invading bacteria counts were modeled using an absorption model in the intestinal tract of the one-compartment model used for pharmacokinetics analysis (Bourne, 1995). The rate of absorption (here, the rate of bacterial invasion, $\frac{d}{dt}N_{invading}$) was determined as the product of the absorption rate constant, μ, and concentration of medicines (extracellular bacterial concentration, $C_{extraceller}$, in this case) in the absorption section, with a spatial upper limit to the amount of medians (upper limit of invading bacteria, N_{max}) absorbed. Therefore, total absorption in the absorption section (in this paper, the invading bacteria count) is defined by the following differential Eq. 5-1, and if the initial number of invading bacteria is set to 0, Eq. 5-1 can be solved as Eq. 5-2.

$$\frac{d}{dt}N_{invading} = \mu C_{extraceller}\left(N_{max} - N_{invading}\right) \quad \text{(Eq. 5-1)}$$

$$N_{invading} = N_{max}(1 - e^{-\mu C_{extraceller} t}) \quad \text{(Eq. 5-2)}$$

This can be transformed into logarithmic form as shown in Eq. 5-3.

$$\mathrm{Log}_{10}\, N_{invading} = \mathrm{Log}_{10}[N_{\max}(1 - e^{-\mu C_{extraceller} t})] \quad \text{(Eq. 5-3)}$$

The model was fitted to the observed invading behavior of each isolate by Bayesian inference regression (parameters: $\mathrm{Log}_{10}\, N_{max}$ and $\mathrm{Log}_{10}\, \mu$). Bayesian inference regression, which

considers uncertainty and variability, was used to estimate the fitting of the invasion model to the observed data. We adopted a normal distribution with standard deviation, σ, as the prior of $\mathrm{Log}_{10}\, N_{invading}$ and uniform distribution as a non-informal prior distribution for each parameter. PyStan (version 2.19) was used for Bayesian parameter estimation; the No-U-Turn sampler was used for the MCMC sample method of posterior parameter distributions. The predictive model equation used for Bayesian parameter estimation is shown in Eq. 5-4.

$$\mathrm{Log}_{10}\, N_{invading} \sim Normal(\mathrm{Log}_{10}[N_{\max}(1 - e^{-\mu C_{extracellert}})], \sigma) \qquad \text{(Eq. 5-4)}$$

5.3. Results

5.3.1. Behaviors of invading C. jejuni count into Caco-2 cells

Fig. 5-1, 5-2 and 5-3 shows that invading *C. jejuni* counts into Caco-2 cells per cm^2 (CFU/cm^2) showed an asymptotic increase (approximate maximum of 4.5 log CFU/cm^2) over time in the three tested strains (Fig. 5-1, 5-2 and 5-3). Each point denotes the mean value of three iterations for each condition, and the error bars denote the standard deviation for each condition. No intracellular invasion of bacteria was observed under some short exposure duration conditions such as 10 s and 1.5 h (no plot is shown in Fig. 5-1, 5-2 and 5-3). Under high-dose conditions such as >5.7 log CFU/mL, the invading *C. jejuni* counts reached a maximum and became almost constant for more than 3 h of co-culture with Caco-2 cells. In contrast, invasion of *C. jejuni* proceeded slowly after low-dose exposure such as <4.5 log CFU/mL. The number of invading *C. jejuni* showed an increasing trend with higher doses for the same exposure duration. Although no intracellular invasion was observed within 10 s exposure at most concentrations, *C. jejuni* exhibited immediate intracellular invasion (<10 s) at higher concentrations (>6.6 log CFU/mL).

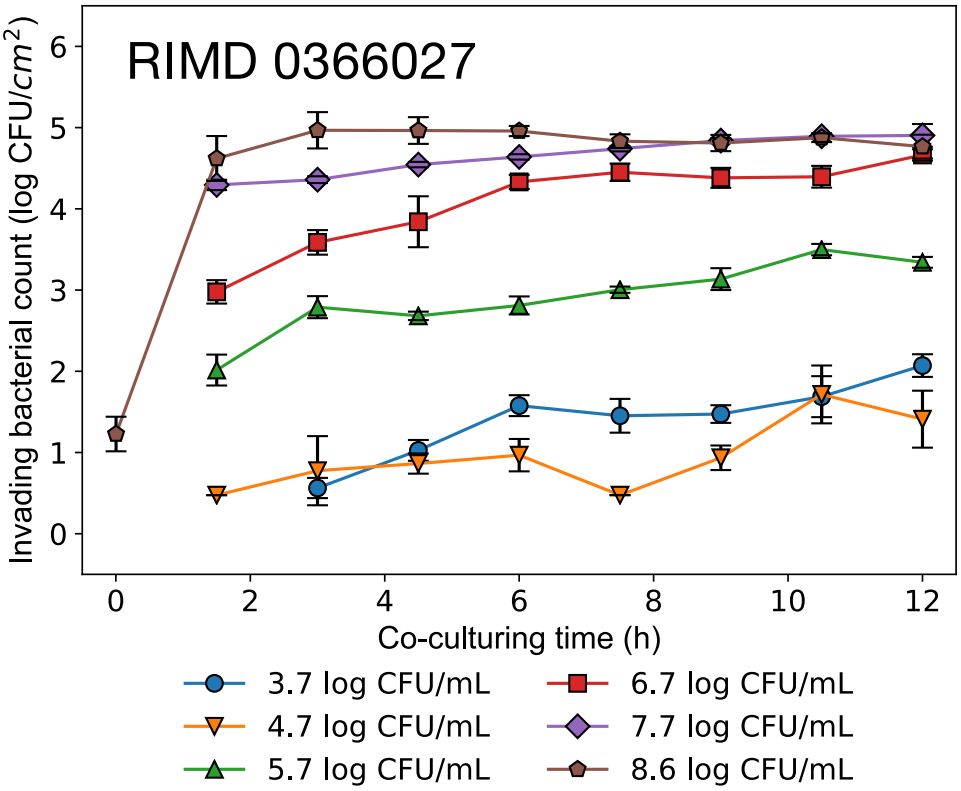


Fig. 5-1. Differences in the number of invading different strains of *Campylobacter jejuni* (RIMD 0366027) into monolayer-cultured Caco-2 cells (RCB0988). Each symbol and line describe the behaviors of each exposure concentration condition. The exposure concentrations (CFU/mL) of each *C. jejuni* strain were approximately 10^3 (circle), 10^4 (insert triangle), 10^5 (triangle), 10^6 (square), 10^7 (plus), and 10^8 (cross).

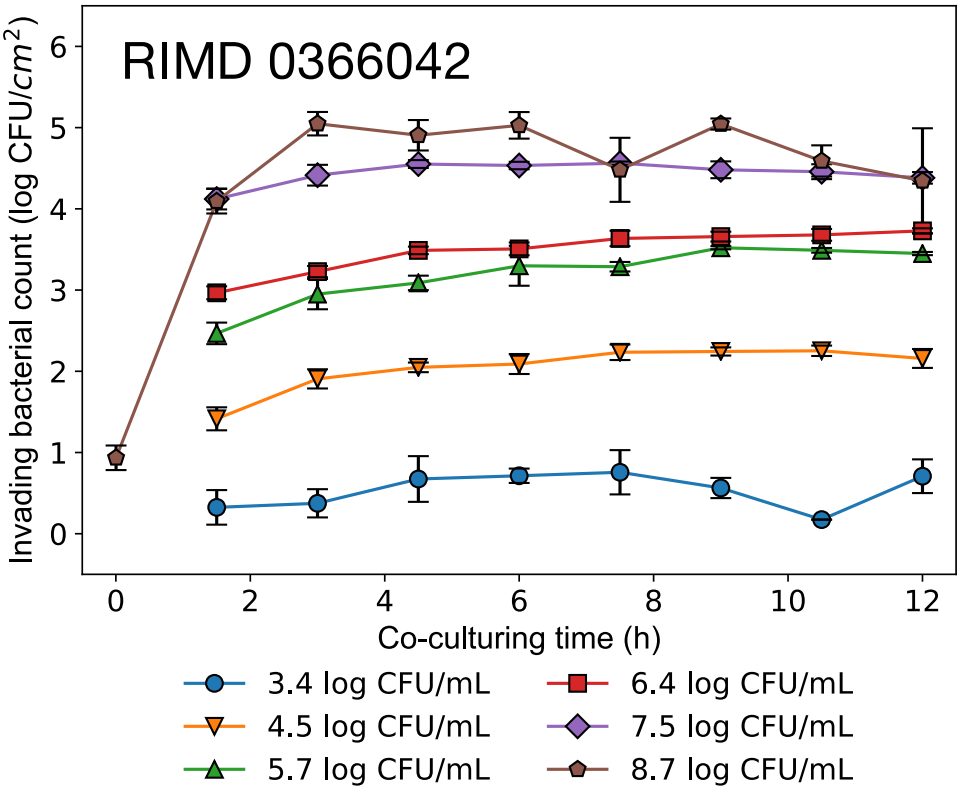


Fig. 5-2. Differences in the number of invading different strains of *Campylobacter jejuni* (RIMD 0366042) into monolayer-cultured Caco-2 cells (RCB0988). Each symbol and line describe the behaviors of each exposure concentration condition. The exposure concentrations (CFU/mL) of each *C. jejuni* strain were approximately 10^3 (circle), 10^4 (insert triangle), 10^5 (triangle), 10^6 (square), 10^7 (plus), and 10^8 (cross).

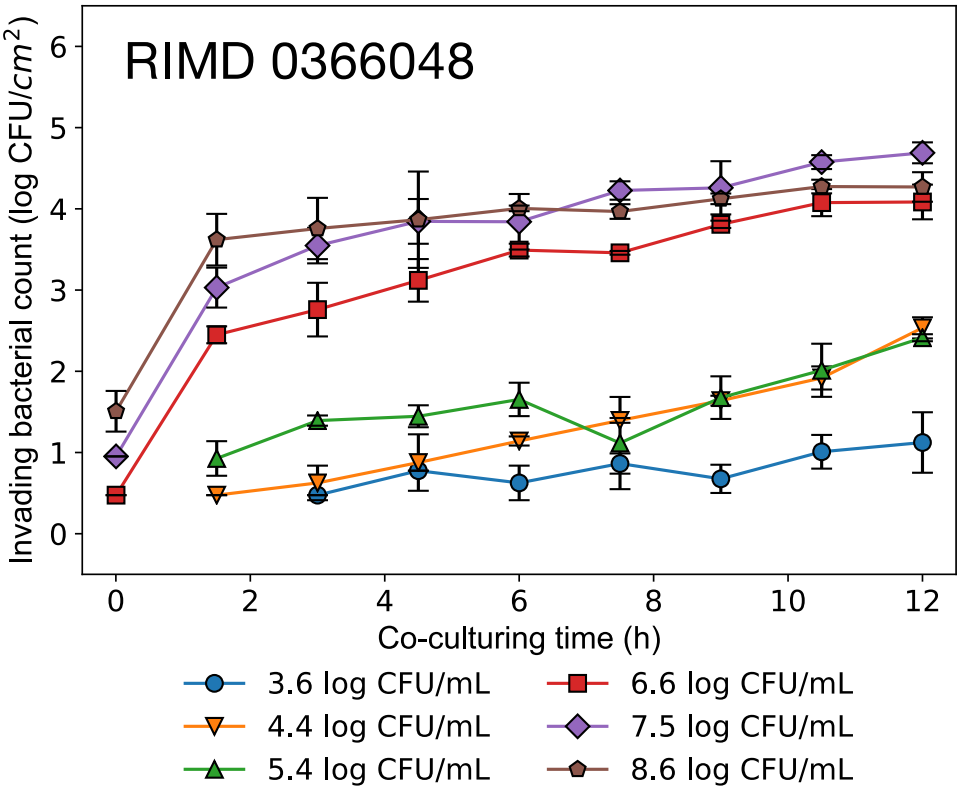


Fig. 5-3. Differences in the number of invading different strains of *Campylobacter jejuni* (RIMD 0366048) into monolayer-cultured Caco-2 cells (RCB0988). Each symbol and line describe the behaviors of each exposure concentration condition. The exposure concentrations (CFU/mL) of each *C. jejuni* strain were approximately 10^3 (circle), 10^4 (insert triangle), 10^5 (triangle), 10^6 (square), 10^7 (plus), and 10^8 (cross).

Comparing the invading counts and the invading ratio, it showed that the invasion ratio (invading bacterial count divided by total exposed bacterial count) did relatively not tend to depend on the exposure concentration except for the highest dose (8.6–8.7 log CFU/mL; Fig. 5-4, 5-5 and 5-6), although the two-way ANOVA has statistically indicated the significant influence of the concentration factors ($p < 0.05$). The invasion ratios of each *C. jejuni* strain were approximately -2.0 (1.0%) for >1.5 h exposure.

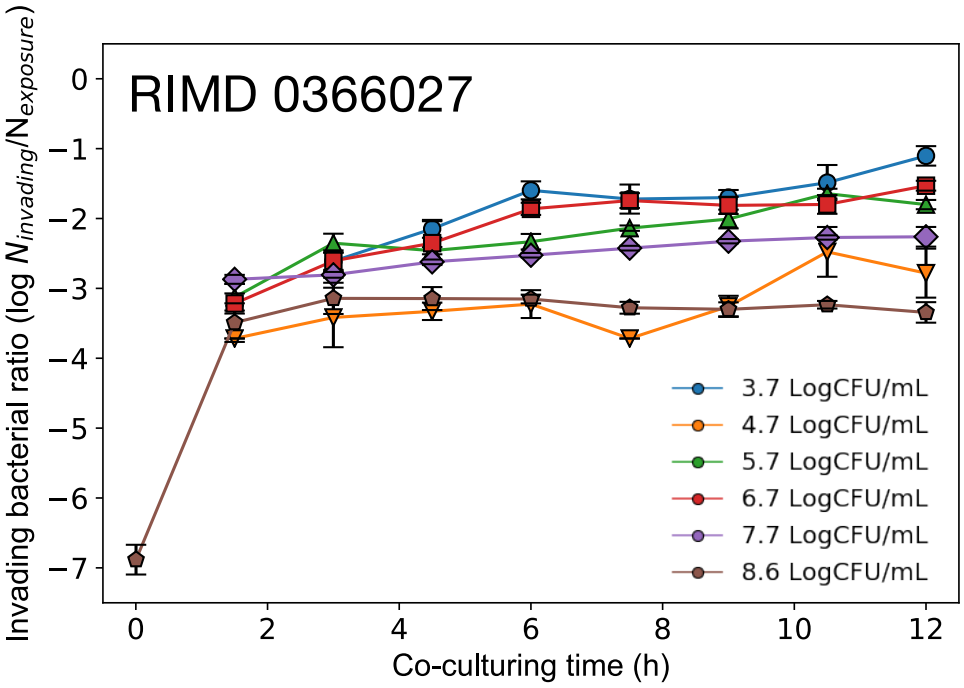


Fig. 5-4. Differences in invading *Campylobacter jejuni* (RIMD 0366027) ratios into monolayer-cultured Caco-2 cells (RCB0988). Each symbol and line describe the behaviors of each exposure concentration condition as in Fig. 5-1.

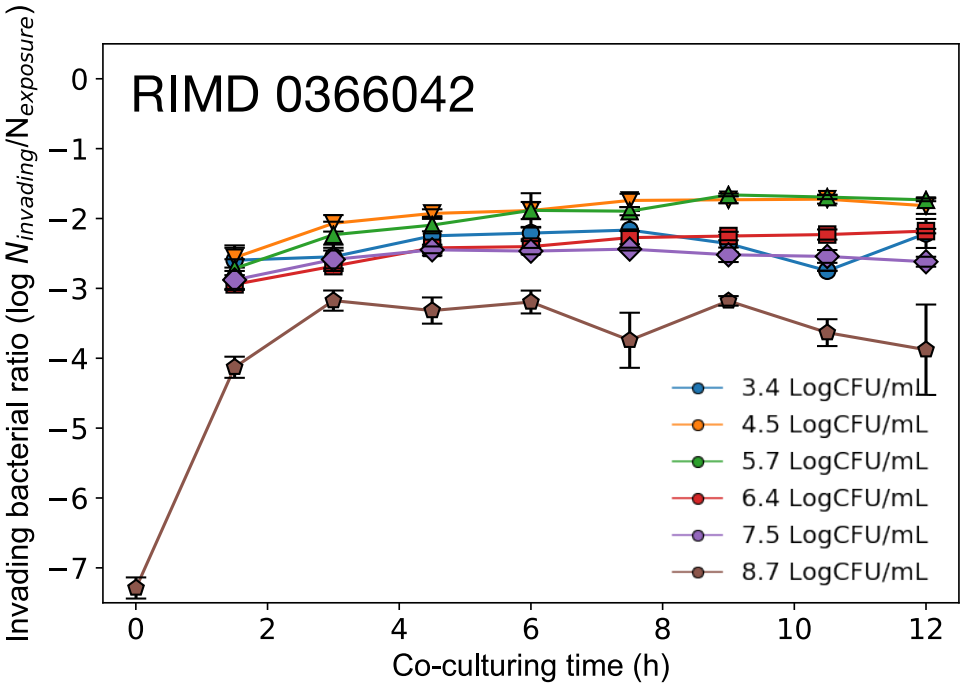


Fig. 5-5. Differences in invading *Campylobacter jejuni* (RIMD 0366042) ratios into monolayer-cultured Caco-2 cells (RCB0988). Each symbol and line describe the behaviors of each exposure concentration condition as in Fig. 5-2.

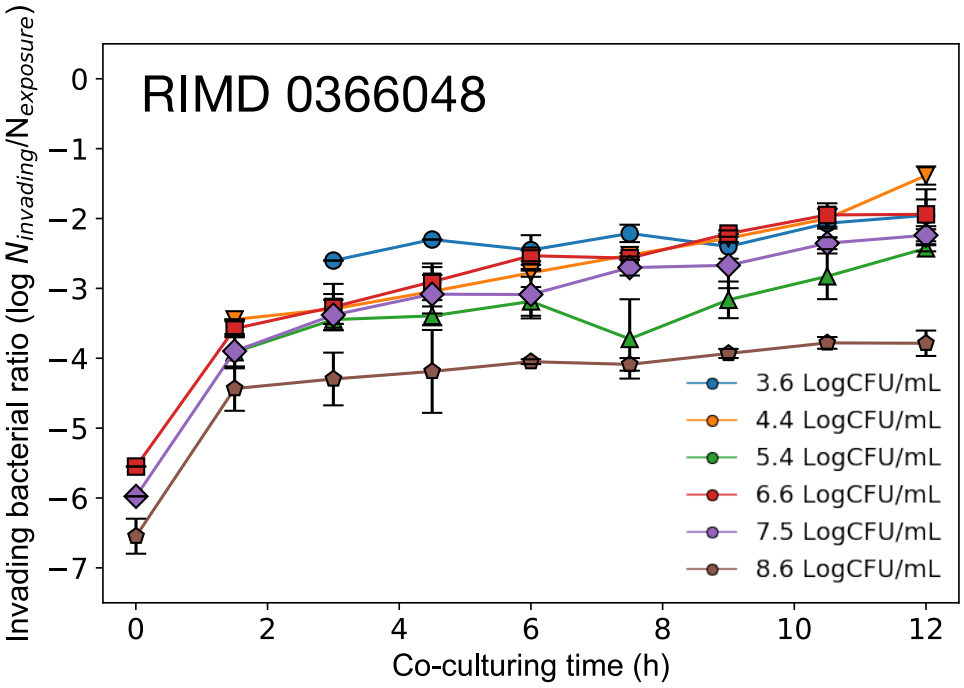


Fig. 5-6. Differences in invading Campylobacter jejuni (RIMD 0366048) ratios into monolayer-cultured Caco-2 cells (RCB0988). Each symbol and line describe the behaviors of each exposure concentration condition as in Fig. 5-3.

5.3.2. Bayesian inference for model parameters for invading C. jejuni

The model parameters for invasion of C. jejuni were successfully estimated by Bayesian inference. The mean values and standard deviations of each parameter derived by the Bayesian estimation and R-hat values representing the convergence of the parameter distribution estimates are summarized in Table 5-1. The estimated posterior distributions converged successfully because the R-hat values for all parameters were lower than 1.1. Fig. 5-7, 5-8 and 5-9 shows the distributions of the estimated parameters and scatter plots and correlation coefficients between parameters. There was a negative correlation between $Log\ N_{\max}$ and $Log\ \mu$ ($-0.79 \leq R \leq -0.84$; R: correlation coefficient), whereas σ was correlated with neither factor ($-0.04 \leq R \leq 0.04$). Fig. 5-10, 5-11 and 5-12 illustrates the changes in invading C. jejuni counts into Caco-2 cells over time based on the estimated parameters and experimentally observed values. The colored gradation ranges from dark to

pale in Fig. 5-10, 5-11 and 5-12, representing 60%, 95%, and 99% prediction intervals in order from the median. Table 5-2 shows the root mean square error of the median predicted value and percentage of observed values within the 99% prediction interval derived from the prediction model of each isolation.

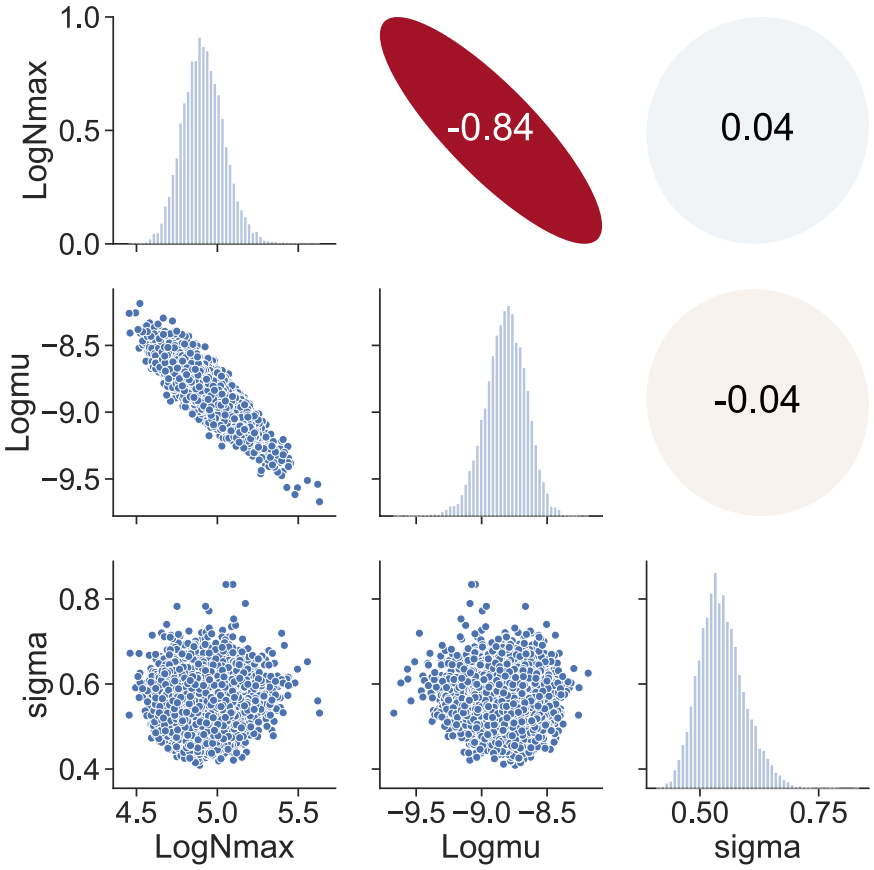


Fig. 5-7. Characteristics of estimated cell-invading model parameters of each bacterial isolate (RIMD 0366027) by Bayesian regression. Relationship of posterior distribution of parameters $\mathbf{Log_{10}}N_{max}$, $\mathbf{Log_{10}}\mu$, and σ (under the diagonal), corresponding histograms (on the diagonal), and correlation coefficients (over the diagonal).

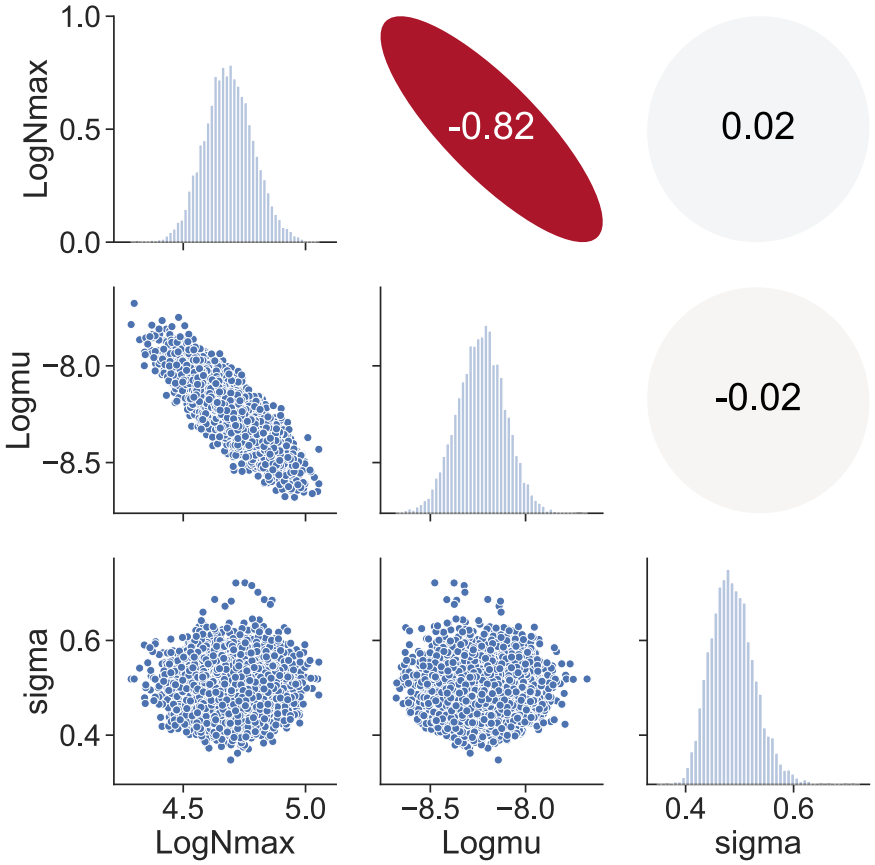


Fig. 5-8. Characteristics of estimated cell-invading model parameters of each bacterial isolate (RIMD 0366042) by Bayesian regression. Relationship of posterior distribution of parameters $\mathbf{Log_{10}}N_{max}$, $\mathbf{Log_{10}}\mu$, and σ (under the diagonal), corresponding histograms (on the diagonal), and correlation coefficients (over the diagonal).

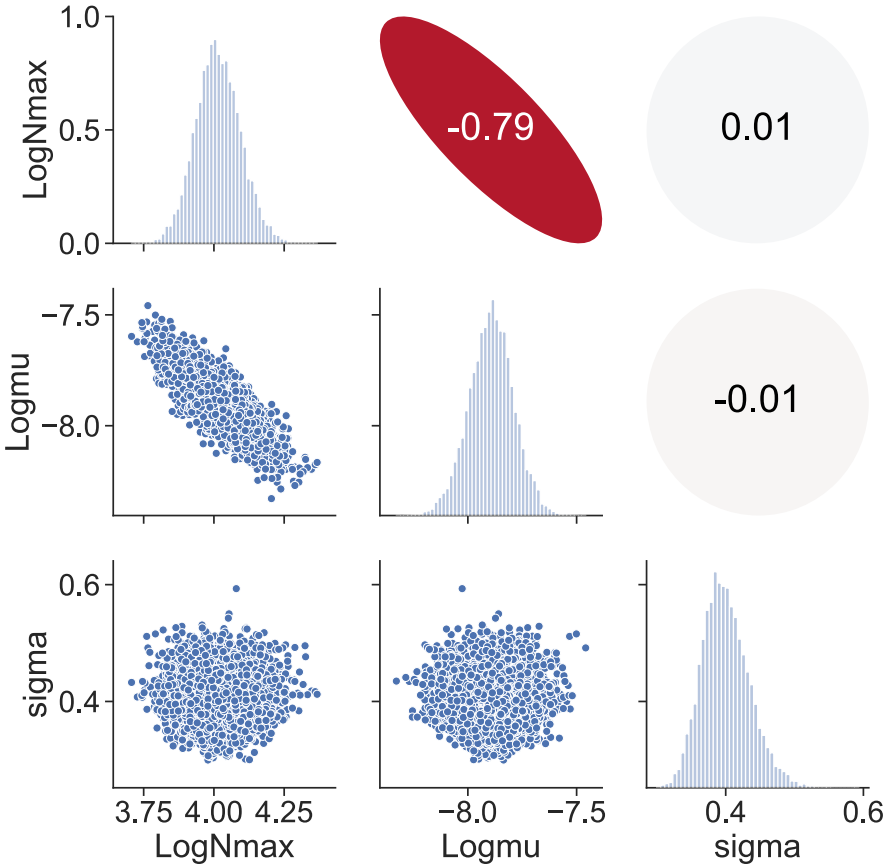


Fig. 5-9. Characteristics of estimated cell-invading model parameters of each bacterial isolate (RIMD 0366048) by Bayesian regression. Relationship of posterior distribution of parameters $\mathbf{Log_{10}}N_{max}$, $\mathbf{Log_{10}}\mu$, and σ (under the diagonal), corresponding histograms (on the diagonal), and correlation coefficients (over the diagonal).

Table 5-1 Parameter values and R-hat values of the estimated model of each isolate

	$Log\ N_{\max}$			$Log\ \mu$			σ		
	Mean	S.D.	R-hat	Mean	S.D.	R-hat	Mean	S.D.	R-hat
RIMD 0366027	4.9	0.13	1.0	-8.8	0.16	1.0	0.55	0.05	1.0
RIMD 0366042	4.7	0.10	1.0	-8.2	0.13	1.0	0.49	0.04	1.0
RIMD 0366048	4.0	0.08	1.0	-7.89	0.10	1.0	0.40	0.03	1.0

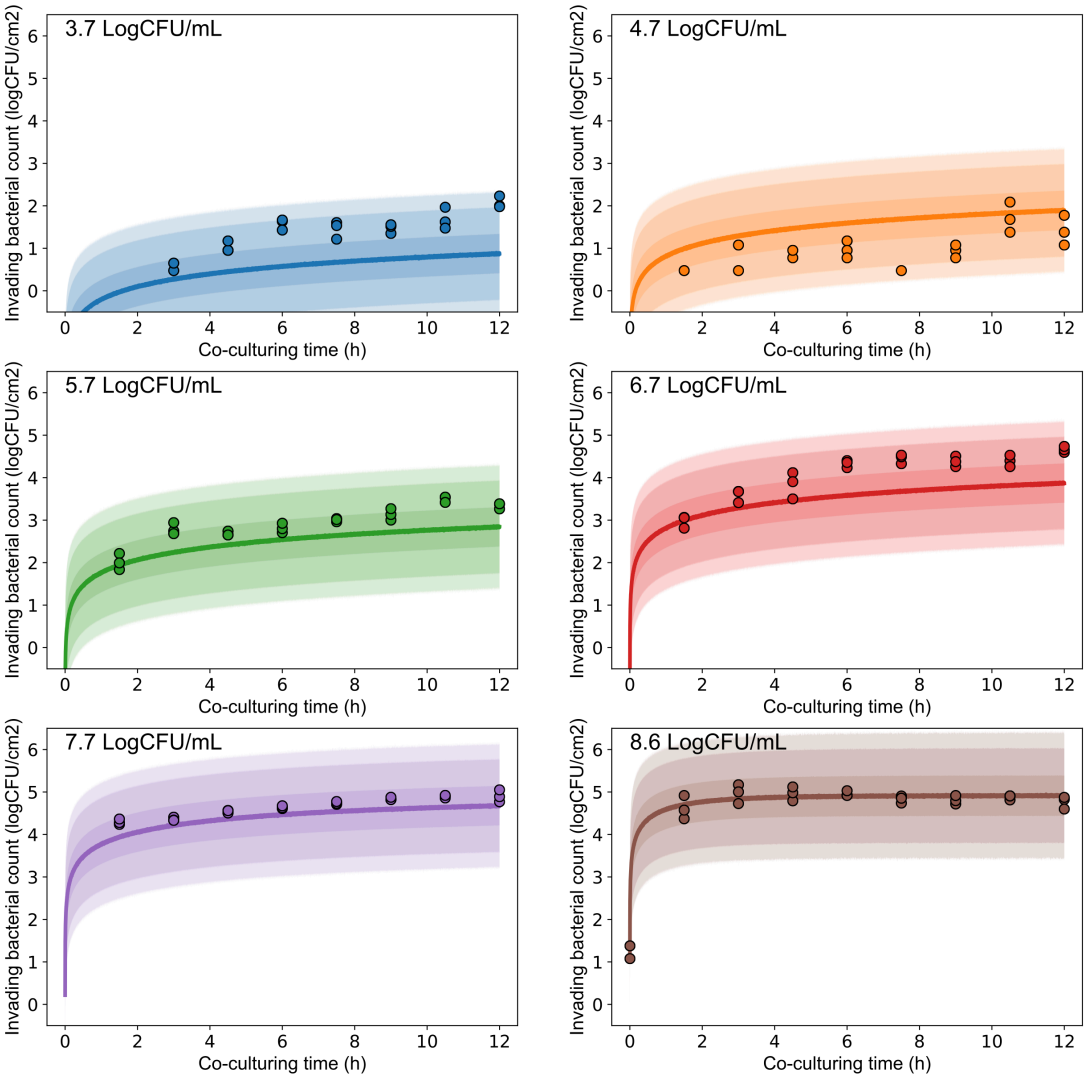


Fig. 5-10. Estimated (curves and ranges) and observed (point) invading bacterial counts of *C. jejuni* (RIMD 0366027) into monolayered Caco-2 cells at each exposure bacterial concentration. Painted ranges show 60%, 95%, and 99% prediction intervals, in order from the median.

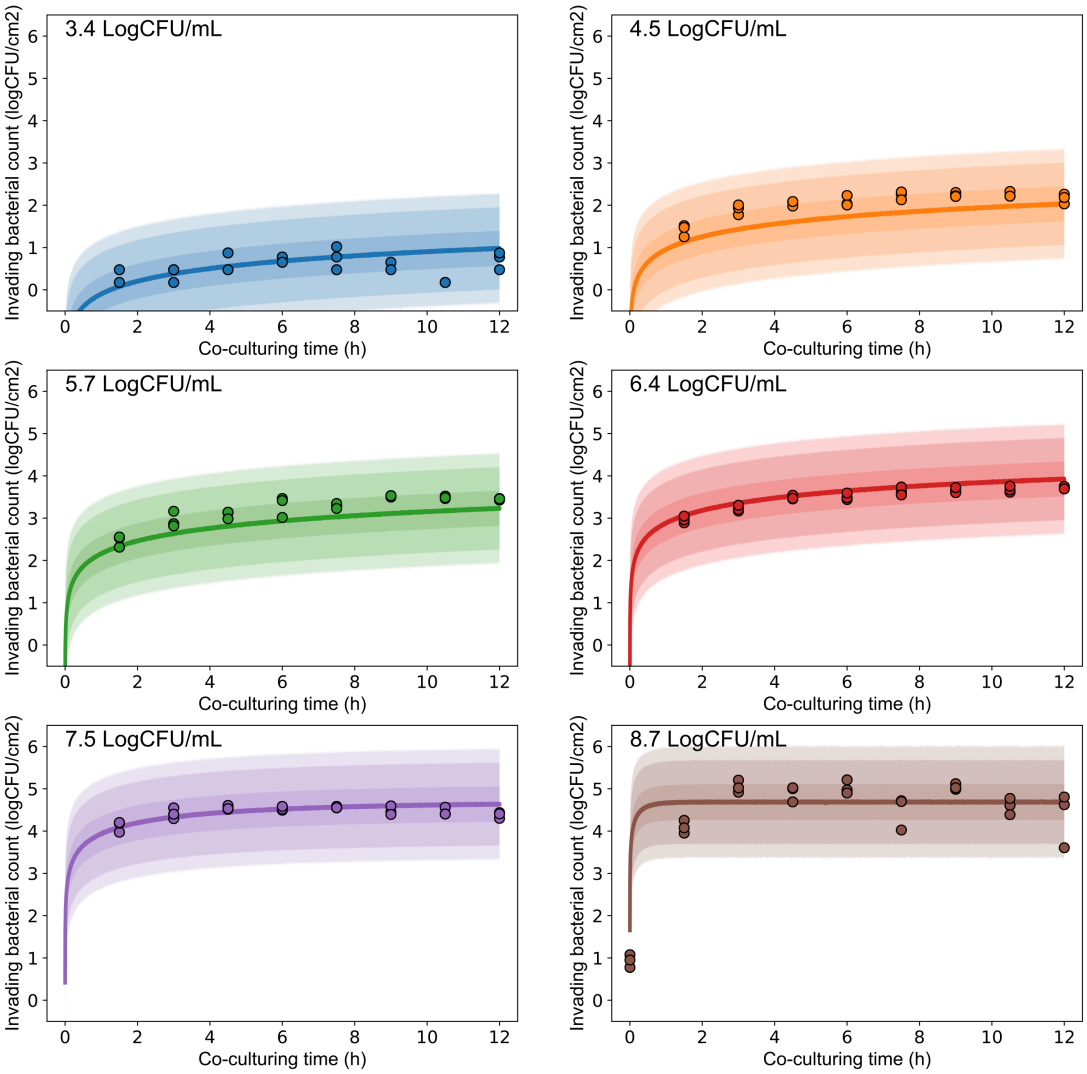


Fig. 5-11. Estimated (curves and ranges) and observed (point) invading bacterial counts of *C. jejuni* (RIMD 0366042) into monolayered Caco-2 cells at each exposure bacterial concentration. Painted ranges show 60%, 95%, and 99% prediction intervals, in order from the median.

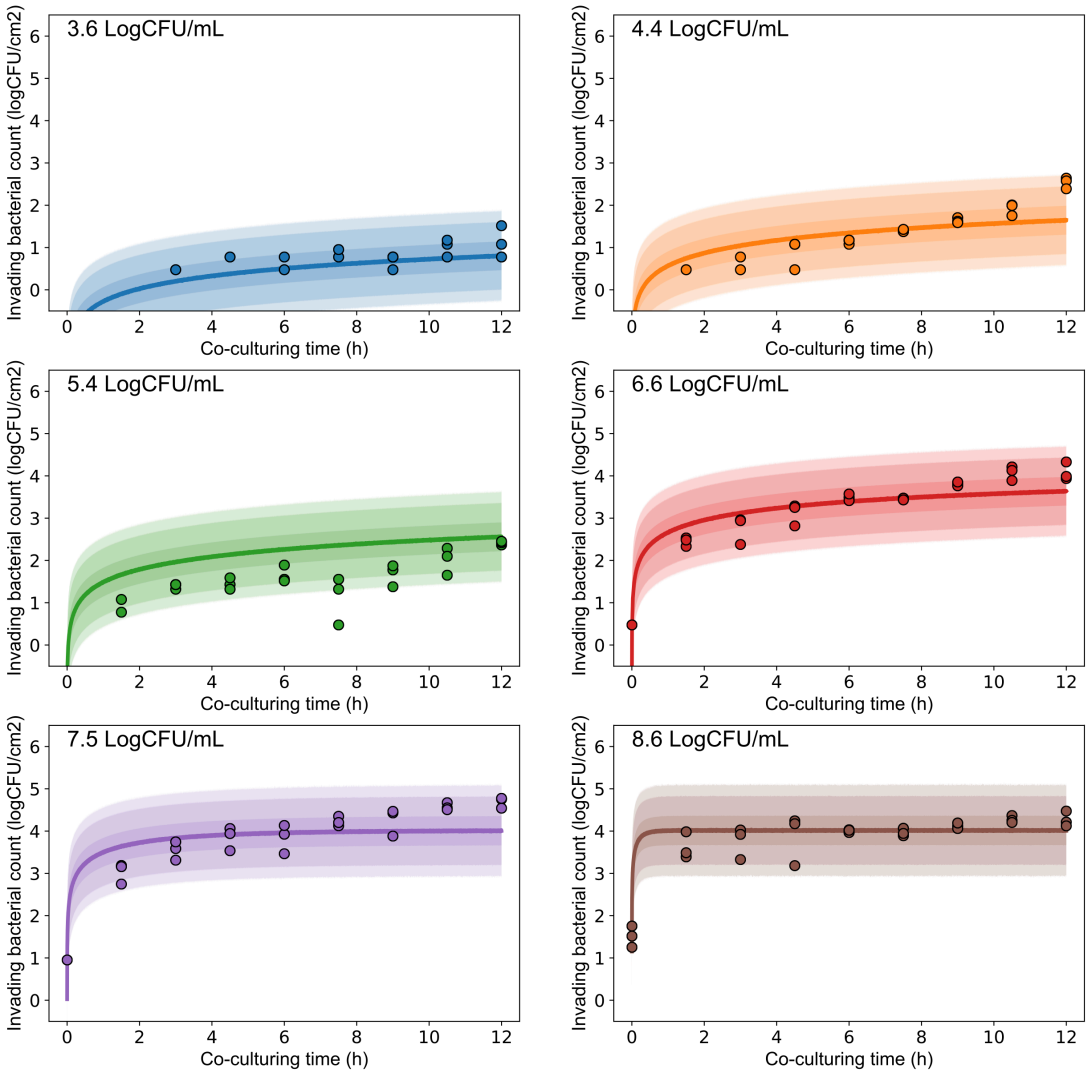


Fig. 5-12. Estimated (curves and ranges) and observed (point) invading bacterial counts of *C. jejuni* (RIMD 0366048) into monolayered Caco-2 cells at each exposure bacterial concentration. Painted ranges show 60%, 95%, and 99% prediction intervals, in order from the median.

Table 5-2 Accuracy of each isolation model in test validation.

	Root mean square error (log CFU)	Accuracy of 99% prediction range (validation data count)
RIMD 0366027	0.53	100% (68)
RIMD 0366042	0.47	96% (75)
RIMD 0366048	0.38	100% (73)

5.4. Discussion

5.4.1. Advantages of the present model

Our results revealing asymptotically increasing changes were similar to those reported in previous studies of the increasing behavior of adherent bacteria counts (Russell & D C Blake, 1994). Other studies on *C. jejuni* cell invasion (Hu & Kopecko, 1999; Mooney et al., 2003) also indicated saturation of invading bacterial counts. Therefore, it could be suggested that the present experiment reproduce general *C. jejuni* adhesion and invasion dynamics into Caco-2 cell layer. In this study, we clarified the temporal changes in invasion behavior of *Campylobacter* into intestinal cells.

According to physiological studies, the mean time required for food to pass through the stomach is 3–4 h (Davis, Hardy, & Fara, 1986), and mean time to reach the colon is 10–12 h (Song, Cho, Jo, Oh, & Kim, 2012). Therefore, the average retention time in the small intestines, which is a microaerobic environment that is most optimal for *C. jejuni*, would be 6–9 h. Thus, the bacterial invasion behavior of intestinal epithelial cells observed in the present study can occur during the actual digestion process. As the ratio of *C. jejuni* invasion into intestinal epithelial cells tended to remain approximately constant at conditions of low exposure concentrations (3.6–7.7 log CFU/mL), bacterial invasion behavior can be predicted at low doses. In addition, the estimation range of the present mathematical model

successfully and accurately described the invading *C. jejuni* counts. No studies have attempted to predict the time-dependent number of cell-invading *C. jejuni* using mathematical models; therefore, our results can be used to study dose-response relationships based on the KEDRF concept.

The present model equation was derived from part of the one-compartment model that estimates chemical absorption behaviors (Bourne, 1995). It was revealed that the rate of change in the *C. jejuni* invasion count depended on the extracellular concentration of dose material, which is same as the nutritional or chemical absorption through human gastrointestinal tracts. Although it seems to be the nutritional absorption originating from only human digestion system is simpler than that of pathogenic invasion into epithelial intestinal cells, which is an interactive bio-phenomenon between human cells and *C. jejuni*, a potential that the absorption model could describe the *C. jejuni* invading into cells was indicated by the result. Additionally, because of the potential of absorption kinetics model describing the cell invasion behavior of *C. jejuni*, there is possibility that the cell invasion behavior of other infectious food poisoning bacteria can also be represented using predictive models of chemical absorption.

The modeling procedure presented in this study based on Bayesian inference separately describes model uncertainty and variability in the parameter and prediction distributions. It has been suggested that prior distributions of the prediction describe experimental uncertainty (19, 20), and the distributions of kinetic parameters describe variability (Aryani, Besten, Hazeleger, & Zwietering, 2015; Besten, Aryani, Metselaar, & Zwietering, 2017; Garre, Zwietering, & Besten, 2020). In this study, by applying normal distribution as a posterior distribution to the prediction (Eq. 5-4), experimental uncertainty in the invading bacterial counts was described as mean values derived from the model equation and standard deviation (σ). In contrast, the parameter distributions describe the variabilities

in biological characteristics. There were two biological variability sources in *C. jejuni* and Caco-2 cells in this study. However, these variability sources were not separately described as parameter distributions, and both variability sources were treated as a combined parameter distribution. The distribution of μ describes variability in the cellular chemotaxis of *C. jejuni* and invasion signal receptor activity of Caco-2 cells. Furthermore, the distribution of N_{max} describes variability in the bacterial invasion capacity of Caco-2 cells. Considering both uncertainty and variability, the present model enables determination of more realistic prediction ranges than those of predictions obtained by non-Bayesian modeling.

Prediction models based on Bayesian estimation can explain the variability and uncertainty of predictive models. The importance of these factors has been proposed in dose-response models (Food and Agriculture Organization of the United Nations/ World Health Organization, 2003), and modeling using Bayesian inference is necessary. Studies have suggested that the Bayesian approach is convenient for estimating the variability and uncertainty in both, exposure assessment and dose-response quantitative microbiological risk assessment of food (Koyama, Aspridou, Koseki, & Koutsoumanis, 2019; Pouillot, Albert, Cornu, & Denis, 2003; Ranta, Lindqvist, Hansson, Tuominen, & Nauta, 2015). Considering the efficacy of describing variability and uncertainty in predicting various bacterial behaviors by Bayesian modeling, Bayesian inference is important not only in dose-response models but also in each key event model for the KEDRF.

5.4.2. Limitations of the present model

The predictive model in this study represents the invasion behavior of C. jejuni into Caco-2 cells; however, this is only an experimental reproduction of the infection mechanism. This is common to all key event models used in the KEDRF. Although several key event models should be combined to estimate the dose-response relationship and its validity should

be assessed by comparison with the human-feeding test and epidemiological estimation data, the validity of human reproduction cannot be assessed only by the experimental methods used in the present study. Whether our in vitro experiments represent the actual intestinal environment remains unclear, and artificial organs can be used to reproduce the intestinal environment, or the conversion factor can develop to correct for the difference.

Only the invasion behavior of C. jejuni into Caco-2 cells was predicted in this study, which does not directly estimate the dose-response relationship. To estimate this relationship, the predictive models for bacterial invading into intestinal cells should be combined with other key events models. Combining all the key models predicting C. jejuni dynamics in the human body, it could be possible to develop a dose-response model of C. jejuni.

5.4.3. How to use the information obtained from the cell invasion model

This estimation model can be used to determine the probability that one or more bacteria will invade cells, $P_{p_invading}$. As at least one or more bacteria must invade intestinal cells to cause infection and disease development, $P_{p_invading}$ can be one indicator of the infection strength $Pp_{invading}$ can be described as follows:

$$\begin{aligned} P_{p_invading} &= 1 - P_{p_not\ invading} \\ &= 1 - \left(P_{s_not\ invading}\right)^{N_{Dose}} \\ &= 1 - \left(1 - P_{s_invading}\right)^{N_{Dose}} \end{aligned} \quad \text{(Eq. 5-5)}$$

where $P_{p_not\ invading}$ denotes the probability that all bacteria will not invade the cell; $P_{s_not\ invading}$ denotes the probability that a single bacterium will not invade the cells; N_{Dose} denotes the dose bacterial count; and $P_{s_invading}$ denotes the probability that a single bacterium will invade the cells. The rate of invading *C. jejuni* ratios into monolayer-cultured Caco-2 cells of 1 cm^2 (Fig. 5-4, 5-5 and 5-6) essentially equal to the probability that a single

bacterium will 1 cm^2 of invade cells, $r_{invading}$. As in Eq. 5-5, $p_{invading}$ can be described using $r_{invading}$:

$$P_{s_invading} = 1 - \left(1 - r_{invading}\right)^S \quad \text{(Eq. 5-6)}$$

where S denotes the surface area of the human small intestine. Substituting Eq. 5-3 for the definition of $r_{invading}$, $r_{invading}$ can be described as follows:

$$r_{invading} = \frac{N_{invading}}{N_{Dose}} = \frac{N_{\max}\left(1-e^{-\mu C_{extracellert}}\right)}{N_{Dose}} = \frac{N_{\max}\left(1-e^{-\frac{\mu N_{Dose} t}{V}}\right)}{N_{Dose}} \quad \text{(Eq. 5-7)}$$

where V denotes the volume of a human small intestine; the extracellular concentration was used as the average concentration in the intestinal fluid, $C_{extraceller} = N_{Dose}/V$. Here, the relationship between $P_{p_invading}$ and $\mathrm{Log}_{10}N_{Dose}$ was numerically derived using the model-estimated invading bacterial count and estimated data on the small intestine from previous studies; S: 32 m^2 from (Helander & Fändriks, 2014); V: 319 mL from (Schliller et al., 2005); t: 7.5 h from (Davis et al., 1986; Song et al., 2012). $P_{p_invading}$ as a function of the ingested dose of *C. jejuni* exhibited the same trend as the reported dose-response relationships (Teunis et al., 2005), as shown in Fig. 5-13; this Fig. also indicates not-significantly differences in $P_{p_invading}$ among strains. A larger μ parameter for each strain was associated with a higher $P_{p_invading}$ of each strain. This suggests that the $P_{p_invading}$ depends on the μ parameter and can indicate the infectious potential of different strains and bacterial species. Although $P_{p_invading}$ was higher than the reported dose-response relationship of *C. jejuni*, other factors will inhibit infection besides invasion into intestinal cells. In this case, other key events in infection, such as inactivation of *C. jejuni* in the stomach or immune system, will be influenced. $P_{p_invading}$ will be useful for deriving the dose-response relationship of an objective pathogen by combining this factor with other key event predictive models.

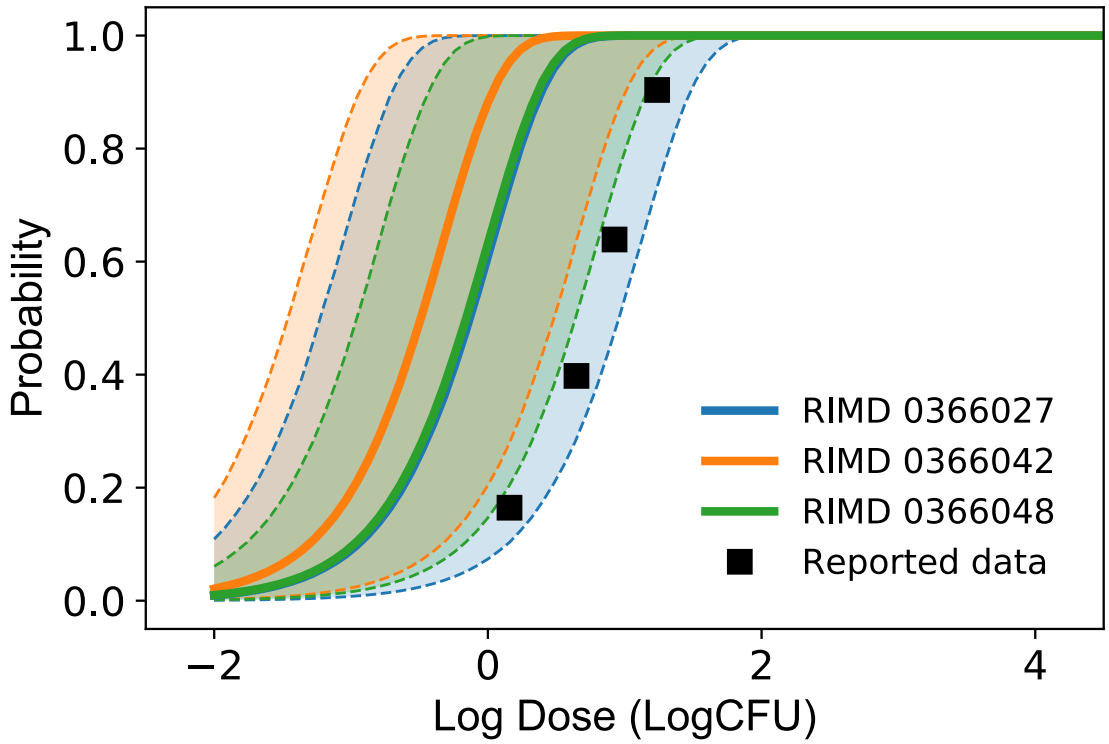


Fig. 5-13. Reported dose-response relationship (Teunis et al., 2005) and relationship between the probability that one or more bacteria of bacterial population invade cells, $P_{p_invading}$ and exposed bacterial counts, $LogN_{Dose}$ of *C. jejuni* (RIMD 0366027, blue; RIMD 0366042, orange; and RIMD 0366048: green). Each colored range indicates the 95% prediction interval derived from the present predictive model of *C. jejuni* invading counts into Caco-2 cells. The reported mean retention time at the small intestine, 7.5 h (Davis et al., 1986; Song et al., 2012), the volume, 319 mL (Schliller et al., 2005), and surface area of small intestine, 32 m^2 (Helander & Fändriks, 2014), were used.

5.4.4. Conclusions

In this study, the invasion behavior of *C. jejuni* into monolayer-cultured intestinal epithelial cells was evaluated *in vitro* and described using a mathematical model based on Bayesian inference, which is useful in constructing a dose-response model based on the KEDRF. Studies are needed to develop a mathematical model to represent the body dynamics of *C. jejuni* at any key event to validate the potential of the KEDRF. This procedure can be

applied to other bacterial species to provide fundamental information for evaluating and developing dose-response models.

5.5. References

Aryani, D. C., Besten, den, H. M. W., Hazeleger, W. C., & Zwietering, M. H. (2015). Quantifying strain variability in modeling growth of Listeria monocytogenes. *International Journal of Food Microbiology*, *208*, 19–29. http://doi.org/10.1016/j.ijfoodmicro.2015.05.006

Besten, den, H. M. W., Aryani, D. C., Metselaar, K. I., & Zwietering, M. H. (2017). Microbial variability in growth and heat resistance of a pathogen and a spoiler: All variabilities are equal but some are more equal than others. *International Journal of Food Microbiology*, *240*, 24–31. http://doi.org/10.1016/j.ijfoodmicro.2016.04.025

Black, R. E., Levine, M. M., Clements, M. L., Hughes, T. P., & Blaser, M. J. (1988). Experimental Campylobacter jejuni Infection in Humans. *The Journal of Infectious Diseases*, *157*(3), 472–479. http://doi.org/10.1093/infdis/157.3.472

Bourne, D. W. A. (1995). Mathematical modeling of pharmacokinetic data (pp. 1–22). CRC Press.

Buchanan, R. L., Havelaar, A. H., Smith, M. A., Whiting, R. C., & Julien, E. (2009). The Key Events Dose-Response Framework: its potential for application to foodborne pathogenic microorganisms. *Critical Reviews in Food Science and Nutrition*, *49*(8), 718–728. http://doi.org/10.1080/10408390903116764

Dasti, J. I., Tareen, A. M., Lugert, R., Zautner, A. E., & Groß, U. (2010). Campylobacter jejuni A brief overview on pathogenicity-associated factors and disease-mediating mechanisms. *International Jl of Medical Microbiology*, *300*(4), 205–211. http://doi.org/10.1016/j.ijmm.2009.07.002

Davis, S. S., Hardy, J. G., & Fara, J. W. (1986). Transit of pharmaceutical dosage forms through the small intestine. *Gut*, *27*(8), 886–892. http://doi.org/10.1136/gut.27.8.886

Evans, M. R., Roberts, R. J., Ribeiro, C. D., Gardner, D., & Kembrey, D. (1996). A milk-borne campylobacter outbreak following an educational farm visit. *Epidemiology & Infection*, *117*(3), 457–462. http://doi.org/10.1017/S0950268800059112

Food and Agriculture Organization of the United Nations/ World Health Organization. (2003). Microbiological risk assessment series 3: hazard characterization for pathogens in food and water, 1–76.

Food and Agriculture Organization of the United Nations/ World Health Organization, World Health Organization. (2003). Microbiological risk assessment series 3: hazard characterization for pathogens in food and water, 1–76.

Garre, A., Zwietering, M. H., & Besten, den, H. M. W. (2020). Multilevel modelling as a tool to include variability and uncertainty in quantitative microbiology and risk assessment. Thermal inactivation of Listeria monocytogenes as proof of concept. *Food Research International*, *137*, 109374. http://doi.org/10.1016/j.foodres.2020.109374

Helander, H. F., & Fändriks, L. (2014). Surface area of the digestive tract – revisited. *Scandinavian Journal of Gastroenterology*, *49*(6), 681–689. http://doi.org/10.3109/00365521.2014.898326

Hu, L., & Kopecko, D. J. (1999). Campylobacter jejuni 81-176 Associates with Microtubules and Dynein during Invasion of Human Intestinal Cells. *Infection and Immunity*, *67*(8), 4171–4182. http://doi.org/10.1128/IAI.67.8.4171-4182.1999

Julien, E., Boobis, A. R., Olin, S. S., The ILSI Research Foundation Threshold Working

Group. (2009). The Key Events Dose-Response Framework: A Cross-Disciplinary Mode-of-Action Based Approach to Examining Dose-Response and Thresholds. *Critical Reviews in Food Science and Nutrition*, *49*(8), 682–689. http://doi.org/10.1080/10408390903110692

Kaakoush, N. O., Castaño-Rodríguez, N., Mitchell, H. M., & Man, S. M. (2015). Global Epidemiology of Campylobacter Infection. *Clinical Microbiology Reviews*, *28*(3), 687–720. http://doi.org/10.1128/CMR.00006-15

Koyama, K., Aspridou, Z., Koseki, S., & Koutsoumanis, K. (2019). Describing Uncertainty in Salmonella Thermal Inactivation Using Bayesian Statistical Modeling. *Frontiers in Microbiology*, *10*, 216. http://doi.org/10.3389/fmicb.2019.02239

Krause-Gruszczynska, M., Rohde, M., Hartig, R., Genth, H., Schmidt, G., Keo, T., et al. (2007). Role of the small Rho GTPases Rac1 and Cdc42 in host cell invasion of Campylobacter jejuni. *Cellular Microbiology*, *9*(10), 2431–2444. http://doi.org/10.1111/j.1462-5822.2007.00971.x

Man, S. M. (2011). The clinical importance of emerging Campylobacter species. *Nature Reviews Gastroenterology & Hepatology*, *8*(12), 669–685. http://doi.org/10.1038/nrgastro.2011.191

Medema, G. J., Teunis, P. F. M., Havelaar, A. H., & Haas, C. N. (1996). Assessment of the dose-response relationship of Campylobacter jejuni, 1–11.

Mooney, A., Byrne, C., Clyne, M., Henry, K. J., Sherman, P., & Bourke, B. (2003). Invasion of human epithelial cells by Campylobacter upsaliensis. *Cellular Microbiology*, *5*(11), 835–847. http://doi.org/10.1046/j.1462-5822.2003.00325.x

Pouillot, R., Albert, I., Cornu, M., & Denis, J.-B. (2003). Estimation of uncertainty and variability in bacterial growth using Bayesian inference. Application to Listeria monocytogenes. *International Journal of Food Microbiology*, *81*(2), 87–104. http://doi.org/10.1016/S0168-1605(02)00192-7

Rahman, S. M. A., Munther, D., Fazil, A., Ben Smith, & Wu, J. (2016). Unraveling the dose-response puzzle of *L. monocytogenes*: A mechanistic approach. *Infectious Disease Modelling*, *1*(1), 101–114. http://doi.org/10.1016/j.idm.2016.09.001

Ranta, J., Lindqvist, R., Hansson, I., Tuominen, P., & Nauta, M. (2015). A Bayesian approach to the evaluation of risk-based microbiological criteria for Campylobacter in broiler meat. *The Annals of Applied Statistics*, *9*(3), 1415–1432. http://doi.org/10.1214/15-AOAS845

Russell, R. G., & D C Blake, J. R. (1994). Cell association and invasion of Caco-2 cells by Campylobacter jejuni. *Infection and Immunity*, *62*(9), 3773–3779.

Schliller, C., Fröhlich, C. P., Giessmann, T., Siegmund, W., Mönnikes, H., Hosten, N., & Weischies, W. (2005). Intestinal fluid volumes and transit of dosage forms as assessed by magnetic resonance imaging. *Alimentary Pharmacology & Therapeutics*, *22*(10), 971–979. http://doi.org/10.1111/j.1365-2036.2005.02683.x

Song, B. K., Cho, K. O., Jo, Y., Oh, J. W., & Kim, Y. S. (2012). Colon transit time according to physical activity level in adults. *Journal of Neurogastroenterology and Motility*, *18*(1), 64–69. http://doi.org/10.5056/jnm.2012.18.1.64

Szymanski, C. M., King, M., Haardt, M., & Armstrong, G. D. (1995). Campylobacter jejuni motility and invasion of Caco-2 cells. *Infection and Immunity*, *63*(11), 4295–4300.

Teunis, P., van den Brandhof, W., Nauta, M., Wagenner, J., van den Kerkhof, H., & van Pelt, W. (2005). A reconsideration of the *Campylobacter* dose–response relation. *Epidemiology & Infection*, *133*(4), 583–592. http://doi.org/10.1017/S0950268805003912

Verhoeckx, K., Cotter, P., López-Expósito, I., Kleiveland, C., Lea, T., Mackie, A., et al. (2015). The Impact of Food Bio-Actives on Gut Health. library.oapen.org

.

World Health Organization. (2009). Risk assessment of *Campylobacter* spp. in broiler chickens: technical report.

Chapter 6 Development of dose-response model for *Campylobacter jejuni* based on human digestive systems

6.1. Introduction

Dose-response models for foodborne pathogens play an important role for assessment and managing risk of food poisoning or foodborne infections. Food safety management systems are developed to systematically prevent outbreaks of foodborne illness. A quantitative approach to food safety control can be realized by development and implementation of quantitative microbial risk assessments (QMRA) for food products in existing safety management systems (Zwietering, 2009). While the exposure assessment of the QMRA helps predict the bacterial response during processing and distribution of foods, dose-response models play a key role in risk characterization, which estimates the probability of illness or infection from pathogen intake counts derived from the exposure assessment. Three main approaches for developing dose-response relationships of foodborne pathogens are available: testing with human volunteers, animal tests, and epidemiological estimation from outbreak data. Although each approach has strengths and limitations, all three approaches have substantial uncertainty owing to the inherent variability in the pathogen, host, and food vehicle (Buchanan, Havelaar, Smith, Whiting, & Julien, 2009; Julien, Boobis, Olin, The ILSI Research Foundation Threshold Working Group, 2009). In addition, it is generally difficult to collect data at a low pathogen concentration to which a person is exposed, and it is difficult to collect relevant data during the response (Buchanan et al., 2009).

An alternative approach has been suggested for establishing dose-response models; the Key Events Dose-Response Framework (KEDRF) (Julien et al., 2009). KEDRF is an approach based on important infection mechanisms causing foodborne illness, called key

events, and available data from digestive systems to gain insight into dose-response relationships. As the method for estimating the dose-response relationship is based on infection mechanisms, KEDRF is expected to have several advantages, such as potential of responding to low-dose infection, considering host health, sex, pathogen strain, and variability.

Few studies have focused on developing dose-response models based on infection mechanisms or key event models describing pathogen response in humans. Koseki et al. (Shige Koseki, Mizuno, & Sotome, 2011) and Koyama et al. (2021) developed key event models that dynamically describe the death of some pathogens in simulated gastric fluid mimicking stomach digestion. Pujol et al. (Pujol, Eisenberg, Haas, & Koopman, 2009) described immune capacities until the occurrence of infection. Pathogens, such as *Listeria*, *Salmonella*, and *Campylobacter,* adhere to and invade intestinal epithelial cells and cause disease (Ribet & Cossart, 2015). Caco-2 cells are commonly used to observe the adhesion and invasion of pathogens to intestinal epithelial cells *in vitro*. We recently developed a model describing the invasion kinetics of pathogens in human intestinal cells (Abe, Koyama, & Koseki, 2021). Although one study has previously estimated the dose-response relationship of *Listeria* through mathematical modeling of bacterial colonization in the human intestine after reductions in the human stomach (Rahman, Munther, Fazil, Ben Smith, & Wu, 2018), this mechanistic dose-response model does not consider cell invasion by the pathogen in terms of infection and that pathogen colonization in the intestines does not always cause infection. The final dose-response relationship needs to describe illness and modeling competitions with the immune system after the invasion of tissues by pathogens and the onset of illness. In these respects, KEDRF is still a developing concept. It is desirable to develop a more sophisticated key events dose-response model to further elucidate the reality of foodborne illness.

It is necessary to incorporate the concept of bioaccessibility and bioactivity in KEDRF to develop a more sophisticated mechanistic dose-response model. The term "bioaccessibility," along with "bioavailability," is a key concept to ascertain nutritional efficiency of food and food formulas developed to improve human health in terms of pharmacokinetics and nutrition (Fernández-García, Carvajal-Lérida, & Pérez-Gálvez, 2009). "Bioaccessibility" is defined as the number of chemicals or nutrients that are released from the gastrointestinal tract tissue, which are made available through blood vessels via absorption. It is evaluated using *in vitro* digestion models, generally simulating gastric or small intestinal digestion, as revealed through a Caco-2 cell uptake test (Galanakis, 2016). While the "Bioaccessibility", "Bioactivity" is the specific effect upon exposure to a substance. If these two concepts are considered for a pathogen, "Bioaccessibility" represents infection with the pathogen and "Bioactivity" represents the onset of illness caused by the pathogen. Infectious foodborne pathogens invade the tissues through the stomach and intestines, causing inflammation in the gastrointestinal tract, or travel to the affected area, such as blood or lymph, and cause symptoms. Pathogens also trigger physiological reactions through the same pathways as nutrients and chemicals (there is also an interaction between pathogen and host, but to simplify). As mentioned in the above paragraphs, conventional dose-response models for foodborne pathogens have not taken into account the infection mechanism in human body. On the other hand, in nutrition and pharmacokinetics, the movement of nutrients and medications in the body has been considered for predicting the effect of them. It would be also necessary to consider the infection mechanism in the human body for estimating more details of the dose-response relationship of foodborne pathogens. At present, it is difficult to experimentally replicate and model the competition between pathogens and immune cells, but the pathways for invading intestinal tissues have been reproduced *in vitro*. The definition of infection is based on bioaccessibility, including

invading into the body or retention in the intestinal tract. On the other hand, the definition of illness or virulence indicates the adverse effects in the human body corresponding to bioactivity. Although the two terms have different definitions, the infection probability should be higher than the illness probability. In this manner, assessing the bioaccessibility and bioactivity of pathogens would be essential to assume a dose-response relationship based on the KEDRF concept.

This study aimed to develop an alternative dose-response model of *Campylobacter jejuni*, which is one of the most dangerous pathogenic bacteria, based on KEDRF, considering food type and host age. We estimated the invasion probability, defined as the probability of infection, accounting for food type in the gastric retention time and age in the gastric pH. The estimated infection probability was compared and validated using actual epidemiological data.

6.2. Materials and methods

6.2.1. Modeling for postprandial gastric pH change among younger and elder individuals

The postprandial pH changes among young and elderly individuals were expressed separately in a mathematical model. The exponential models (Eq. 6-1) were fitted to the reported pH changes after a standard meal (1000 kcal) for young (Dressman et al., 1990) and elderly individuals (Russell et al., 1993):

$$pH_{(t)} = pH_0 e^{-k_{pH} t} + pH_{min} \quad (6\text{-}1),$$

where $pH_{(t)}$ denotes the pH at a time after food intake, t; pH_0 denotes pH immediately after a meal; k_{pH} denotes the decreasing rate of pH; pH_{min} denotes the convergence value of pH. The parameters were estimated using Bayesian inference through pystan (ver. 2.19.). The normal distribution, which is generally used, was adopted as the prior distribution of pH, as distributions of the reported data were contrasting.

6.2.2. Pathogen survival in stomach with between- and within-strain variability

The survival of *C. jejuni* was described using a previously reported dynamic survival model of *C. jejuni* (Eq. 6-2) under artificial gastric conditions using Bayesian inference (Koyama et al., 2021). The between- and within-strain variability reduction model was constructed from the data of 11 strains of *C. jejuni* (RIMD 0366026, RIMD 0366027, RIMD 0366028, RIMD 0366029, RIMD 0366042, RIMD 0366043, RIMD 0366044, RIMD 0366048, RIMD 0366049, RIMD 0366050, and RIMD 0366051).

$$log_{10}\, S_{g(t+\Delta t)} = -\left(\frac{t^{*}+\Delta t}{\delta_{(\overline{pH})}}\right)^{p_{(\overline{pH})}} \tag{6-2. a}$$

$$t^{*} = \delta_{(\overline{pH})}\left(-log_{10}\, S_{g(t)}\right)^{\frac{1}{p}}$$

$$\begin{cases} ln(\delta_{(\overline{pH})}) = a \times pH + b \\ ln(p_{(\overline{pH})}) = e \times pH + f \end{cases} \tag{6-2. b}$$

$$\begin{pmatrix} a_k \\ b_k \\ e_k \\ f_k \end{pmatrix} \sim MultiNormal_Cholesky\left(\begin{pmatrix} a_0 \\ b_0 \\ e_0 \\ f_0 \end{pmatrix}, \Sigma_{chol}\right) \tag{6-2. c}$$

where $S_{g(t)}$ denotes the bacterial survival ratio defined as the ratio of the surviving bacterial counts divided by the initial bacterial counts; p denotes the power parameter of the Weibull model; δ denotes the time of the first decimal reduction of the Weibull model; and $\overline{pH}$ denotes the mean pH during the time intervals from t to $t + \Delta t$ as $\overline{pH} = \frac{pH_{(t)}+pH_{(t+\Delta t)}}{2}$. The parameters of the primary model, δ and p, were defined using the parameters of the secondary model (a_k, b_k, e_k, f_k), following the multivariate normal distribution of Cholesky parameterization, in which Σ_{chol} is the Cholesky factor of the covariance matrix of $log(p_{(k,\overline{pH})})$ and $log(\delta_{(k,\overline{pH})})$ of all strains.

6.2.3. Bacterial transfer to the small intestine

Changes in the gastric retention ratio were described as the cumulative gamma distribution, which is used to describe the waiting time of traffic jams and transmitting times. Comparing the transfer time of solid foods and liquid foods, the effect on the cell invasion ability due to differences in food type was estimated. The changes in gastric retention ratio were described using the following cumulative gamma distribution fitted to the reported change in the gastric retention ratio after solid and liquid meals (Hellström et al., 2006):

$$R_g = 1 - \frac{1}{\Gamma_{(\alpha)}}\gamma_{(\alpha,\beta t)} \quad (6\text{-}3),$$

where R_g is the gastric retention ratio; α is the shape parameter; β is the rate parameter of gamma distribution; $\Gamma_{(\alpha)}$ is the gamma function $\Gamma_{(\alpha)} = \int_0^\infty e^{-u}u^{\alpha-1}\,du$; $\gamma_{(\alpha,\beta t)}$ is the lower incomplete gamma function $\gamma_{(\alpha,\beta t)} = \sum_{k=0}^{\infty}\frac{(\beta t)^{\alpha+k}e^{-\beta t}}{\alpha(\alpha+1)\ldots(\alpha+k)}$.

The combined equation of pH, pathogenic survival, and gastric retention model, as well as the ratio of the surviving pathogen transfer to the intestine, $r_{intestine}$, was described (Eq. 6-4; graphically description: Supplementary Fig. 6-S1), and discretely expressed as shown in Eq. 6-4**b**:

$$r_{intestine,(t)} = \int_0^t S_{g(s)}\frac{dR_g}{ds}\,ds \quad (6\text{-}4.\ a)$$

$$r_{intestine,(t_k)} = \sum_{i=1}^{k}\frac{S_{(t_i)}}{n} \quad (6\text{-}4.\ b)$$

where s denotes an operator; t_i denotes the simulated gastric retention times from the gamma distributions; n denotes the total simulation counts from the gamma distributions; k denotes any natural number between 1 and n. Using Eq. 6-4, the survival pathogen transit counts, $N_{intestinal}$, were derived as follows:

$$N_{intestine} = r_{intestine}N_{dose} \quad (6\text{-}5)$$

where N_{dose} denotes the intake counts of pathogens.

6.2.4. Bacterial invasion in intestinal cells

Invasion of *C. jejuni* was described using a modified predictive model based on a previously reported *C. jejuni* model (Abe et al., 2021) (RIMD 0366027, RIMD 0366042, and RIMD 0366048) applying invasion count, $N_{invading}$, to Caco-2 cells as follows:

$$\frac{d}{dt}N_{invading} = \mu\frac{N_{exposure}-N_{invading}}{V}\left(SN_{max} - N_{invading}\right) \quad (6\text{-}6)$$

where μ, $N_{exposure}$, N_{max}, V, and S denote the cell invasion rate, the pathogen exposure count, the spatial maximum invading pathogen count per 1 cm^2, the volume of intestinal juice (319 mL) (Schliller et al., 2005) and the surface area of the small intestine (32 m^2), respectively (Helander & Fändriks, 2014).

6.2.5. Retention time in the small intestine

The cumulative gamma distribution was fitted to the change in the small intestinal retention ratio, $R_{intestinal}$, as the reported colonic filling ratio was as follows (Read et al., 1986):

$$R_{intestinal} = 1 - \frac{1}{\Gamma_{(\alpha)}}\gamma_{(\alpha',\beta' t)} \quad (6\text{-}7)$$

Considering Eq. 6-7, small intestinal retention time, $t_{intestinal}$, follows the gamma distribution α' as a shape parameter and β' as a rate parameter; $Gamma(\alpha', \beta')$ as follows:

$$t_{intestinal} \sim Gamma(\alpha', \beta') \quad (6\text{-}8)$$

6.2.6. Invasion probability in human tissues

The probability of pathogen invasion into the cells was determined as previously described (Abe et al., 2021). One or more C. jejuni predicted infection probabilities were derived from the models as follows:

$$P_{invading} = 1 - \left(1 - \frac{N_{invading\,(t_{intestinal})}}{N_{Dose}}\right)^{N_{Dose}} \quad (6\text{-}9)$$

Spearman's rank correlation coefficients between $P_{invading}$ and the parameters were established as a sensitivity analysis of the current dose-response model.

6.2.7. Computation

All the computations were calculated under the Anaconda distribution (Python 3.7.7) (See data availability section). All the bayesian inference have been done with No-U-Turn-Sampler MCMC.

6.3. Results

6.3.1. Defining the key events of campylobacteriosis infection

The key events of the infection mechanism for this study were designed on the basis of the KEDRF report (Buchanan et al., 2009). Since it is difficult to quantitatively assess pathogens in the human body tissues such as blood vessels or lymphatic system, this study considered the probability of invasion into the small intestinal endothelial cells as the infection probability. The following were identified as key events: (i) pathogen reduction in the stomach; (ii) transfer to the small intestine from the stomach; (iii) pathogen invasion into small intestinal epithelial cells. The influence of *C. jejuni* growth in intestines were omitted because it is reported that the invasion rate of *C. jejuni* is much faster than *C. jejuni* growth rate in broth medium (Abe et al., 2021). The Fig. 6-1 shows the diagram of the constructed model in this study, and the abbreviations are summarized in Table 6-1. Each key event was modeled by referring to data from literatures, and MCMC (Markov Chain Monte Carlo) simulations were performed to derive the probability of *C. jejuni* invading small intestinal cells based on the developed models.

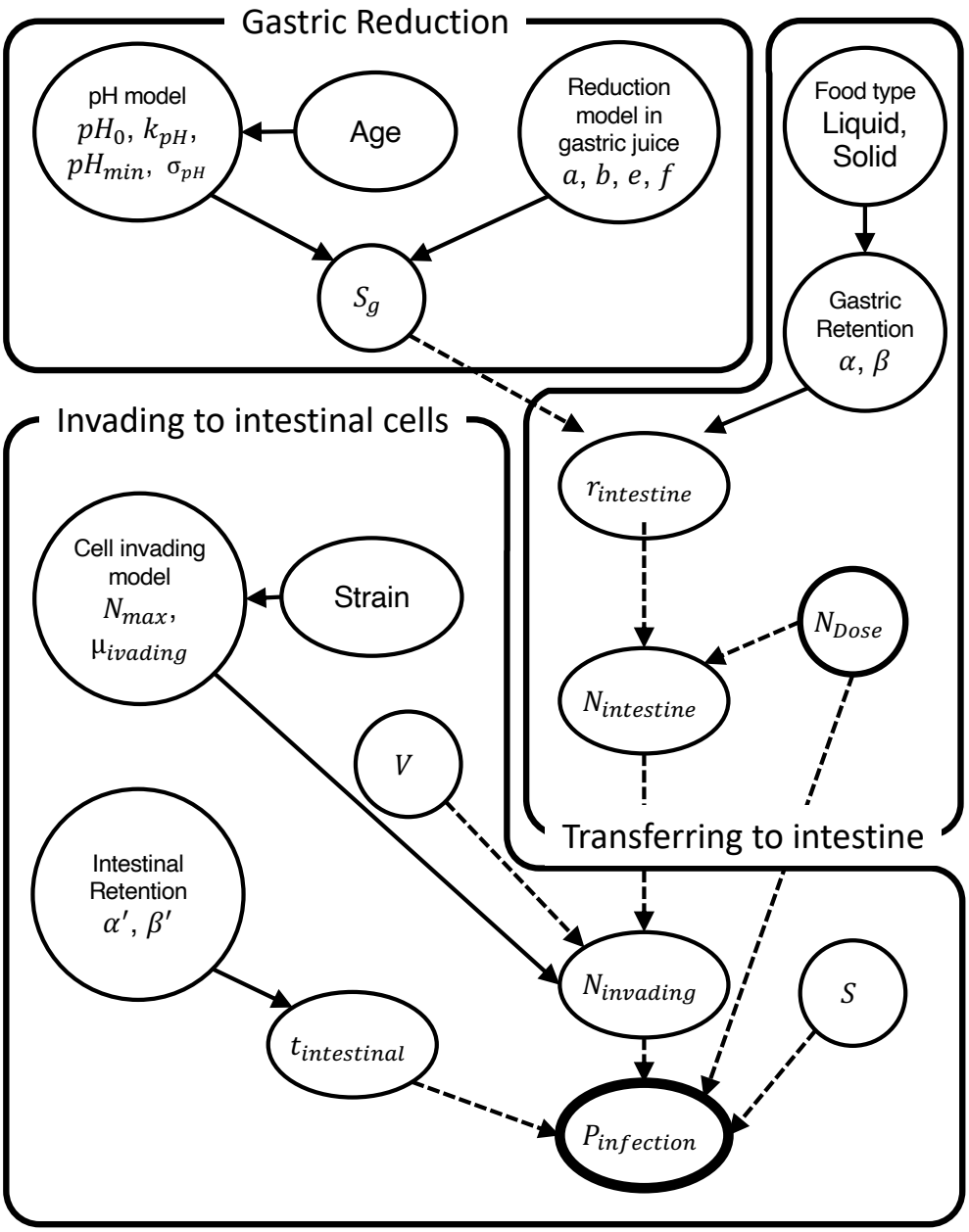


Fig. 6-1. Directed acyclic graph of the model parameters and factors. Solid arrows indicate distributions, dashed arrows deterministic functions. The abbreviations and details of components are summarized in Table 6-1.

Table 6-1. Details of components in the constructed key events dose-response model

Abbreviation	Section	Detail of components	Data source
N_{dose}	Dose	Pathogen count intake	Describing variables
pH_0	pH change of gastric juice after meal	pH immediately after meal	Younger pH: Dressman et al., [19] Elder pH: Russel et al., [20]
k_{pH}		Rate of decrease in pH	
pH_{min}		Minimum pH value	
σ_{pH}		S.D. of pH prediction	
a	Pathogen reduction model in gastric juice	Secondary parameter of δ	Takeoka et al., in submission
b			
e		Secondary parameter of p	
f			
S_g		Survival pathogen ratio in gastric juice	Computables
α	Gastric retention of food	Shape parameter of gamma distribution	Hellström et al., [21]
β		Rate parameter of gamma distribution	
$r_{intestine}$	Transit of pathogen	Survival pathogen transit ratio to intestine	Computables
$N_{intestine}$		Survival pathogen transit count to intestine	Computables
V	Cell invasion of pathogens	Volumes of small intestine	Schiller et al., [22]
N_{max}		Maximum invading counts to 1 cm^2 of cell layer	Abe et al., [6]
μ		Cell-invading rate	
$\sigma_{invading}$		S.D. of invading pathogen count prediction	
S		Surface area of intestine	Helander et al., [23]
α'	Intestinal retention of food	Shape parameter of gamma distribution	Read et al., [24]
β'		Rate parameter of gamma distribution	
$t_{intestinal}$		Intestinal retention time	Computables
$P_{infection}$	Calculation of invading probability	Infection (invading) probability	Objective variables

6.3.2. Gastric bacterial reduction

The reported changes in the pH of young (Dressman et al., 1990) and elderly (Russell et al., 1993) individuals could be successfully described using an exponential model (Fig. 6-2). The reference data were derived from the Heidelberg capsules which measured the gastric pH of 34 young subjects (sex, 18 female, 16 male; range, 21-35 years old) and 79 elderly subjects (sex, 49 female, 31 male; range, 65-83 years old) after a simulated standard

meal consisting of 6 oz of hamburger, 2 slices of bread, 2 oz of hash brown potatoes, 1tbsp each of ketchup and mayonnaises, 1 oz each of tomato and lettuce, and 8 oz of milk (for a total of 1000 kcal) (Dressman et al., 1990; Russell et al., 1993). All the estimated parameters of the exponential model were convergent for pH changes after liquid and solid meals among young and elderly individuals (Supplementary Fig. 6-S2) because the Gelman-Rubin convergence statistic (R-hut value) of parameter distributions was 1.0. The estimation of the fitted exponential model indicated that the changes in the pH in the stomachs of elderly individuals were broader than those of young individuals (Fig. 6-2).

The reduction behaviors of *C. jejuni* in young and elderly people's stomach after meal were calculated based on a reported predictive model for *C. jejuni* reduction in gastric juices (Koyama et al., 2021), and the differences in those were shown to be due to differences in pH (Fig. 6-3). The calculated survival ratio of elderly individuals after ingestion of liquid and solid foods was higher than that of the calculated survival transit ratio of young individuals.

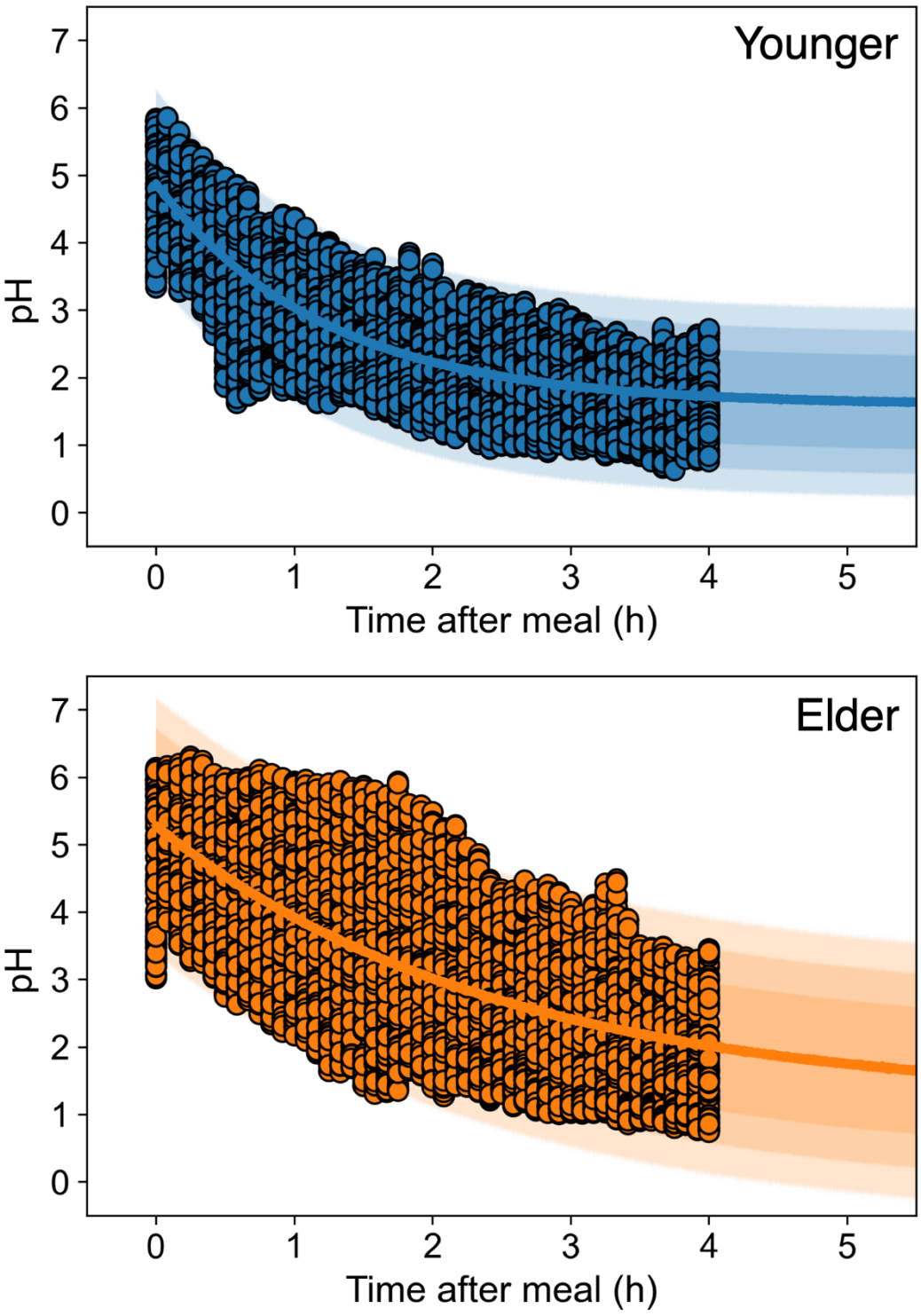


Fig. 6-2. Changes in the observed pH in human stomach after-meal pH data (points) of young (upper; Dressman et al., 1990) and elderly (lower; Russel et al., 1993) people, and the prediction band derived from the exponential model. The estimated parameter traceplots and distributions of Bayesian MCMC in supplementary information (Fig. 6-S2).

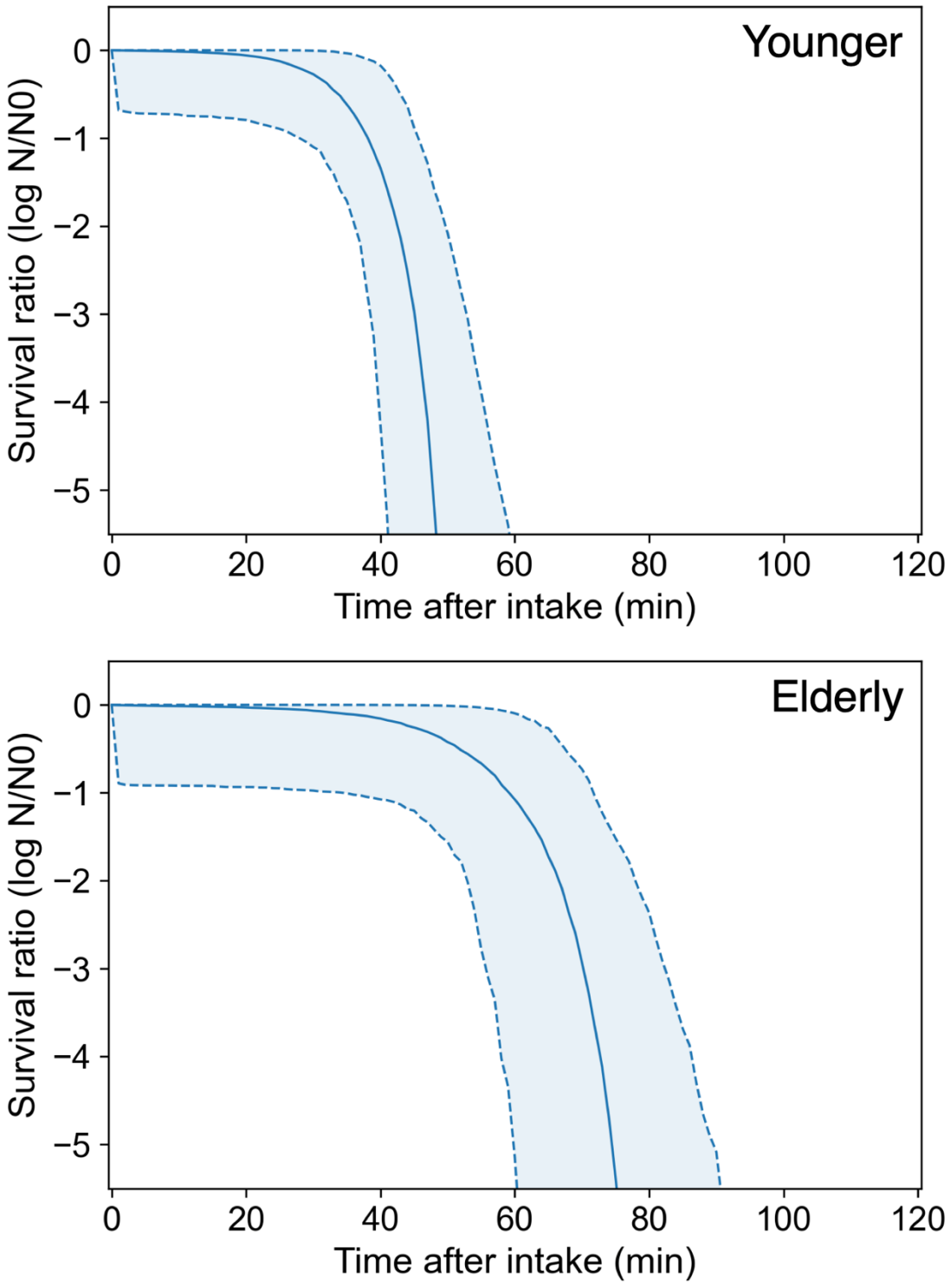


Fig. 6-3. Predicted after-meal survival curves (solid curve: median, dash curve and covered range: 90% prediction band) of *C. jejuni* in the stomach of young (upper) and elderly (lower) people derived from a predictive model for *C. jejuni* reduction in gastric juice (Koyama et al., 2021).

6.3.3. Bacterial transfer to the small intestine

The reported changes in the retention ratio in the stomach for solids and liquids (Hellström, Grybäck, & Jacobsson, 2006) could be successfully described as a cumulative gamma distribution (Fig. 6-4**a**). The reported gastric emptying curves for a solid (^{99m}Tc-labelled omelets) and liquid (^{111}In-labelled soft drink) meal in a healthy volunteer; liquid emptying begins instantly in an exponential fashion, while the linear emptying of solid foods begins after the lag phase (Hellström et al., 2006). Estimated parameter distributions converged with Bayesian inference because all R-hut values of parameter distributions were 1.0 (Supplementary Fig. 6-S3). The mean (± standard deviation) time of estimated gastric retention of solid foods was 1.5 ± 0.52 h, and the mean of estimated gastric retention of liquid foods was 0.77 ± 0.84 h. The survival ratio of intestinal transit varied with food type and age (Fig. 6-5). There was a significant difference in the survival transit ratio in young and elderly people after eating solid food. While, there was not notably difference between survival transit ratio of young and elderly individuals after eating liquid foods (Fig. 6-5a and 6-5b). In addition, considering food type difference, there was a difference in the estimated survival pathogen transit ratio regardless of age (Fig. 6-5). The gamma distribution is used to describe distributions of the waiting time and applied to waiting times for traffic jams and internet connecting times. This distribution could be appropriate to describe the time it takes for food (pathogens) entering the stomach to travel to the intestines.

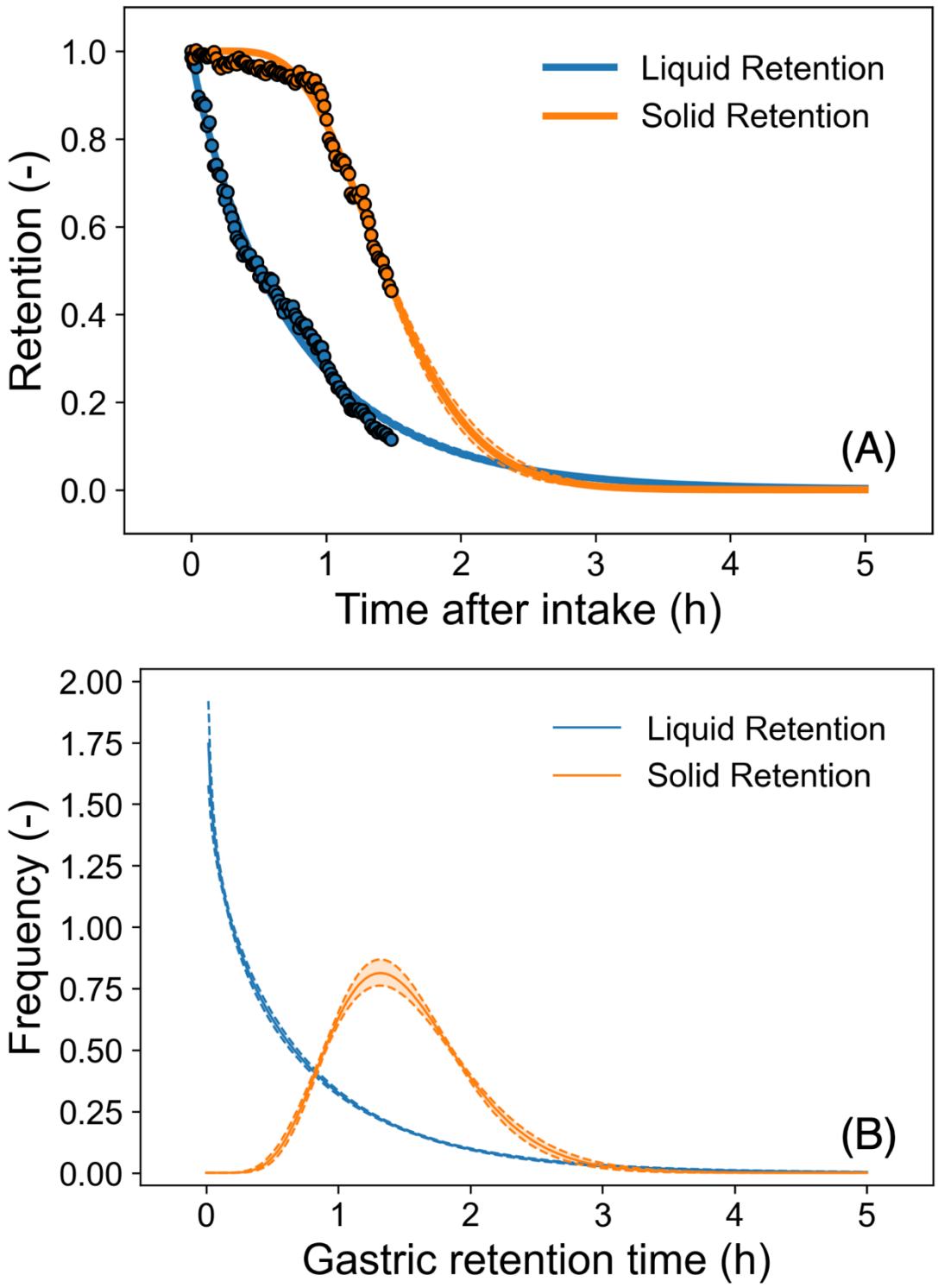


Fig. 6-4. Reported retention ratio (a; point; Hellström et al., 2006) & predicted cumulative gamma distributions (a and b; solid curve: median, dash curve and covered range: 95% prediction band) for gastric retention time. The estimated parameter traceplots and distributions of Bayesian MCMC in supplementary information (Fig. 6-S3).

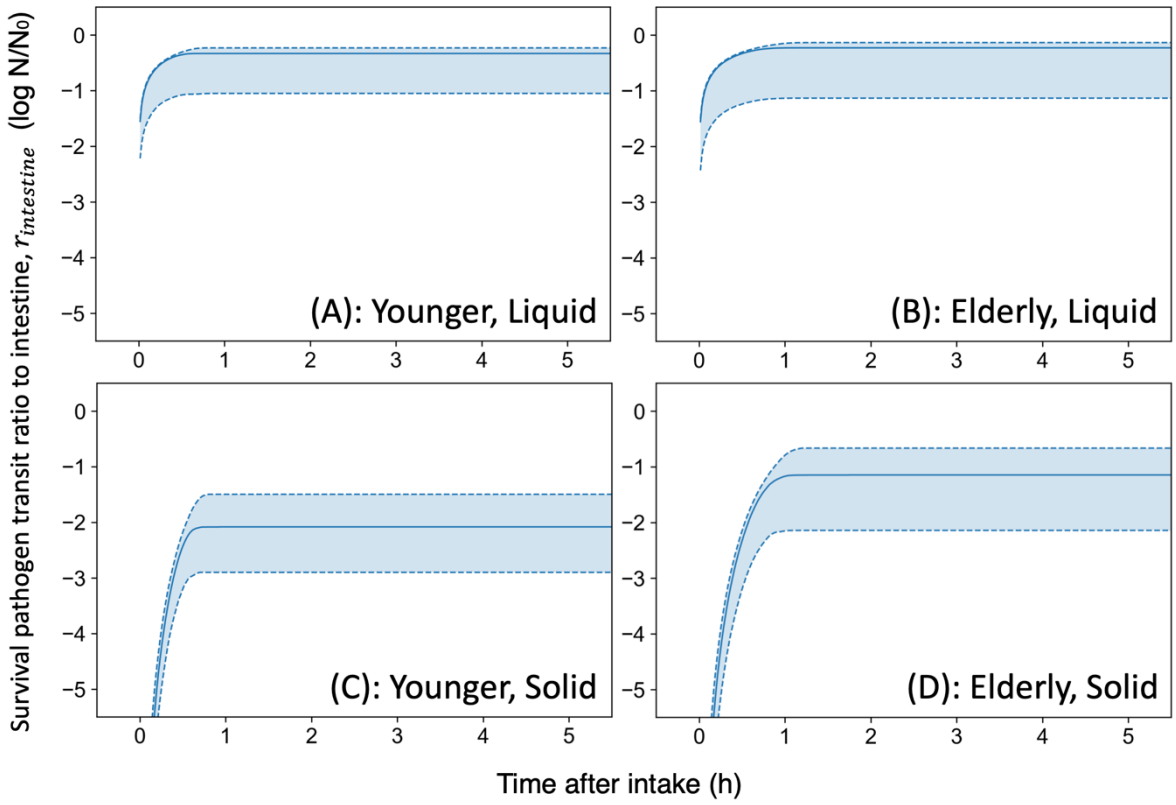


Fig. 6-5. Calculated transferred survival ratio (solid curve: median, dash curve and covered range: 90% prediction band) in intestine under each condition (a: young and liquid food, b: elderly and liquid food, c: young and liquid food, d: elderly and solid food).

6.3.4. Retention time in the small intestine

The reported the colonic (large intestine) filling ratio (Read, Al-Janabi, Holgate, Barber, & Edwards, 1986) could be successfully described as a cumulative gamma distribution (Fig. 6-6**a**), and the distribution of the time for food to move to the large intestine after a meal were estimated with the gamma distribution using Bayesian inference (Fig. 6-6**b**). The reported colonic filling data was derived from ^{99m}Tc-labelled mashed potatoes (Read et al., 1986). The estimated parameter distributions converged with Bayesian inference since all R-hut values of parameter distributions were 1.0 (Supplementary Fig. 6-S4). The mean time of estimated intestinal retention was 5.8 ± 2.0 h.

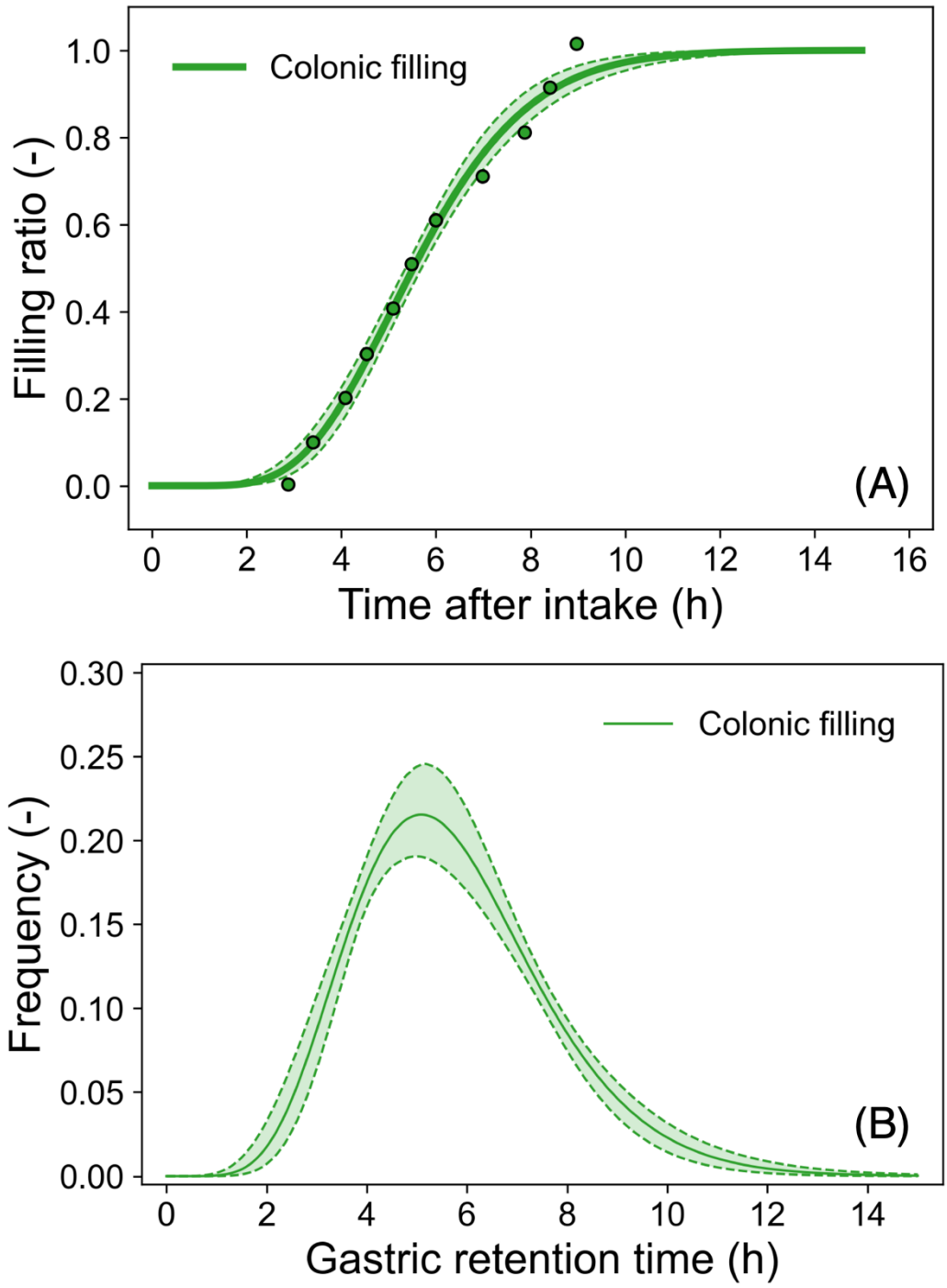


Fig. 6-6. Reported colonic (large intestine) filling ratio (a; points; Read et al., 1986) and predicted cumulative (a) and density (b) gamma distribution for the time for food to move from the small intestine to the large intestine after a meal (solid curve: median, dash curve and covered range: 95% prediction band). The estimated parameter traceplots and distributions of Bayesian MCMC in supplementary information (Fig. 6-S4).

6.3.5. Probability of infection in human intestinal cells

The predicted infection probabilities of *C. jejuni* derived using the predicting cell-invading model of *C. jejuni* (Abe et al., 2021) and they varied with food type and age (Fig. 6-7). Comparing influence of the *C. jejuni* strain onto the predicted dose-response relationship, there were no significant differences in doses of the predicted dose-response relationships of infection probability among the three strains (within 0.5 log CFU gaps; Supplementary Fig. 6-S7, 6-S8, and 6-S9) These strains were used in the referenced studies (Abe et al., 2021; Koyama et al., 2021) of predicting the reduction behavior by gastric juice and the cell-invading behavior (RIMD 0366027, RIMD 0366042 and RIMD 0366048) and had been isolated from patients of actual foodborne disease (http://rceid.biken.osaka-u.ac.jp/LIST2012(1392).htm; accessed: May 18, 2021). The predicted infection probability of all three *C. jejuni* strains is shown in Fig. 6-7. Young and elderly individuals consuming liquid food (young-liquid and elderly-liquid, respectively), as well as elderly individuals consuming solid food (elderly-solid) estimated infection probabilities were similar to the reported illness probabilities derived from actual *C. jejuni* outbreak for children (range, 8-13 years old) with bovine milk (Teunis et al., 2005), and all three strains' 95% prediction bands covered the reported dose-response relationship despite of the completely difference of data source type, which means that one is the real outbreak data and the other is the data of human digestive and *C. jejuni* reductions. The root mean square error (RMSE) of the median prediction of young-liquid, elderly-solid, and elderly-liquid groups were 0.69, 0.84, and 0.21 log CFU, respectively, when the logarithms of pathogen dose were assumed as objective variables. In contrast, the RMSE of the median prediction of the young-solid group was 1.2 log CFU and the 95% prediction band did not cover the reported dose-response relationship. The estimated infection probabilities for the young-liquid and elderly-liquid conditions were almost identical (0.2 log CFU gap). In contrast, the young-solid and elderly-solid conditions

resulted in a gap of about 1.0 log CFU. The combination of conditions with the largest difference in estimates was young-solid and elderly-liquid, resulting in a difference of almost 2.0 log CFU.

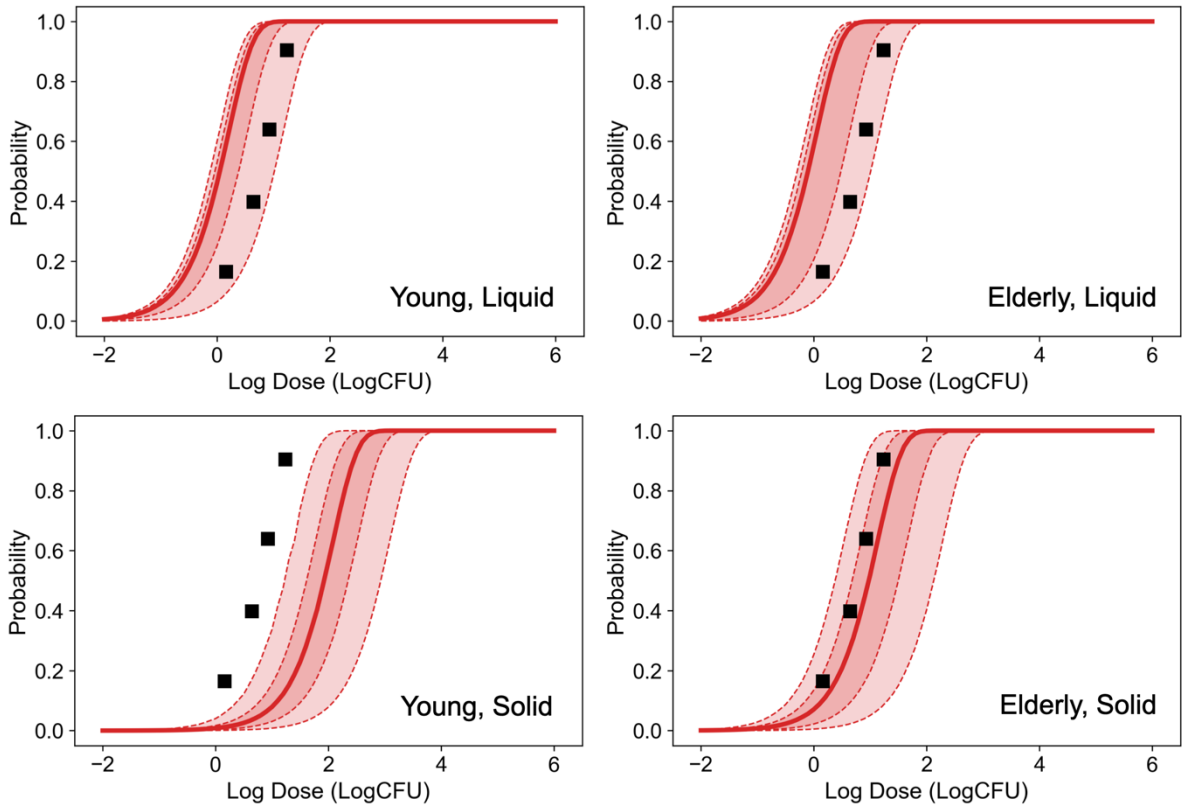


Fig. 6-7. Predicted infection probability (solid curve: median, dash curve and covered range: 60% and 95% prediction band) of *C. jejuni* (total of all three strains) under each condition (Same position as Fig. 6-5) and the reported ill probability of milk outbreak for children (8-13 years old) with milk (square; Teunis et al., 2005).

6.3.6. Sensitivity analysis of the framework for estimating invasion probability

Fig. 6-8 shows the Spearman's rank correlation coefficients of model components (e.g., food type, model parameters, $N_{intestine}$, and $t_{intestinal}$) against the infection probability. The upper factors in Fig. 6-8 were more relevant to the estimated infection probability. The indicators of liquid and solid food were set as 0 and 1, respectively, and the indicators of the strains were set as follows: RIMD 0366027, 1; RIMD 0366042, 2; and

RIMD 0366048, 3. The indicators for age were set as the mean age of individuals subjected to the pH test (young: 25; elderly: 71). The most relevant factor against the infection probability was the cell-invading pathogen count (R: 0.95; p-value < 10^{-6}). The second position of the relevant factor was the logarithm of pathogen count intake (R: 0.90; p-value < 10^{-6}). Since the infection probability was directly derived from these two factors, it is natural that these factors have the most relevance. The third position of the relevant factor was the intestinal survival ratio (R: 0.26; p-value < 10^{-6}). The relevant factors from the first to the third place were computable. The most important factors in the parametric factors were the food type (R: -0.25; p-value < 10^{-6}), the second factor was the shape parameter of the gamma distribution for gastric retention (R: -0.22; p-value < 10^{-6}), and the third factor was the rate parameter of the gamma distribution for gastric retention (R: -0.21; p-value < 10^{-6}). The factors with a p-value more than 0.05 were intestinal retention α (p-value: 0.06), intestinal retention β (p-value: 0.11), stomach reduction a (p-value: 0.11) , stomach reduction b (p-value: 0.38) , stomach reduction e (p-value: 0.058) , stomach reduction f (p-value: 0.15), invasion ratio (p-value: 0.175), and invasion $LogN_{max}$ (p-value: 0.051).

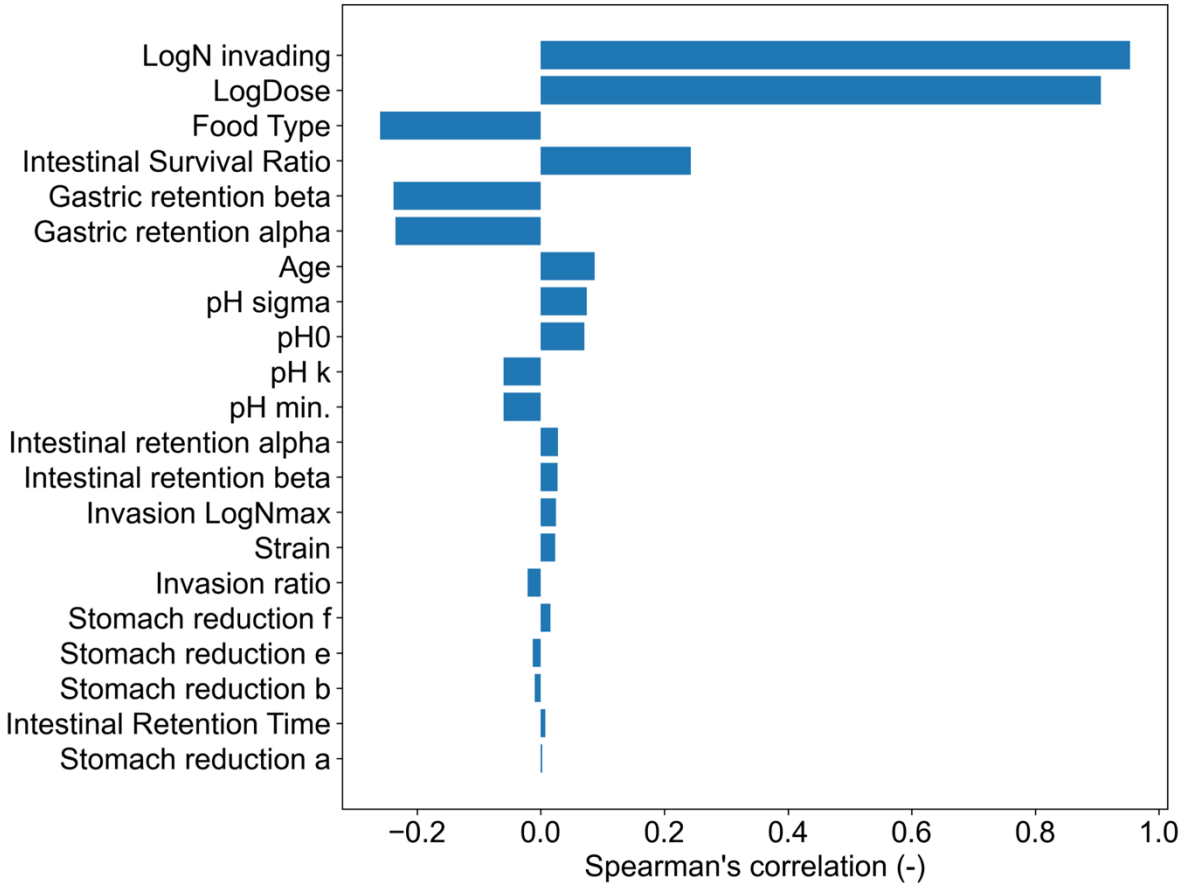


Fig. 6-8. Spearman's ranked correlation coefficients of parameter and computable factors against the predicted infection probability. Factors located at the upper position of this figure have a stronger relevance to infection probability.

6.4. Discussion

Here, this study aimed to develop an alternative dose-response model of *C. jejuni*, one of the most dangerous pathogenic bacteria, through KEDRF, considering food type and host age. There are few human test studies with a dose response effect (increasing trend with dose) for infection probability and data with a dose response effect are only for illness probability (Teunis, Bonačić Marinović, Tribble, Porter, & Swart, 2018). For these reasons, in order to assess the validity of the infection probability estimates, the illness probability was used in this study as a factor that cannot be simply compared but has a very strong association. Despite the completely different approach to estimating the dose-response

relationship using conventional methods, the combining predictive models developed in this study based on the KEDRF (Fig. 6-1) covered the reported illness probability of campylobacteriosis (Teunis et al., 2005). It seems that the KEDRF has a potential to appropriately predict *C. jejuni* infection probability. The reported dose-response relationship (illness probability) resulted from contaminated milk consumption (Teunis et al., 2005), which could be properly predicted from among predictions infection probability of the KEDRF dose-response model of this study for both young and elderly individuals ingesting liquid foods. The predicted infection probability in this study is also similar to that reported by Teunis et al. 2018, who collected and estimated multiple epidemiological data (Blaser, Sazie, & Williams, 1987; Evans, Roberts, Ribeiro, Gardner, & Kembrey, 1996; Korlath, Osterholrn, Judy, Forfang, & Robinson, 1985; van den Brandhof, Wagenner, & van den Kerkhof, 2003). However, it should be noted that there were small but unignorable RMSEs of young and elderly individuals ingesting liquid foods (0.69 and 0.84 log CFU, respectively; Fig. 6-7) with a reported dose-response relationship. The infection probability according to the dose-response relationship estimated in this study was based on the probability of invasion into intestinal cells. Because the immune system prevents symptoms of the illness after the invasion of the intestinal tissue, the illness probability being lower than the infection probability is natural.

The predicted results of this study showed a possibility that *C. jejuni* could invade the intestinal tissues and infect the human body even at a dose as low as 1–10 CFU. The previously reported epidemiological data on milk consumption also exhibited the occurrence of the disease at low doses. In contrast, the dose-response of *C. jejuni* demonstrated herein showed a discrepancy with the previously reported model (Black, Levine, Clements, Hughes, & Blaser, 1988), which is also the most widely used dose-response relationship for *C. jejuni* in QMRA. The infection probability reported by Black et al. (Black et al., 1988) was based

on the presence of *C. jejuni* in stools, the definition of which was completely different from that examined in this study. The difference in definition might be the reason for the difference in the prediction results. It has been reported that *C. jejuni* growth is inhibited upon competition with the extended-spectrum β-lactamase-producing bacteria, including some strains of *Escherichia coli*, which are widespread in nature (Hazeleger, Jacobs-Reitsma, & Besten, 2016). Many recent studies have reported that the healthy population is asymptomatically colonized with ESBL-E (Islam et al., 2018; van Duijkeren et al., 2018), with colonization frequencies could be ranged up to 50% (Kiratisin et al., 2008). In the colon, which is not an optimum environment for *C. jejuni* because of the anaerobic environment, the number of viable *C. jejuni* may decrease owing to competition with other intestinal bacteria. *C. jejuni* could be reduced before it is detected in the stool owing to competition with intestinal microbiota for nutrients or competitive effects in the gut, such as the Jameson effect (Jameson, 1962). Considering the actual behavior of *C. jejuni* in the human body, it is better to discuss infection probability defined as the invasion probability not as the existence/absence of pathogens in stool, for development of dose-response models.

While the results for the prediction were similar to those reported for illness probabilities derived from actual *C. jejuni* outbreak (Teunis et al., 2005), it was also possible to show the effectiveness of the implementation of the computational framework based on KEDRF. In particular, the results will be considered very beneficial, because the dose-response relationship depends on the food type and the age of the host. The FAO/WHO risk assessment for *Listeria* also emphasizes the importance of dose-response relationships in elderly and high-risk populations (Food & Agriculture Organization, 2004). In particular, the results of this study indicated a large difference in the infection probability (Young: 1.9 log CFU; Elderly: 1.1 log CFU; Fig. 6-7) among the food types. In the sensitivity analysis, the factor related to the food type had the largest correlation among the parameters. Fig. 6-5

shows that when consuming liquid food, the number of *C. jejuni* reaching the intestines was higher than that when consuming solid food owing to the difference in the gastric retention time. The difference in the predicted infection probability between solid and liquid foods was due to the difference in the gastric retention time (Fig. 6-8). KEDRF has the potential to estimate the probability of infection in young children since the difference between the elderly and young individuals was considered in this study. Comparing to food type or host age variability, the strain variability used in this study had relatively weak relevance for infection probability (food type: -0.25, Host age: 0.10, strain: 0.023; Fig. 6-8). However, from a molecular biological point of view, the strong variability of *C. jejuni* virulence has been reported that the virulence changes depending on the host species (Atterby et al., 2018; Mourkas et al., 2020). The strain factor used in this study, which included only three, have influence in reduction behaviors in gastric juices and in the invasion behaviors into the intestinal tissue. Because the three strains compared in this study, which are all isolated from human disease, are not sufficient to determine the overall strain variability of *C. jejuni*, it cannot be concluded that the effect of strain variability on infection risk is weak. Nevertheless, the KEDRF concept, which can simultaneously consider various conditions such as food type and host or strain variability, would be a useful tool for estimating dose-response relationships (Buchanan et al., 2009; Julien et al., 2009).

Key event models using Bayesian inference are important in KEDRF, where predictions are chained for each key event (Abe et al., 2021). This study attempted to illustrate the variability and uncertainty of pathogen behavior and the environment of the gastrointestinal tract based on Bayesian inference. Modeling using Bayesian inference has been used to describe various bacterial behaviors, such as the growth and death of various bacteria, as a method that can represent variability and uncertainty (Abe et al., 2021; Garre, Zwietering, & Besten, 2020; Huang & Li, 2020; Koyama, Aspridou, Koseki, &

Koutsoumanis, 2019). In addition, KEDRF suggests that modeling the individual variability of the digestive process in different hosts will lead to a better understanding of food poisoning incidents such as the digestive modeling in this study (Fig. 6-2). The use of Bayesian inference to represent not only bacterial but also host variability will allow the estimation of appropriate dose-response relationships using mechanistic approaches.

Although this study has shown that KEDRF is a useful procedure for predicting dose-response relationships of *C. jejuni*, KEDRF is also effective for other types of bacteria (Buchanan et al., 2009). The approach used in this study consisted of a mathematical prediction model based on predictive microbiology and pharmacokinetics. The growth and death of various other pathogens, as well as the cited *C. jejuni* model (Abe et. al. 2021; Koyama et al., 2021), have been described using predictive models (Ross, McMeekin, & Baranyi, 2014). For many other pathogens, the present method can be applied to calculate the intestinal viable bacterial count using gastric retention time and survival kinetics in the stomach, independent of the pathogen type. In addition, the KEDRF would have potentials to take into account of the infection mechanisms identified by molecular biology, and it could bring us the possibility to apply fundamental information of infection mechanisms elucidated by molecular biological approaches to the macroscopic output of actual food sanitation management sites. In this manner, development of dose-response models based on KEDRF will be expected for various foodborne pathogens, combining various mechanisms for estimating infection risks.

However, the dose-response model based on KEDRF presented in this study still has certain limitations. The present study did not consider the growth of *C. jejuni* in the intestines because its growth rate is slower than its invasion rate (Abe et al., 2021). In contrast, a growth model is needed for fast-growing pathogenic bacteria, such as *E. coli* or *Salmonella*. Modeling the interactions between the immune system and pathogens is also required. It has

been suggested that the probability of infection may be high, but the illness may not develop (Teunis et al., 2018). Modeling the effect of immunity on pathogens will be necessary to predict the probability of illness. Furthermore, since the available data on the gastrointestinal tract were limited, the effect of age was reflected only in the pH change and the effect of food type was reflected only in the residence time in the stomach in this study. However, for a more realistic prediction, data corresponding to age and food types in all gastrointestinal environments, such as pH change, gastric retention time, and intestinal retention time, are needed. For more realistic and appropriate predictions of the dose-response relationship based on KEDRF, it is necessary to study all the factors of infection mechanisms including not only immune modeling and additional environmental data of the gastrointestinal tract under various conditions but also perspectives of omics, molecular microbiology, and medical microbiology.

In conclusion, the behavior of *C. jejuni* in the gastrointestinal tract based on the KEDRF was predicted via mathematical models using Bayesian inference (Fig. 6-1 to 6-6). Moreover, the respective dose-response relationships for combinations of age (young, elderly) and food type (liquid, solid) were also estimated (Fig. 6-7). The results of the dose-response model of KEDRF showed similar results to the reported dose-response relationship (Teunis et al., 2005; Fig. 6-7). Furthermore, sensitivity analysis of the prediction results showed that gastric retention time was the most relevant factor among the key events from ingestion to invasion (Fig. 6-8). This study demonstrated a large potential for the development of a novel dose-response model based on KEDRF. The dose-response model based on KEDRF will allow us to estimate the dose-response relationships of various pathogens with various factors, such as age, sex, chronic illness, food type, and others based on their actual infection mechanisms.

6.5. References

Abe, H., Koyama, K., & Koseki, S. (2021). Modeling Invasion of Campylobacter jejuni into Human Small Intestinal Epithelial-Like Cells by Bayesian Inference. Applied and Environmental Microbiology, 87(1), 687. http://doi.org/10.1128/AEM.01551-20

Atterby, C., Mourkas, E., Méric, G., Pascoe, B., Wang, H., Waldenström, J., et al. (2018). The Potential of Isolation Source to Predict Colonization in Avian Hosts: A Case Study in Campylobacter jejuni Strains From Three Bird Species. Frontiers in Microbiology, 9. http://doi.org/10.3389/fmicb.2018.00591

Black, R. E., Levine, M. M., Clements, M. L., Hughes, T. P., & Blaser, M. J. (1988). Experimental Campylobacter jejuni Infection in Humans. The Journal of Infectious Diseases, 157(3), 472–479. http://doi.org/10.1093/infdis/157.3.472

Blaser, M. J., Sazie, E., & Williams, L. P. (1987). The Influence of Immunity on Raw Milk—Associated Campylobacter Infection. Jama, 257(1), 43–46. http://doi.org/10.1001/jama.1987.03390010047026

Buchanan, R. L., Havelaar, A. H., Smith, M. A., Whiting, R. C., & Julien, E. (2009). The Key Events Dose-Response Framework: its potential for application to foodborne pathogenic microorganisms. Critical Reviews in Food Science and Nutrition, 49(8), 718–728. http://doi.org/10.1080/10408390903116764

Dressman, J. B., Berardi, R. R., Dermentzoglou, L. C., Russell, T. L., Schmaltz, S. P., Barnett, J. L., & Jarvenpaa, K. M. (1990). Upper Gastrointestinal (GI) pH in Young, Healthy Men and Women. Pharmaceutical Research, 7(7), 756–761. http://doi.org/10.1023/A:1015827908309

Evans, M. R., Roberts, R. J., Ribeiro, C. D., Gardner, D., & Kembrey, D. (1996). A milk-borne campylobacter outbreak following an educational farm visit. Epidemiology & Infection, 117(3), 457–462. http://doi.org/10.1017/S0950268800059112

Fernández-García, E., Carvajal-Lérida, I., & Pérez-Gálvez, A. (2009). In vitro bioaccessibility assessment as a prediction tool of nutritional efficiency. Nutrition Research, 29(11), 751–760. http://doi.org/10.1016/j.nutres.2009.09.016

Food & Agriculture Organization. (2004). Risk Assessment of Listeria Monocytogenes in Ready-to-eat Foods.

Galanakis, C. M. (2016). Nutraceutical and Functional Food Components. Academic Press.

Garre, A., Zwietering, M. H., & Besten, den, H. M. W. (2020). Multilevel modelling as a tool to include variability and uncertainty in quantitative microbiology and risk assessment. Thermal inactivation of Listeria monocytogenes as proof of concept. Food Research International, 137, 109374. http://doi.org/10.1016/j.foodres.2020.109374

Hazeleger, W. C., Jacobs-Reitsma, W. F., & Besten, den, H. M. W. (2016). Quantification of Growth of Campylobacter and Extended Spectrum β-Lactamase Producing Bacteria Sheds Light on Black Box of Enrichment Procedures. Frontiers in Microbiology, 7(1503), 884. http://doi.org/10.3389/fmicb.2016.01430

Helander, H. F., & Fändriks, L. (2014). Surface area of the digestive tract – revisited. Scandinavian Journal of Gastroenterology, 49(6), 681–689. http://doi.org/10.3109/00365521.2014.898326

Hellström, P. M., Grybäck, P., & Jacobsson, H. (2006). The physiology of gastric emptying. Best Practice & Research Clinical Anaesthesiology, 20(3), 397–407. http://doi.org/10.1016/j.bpa.2006.02.002

Huang, L., & Li, C. (2020). Growth of Clostridium perfringens in cooked chicken during cooling: One-step dynamic inverse analysis, sensitivity analysis, and Markov Chain Monte Carlo simulation. Food Microbiology, 85, 103285. http://doi.org/10.1016/j.fm.2019.103285

Islam, S., Selvarangan, R., Kanwar, N., Rendie McHenry, James D Chappell, Natasha Halasa, et al. (2018). Intestinal Carriage of Third-Generation Cephalosporin-Resistant

and Extended-Spectrum β-Lactamase-Producing Enterobacteriaceae in Healthy US Children | Journal of the Pediatric Infectious Diseases Society | Oxford Academic. Clinical Infectious Diseases. http://doi.org/10.1093/jpids/pix045

Jameson, J. E. (1962). A discussion of the dynamics of salmonella enrichment. Epidemiology & Infection, 60(2), 193–207. http://doi.org/10.1017/S0022172400039462

Julien, E., Boobis, A. R., Olin, S. S., The ILSI Research Foundation Threshold Working Group. (2009). The Key Events Dose-Response Framework: A Cross-Disciplinary Mode-of-Action Based Approach to Examining Dose-Response and Thresholds. Critical Reviews in Food Science and Nutrition, 49(8), 682–689. http://doi.org/10.1080/10408390903110692

Kiratisin, P., Chattammanat, S., Sa-Nguansai, S., Dansubutra, B., Nangpatharapornthawee, P., Patthamalai, P., et al. (2008). 2-year trend of extended-spectrum β-lactamase-producing Escherichia coli and Klebsiella pneumoniae in Thailand: an alert for infection control | Transactions of The Royal Society of Tropical Medicine and Hygiene | Oxford Academic. Clinical Infectious Diseases, (102), 460–464. http://doi.org/10.1016/j.trstmh.2008.02.005

Korlath, J. A., Osterholrn, M. T., Judy, L. A., Forfang, J. C., & Robinson, R. A. (1985). A Point-Source Outbreak of Campylobacteriosis Associated with Consumption of Raw Milk. The Journal of Infectious Diseases, 152(3), 1–5.

Koseki, Shige, Mizuno, Y., & Sotome, I. (2011). Modeling of pathogen survival during simulated gastric digestion. Applied and Environmental Microbiology, 77(3), 1021–1032. http://doi.org/10.1128/AEM.02139-10

Koyama, K., Aspridou, Z., Koseki, S., & Koutsoumanis, K. (2019). Describing Uncertainty in Salmonella Thermal Inactivation Using Bayesian Statistical Modeling. Frontiers in Microbiology, 10, 216. http://doi.org/10.3389/fmicb.2019.02239

Mourkas, E., Taylor, A. J., Méric, G., Bayliss, S. C., Pascoe, B., Mageiros, L., et al. (2020). Agricultural intensification and the evolution of host specialism in the enteric pathogen *Campylobacter jejuni*. Proceedings of the National Academy of Sciences of the United States of America, 117(20), 11018–11028. http://doi.org/10.1073/pnas.1917168117

Pujol, J. M., Eisenberg, J. E., Haas, C. N., & Koopman, J. S. (2009). The Effect of Ongoing Exposure Dynamics in Dose Response Relationships. PLoS Computational Biology, 5(6), e1000399. http://doi.org/10.1371/journal.pcbi.1000399

Rahman, A., Munther, D., Fazil, A., Ben Smith, & Wu, J. (2018). Advancing risk assessment: mechanistic dose–response modelling of Listeria monocytogenes infection in human populations. Royal Society Open Science, 5(8), 180343. http://doi.org/10.1098/rsos.180343

Read, N. W., Al-Janabi, M. N., Holgate, A. M., Barber, D. C., & Edwards, C. A. (1986). Simultaneous measurement of gastric emptying, small bowel residence and colonic filling of a solid meal by the use of the gamma camera. Gut, 27(3), 300–308. http://doi.org/10.1136/gut.27.3.300

Ribet, D., & Cossart, P. (2015). How bacterial pathogens colonize their hosts and invade deeper tissues. Microbes and Infection, 17(3), 173–183. http://doi.org/10.1016/j.micinf.2015.01.004

Ross, T., McMeekin, T. A., & Baranyi, J. (2014). Predictive Microbiology and Food Safety. Encyclopedia of Food Microbiology (Second Edition, pp. 59–68). Elsevier. http://doi.org/10.1016/B978-0-12-384730-0.00256-1

Russell, T. L., Berardi, R. R., Barnett, J. L., Dermentzoglou, L. C., Jarvenpaa, K. M., Schmaltz, S. P., & Dressman, J. B. (1993). Upper Gastrointestinal pH in Seventy-Nine Healthy, Elderly, North American Men and Women. Pharmaceutical Research, 10(2), 187–196. http://doi.org/10.1023/A:1018970323716

Schliller, C., Fröhlich, C. P., Giessmann, T., Siegmund, W., Mönnikes, H., Hosten, N., & Weischies, W. (2005). Intestinal fluid volumes and transit of dosage forms as assessed by magnetic resonance imaging. Alimentary Pharmacology & Therapeutics, 22(10), 971–979. http://doi.org/10.1111/j.1365-2036.2005.02683.x

Teunis, P. F. M., Bonačić Marinović, A., Tribble, D. R., Porter, C. K., & Swart, A. (2018). Acute illness from Campylobacter jejuni may require high doses while infection occurs at low doses. Epidemics, 24, 1–20. http://doi.org/10.1016/j.epidem.2018.02.001

Teunis, P., van den Brandhof, W., Nauta, M., Wagenner, J., van den Kerkhof, H., & van Pelt, W. (2005). A reconsideration of the Campylobacter dose–response relation. Epidemiology & Infection, 133(4), 583–592. http://doi.org/10.1017/S0950268805003912

van den Brandhof, W., Wagenner, J., & van den Kerkhof, H. (2003). An outbreak of campylobacteriosis after drinking unpasteurized milk, 2002, the Netherlands. Int. J. Med. Microbiol., 293 (143).

van Duijkeren, E., Wielders, C. C. H., Dierikx, C. M., van Hoek, A. H. A. M., Hengeveld, P., Veenman, C., et al. (2018). Long-term Carriage of Extended-Spectrum β-Lactamase–Producing Escherichia coli and Klebsiella pneumoniae in the General Population in The Netherlands | Clinical Infectious Diseases | Oxford Academic. Clinical Infectious Diseases. http://doi.org/10.1093/cid/cix1015

Zwietering, M. H. (2009). Quantitative risk assessment: Is more complex always better?: Simple is not stupid and complex is not always more correct. International Journal of Food Microbiology, 134(1-2), 57–62. http://doi.org/10.1016/j.ijfoodmicro.2008.12.025

6.6. Supplementary materials

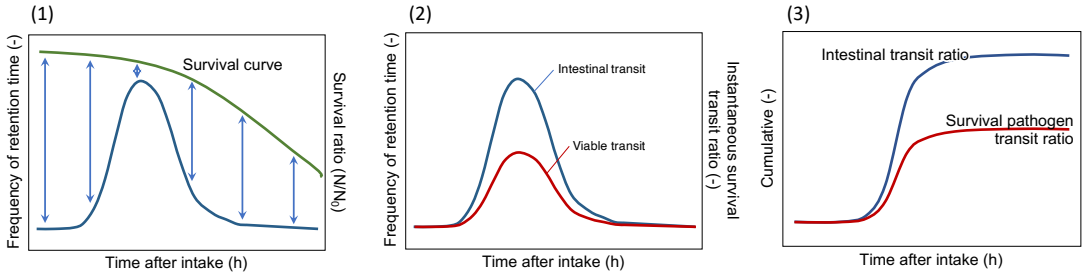


Figure 6-S1. The scheme of the calculation for survival pathogen transit ratio from stomach to intestine (Eq. 4). (1): It is assumed that the intestinal transit rate of pathogen is equal to that of food. The survival ratio of the instantaneous pathogen transit corresponds to the instantaneous value of the survival curve. (2): Multiply the instantaneous values of survival curve and intestinal transit to calculate the instantaneous values of viable transit. (3): Integrating intestinal transit gives the ratio of all pathogens (dead or alive) that have transferred into an intestine. Similarly, the integral of viable transit represents the survival transit ratio of pathogens that have transferred into an intestine.

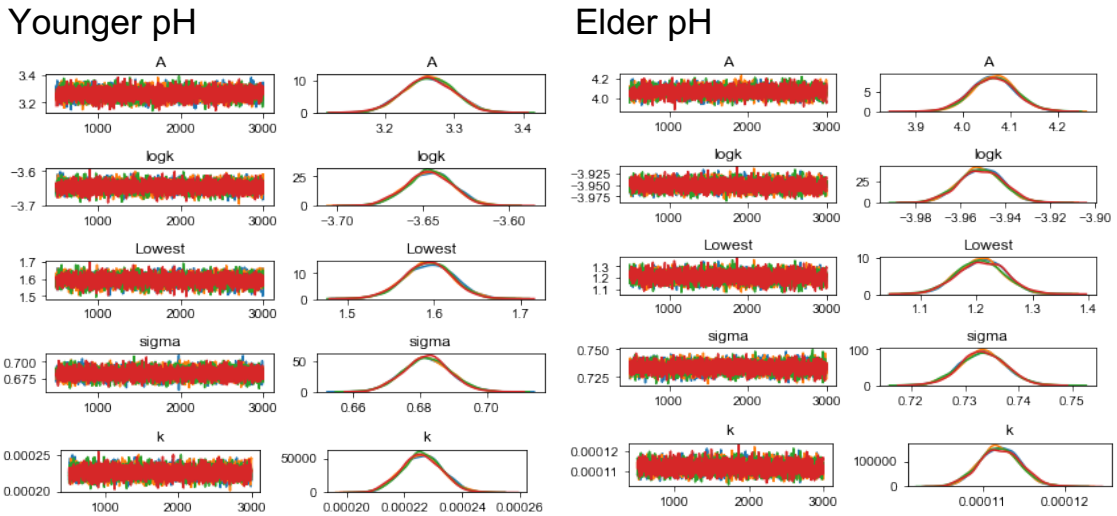


Figure 6-S2. Trace-plots and posterior distributions for estimated parameters of younger and elderly people's pH change by Bayesian inference. Each color indicates each trace-plot and each distribution of the MCMC chain.

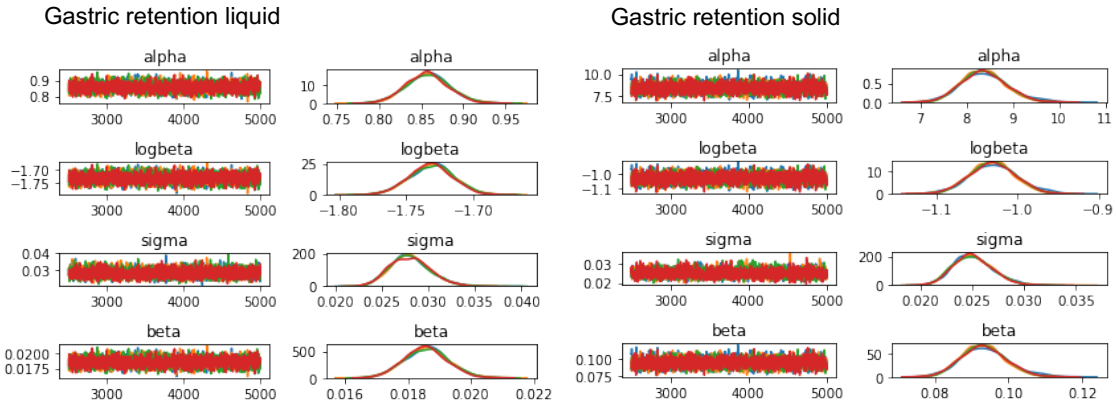


Figure 6-S3. Trace-plots and posterior distributions for estimated parameters of gastric retention of liquid and solid by Bayesian inference. Each color indicates each trace-plot and each distribution of the MCMC chain.

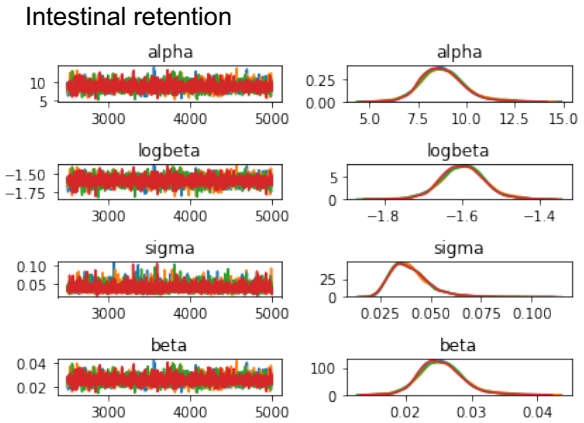


Figure 6-S4. Trace-plots and posterior distributions for estimated parameters of gastric retention of liquid and solid by Bayesian inference. Each color indicates each trace-plot and each distribution of the MCMC chain.

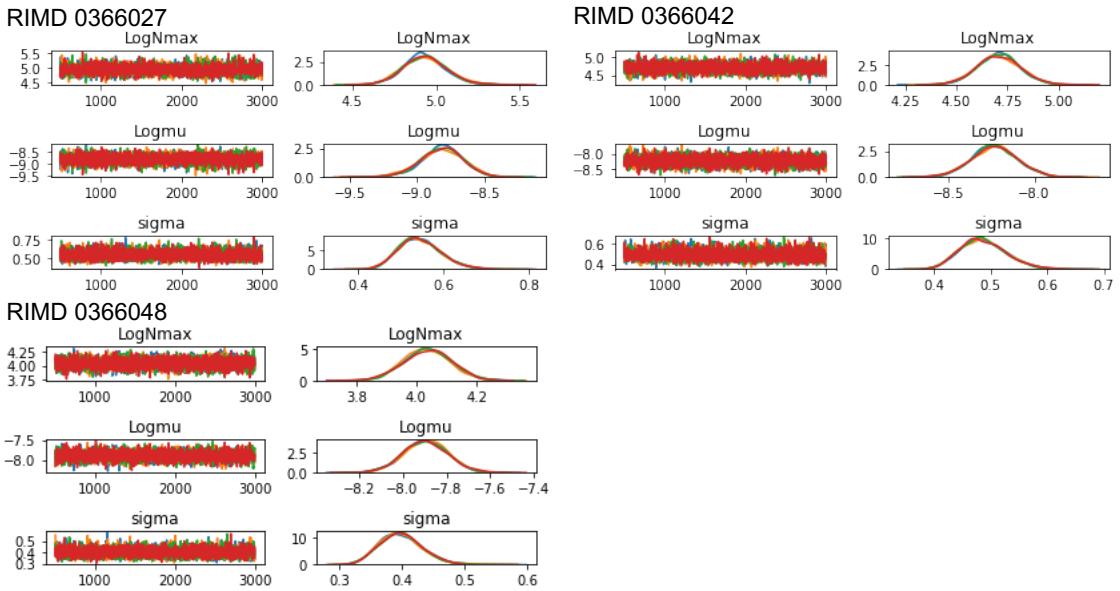


Figure 6-S5. Trace-plots and posterior distributions for estimated parameters of the modified model from reported cell-invasion model (Abe et., 2021) of C. jejuni (RIMD 0366027, 0366042 and 0366048) by Bayesian inference. Each color indicates each trace-plot and each distribution of the MCMC chain.

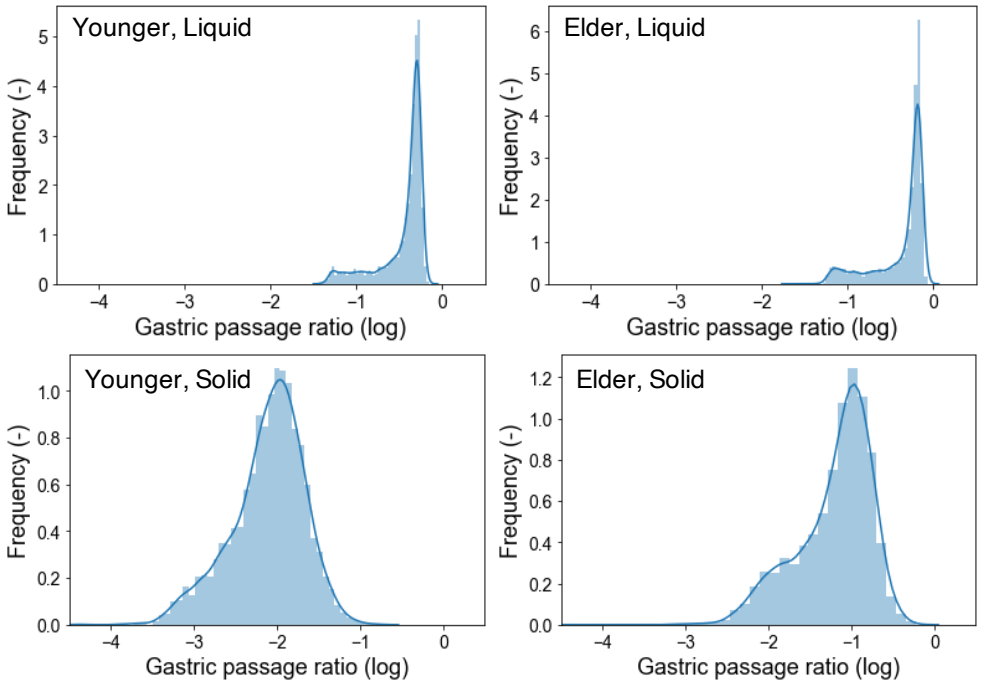


Figure 6-S6. Histograms and kernel distributions (solid) of final survival transit ratio (12 hours after meal). Host age and food type were, from top left: Young-Liquid; Elderly-Liquid; Young-Solid and Elderly-Solid.

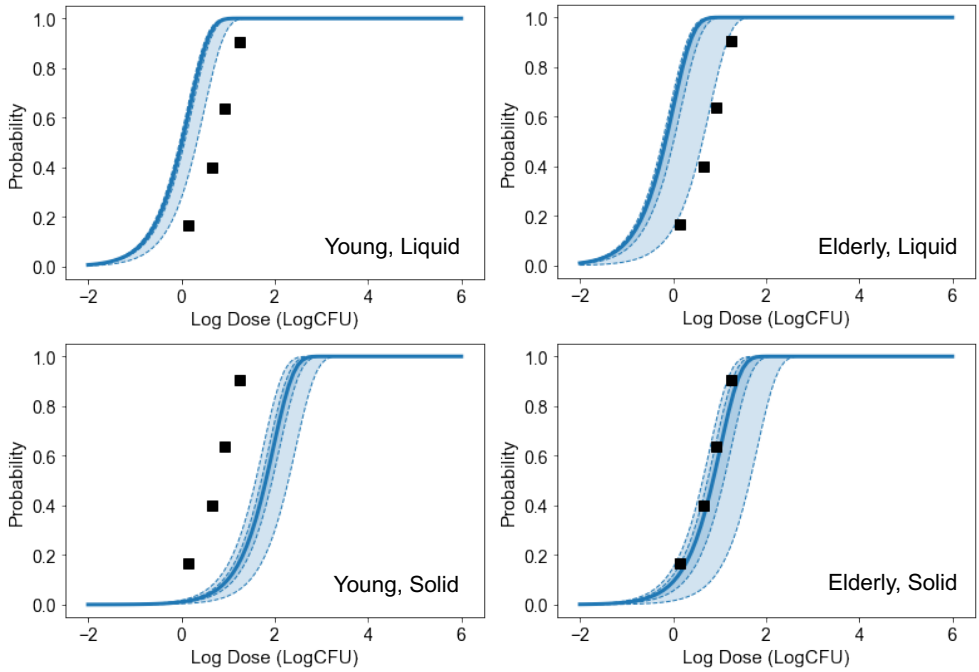


Figure 6-S7. Cell invading probability (solid curve: median, dash curve and covered range: 60% and 95% prediction band) of C. jejuni (RIMD 0366027) under each condition (Same position as Fig. 6-7) & reported ill probability of milk outbreak against children (squares; Teunis et al., 2005).

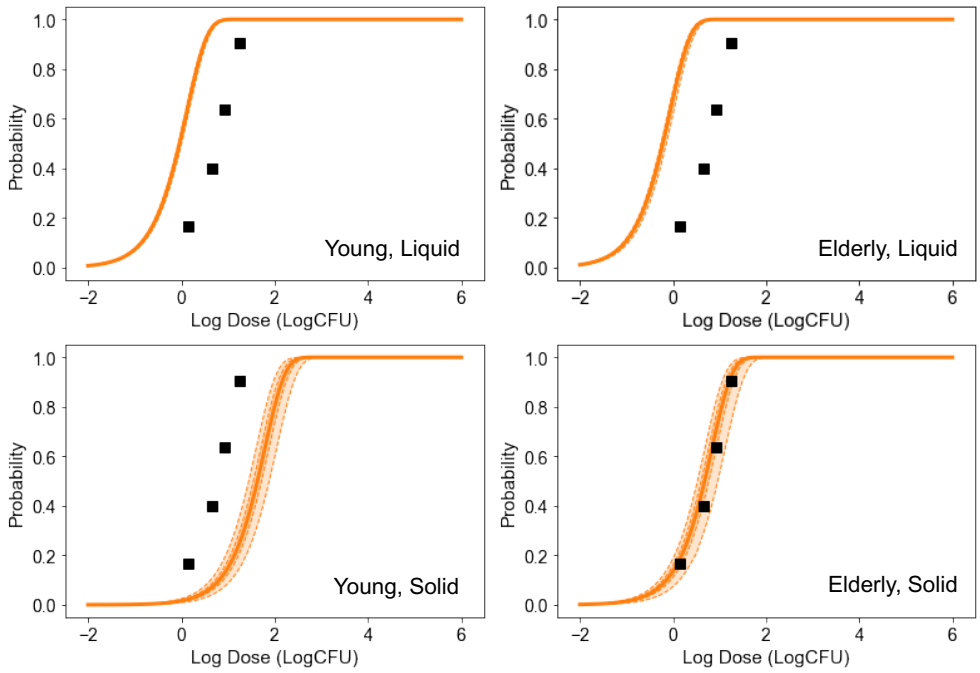


Figure 6-S8. Cell invading probability (solid curve: median, dash curve and covered range: 60% and 95% prediction band) of *C. jejuni* (RIMD 0366042) under each condition (Same position as Fig. 6-7) & reported ill probability of milk outbreak against children (squares; Teunis et al., 2005).

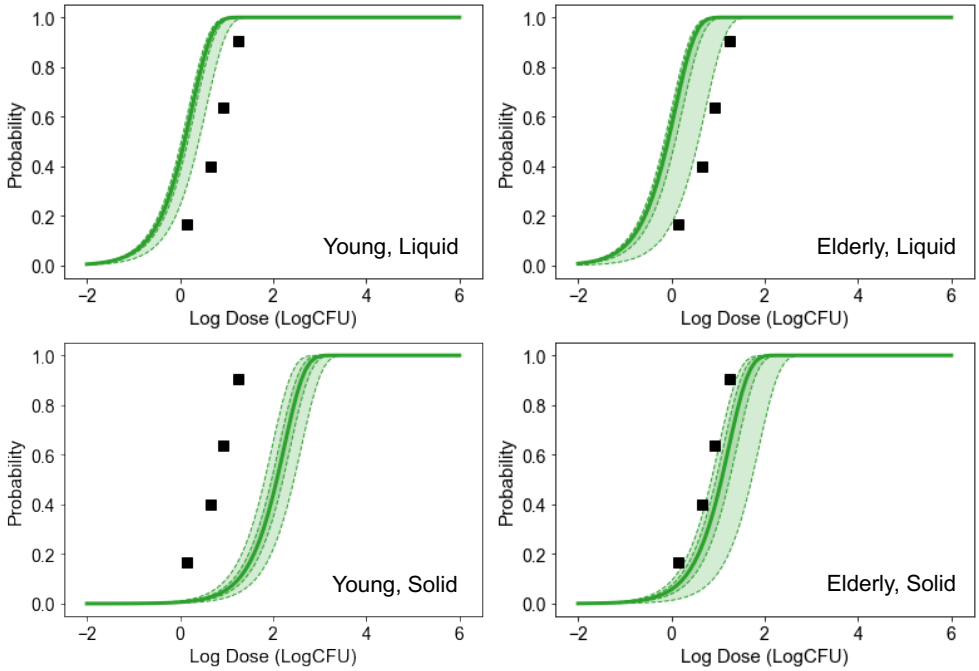


Figure 6-S9. Cell invading probability (solid curve: median, dash curve and covered range: 60% and 95% prediction band) of *C. jejuni* (RIMD 0366048) under each condition (Same position as Fig. 6-7) & reported ill probability of milk outbreak against children (squares; Teunis et al., 2005).

Chapter 7 Elucidation of relevant factors to foodborne listeriosis on pasteurized milk from quantitative microbial risk assessment

7.1. Introduction

No matter how advanced the processing and preservation technology is, the risk of foodborne illness will never be reduced to completely zero (Zwietering, Garre, Wiedmann, Robert L Buchanan, 2021). Worldwide annually 600 million people suffer from foodborne diseases (World Health Organization, 2015). Therefore, controlling the risk of foodborne illness is an essential process to protect public health. Hazard Analysis Critical Control Point (HACCP) is broadly used to manage and control the safety of foods. HACCP is a management system in which food safety is addressed by analysing and controlling biological, chemical, and physical hazards from raw material production, procurement and handling, to manufacturing, distribution and consumption of the finished product (FDA, 2018). HACCP identifies the critical control points (CCP) from an analysis of the risk for the food processing flow and manages the safety of foods by controlling these CCP. To ensure food safety using this method, it is necessary to identify the key factors or the combinations of factors that contribute to the food safety risks. However, it is difficult to trace back and identify the characteristics of processes, distribution, and storage until consumption of the foods that caused foodborne illness outbreaks.

Therefore, this study focused on Quantitative Microbiological Risk Assessment (QMRA), which quantifies the risk of foodborne illness by simulating the effects of environmental conditions and bacterial characteristics on foodborne illness in a food chain. QMRA combines existing laboratory and surveillance databases with computational techniques to yield models that predict public health outcomes (Dennis, Buchanan, & Miller, 2002). Furthermore, since it is a computer simulation, all the factors in the food chain can be

saved to analyse in detail the scenarios that caused the foodborne illnesses, different from the analysis of actual foodborne illness incidents.

In order to elucidate the relevant factors that determine the foodborne risk, it is necessary to consider the output method of QMRA. Often as output, the log concentration or the log risk or risk is correlated to the input factors in sensitivity analyses as part of QMRA. However, since many parts of the risk distribution are not practically relevant for the actual risk, this might result in artefacts. Revealing the relationship with actual risk may require deriving correlations using outputs that directly indicates the occurrence of the foodborne illness. In addition, the log concentration or the log risk, which are often calculated in QMRA, are difficult to grasp intuitively and often confuse risk managers or decision makers. Expressing risk as a natural number, such as the number of occurrences of foodborne illness, would make it easier to understand and more realistic.

Note, however, that the method deriving natural number outputs may be computationally demanding. Basically, foods distributed to the market are safe products, and the residual risks of the foods are very low. However, no matter how low the probability is, if the food is consumed in large quantities by large population, the residual risk accumulates with the amount consumed, and the number of cases of foodborne illness increases. To illustrate this, although the risk per serving is higher for unpasteurized milk than for pasteurized milk, a report estimated a higher foodborne illness risk (cases/year/million population) for pasteurized milk food than for unpasteurized milk due to the very large difference in consumption frequency (U.S. Food and Drug Administration, 2003). Therefore, the risk of foodborne illness for foods consumed in large quantities should be estimated in conjunction with the number of servings. In this case, it is necessary to adjust the number of simulations according to the number of servings for natural number QMRA outputs. This

results in a large computational load and has not been widely performed in previous research on QMRA.

So, this study focuses on the pasteurised milk's food chain as model chain with relatively high food consumption frequency and relatively low food safety risk to reveal the relevant factors of the pasteurised milk's food chains that determine the listeriosis cases, and to identify the points that should be controlled rigorously. Unlike many other QMRAs, the actual cases of illness in this analysis were investigated as natural numbers and correlated to the input factors. The output type for the present QMRA, illness occurrence, indicates whether the simulated scenario iteration caused illnesses or not, and what factors or combinations of factors actually are responsible for causing the illness. Since the residual risk is very low in well-controlled processes like pasteurization of milk, a huge number of iterations need to be run to get to an actual number of illness cases in such a QMRA. Therefore, this study conducted 10 billion iterations of the QMRA. In addition, the sensitivity analysis demonstrated the food chain factor's correlations with illness occurrence and those with the logarithm of pathogen concentration at the moment of consumption.

7.2. Materials and methods

7.2.1. Thermotolerance model for Listeria monocytogenes in milks from metadata based on Bayesian inference

7.2.1.1. Metadata preparation

For describing thermotolerance variation with the Bayesian modelling technique, a reported dataset was referenced from a metadata collection study (Asselt & Zwietering, 2006). The dataset of Van Asselt & Zwietering (2006) included 226 *D*-values for at least 16 strains of *Listeria monocytogenes*, including unidentified strains, heated between 50°C and 75°C in milk.

7.2.1.2. Description and estimation of *D*-value variability with Bayesian inference

A secondary model for thermotolerance (*D*-values) of heated *Listeria monocytogenes* was fitted to the referenced meta-dataset based on Bayesian inference to describe thermotolerance variation, which is a mixture of variability and uncertainty. The Bayesian *D*-value model was constructed based on most common secondary model for *D*-value like as following prior distribution.

$$\mathrm{Log}\, D_a \sim \mathrm{Normal}\left(-\frac{\mathrm{T}_a - \mathrm{T}_{ref,heat}}{z_b} + \mathrm{Log}\, D_{ref,b},\ \sigma_{\mathrm{Log}\, D,b}\right) \quad (7\text{-}1)$$

The $\mathrm{Log}\, D_a$ and T_a were the each referenced dataset ($a = 1, 2, 3, \ldots, 226$), and z_b and $\mathrm{Log}\, D_{ref,b}$ and $\sigma_{\mathrm{Log}\, D,b}$ were the each estimated parameters with Bayesian inference (the iteration number for estimating posterior distributions:$b = 1, 2, 3, \ldots, 100000$). The all of log or Log in this study indicate the common logarithm with base 10. For the estimated parameters, $\mathrm{Log}\, D_{ref,b}$ and $\sigma_{\mathrm{Log}\, D,b}$, the uninformative distribution, Uniform [-infinite, infinite], was adopted as the prior distribution. Especially, the half Cauchy distribution as the prior distribution for the estimated standard deviation of $\mathrm{Log}\, D$, $\sigma_{\mathrm{Log}\, D,b}$ as following:

$$\sigma_{\mathrm{Log}\, D,b} \sim \mathrm{Cauchy}(0,\ 1) \qquad (\sigma_{\mathrm{Log}\, D,b} > 0) \quad (7\text{-}2).$$

The half Cauchy distribution has been recommended and commonly used for the prior distribution for standard deviations (Gelman, 2006; Polson & Scott, 2012). The reference temperature for the *D*-value model, $\mathrm{T}_{ref,heat}$, was sat as 62.3°C which was the average temperature of the referenced dataset.

7.2.2. Growth model for Listeria monocytogenes in milks based on Bayesian inference

7.2.2.1. Metadata preparation

For describing the growth rate variation with the Bayesian modelling technique, a reported dataset was referenced from a metadata collection. The referenced dataset included

111 growth rates for at least 14 strains of *Listeria monocytogenes*, including unidentified strains, incubated between 0°C and 20°C in milk.

7.2.2.2. Description and estimation of growth rate variation with Bayesian inference

A secondary model for growth rate (μ-values) of incubated *Listeria monocytogenes* in milk was fitted to the referenced meta-dataset based on Bayesian inference to describe growth rate variation, which is a mixture of variability and uncertainty. The Bayesian growth rate model was constructed based on most common secondary model, the gamma model for growth rate (Zwietering, Wijtzes, Rombouts, & Riet, 1993) like as following prior distribution.

$$\sqrt{\mu_c} \sim \text{Normal}\left(\sqrt{\mu_{ref,d}} \times \frac{T_c - T_{min,d}}{T_{ref,growth} - T_{min,d}},\ \sigma_{\sqrt{\mu},d}\right) \quad (7\text{-}3)$$

The $\sqrt{\mu_c}$ and T_c were the each referenced dataset ($c = 1, 2, 3, \dots, 111$), and $T_{min,d}$ and $\sqrt{\mu_{ref,d}}$ and $\sigma_{\sqrt{\mu},d}$ were each estimated parameters with Bayesian inference (the iteration number for estimating posterior distributions: $d = 1, 2, 3, \dots, 100000$). For the estimated parameters, $T_{min,d}$ and $\sqrt{\mu_{ref,d}}$, the uninformative distribution, Uniform [-infinite, infinite], was adopted as the prior distribution. Especially, the half Cauchy distribution as the prior distribution for the estimated standard deviation of $\sqrt{\mu}$, $\sigma_{\sqrt{\mu},d}$ as following:

$$\sigma_{\sqrt{\mu},d} \sim \text{Cauchy}(0,\ 1) \qquad (\sigma_{\sqrt{\mu},d} > 0) \quad (7\text{-}4).$$

The reference temperature for the growth rate model, $T_{ref,growth}$, was sat as 8.52°C which was the average temperature of the referenced dataset.

7.2.3. Food-chain calculation frame & conditions

This study has adopted the simple one-way model for the exposure assessment with the Monte Carlo simulation. The exposure assessment has considered storages on farm, pasteurisations, distributing from factory to retail store, storages on retail store, and storages

at domestic fridges. Therefore, it was the five-phase model. for the quantifications for growth and reduction behaviour, the linear models without lag phases. The all of random variables for Monte Carlo simulations were defined from referenced datasets (Table 7-1) with individual random seeds through the Numpy.random library (version 1.18.5).

Table 7-1a Variables used in the QMRA simulation

Parameters	Units	Notation	Description	Source
Contaminated probability of bulk tank	(-)	$P_{prevalence}$	$P_{prevalence,i}$	
		i	Classification ([1, 2], [0.5, 0.5]) *	
		$P_{prevalence,1}$	0.032	Meyer-Broseta et al., 2003
		$P_{prevalence,2}$	0.022	Dalzini et al., 2016
Contaminated occurrence	(-)	W_{cont}	$Bernoulli(< P_{prevalence})$ If contaminated $W_{cont} = 1$, if not $W_{cont} = 0$.	
Initial concentration	log CFU/ mL	Log C_0	Log $C_{0,i}$	
		Log $C_{0,1}$	Cumulative ([-7.29, -6.72, -6.14, -5.55, -4.97, -4.40, -3.81, -3.21, -2.64, -2.05, -1.48, -0.905, -0.309, 0.260, 0.830], [9.39×10^{-6}, 2.84×10^{-5}, 5.62×10^{-5}, 1.43×10^{-4}, 6.08×10^{-4}, 1.79×10^{-3}, 6.98×10^{-3}, 0.0163, 0.0603, 0.150, 0.415, 0.776, 0.948, 0.974, 1.0])	Meyer-Broseta et al., 2003
		Log $C_{0,2}$	Cumulative ([-1.4, 0, 1, 2, 3, 4], [0, 0.128, 0.822, 0.904, 0.941, 1.0])	Dalzini et al., 2016
Temperature of on-farm storage	°C	T_{farm}	Cumulative ([-0.25, 0.25, 0.75, 1.25, 1.75, 2.25, 2.75, 3.25, 3.75, 4.25, 4.75, 5.25, 5.75, 6.25, 6.75, 7.25, 7.75, 8.25, 8.75, 9.25, 9.75, 10.25, 10.75, 11.25, 11.75, 12.25], [0, 0.000792, 0.000792, 0.00301, 0.0112, 0.06289, 0.151, 0.355, 0.556, 0.723, 0.809, 0.867, 0.910, 0.942, 0.96, 0.983, 0.990, 0.994, 0.997, 0.9987, 0.9992, 0.9996, 0.9998, 0.9998, 0.9998, 1.0])	Servello et al., 2004
Time of on-farm storage	h	$time_{farm}$	PERT (1.5, 12, 36)	Barker et al., 2013
Growth rate on farm storage	log CFU/ mL/h	μ_{farm}	If $T_{farm} < T_{min,d'}$: 0 else: $\left[\text{Normal}\left(\sqrt{\mu_{ref,d'}} \times \frac{T_{farm} - T_{min,d'}}{T_{ref,growth} - T_{min,d'}},\ \sigma_{\sqrt{\mu},d'}\right)\right]^2$ $T_{ref,growth}$: 8.52ºC (Mean of dataset) Bayesian MCMC iteration: 100000 Parameters: Mean (S.D.) μ_{ref}: 0.0283 (8.8×10^{-4}) T_{min}: -3.47 (0.54) $\sigma_{\sqrt{\mu}}$: 0.0275 (1.9×10^{-3})	Bayesian model in this study
		d'	Discrete Uniform (1, 100000)	
Maximum population density	log CFU/ mL	$MPD_{(T)}$	Uniform (6.5, 7.5) (T<5) Uniform (7.0, 8.0) (5≤T<7) Uniform (7.5, 8.5) (T≥7)	FDA, 2003
Concentration after on-farm storage	log CFU/ mL	Log C_{farm}	Min (Log $C_0 + \mu_{farm} time_{farm}$, $MPD_{(T_{farm})}$)	Linear growth and stationary model

Table 7-1b Variables used in the QMRA simulation

Parameters	Units	Notation	Description	Source
Temperature of thermal inactivation	°C	T_{heat}	PERT ($T_{heat,k} - \varepsilon_{T,heat,j}$, $T_{heat,k}$, $T_{heat,k} + \varepsilon_{T,heat,j}$)	This study
		j	Classification ([1, 2, 3, 4], [0.25, 0.25, 0.25, 0.25]) *	
		k	Classification ([1, 2, 3, 4], [0.25, 0.25, 0.25, 0.25]) *	
		$T_{heat,1}$	72	Melini et al., 2017
		$T_{heat,2}$	72.5	This study
		$T_{heat,3}$	74	This study
		$T_{heat,4}$	75	Melini et al., 2017
		$T_{heat,5}$	85 **** (Only for scenario analysis)	Melini, et al. 2017
Variation magnitude of heating temperature	°C	$\varepsilon_{T,heat,1}$	0.05	This study
		$\varepsilon_{T,heat,2}$	0.25	
		$\varepsilon_{T,heat,3}$	0.5	
		$\varepsilon_{T,heat,4}$	1	
Time of thermal inactivation	s	$time_{heat}$	PERT ($time_{heat,k}(1 - \varepsilon_{time,heat,l})$, $time_{heat,k}$, $time_{heat,k}(1 + \varepsilon_{time,heat,l})$)	This study
		l	Classification ([1, 2, 3, 4], [0.25, 0.25, 0.25, 0.25]) *	
		$time_{heat,1}$	15	Melini et al., 2017
		$time_{heat,2}$	20	This study
		$time_{heat,3}$	20	This study
		$time_{heat,4}$	20	Melini et al., 2017
Variation magnitude of heating time	(-)	$\varepsilon_{time,heat,1}$	0.01	This study
		$\varepsilon_{time,heat,2}$	0.05	
		$\varepsilon_{time,heat,3}$	0.10	
		$\varepsilon_{time,heat,4}$	0.25	
D-value at heating temp.	min	$D_{(T_{heat})}$	$10^{\text{Normal}\left(-\frac{T_{heat}-T_{ref,heat}}{z_{b'}}+\text{Log}\,D_{ref,b'},\ \sigma_{\text{Log}\,D,b'}\right)}$ $T_{ref,heat}$: 62.3ºC (Mean of dataset) Bayesian MCMC iteration: 100000 Parameters: Mean (S.D.) z: 6.37 (0.14) D_{ref}: 0.81 (0.04) $\sigma_{\text{Log}\,D}$: 0.29 (0.01)	Bayesian model in this study
		b'	Discrete Uniform (1, 100000)	
Concentration after heating	log CFU/mL	Log C_{heat}	Log $C_{farm} - \frac{time_{heat}}{60D_{(T_{heat})}}$	Linear reduction model
Package size	mL	$Size_{pack}$	1000	This study
Pathogen counts in a package after heating	CFU /pack	N_{heat_pack}	$\text{Poisson}\left(Size_{pack}10^{\text{Log}\,C_{heat}}\right)$	
Temperature of distributing storage	°C	T_{dist}	Normal (6.66, 1.64)	Koutsoumanis et al., 2010
Time of distributing storage	h	$time_{dist}$	Weibull (1.98, 4.33)	Koutsoumanis et al., 2010

Table 7-1c Variables used in the QMRA simulation

Parameters	Units	Notation	Description	Source
Growth rate on distributing storage	log CFU/ mL/h	μ_{dist}	If $T_{dist} < T_{min,d'}$: 0 else: $\left[\text{Normal}\left(\sqrt{\mu_{ref,d'}} \times \frac{T_{dist} - T_{min,d'}}{T_{ref,growth} - T_{min,d'}},\ \sigma_{\sqrt{\mu},d'}\right)\right]^2$	Bayesian model in this study
Pathogen count after distributing	CFU/ pack	N_{dist}	If $N_{heat_pack} > Size_{pack} \times 10^{\text{MPD}(T_{dist})}$: N_{heat_pack} else: Min (N_{heat_pack} + Negbin$\left(N_{heat_pack}, 10^{-\mu(T_{dist})time_{dist}}\right)$, $Size_{pack} \times 10^{\text{MPD}(T_{dist})}$)	Linear growth and stationary model
Concentration after distributing	log CFU/ mL	$\text{Log}C_{dist}$	$\text{Log}\left(\frac{N_{dist}}{Size_{pack}}\right)$	
Temperature of retail storage	°C	T_{retail}	Normal (4.98, 2.9)	Koutsoumanis et al., 2010
Time of retail storage	h	$time_{retail}$	Cumulative ([0, 5, 15, 25, 35, 45, 55, 65, 75, 85, 95, 105], [0, 0.0198, 0.443, 0.718, 0.85, 0.916, 0.951, 0.970, 0.982, 0.992, 0.997, 1.0])	Koutsoumanis et al., 2010
Growth rate on retail storage	log CFU/ mL/h	μ_{retail}	If $T_{retail} < T_{min,d'}$: 0 else: $\left[\text{Normal}\left(\sqrt{\mu_{ref,d'}} \times \frac{T_{retail} - T_{min,d'}}{T_{ref,growth} - T_{min,d'}},\ \sigma_{\sqrt{\mu},d'}\right)\right]^2$	Bayesian model in this study
Pathogen count after retail storage	CFU/ pack	N_{retail}	If $N_{dist} > Size_{pack} \times 10^{\text{MPD}(T_{retail})}$: N_{dist} else: Min (N_{dist} + Negbin$\left(N_{dist}, 10^{-\mu(T_{retail})time_{retail}}\right)$, $Size_{pack} \times 10^{\text{MPD}(T_{retail})}$)	Linear growth and stationary model
Concentration after retail storage	log CFU/ mL	$\text{Log}C_{retail}$	$\text{Log}\left(\frac{N_{retail}}{Size_{pack}}\right)$	
Temperature of domestic storage	°C	$T_{domestic}$	Classification ([Normal (7.57, 2.95), Normal (6.31, 2.66), Normal (6.69, 3.29), Normal (8.40, 3.00)], [0.25, 0.19, 0.05, 0.51]) *	Koutsoumanis et al., 2010
Time of domestic storage	day	$time_{domestic}$	Cumulative ([0, 1, 2, 3, 4, 5], [0, 0.23, 0.74, 0.96, 0.98, 1.0])	Koutsoumanis et al., 2010
Growth rate on domestic storage	log CFU/ mL/h	$\mu_{domestic}$	If $T_{domestic} < T_{min,d'}$: 0 else: $\left[\text{Normal}\left(\sqrt{\mu_{ref,d'}} \times \frac{T_{domestic} - T_{min,d'}}{T_{ref,growth} - T_{min,d'}},\ \sigma_{\sqrt{\mu},d'}\right)\right]^2$	Bayesian model in this study

Table 7-1d Variables used in the QMRA simulation

Parameters	Units	Notation	Description	Source
Pathogen count after domestic storage	CFU/ pack	$\mathrm{N}_{domestic}$	If $N_{retail} > Size_{pack} \times 10^{\mathrm{MPD}_{(T_{domestic})}}$: N_{retail} else: Min ($N_{retail} + \mathrm{Negbin}\left(N_{retail}, 10^{-\mu_{(T_{domestic})} time_{domestic}}\right)$, $Size_{pack} \times 10^{\mathrm{MPD}_{(T_{domestic})}}$)	Linear growth and stationary model
Concentration after domestic storage	log CFU/ mL	Log $C_{domestic}$	$\mathrm{Log}\left(\frac{\mathrm{N}_{domestic}}{Size_{pack}}\right)$	
Serving size	mL	$Size_{serve}$	Cumulative ([0, 238, 239, 476, 714], [0, 0.50, 0.75, 0.95, 1.0])	WHO/FAO , 2004
Dose level	CFU	$Dose$	$\mathrm{Poisson}\left(\mathrm{N}_{domestic}\frac{Size_{serve}}{Size_{pack}}\right)$	
r-value	(-)	r	Classification ($[r_{Intermediate}, r_{Perinatal}, r_{Elder}]$, [0.823, 5.71×10^{-3}, 0.171]) *	FDA, 2003
		$\log r_{Intermediate}$	Normal (-14.11, 1.62)	Pouillot et al., 2015
		$\log r_{Perinatal}$	Normal (-11.70, 1.62)	Pouillot et al., 2015
		$\log r_{Elder}$	Normal (-12.83, 1.62)	Pouillot et al., 2015
Illness probability	-	P_{ill}	$1 - e^{-rDose}$	WHO/FAO , 2004
Illness occurrence	(-)	W_{ill}	$\mathrm{Bernoulli}(< P_{ill})$ If illness $W_{ill} = 1$, if not $W_{ill} = 0$	

* Classification ($[A, B, C]$, $[p_A, p_B, p_C]$) denotes the function for divisions to cases; the output value derived from the function is assigned to A with a probability of p_A, to B with a probability of p_B, and to C with a probability of p_C.

** The valuables of i, j, k, and l denotes the indicator for divisions to cases.

*** The b' denotes the indicator for the parameter set number from Bayesian MCMC for the developed reduction model; The d', d'', d''', and d'''' denote the indicators for the parameter set number from Bayesian MCMC for the developed growth model.

**** 85ºC heating was used only for scenario analysis.

***** Log 0 was calculated as the negative infinity.

7.2.3.1. Prevalence and initial concentration

The simulated initial concentrations, Log C_0, were defined with the couples of datasets of prevalence (contaminated ratios) and initial contamination level. The initial concentration of *L. monocytogenes* in milk characterized as a cumulative distribution (Table 7-1) derived from two dataset (Dalzini et al., 2016; Meyer-Broseta, Diot, Riviere, & Cerf, 2003) of prevalence and initial concentration of *L. monocytogenes* were used for the Monte Carlo simulations.

The first step was to define whether the milk was contaminated or not, W_{cont}. The W_{cont} were defined from Bernoulli distribution which generates dummy variable (0 or 1). The 1 of W_{cont} indicates the milk is contaminated, while the 0 of W_{cont} indicates the milk is NOT contaminated. The Bernoulli follows the prevalence dataset. The choice of which of the two referenced datasets to use was selected randomly on a 50/50 basis. After generating the W_{cont}, if W_{cont} was 1, the initial concentration was generated with the cumulative distribution derived from the chosen dataset.

7.2.3.2. On-farm time, temperature and growth of *L. monocytogenes* in milk

The distributions of the temperature, T_{farm}, (Servello, Hill, & Lencki, 2004) and the storage time, $time_{farm}$, (Barker & Goméz-Tomé, 2013) on farm were used for generating the Monte Carlo simulations. The on-farm storage temperatures were randomly determined from cumulative distribution referenced from Servello et al., 2004, and the on-farm times were randomly determined from the PERT distribution referenced from Barker et al., 2013 (Table 7-1). The PERT distribution is widely used in risk analysis branches, and it is decided by three parameters, the minimum, mode and maximum value. The generated storage conditions in this study were assumed as constant and used for the calculation of *L. monocytogenes* growth on farm storage.

The growth rates on farm storage were also randomly determined from the Bayesian model we developed in this study (see above the section: Growth model for *Listeria monocytogenes* in milks based on Bayesian inference). The Bayesian model has numerous parameter-sets for describing the variation of estimates. In each iteration, the ID of the parameter set were determined by the discrete uniform distribution (Table 7-1: Discrete Uniform (1, 100000)). The parameter set used in on-farm section was used in whole growth section for one iteration including the distributing, retail and domestic storage section. After determination of the parameter set for the growth behaviour, the root of growth rate at the on-farm temperature $\sqrt{\mu_{farm}}$ was determined by normal distribution using the secondary model (Eq. 7-3) and the chosen parameter set. For analysing the relevance effect of variability of the growth rate, μ, of *L. monocytogenes*, the deviations of the $\sqrt{\mu_T}$ were defined as the difference from the median of the simulated $\sqrt{\mu_T}$. The deviations were calculated in each temperature. The linear growth and stationary growth model was used for the growth estimation during all of storages in this study. The referenced Maximum Population Density (MPD) (U.S. Food and Drug Administration, 2003)depended on temperature of growth environment. It was assumed that once pathogens increased, they could not be reduced except by pasteurisation in this study. The pathogen concentrations after on-farm storage, Log C_{farm}, were defined as Min (Log $C_0 + \mu_{farm} time_{farm}$, $\mathrm{MPD}_{(T_{farm})}$) according to the linear and stationary model of bacterial growth. The pathogen count ratio of growth by on-farm storage, Δ Log C_{farm}, were defined as the difference in the logarithms of pathogen concentration before and after storage as Log C_{farm} − Log C_0.

7.2.3.3. Heating conditions of pasteurization and thermotolerance of *L. monocytogenes* in milk

The thermal conditions of pasteurisation in this study were 72ºC-15 seconds, 72.5ºC-20 seconds, 74ºC-20seconds, 75ºC-seconds and 85ºC-20 seconds. The 85ºC-20seconds condition was used only for the scenario analysis after described. The four thermal conditions (72ºC-15 seconds, 72.5ºC-20 seconds, 74ºC-20seconds and 75ºC-seconds) were used for 10 billion QMRA simulations. The target of the thermal condition of each iteration was randomly determined with the same probability. After the determination of the target thermal condition, the magnitude of the error of the thermal condition, $\varepsilon_{T,heat}$ and $\varepsilon_{time,heat}$, was determined in each iteration. As the variation of magnitude, the four patterns were prepared for heating temperature and time. For the magnitude of heating temperature, ±0.05ºC, ±0.25ºC, ±0.5ºC, and ±1.0ºC, and for the that of the heating time, ±1%, ±5%, ±10%, and ±25% of target time were adopted in this QMRA simulations. Each error was randomly selected with the same probability. The simulated thermal condition (heating temperature (ºC): T_{heat}; heating time (sec): $time_{heat}$) were defined by the PERT distribution. The mode of the PERT distributing was assumed as the target thermal condition in each iteration, and the minimum and maximum of PERT distribution was assumed as the errors of the conditions. For analysing the relevance effect of errors of the thermal conditions, the deviation from target heating conditions were defined as the deference of heating condition from the target heating conditions of each iteration.

The thermotolerance of pathogen (D-value) were randomly selected from the developed Bayesian predictive model in this study. Same as the growth bayesian model, the Bayesian model for pathogen reductions has numerous parameter-sets for describing the variation of estimates. In each iteration, the ID of the parameter set were determined by the discrete uniform distribution (Table 7-1: Discrete Uniform (1, 100000)). After determination of the parameter set for the reduction behaviour, the common logarithm of D-value (min), $\mathrm{Log}\, D_{(T_{heat})}$, was determined by normal distribution using the secondary model (Eq. 7-1) and

the chosen parameter set. For analysing the relevance effect of variability of the thermotolerance of *L. monocytogenes*, the deviations of the $\mathrm{Log}\, D_{(T)}$ were defined as the difference from the median of the simulated $\mathrm{Log}\, D_{(T)}$. The deviations were calculated in each temperature. The D-value model was used for the estimation of the pathogen concentrations after pasteurisations, $\mathrm{Log}\, C_{heat}$, as $\mathrm{Log}\, C_{farm} - \frac{time_{heat}}{60 D_{(T_{heat})}}$. The pathogen count ratio of reduction by pasteurisation, $\Delta\, \mathrm{Log}\, C_{heat}$, were defined as the difference in the logarithms of pathogen concentration before and after pasteurisation as $\mathrm{Log}\, C_{heat} - \mathrm{Log}\, C_{farm}$.

For considering the effect of packing of milk, the pathogen count and change of that were discretely calculated. The package size, $Size_{pack}$, was defined as 1000 mL, and the pathogen counts after packing (CFU/pack), N_{heat_pack}, were simulated with the Poisson distribution as $\mathrm{Poisson}\left(Size_{pack} 10^{\mathrm{Log}\, C_{heat}}\right)$. The Poisson distribution describes the variations of the separated bacterial count from the average value of bacterial counts (Koyama, Hokunan, Hasegawa, Kawamura, & Koseki, 2016). After packing, all of the growth estimation was calculated in discretely methods.

7.2.3.4. Distributing time, temperature and growth of *L. monocytogenes* in milk

The distributions of the distributing temperature, T_{dist}, and the distributing storage time, $time_{dist}$, were used for generating the Monte Carlo simulations. The distributing storage conditions were randomly determined from referenced distributions (Koutsoumanis, Pavlis, Nychas, & Xanthiakos, 2010) which are the normal distribution for T_{dist} and the Weibull distribution for $time_{dist}$ (Table 7-1).

The growth rates during distributing were also randomly determined from the Bayesian model we developed in this study same as the growth rate on farm. The ID of the parameter set were already determined in on-farm section, so the root of growth rate at the

distributing temperature $\sqrt{\mu_{dist}}$ was determined by normal distribution using the secondary model (Eq. 7-3) and the chosen parameter set. As same as on-farm growth, the deviations of $\sqrt{\mu_T}$ were calculated, and the pathogen concentrations were defined by the linear and stationary growth model. The growths were calculated discretely. Therefore, the pathogen count per one package after distributing, N_{dist}, was defined as Min ($N_{heat_pack} +$ $\mathrm{Negbin}\left(N_{heat_pack}, 10^{-\mu_{(T_{dist})}time_{dist}}\right)$, $Size_{pack} \times 10^{\mathrm{MPD}_{(T_{dist})}}$) using the negative binomial distribution (Nauta, 2001). Therefore, the pathogen concentration after distributing, $\mathrm{Log}\ C_{dist}$, was derived as $\mathrm{Log}\left(\frac{\mathrm{N}_{dist}}{Size_{pack}}\right)$. The pathogen count ratio of growth by distributing, $\Delta\ \mathrm{Log}\ C_{dist}$, were defined as the difference in the logarithms of pathogen concentration before and after pasteurisation as $\mathrm{Log}\ C_{dist} - \mathrm{Log}\ C_{heat}$. If the pathogen count per package was 0, the calculations of the pathogen count ratio of growth were skipped because the logarithm of the concentration will be the minus infinite.

7.2.3.5. Retail time, temperature, and growth of *L. monocytogenes* in milk

The distributions of the retail temperature, T_{retail}, and the retail storage time, $time_{retail}$, were used for generating the Monte Carlo simulations. The retail storage conditions were randomly determined from referenced distributions (Koutsoumanis et al., 2010) which are the normal distribution for T_{retail} and the cumulative distribution based on the referenced data for $time_{retail}$ (Table 7-1).

The growth rates during distributing were also randomly determined from the Bayesian model we developed in this study same as the growth rate on farm. The ID of the parameter set were already determined in on-farm section, so the root of growth rate at the distributing temperature $\sqrt{\mu_{retail}}$ was determined by normal distribution using the secondary model (Eq. 7-3) and the chosen parameter set. As same as on-farm growth, the deviations of

$\sqrt{\mu_T}$ were calculated, and the pathogen concentrations were defined by the linear and stationary growth model. The growths were calculated discretely. Therefore, the pathogen count per one package after distributing, N_{retail}, was defined as Min ($N_{dist} +$ $\mathrm{Negbin}\left(N_{dist}, 10^{-\mu_{(T_{retail})}time_{retail}}\right)$, $Size_{pack} \times 10^{\mathrm{MPD}_{(T_{retail})}}$) using the negative binomial distribution (Nauta, 2001). If the Log C_{dist} was higher than $\mathrm{MPD}_{(T_{retail})}$, the Log C_{retail} was defined as equal to the Log C_{dist}. Therefore, the pathogen concentration after distributing, Log C_{retail}, was derived as $\mathrm{Log}\left(\frac{\mathrm{N}_{retail}}{Size_{pack}}\right)$. The pathogen count ratio of growth by distributing, Δ Log C_{retail}, were defined as the difference in the logarithms of pathogen concentration before and after pasteurisation as Log C_{retail} − Log C_{dist}. If the pathogen count per package was 0, the calculations of the pathogen count ratio of growth were skipped because the logarithm of the concentration will be the minus infinite.

7.2.3.6. Domestic time, temperature, and growth of *L. monocytogenes* in milk

The distributions of the domestic storage temperature, $T_{domestic}$, and the domestic storage time, $time_{domestic}$, were used for generating the Monte Carlo simulations. The retail storage conditions were randomly determined from referenced distributions (Koutsoumanis et al., 2010) which are the normal distribution for $T_{domestic}$ and the cumulative distribution based on the referenced data for $time_{domestic}$ (Table 7-1).

The growth rates during distributing were also randomly determined from the Bayesian model we developed in this study same as the growth rate on farm. The ID of the parameter set were already determined in on-farm section, so the root of growth rate at the distributing temperature $\sqrt{\mu_{domestic}}$ was determined by normal distribution using the secondary model (Eq. 7-3) and the chosen parameter set. As same as on-farm growth, the deviations of $\sqrt{\mu_T}$ were calculated, and the pathogen concentrations were defined by the

linear and stationary growth model. The growths were calculated discretely. Therefore, the pathogen count per one package after distributing, $N_{domestic}$, was defined as Min (N_{retail} + Negbin$\left(N_{retail}, 10^{-\mu_{(T_{domestic})}time_{domestic}}\right)$, $Size_{pack} \times 10^{\mathrm{MPD}_{(T_{domestic})}}$) using the negative binomial distribution (Nauta, 2001). If the Log C_{retail} was higher than $\mathrm{MPD}_{(T_{domestic})}$, the Log $C_{domestic}$ was defined as equal to the Log C_{retail}. Therefore, the pathogen concentration after distributing, Log $C_{domestic}$, was derived as Log $\left(\frac{N_{domestic}}{Size_{pack}}\right)$. The pathogen count ratio of growth by distributing, Δ Log $C_{domestic}$, were defined as the difference in the logarithms of pathogen concentration before and after pasteurisation as Log $C_{domestic}$ − Log C_{retail}. If the pathogen count per package was 0, the calculations of the pathogen count ratio of growth were skipped because the logarithm of the concentration will be the minus infinite.

7.2.3.7. Consumption conditions and pathogenicity of *L. monocytogenes*

The serving size per one serve of consumption was referenced data (Food and Agriculture Organization/ World Health Organization, 2021) and generated as random numbers following to the cumulative distribution based on the referenced data. The hosts consuming the simulated milk were randomly selected from three types of host populations: intermediate, perinatal, and elderly. The host classification probability was derived based on reported data of the estimated number of annual servings of pasteurised milk consumed by the host populations (intermediate: 7.2×10^{10}, perinatal: 5.0×10^{8}, and elderly: 1.5×10^{10}; (U.S. Food and Drug Administration, 2003)). The pathogenicity, Log r value of dose response model, was randomly generated from the referenced normal distribution depends on the host populations (intermediate: $\mathrm{Normal}(-14.11, 1.62)$, perinatal: $\mathrm{Normal}(-11.70, 1.62)$, and elderly: $\mathrm{Normal}(-12.83, 1.62)$; (Pouillot, Hoelzer, Chen, & Dennis, 2015)). The illness

probability per one serve, P_{ill}, was determined by the exponential model defined as $1 - e^{-rDose}$.

7.2.4. Illness occurrence from illness probability per one serving

The illness occurrence, W_{ill}, indicates whether the simulated scenario causes illness or not defined by the Bernoulli distribution that has the illness probability as the threshold. The 1 of W_{ill} indicates the food chain caused illness, while the 0 of W_{ill} indicates the food chain did NOT cause illness. The number of illness cases was derived from numerous iterations of food chain simulation.

7.2.5. Sensitivity analysis for elucidating the relevance factors to listeriosis

For elucidating the relevance of each factor to QMRA results, the Spearman's ranked correlation coefficients of variable factors were derived. For a comparison, both of the correlations against to the pathogen log concentration at eating, Log $C_{domestic}$, and against to the illness occurrence, W_{ill}. Due to the limitation of used computer spec (MacBook pro, 13inch, M1-CPU, 2020), the calculation of the Spearman's correlation of 10 billion simulations were conducted separately by 10 times of calculation: 1 billion simulations for one correlation calculation.

7.2.6. Scenario analysis for different thermal condition target

For analysing the difference in effect of the simulated thermal target (72-75ºC; 15-20 sec) and higher target (85ºC; 20 sec), the scenario analysis of the different thermal condition target was conducted. Only the heating condition targets were fixed, and a billion iterations of QMRA simulations were performed for each heating target. Other variable factors and calculation were completely same as the above simulation framework. As the output, not only

illness occurrence, W_{ill}, but also the average of the illness probability per one serve, $\overline{P_{ill}}$ were derived in the scenario analysis.

7.3. Results

7.3.1. Bayesian model fitting

Bayesian secondary models for describing the reduction behaviour by pasteurisations and the growth behaviour at low temperature of *L. monocytogenes* in milk were successfully fitted to each metadata, the r-hut values of all estimated parameters were 1.0 which indicate the estimation of posterior parameter distribution were convergence. The estimated 95% confidence and predicted band of reduction and growth were showed in Fig. 7-S1. The estimated parameter means, and the standard deviations were indicated at the Bayesian reduction and growth model cells in Table 7-1.

7.3.2. Illness cases and expected value of illness probability

The illness occurrences of 61 cases were estimated by the 10 billion iterations of QMRA simulation for listeriosis from pasteurised milk. Therefore, the illness probability derived from the Illness occurrence was 6.1×10^{-8}. The sum of the estimated P_{ill}, which can be assumed as the expected value of illness cases, were calculated as 61.6. Therefore, the expected illness probability was calculated as 6.2×10^{-8}. The simulation of 10 billion servings had taken almost 3 weeks on the latest laptop (MacBook pro, M1, 2020) when the simulation was done. The details of condition and the concentration changes were showed in Table 7-2.

Table 7-2a Conditions in the illness cases

Illness ID Num.	Initial level (log CFU/mL)	Farm temp. (℃)	Farm time (h)	√μ variability on farm	Growth ratio on farm (log CFU/CFU)	Target heating temp. (℃)	Target heating time (sec)	Heating temp. (℃)	Heating time (sec)	Log D variability (log min)
1	0.06	8.7	8.9	0.026	0.35	72	15	71.9	15.1	0.92
2	0.66	4.3	23.4	0.035	0.49	72	15	71.9	14.9	0.70
3	3.24	2.8	27.9	0.000	0.21	72.5	20	72.5	20.1	0.48
4	3.05	3.6	16.0	-0.005	0.14	74	20	74.0	17.0	1.01
5	-0.36	3.2	13.1	-0.003	0.11	72.5	20	72.3	19.2	0.66
6	0.65	4.0	8.2	0.017	0.12	72	15	72.0	15.5	0.84
7	1.08	2.7	22.2	0.005	0.18	72	15	72.0	15.3	0.62
8	0.36	7.3	29.9	-0.024	0.47	72	15	72.4	15.0	0.84
9	3.62	4.8	16.3	-0.027	0.13	72	15	72.0	15.2	0.51
10	3.67	4.7	20.6	0.002	0.28	72	15	72.0	15.0	0.69
11	0.39	4.1	15.1	0.006	0.19	72	15	72.0	16.1	0.56
12	-1.49	6.2	6.9	-0.037	0.07	72	15	72.0	14.9	0.96
13	2.55	5.0	20.0	0.009	0.32	72	15	72.0	15.3	0.22
14	3.32	3.2	14.1	-0.005	0.11	72	15	71.9	15.3	0.97
15	3.95	4.7	27.0	-0.035	0.17	72	15	71.8	13.9	0.55
16	0.44	7.2	8.1	0.008	0.20	72	15	71.9	17.2	0.76
17	-0.16	4.6	9.5	0.026	0.18	72	15	72.2	15.1	0.79
18	3.42	8.7	8.4	-0.053	0.11	72	15	72.0	14.4	0.59
19	2.30	5.4	5.3	-0.009	0.07	72	15	71.9	15.2	0.34
20	2.36	6.6	16.7	0.034	0.50	72	15	72.0	14.5	0.32
21	3.83	3.5	10.6	0.015	0.14	74	20	73.3	19.7	0.80
22	3.13	3.2	6.5	0.006	0.06	72	15	72.2	14.5	0.56
23	0.94	4.7	9.5	-0.044	0.05	72	15	71.2	15.0	0.56
24	3.52	4.7	15.7	0.033	0.33	72	15	72.2	14.2	0.59
25	3.48	3.6	8.9	0.040	0.17	72	15	72.0	11.9	0.49
26	3.68	4.1	18.6	0.018	0.29	72	15	72.0	15.0	0.21
27	0.76	2.9	22.9	0.000	0.18	72	15	72.0	15.3	1.03
28	2.16	2.4	10.9	-0.010	0.06	72.5	20	72.5	20.7	0.80
29	3.91	5.3	11.0	0.006	0.18	72	15	71.6	14.6	0.56
30	0.74	2.6	17.7	-0.009	0.10	72	15	72.0	14.7	0.46
31	3.74	3.5	15.1	0.004	0.16	72	15	72.1	15.0	0.52
32	1.81	5.7	4.9	-0.017	0.06	72	15	72.0	14.7	0.54
33	0.95	2.8	7.1	0.029	0.10	72	15	72.0	15.1	0.75
34	4.00	4.8	15.1	-0.071	0.03	72	15	72.0	14.8	0.73
35	-0.55	4.2	19.6	0.040	0.42	72	15	72.0	15.0	0.76
36	3.81	3.3	11.1	0.063	0.27	72.5	20	72.5	20.1	0.77
37	0.97	6.6	19.6	0.077	0.92	72	15	72.0	14.4	0.98
38	2.06	4.1	18.3	-0.029	0.11	72	15	72.0	14.4	0.35
39	1.71	6.0	22.7	-0.041	0.19	72.5	20	72.5	20.0	0.73
40	3.47	6.1	12.3	-0.006	0.20	72	15	72.0	14.9	0.45
41	3.87	6.6	22.3	0.044	0.76	72	15	72.0	14.9	0.56
42	3.94	2.1	9.8	0.000	0.06	72.5	20	72.2	20.5	0.70
43	1.41	3.5	7.9	-0.002	0.07	72	15	72.0	14.9	0.44
44	0.47	3.3	24.3	-0.046	0.06	72	15	72.1	15.0	0.80
45	3.84	4.2	14.7	-0.058	0.03	72	15	72.0	14.9	0.17
46	3.54	4.9	12.0	0.004	0.17	72.5	20	72.0	19.9	0.66
47	3.41	6.6	15.3	0.020	0.39	72	15	72.2	14.1	0.70
48	1.01	3.3	11.2	0.010	0.12	72.5	20	72.0	23.4	1.19
49	0.72	6.3	10.3	0.043	0.33	72	15	72.0	14.6	0.64
50	0.37	4.9	16.6	0.037	0.39	72	15	71.7	15.1	0.56
51	0.07	1.9	6.8	0.017	0.06	72	15	72.0	11.6	0.68
52	0.91	3.1	18.1	0.008	0.18	74	20	73.9	20.0	1.09
53	3.59	3.7	8.5	-0.019	0.05	72.5	20	72.4	18.6	0.66
54	1.05	3.8	14.5	0.011	0.18	72	15	72.0	15.0	0.40
55	2.66	3.0	17.3	-0.035	0.05	72.5	20	72.3	20.4	0.73
56	0.80	2.7	9.0	0.008	0.08	72	15	72.0	14.5	0.73
57	2.47	3.6	9.7	-0.030	0.05	72	15	72.0	14.9	0.88
58	3.85	3.0	21.0	-0.014	0.12	72	15	71.5	13.1	0.68
59	-0.35	4.6	5.3	0.022	0.10	74	20	73.8	20.4	0.97
60	3.90	6.1	6.2	-0.013	0.09	72	15	72.0	14.1	0.58
61	3.75	4.0	23.4	-0.002	0.24	72	15	72.0	13.8	0.64
Quantile										
0.25	-1.5	3.0	9.4	-0.018	0.1	72	15	72.2	16.7	-0.21
0.5	-0.7	3.6	13.7	0.001	0.1	72.5	20	73.2	19.9	-0.01
0.75	0.4	4.4	18.6	0.019	0.2	74	20	74.5	20.1	0.19

Table 7-2b Conditions in the illness cases

Illness ID Num	Reduction ratio by heating (log CFU/CFU)	Distributing temp. (℃)	Distributing time (h)	√μ variability on distributing	Growth ratio on distributing (log CFU/CFU)	Retail temp. (℃)	Retail time (day)	√μ variability on retail
1	-1.1	7.7	6.6	0.011	0.17	3.4	1.5	0.027
2	-1.9	8.1	2.8	0.013	0.09	2.9	0.6	0.028
3	-5.3	5.1	3.8	-0.013	0.03	8.1	3.9	0.002
4	-2.3	9.3	5.2	-0.003	0.17	8.0	2.2	-0.008
5	-3.2	7.0	4.4	-0.016	0.00	10.4	0.4	0.006
6	-1.5	11.2	4.3	-0.035	0.16	5.8	0.7	-0.012
7	-2.5	7.4	9.7	-0.009	0.19	3.3	0.5	0.001
8	-1.7	7.5	4.0	-0.021	0.06	3.1	1.3	0.028
9	-3.1	5.1	0.8	0.011	0.01	8.8	2.4	0.027
10	-2.1	7.0	2.0	-0.032	0.03	8.9	3.7	0.033
11	-2.9	7.5	4.0	0.004	0.00	4.9	1.0	-0.048
12	-1.1	8.8	4.3	-0.014	0.22	6.5	0.9	0.002
13	-6.3	6.3	0.9	-0.039	0.00	4.0	1.1	0.013
14	-1.0	6.1	4.6	0.004	0.09	1.6	0.6	0.003
15	-2.4	5.9	8.3	-0.018	0.11	9.2	2.2	0.055
16	-1.9	9.1	5.8	0.002	0.14	3.0	0.3	-0.007
17	-1.8	5.7	3.0	0.004	0.10	5.1	1.0	-0.005
18	-2.4	5.7	3.5	-0.022	0.04	3.0	0.3	0.016
19	-4.5	7.7	2.4	0.030	0.00	5.9	0.5	0.059
20	-4.6	6.1	5.8	0.029	0.16	3.8	0.9	0.003
21	-3.2	5.9	10.3	0.024	0.25	7.7	1.7	-0.004
22	-2.8	6.5	2.6	0.026	0.08	-1.2	0.9	0.010
23	-2.0	3.9	4.2	0.018	0.09	2.7	2.5	-0.013
24	-2.6	6.8	3.8	-0.002	0.08	3.6	0.4	0.052
25	-2.5	8.4	2.6	0.033	0.11	8.3	0.8	0.046
26	-6.1	6.2	0.7	0.003	0.00	10.1	0.7	0.016
27	-1.0	8.2	5.2	0.014	0.17	14.4	2.9	0.041
28	-2.6	7.2	9.2	-0.015	0.15	5.5	0.9	-0.001
29	-2.3	6.1	5.1	-0.037	0.05	6.0	1.1	0.053
30	-3.5	6.2	3.6	0.053	0.30	3.5	0.9	0.027
31	-3.2	4.6	4.3	0.023	0.08	8.3	1.9	-0.008
32	-2.9	6.7	11.3	-0.019	0.14	-3.2	2.1	-0.016
33	-1.8	5.0	3.3	-0.011	0.03	7.9	0.8	0.010
34	-1.9	3.8	6.6	0.013	0.09	6.2	2.0	0.050
35	-1.7	10.1	2.4	-0.007	0.11	0.9	0.3	-0.020
36	-2.8	7.0	4.0	0.029	0.12	6.0	0.9	0.011
37	-1.0	9.7	3.9	0.052	0.22	5.5	1.3	-0.002
38	-4.4	6.1	4.8	-0.026	0.07	7.7	3.6	0.081
39	-3.0	6.9	7.3	-0.044	0.07	4.9	1.2	0.012
40	-3.5	3.9	0.1	-0.009	0.00	8.6	2.4	0.016
41	-2.8	7.7	3.9	0.034	0.14	5.3	2.6	0.009
42	-3.0	6.1	1.8	0.014	0.04	7.3	1.3	-0.005
43	-3.7	8.7	5.3	0.022	0.37	11.4	0.7	-0.006
44	-1.6	8.4	2.2	0.007	0.06	3.4	0.3	0.034
45	-6.6	6.5	1.3	-0.046	0.00	8.0	0.6	-0.008
46	-3.0	5.4	3.2	0.004	0.05	10.9	3.4	0.008
47	-2.0	8.6	5.2	0.008	0.16	2.2	1.5	0.061
48	-1.0	8.5	3.6	0.054	0.18	5.6	3.4	0.011
49	-2.3	8.7	1.0	0.006	0.02	7.9	0.5	0.049
50	-2.5	6.4	2.6	0.012	0.04	5.5	0.3	-0.034
51	-1.6	7.6	0.4	0.001	0.01	9.3	3.2	0.023
52	-2.2	7.3	6.0	0.020	0.18	5.1	1.5	0.007
53	-3.2	3.8	3.0	0.008	0.03	7.5	3.6	-0.039
54	-4.1	11.3	8.1	0.004	0.00	11.5	3.0	0.003
55	-2.8	6.8	4.0	0.059	0.14	-1.2	0.9	0.020
56	-1.8	5.7	5.3	0.030	0.15	5.6	0.6	-0.018
57	-1.3	5.2	2.5	-0.020	0.03	7.2	0.4	0.007
58	-1.5	3.9	2.9	0.026	0.05	4.8	4.0	0.019
59	-2.9	10.6	2.5	0.003	0.00	5.0	0.6	-0.011
60	-2.5	4.9	3.9	0.000	0.05	2.4	0.3	-0.013
61	-2.0	2.9	3.8	-0.003	0.03	12.0	1.2	0.003
Quantile								
0.25	-37.6	5.6	2.3	-0.018	0.0	3.0	0.4	-0.018
0.5	-20.8	6.7	3.6	0.001	0.0	5.0	0.7	0.001
0.75	-11.4	7.8	5.1	0.019	0.1	6.9	1.1	0.019

Table 7-2c Conditions in the illness cases

Illness ID Num.	Growth ratio on retail (log CFU/CFU)	Domestic temp. (°C)	Domestic time (day)	√μ variability on domestic	Growth ratio on domestic (log CFU/CFU)	Serving size (mL)	Pathogenicity (Log r value)	Subject group	Log Dose (log CFU)
1	0.56	11.8	3.8	0.073	7.5	63	-9.2	Elder	9.2
2	0.19	11.0	4.7	0.094	8.8	238	-11.8	Intermediate	10.8
3	2.39	14.0	4.6	0.043	7.8	619	-10.3	Elder	11.2
4	1.22	13.1	3.9	0.007	5.4	13	-8.3	Elder	8.7
5	0.60	17.0	4.8	0.033	10.8	637	-11.5	Intermediate	11.2
6	0.24	17.6	3.8	0.001	8.1	139	-9.1	Elder	9.9
7	0.17	15.8	2.7	0.045	6.3	237	-8.5	Elder	7.9
8	0.46	14.9	4.7	0.022	8.7	162	-8.7	Elder	10.6
9	2.30	9.0	2.4	0.012	2.0	332	-8.7	Elder	7.4
10	3.83	9.4	1.2	-0.010	0.8	238	-8.4	Elder	8.9
11	0.08	16.1	4.3	0.038	10.0	168	-9.2	Elder	10.0
12	0.68	13.1	4.9	0.052	9.5	229	-10.1	Elder	10.2
13	0.00	15.1	3.7	0.057	9.0	210	-10.3	Intermediate	8.3
14	0.08	13.6	4.1	0.074	5.3	165	-11.3	Perinatal	10.1
15	2.90	10.0	1.9	0.008	1.8	131	-8.5	Elder	8.6
16	0.05	14.9	3.9	-0.008	5.9	107	-7.2	Intermediate	6.8
17	0.41	16.5	4.1	0.034	9.0	135	-10.2	Intermediate	10.0
18	0.08	14.3	3.9	0.029	6.4	239	-9.1	Intermediate	10.1
19	0.15	14.4	4.9	0.053	10.3	462	-12.7	Intermediate	10.9
20	0.22	12.4	4.7	0.067	9.4	24	-9.8	Intermediate	9.4
21	0.96	15.0	2.1	-0.022	2.8	239	-7.3	Intermediate	7.1
22	0.04	13.9	3.8	0.032	6.9	286	-11.2	Elder	9.9
23	0.38	13.2	3.4	0.095	8.7	238	-8.0	Elder	10.5
24	0.22	15.9	4.2	0.031	6.7	119	-10.6	Elder	10.3
25	0.83	11.8	2.8	0.077	5.7	436	-8.9	Elder	10.3
26	0.00	18.2	4.2	0.025	11.0	165	-10.6	Intermediate	10.2
27	5.92	7.4	1.5	0.032	1.2	455	-9.8	Elder	9.9
28	0.33	9.3	4.9	0.004	3.9	395	-8.8	Intermediate	6.7
29	0.93	11.7	2.8	0.005	3.2	239	-10.4	Elder	8.3
30	0.40	15.8	4.6	0.060	10.0	457	-9.7	Elder	10.3
31	1.11	12.2	4.9	0.006	5.8	693	-10.6	Elder	10.5
32	0.02	13.1	4.9	0.024	7.8	23	-8.2	Perinatal	8.3
33	0.53	13.6	3.9	0.053	7.9	22	-9.3	Intermediate	9.0
34	1.63	12.5	2.7	0.034	3.7	122	-10.0	Perinatal	9.7
35	0.03	16.3	4.9	0.026	9.7	382	-10.3	Intermediate	10.7
36	0.45	10.3	5.0	0.037	6.3	104	-8.5	Perinatal	10.2
37	0.50	15.1	4.5	0.018	5.9	239	-9.7	Intermediate	9.9
38	5.21	16.2	2.4	0.008	4.5	239	-10.6	Elder	9.9
39	0.48	16.0	4.6	0.057	8.9	672	-10.7	Intermediate	11.3
40	2.02	13.9	3.3	-0.006	4.5	12	-8.4	Intermediate	7.8
41	1.08	11.7	2.9	0.081	4.9	436	-10.6	Intermediate	10.6
42	0.64	14.2	4.7	-0.008	6.3	381	-10.8	Elder	10.6
43	0.73	11.7	4.8	0.024	6.5	238	-9.1	Elder	7.9
44	0.18	11.6	4.7	0.058	8.1	53	-8.7	Intermediate	9.0
45	0.30	15.7	3.2	0.063	9.1	238	-10.7	Intermediate	8.8
46	3.53	8.4	3.0	-0.006	1.8	147	-7.7	Intermediate	8.3
47	0.71	11.9	4.7	0.044	5.7	44	-11.7	Intermediate	10.0
48	1.55	13.0	4.2	0.004	5.4	238	-10.9	Elder	9.6
49	0.57	12.6	4.4	0.059	8.4	110	-8.6	Intermediate	9.9
50	0.06	11.7	4.6	0.071	8.7	110	-8.9	Intermediate	9.4
51	3.02	14.2	2.8	0.026	5.0	98	-8.2	Elder	8.5
52	0.56	15.6	4.8	-0.001	7.9	238	-9.4	Intermediate	9.9
53	1.14	16.7	4.1	0.017	6.5	238	-11.1	Intermediate	10.6
54	3.49	13.7	3.5	0.010	5.3	425	-9.1	Intermediate	8.9
55	0.06	10.8	4.8	0.032	6.2	87	-10.0	Elder	8.3
56	0.23	13.4	3.7	0.065	8.0	218	-8.6	Elder	9.8
57	0.23	12.2	2.9	0.029	4.2	163	-8.7	Intermediate	7.9
58	1.74	5.7	1.7	0.043	1.2	467	-8.2	Intermediate	8.1
59	0.00	14.3	4.9	0.046	9.9	306	-9.6	Elder	9.7
60	0.03	12.6	4.8	0.036	6.7	43	-9.8	Elder	9.9
61	1.41	13.5	2.7	0.036	4.7	520	-11.2	Intermediate	10.8
Quantile									
0.25	0.0	5.6	1.0	-0.018	0.3	119	-15.0	-	0.7
0.5	0.2	7.7	1.5	0.001	0.8	238	-13.9	-	1.5
0.75	0.5	9.8	2.0	0.019	1.4	239	-12.7	-	2.5

7.3.3. The change of pathogen concentration during food chain

The change of listeria concentrations during the simulated food chains were showed in upper figure of the Fig. 7-1, and the boxplot of initial contamination level (log CFU/mL) and the changing ratio ($\Delta\mathrm{Log}\ C$: log CFU/CFU) were showed in the lower figure of the Fig. 7-1. The initial contamination level was -5 to 5 log CFU/mL. The reduction ratios of whole scenarios had the greatest variance in the changes of concentrations: the median was -20 log CFU/CFU, but the minimum was -77 log reduction, and the maximum was almost 0 log reduction. Furthermore, the lines of concentration changes of illness occurred scenario were showed in the upper figure of Fig. 7-1, and each line indicates each concentration change of illness scenario (we called “spaghetti plot”). The spaghetti plot can indicate the linkage of concentration changes per one illness scenario. The estimated number of illness cases was 61, so there is 61 orange lines in Fig. 7-1. Compared to the concentration change of whole scenarios, the concentration change of illness tended to be much initial contamination level and much less reduction in the pasteurisation section and greater growth in the domestic storage section.

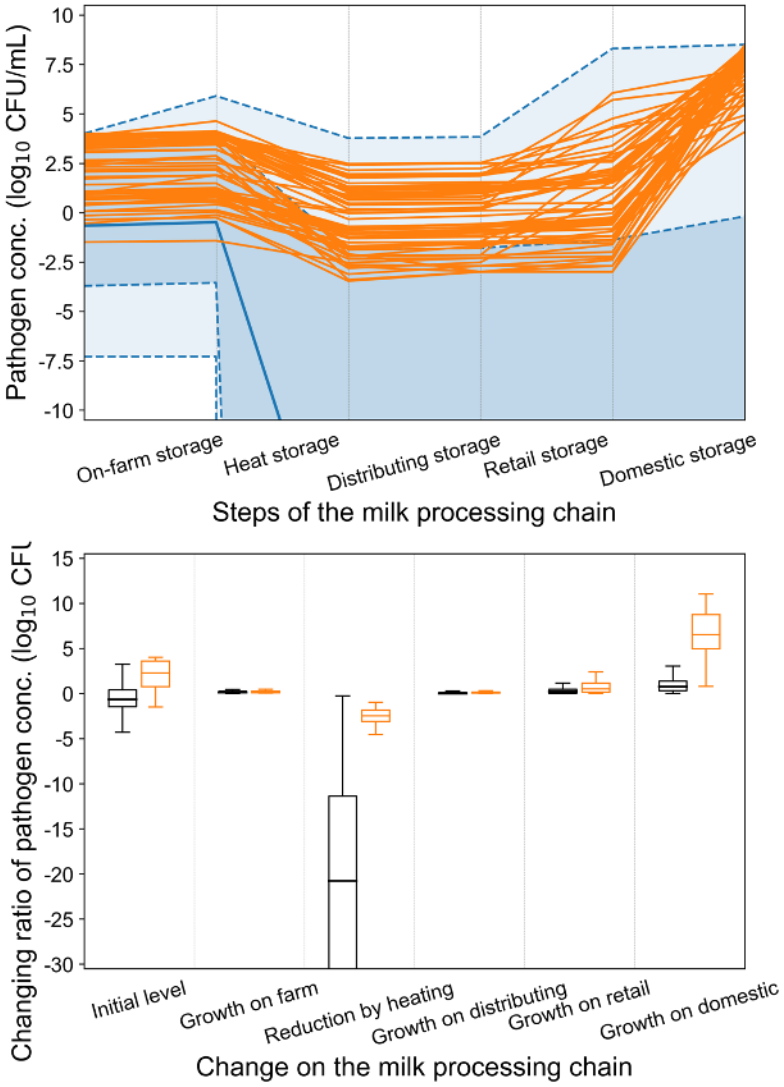


Fig. 7-1. The comparison of listeria concentration changes in whole scenario and illness occurred scenario. The prediction band (upper figure; Max-Min: light blue; 99%: blue; median: solid blue line) of the change in listeria concentration in milk during the simulated food chains, and the concentration change in case of illness occurrence (upper figure; 61 orange lines; spaghetti plot). The boxplot of the initial contamination level (log CFU/mL) and the changing ratio (log CFU/CFU) by storages and pasteurisation in whole scenario (lower; black boxplot) and illness occurred scenario (lower; orange boxplot). The prediction range and box plot were based on only the situation of the milk contaminated.

7.3.4. L. monocytogenes dose per one pasteurized milk serve

The distribution of listeria Log dose of contaminated dose scenario. In this plot, the zero-dose scenario were omitted because the zero CFU will be calculated as minus infinite log CFU. The ratio of the contaminated dose scenario was 0.04% of the whole simulated scenario. And the orange bars indicate the location of dose in scenarios with illness. The scale and grid of x-axis in orange-bar-figure depend on the blue distribution. This type of figure, which we called “barcode chart”, makes it easier to compare and to understand the speciality or the uniqueness of illness scenario. The Fig. 7-2 shows the righter shift of barcode compared to blue distribution and it indicates that there is uniqueness of illness scenarios in dose, which is a well-known fact. The almost of contaminated dose levels were lower than 6 log CFU but the minimum dose in illness scenarios were 6.7 and the almost of illness doses were higher than 8 log CFU which is in the extremely upper tail end.

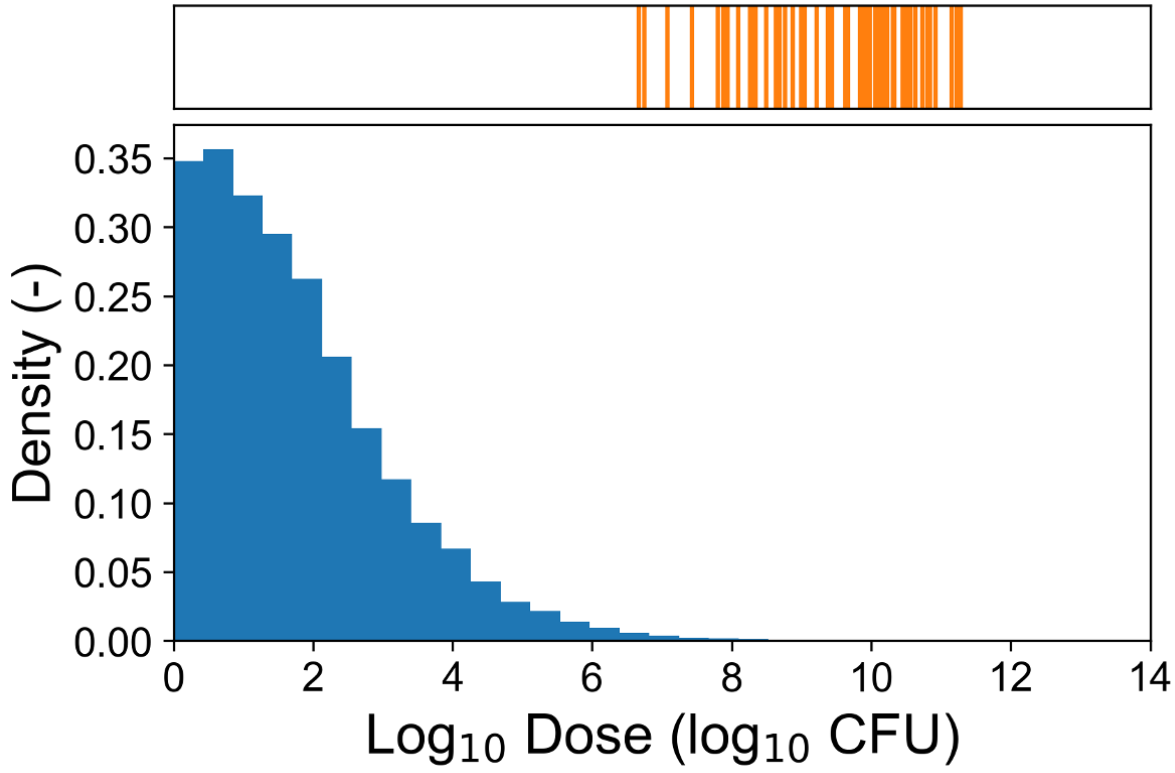


Fig. 7-2. The distribution of the estimated *L. monocytogenes* dose from pasteurised milk (blue distribution) and its location in scenarios with illness (orange bar above ; barcode chart). The scale and x-axis grid of the above orange barcode chart is same as that of the below blue distribution of Log dose of contaminated dose scenario. The contaminated dose scenario was the 0.04% of whole scenario: the doses of the 99.96% of whole simulated scenario were zero.

7.3.5. Distribution of deltas of pathogen concentration

The distributions and the barcode charts of the initial contamination level, the growth ratio on farm, the reduction ratio by pasteurization, the growth ratio on distributing, the growth ratio on retail storage and the growth ratio on domestic storage were showed in Fig. 7-3. As mentioned above, the shift of the barcode can be used to roughly determine whether illness scenarios had specific or not on each distribution. For example, the growths on farm and distributing seem not to be relevant to illness occurrence but the reduction by

pasteurisation and the growth on domestic storage seem to be relevant to the illness occurrence, because all illness scenarios in reductions were higher than the mode of whole distribution (almost -9 log CFU/CFU), and many of the illness scenarios in domestic storage were in the extremely upper tail end of the whole contaminated distribution.

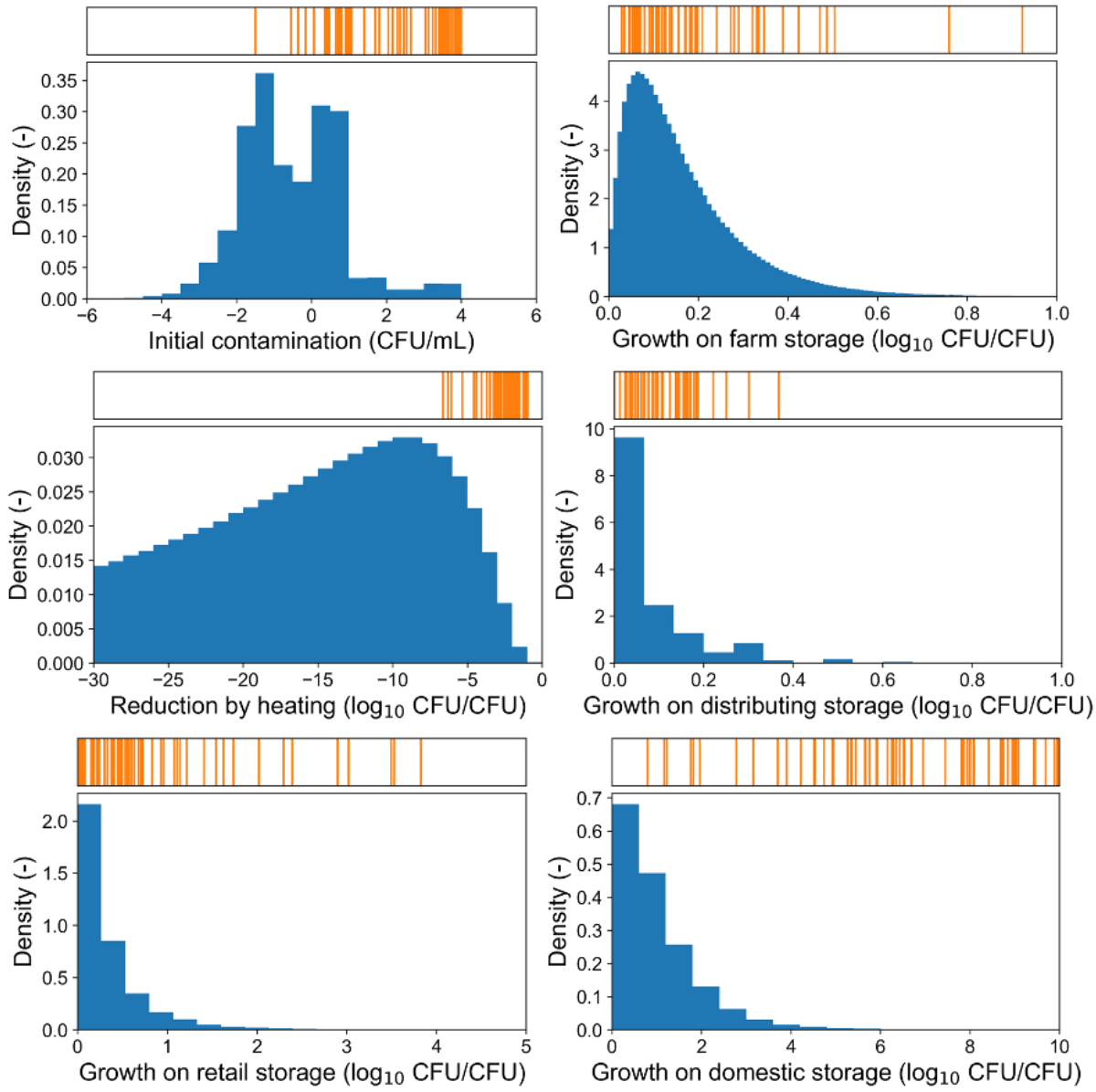


Fig. 7-3. The distributions of the estimated pathogen behaviour (blue distribution) of *L. monocytogenes* in raw milk and its location in scenarios with illness (orange bars; A: initial contamination level; B: growth ratio on farm storage; C: reduction ratio by pasteurisation; D: growth ratio on distributing storage; E: growth ratio on retail storage; F: growth ratio on domestic storage). The scale and x-axis grid of the above orange barcode chart is same as that of the below blue distribution. All of distributions depend on only the contaminated situations in each stage.

7.3.6. Sensitivity analysis of each factor to pathogen log concentration at eating & illness occurrence

Next, this section focuses on the importance of each factor in more detail. Both of the Spearman's correlation coefficients, ρ, to the *L. monocytogenes* final contamination level at the moment of consumption and to the illness occurrence after consumption were compared (Fig. 7-4). There is difference in the relative order of relevance magnitudes. For the final contamination level, the greatest relevant factor was Log D deviation ($\rho_{\mathrm{Log}D\ \mathrm{deviation}|\mathrm{Log}C_{domestic}}$: 0.20), followed by heating temperature ($\rho_{T_{heat}|\mathrm{Log}C_{domestic}}$: -0.14), initial contamination level ($\rho_{\mathrm{Log}C_0|\mathrm{Log}C_{domestic}}$: 0.13) and heating time ($\rho_{time_{heat}|\mathrm{Log}C_{domestic}}$: 0.12), which had relatively stronger relevance. The correlations of storage factors and the growth rate variability for the final levels were relatively lower ($\rho_{T_{domestic}|\mathrm{Log}C_{domestic}}$: 0.00042, $\rho_{time_{domestic}|\mathrm{Log}C_{domestic}}$: 0.00057, $\rho_{\sqrt{\mu}_{domestic}|\mathrm{Log}C_{domestic}}$: 0.00036, etc.). On the other hand, according to the correlations on the illness occurrence, the logarithm r parameter of dose-response model which indicates the pathogenicity variability had relatively the greatest relevance ($\rho_{\mathrm{Log}r|W_{ill}}$: 0.0012), following by Log D deviation ($\rho_{\mathrm{Log}D\ \mathrm{deviation}|W_{ill}}$: 0.0012), domestic storage time ($\rho_{time_{domestic}|W_{ill}}$: 0.0011), domestic storage temperature ($\rho_{T_{domestic}|W_{ill}}$: 0.0010), initial contamination level ($\rho_{\mathrm{Log}C_0|W_{ill}}$: 0.00095), heating temperature ($\rho_{T_{heat}|W_{ill}}$: -0.00080), the $\sqrt{\mu}$ deviation on domestic storages ($\rho_{\sqrt{\mu}_{domestic}|W_{ill}}$: 0.00073) and heating time ($\rho_{time_{heat}|W_{ill}}$: -0.00067). Although the domestic storage conditions had lower relevance to the final contamination level, the domestic condition had great relevance to the illness occurrence.

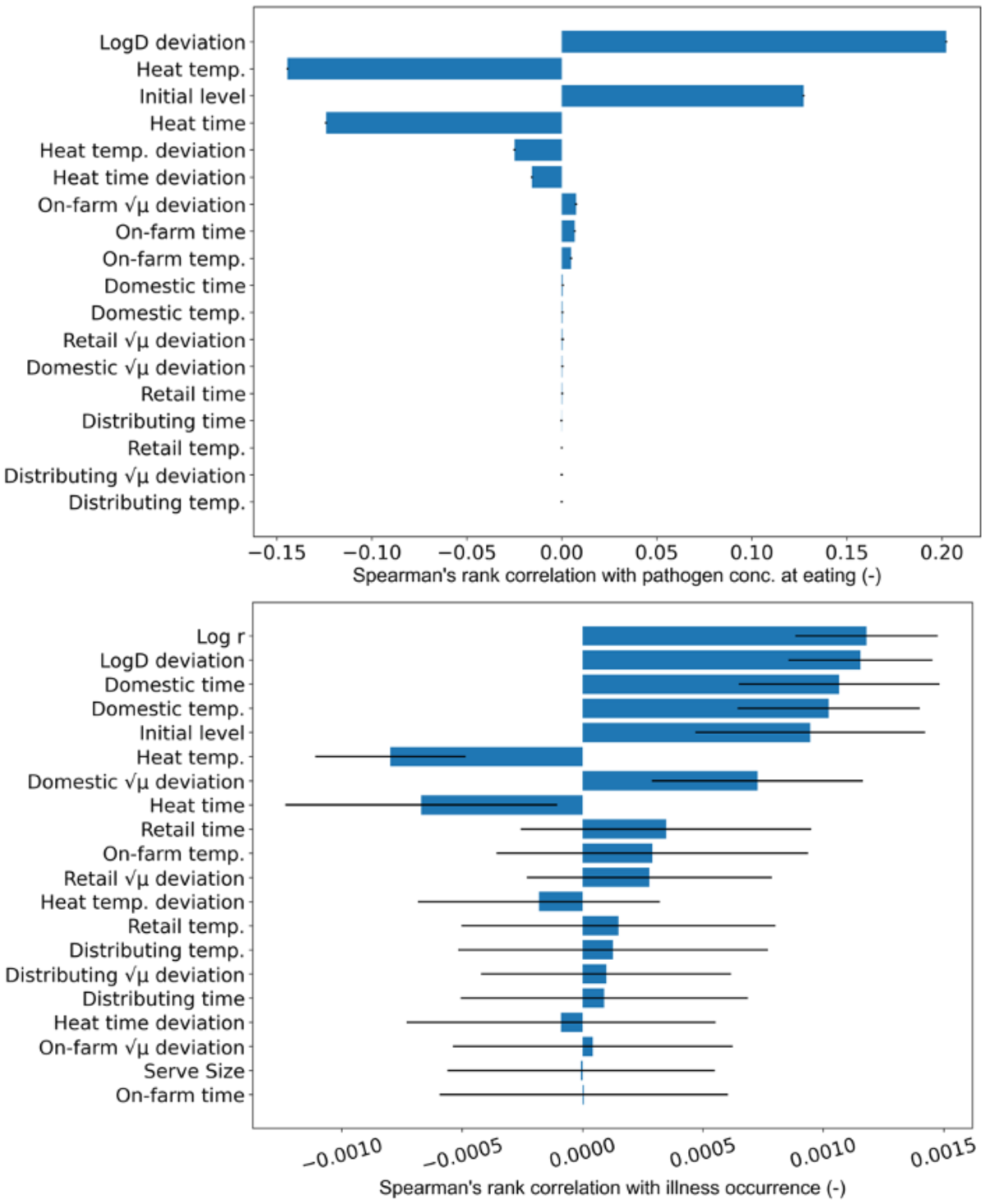


Fig. 7-4. The Spearman's correlation coefficients of the impact of stochastic variable factors on the final contamination levels of *L. monocytogenes* at the moment of consumption (upper figure) and on the illness occurrence (lower figure). The error bars indicate the standard deviation of ten times of the correlation estimations. Factors with stronger correlation coefficients are located at the top.

7.3.7. Uniqueness in time-temperature condition

Although it is well-known fact, the lower heating temperature and the shorter heating time bring us more listeriosis cases: there are a right shift of orange barcode compared to the whole distribution of the heating temperature (Fig. 7-5A) and a left shift of barcode compared to that of heating time (Fig. 7-5B). Focused on the heating target, the 72 ºC-15 sec scenario brought 47 illness cases; the 72.5 ºC-20 sec scenario brought 10 cases; the 74ºC-20 sec scenario brought 4 cases; and the 75ºC-20 sec scenario brought no illness cases.

The almost of illness scenario stored pasteurised milks at higher temperature than 7.5ºC on domestic storages for longer time than 2 days (Fig. 7-6); there are right shifts of barcode. Especially, the higher temperature than 10ºC and that of longer time than 4 days had a high density of illness conditions. For the other time-temperature conditions, there was no shift of barcode chart compared to the whole distributions (Fig. 7-S2).

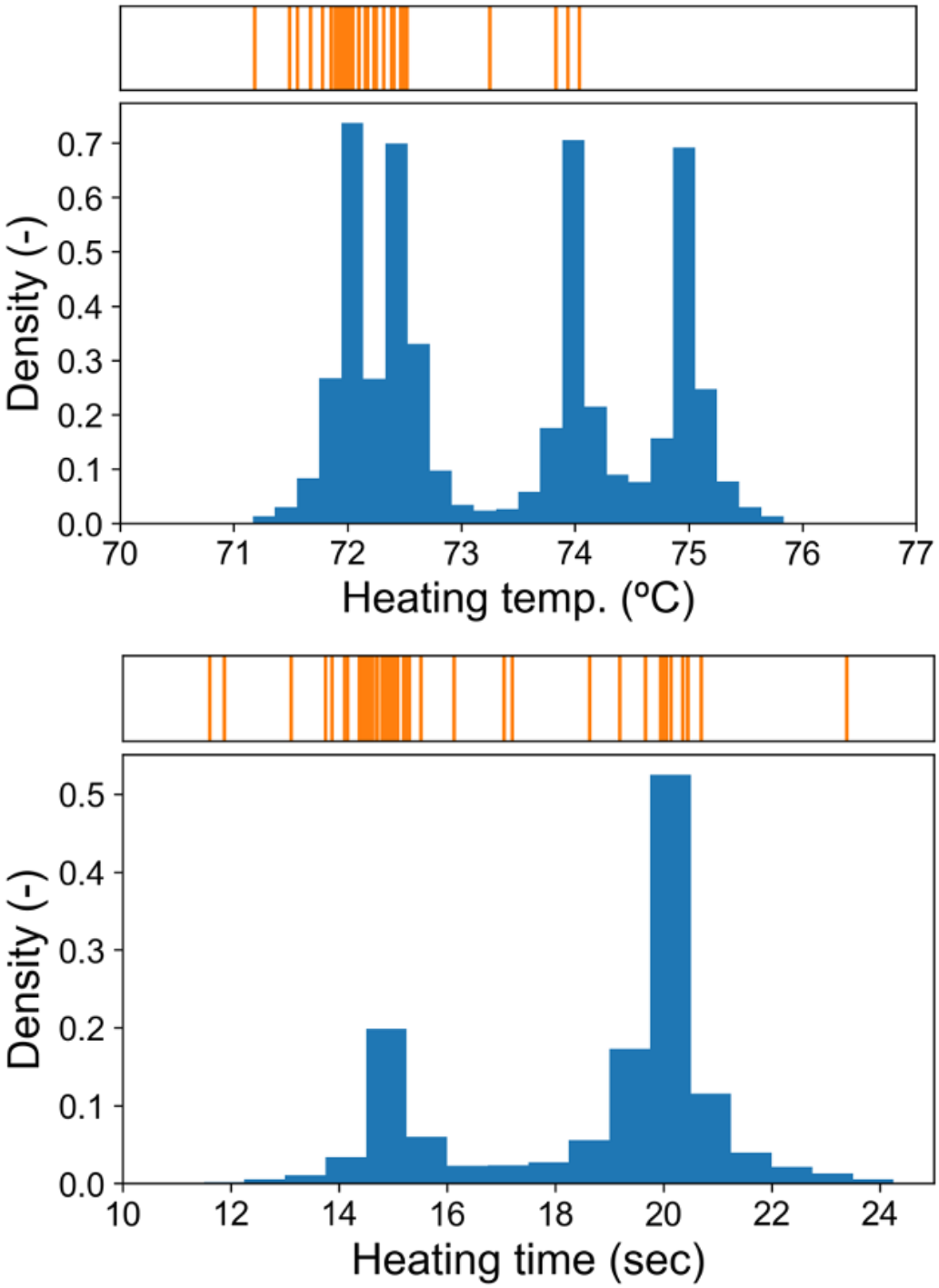


Fig. 7-5. The distributions of the pasteurization temperature: A and time: B (blue distribution) and its location in scenarios with illness (orange bars). The scale and x-axis grid of the above orange barcode chart is same as that of the below blue distribution.

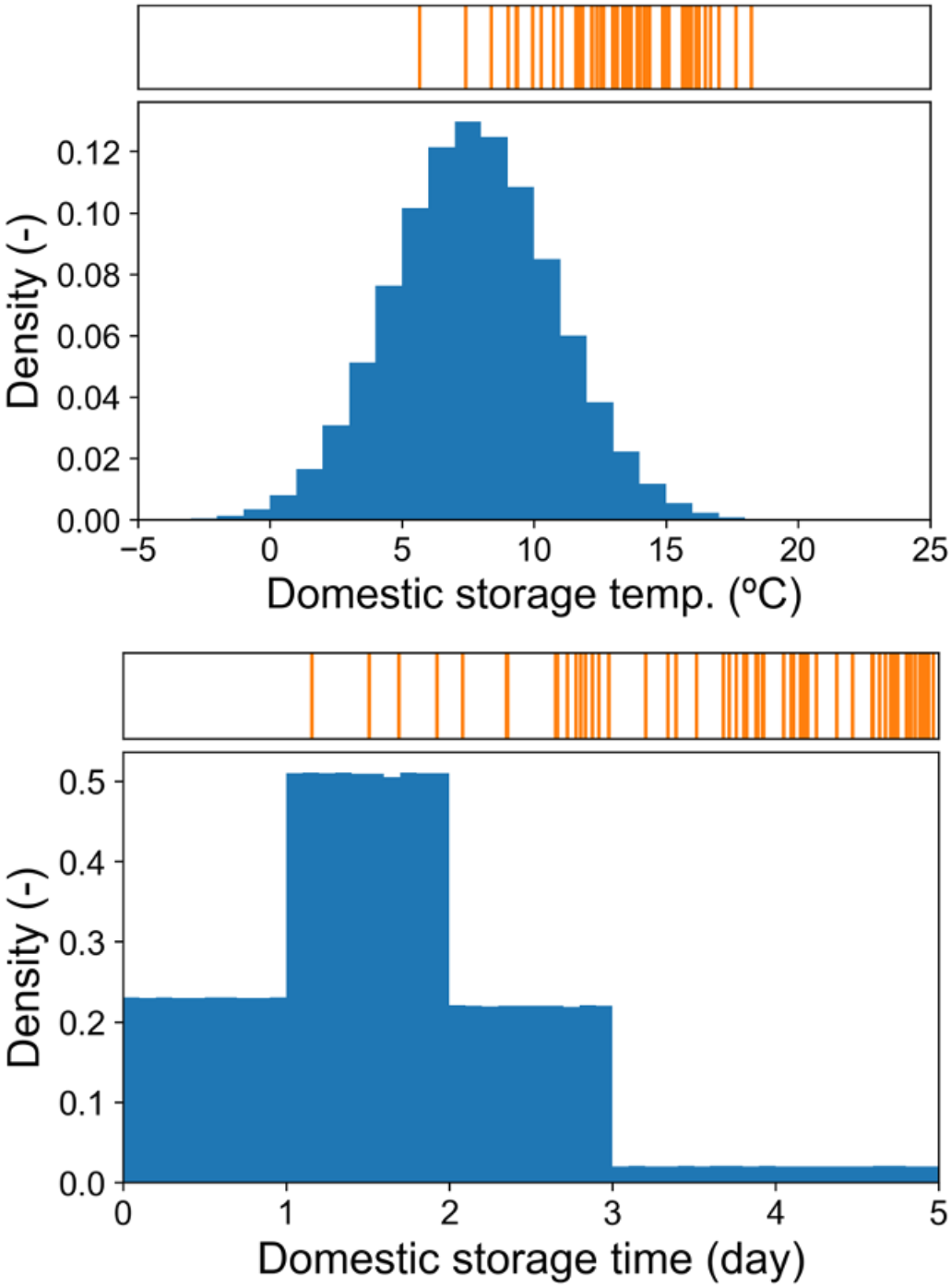


Fig. 7-6. The distributions of the domestic storage temperature: A and the time: B (blue distribution) and its location in scenarios with illness (orange bars). The scale and x-axis grid of the above orange barcode chart is same as that of the below blue distribution.

7.3.8. Uniqueness in pathogen characteristics

The pathogen's characteristics, which are factors beyond the control of techniques, had also relevance to the illness occurrence. There was clear right shift of barcode in the listeria's thermotolerance deviation, the $\sqrt{\mu}$ deviation on domestic storages and the pathogenicity (Fig. 7-7). Especially, in thermotolerance and the pathogenicity, all the characteristic occurred illness were higher than each mode of whole distribution. In the other pathogen's characteristics, there was no significant shift (the $\sqrt{\mu}$ deviation on farm, distributing and retail storage: Fig. S3).

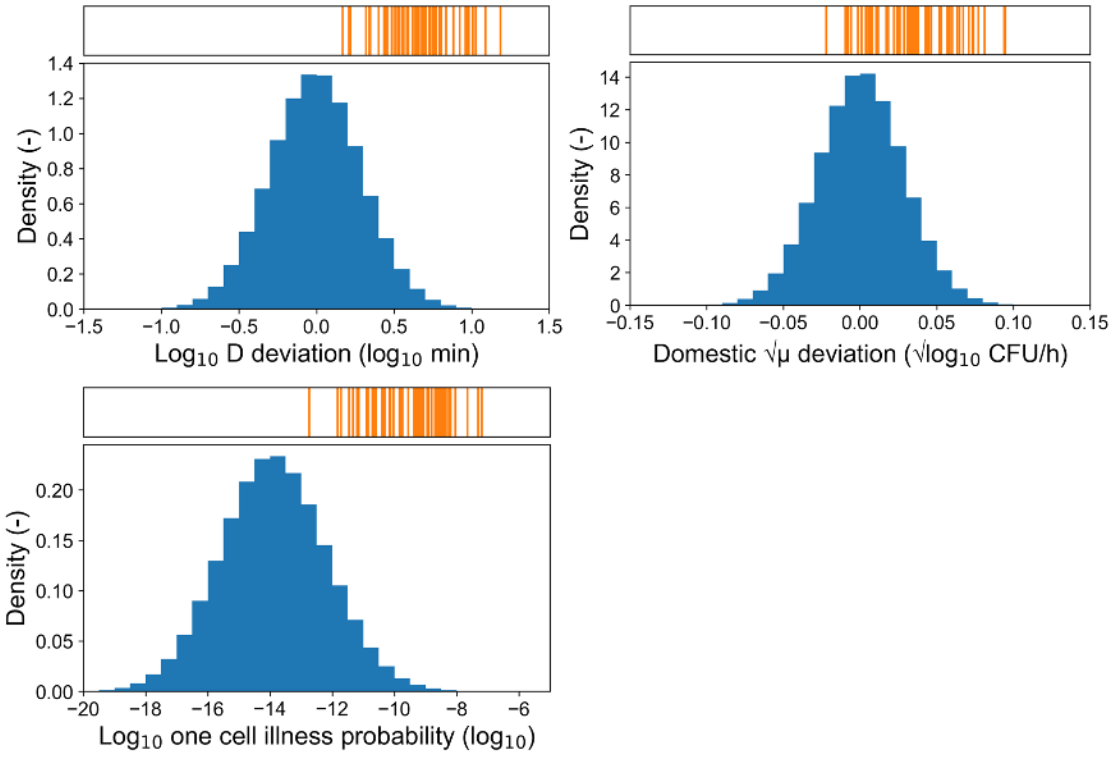


Fig. 7-7. The distributions (blue) of the Log D deviation from the medians at each heating temperature: A, the √μ deviation during domestic storage: B, the one cell illness probability of dose-response model: C, and its location in scenarios with illness (orange bars). The scale and x-axis grid of the above orange barcode chart is same as that of the below blue distribution.

7.3.9. Scenario analysis for thermal condition target

As same as the result of the Fig. 7-5, the scenario analysis for the thermal condition target indicated that the lower heating temperature and the shorter heating time bring us more listeriosis cases (Table 7-3). The risk of illness of the 72ºC-15 sec scenario had the twice of the risk of 72.5ºC-20 sec, 3.6 times of the risk of the 74ºC-20 sec, 23 times of the risk of 75ºC-20 sec heating scenario. The risk of the 85ºC-20 sec was calculated as the extremely low like lower than the computation limitation ($<10^{24}$). Focused on the illness cases per 10^8 servings, it was difficult to see the differences between the heating target conditions.

Table 7-3 Results of scenario analysis

Thermal condition	Average of P ill	Illness cases per 100 million
72ºC 15 sec	2.84×10^{-8}	2
72.5ºC 20 sec	1.41×10^{-8}	2
74ºC 20 sec	7.82×10^{-9}	1
75ºC 20 sec	1.24×10^{-9}	0
85ºC 20 sec	$<10^{-16}$	0

7.4. Discussion

The results of 61 illness cases per 10 billion servings (6.1×10^{-9}) this study derived was similar to the estimation of QMRAs by other official organizations, although there is a little difference. The estimation by World Health Organization and Food and Agriculture Organization was 50 illness cases per 10 billion servings (0.005 illness per 1,000,000 servings) (WHO/FAO, 2004), and that by Food and Drug Administration was 10 illness cases per 10 billion servings (1.0×10^{-9} illness per serving) (FDA/USDA, 2003). Therefore, the result of this study can indicate a part of validity.

Focusing on the pathogen dose of the food chain scenarios where food illnesses occurred, all of them had a dose above 6 log CFU. This result would indicate the listeriosis characteristic that *L. monocytogenes* needs doses above 6 log CFU to cause the illness. Comparing doses of illness scenario with the whole distribution (blue distribution), it shows

that there are illness situations on the tail end of the probability distribution, indicating that the situation in which foodborne illness occurs is an "extreme" outcome.

The results of this study indicate that foodborne illness is not caused by a single factor alone. The combination of inadequate pasteurization in the heating section and poor storage conditions was found to be one of the factors contributing to listeriosis. The spaghetti plot indicated that the combination of insufficient inactivation and drastic growth on storage conditions (retail or domestic) causes the listeriosis. The factors in the pasteurization section (heating temperature, time, and Log D) had great relevance to the final contamination level, which was similar to the order of importance reported previously (den Besten et. al., 2017). Especially, thermotolerance (Log D) has a relatively strong correlation with illness occurrence, which is indicating the importance of modeling the variability of thermotolerance. Comparing the importance of the Log D variability and the deviation from the thermal condition target, it was estimated that the deviation from the target was less important than the Log D variability for the illness occurrence. The maximum deviate range assumed in this study was ±1ºC for heating temperature and ±25% for heating time. At first impression, the deviation can be estimated to be very large, however, the estimation results (Fig. 7-4 bottom) estimated to be relatively insignificant. Since the thermotolerance variability is very large, mitigation of the condition target can be dangerous even if the thermal condition severely controlled. According to the scenario analysis (Table 7-2), raising the thermal pasteurization target would be the most feasible and easy-to-implement risk management method available to producers. On the other hand, the domestic storage condition had relatively great relevance to the illness occurrence. The barcode chart (Fig. 7-6) showed that listeriosis was more likely to occur when the storage conditions were above 10ºC in fridge, which is generally considered dangerous. Sensitivity analysis to illness occurrence also showed the relevance of storage conditions in costumers' home. However, these

costumers' behaviors are difficult to control. The storage conditions in the home can only be dealt with food producers through warning labels, setting shelf life, or time-temperature indicator (TTI). The results on domestic storage conditions can also be useful for consumers and refrigerator developers to clearly show the importance of maintaining low temperatures. Appropriate use of refrigerators by consumers will be expected to greatly reduce the incidence of listeriosis. In the case of listeriosis from pasteurized milk, the results showed the effectiveness of the following options: the current pasteurization with severe control of storage condition for milk tastes; the more stringent pasteurization with current storage condition for extension of shelf life. Few cases of listeriosis occurred even when the storage temperature in the home was below 10°C (Table 7-S1, Illness ID: 9, 10, 27, 28, 46, and 58). In particular, in the Illness ID 58 simulation, foodborne illness occurred despite the fact that the storage temperature in the home was 5.7ºC. Focusing on other factors of ID 58, this study found that the initial bacterial count was 3.9 log CFU/mL, a very high concentration, and the bactericidal effect of pasteurization was only -1.5 log CFU/mL. In addition, the one cell innless probability in ID 58 was strong (-8.2 log). It was estimated that even if the storage conditions in the home were severely controlled below 10ºC, food borne illness could still occur very rarely (probability of 6×10^{-10} in our estimation) due to other factors.

However, as can be seen in Fig. 7-1 and 7-4, the pathogen dose is not the only important factor but also the pathogenicity is strongly related to the incidence of foodborne illness, which clearly indicates that analysis considering risk characterization is important in discussing foodborne illness outbreaks and consumer health.

The difference in the order of importance may be most curious point. It is generally known that intaking a larger number of *L. monocytogenes* can easily lead to listeriosis. Therefore, the concept of sensitivity analysis for the results of exposure assessment was to promote indirect discussion of the susceptibility to listeriosis by discussing the correlation

coefficients for the number or the concentration of pathogens at eating. However, the result of Fig. 7-4 showed that there was difference in the order of important factor. It can be expected that the reason for that lie on the dose-response relationship of *L. monocytogenes*. On the pathogens *like L. monocytogenes* that need amount of pathogens more than 6 log CFU, the dose less than the amount has no effect on the illness occurrence at all. In other words, in the case of listeria, concentrations such as 3 or 2, -1 log CFU have no effect on the incidents of listeriosis. The output type of Illness occurrence proposed in this study is 0 or 1 to directly describe the illness occurrence. However, in the sensitivity analysis for the bacteria concentration at the time of consumption, which is often used, the correlation in the low dose range, which is irrelevant to the occurrence of listeriosis, is also evaluated. It is expected that may have indicated the difference in the order of relevant factors between pathogen concentration and illness occurrence. Although the illness probabilities take values between 0 and 1, most estimated probabilities were almost zero, but very rare probabilities such as 0.8 were also estimated. Spearman's correlation coefficients, which is often used in sensitivity analysis of QMRA, is an index to discuss the correlation between the ranks of each set. Therefore, it is a very effective method for looking at correlations in sets such as QMRA, where the estimation results have a skewed distribution. While the Spearman's correlation has the advantage, it has a demerit that there is not a similar numerical difference for the same rank difference. The distribution of illness probability was skewed, which is highly zero-inflated. Therefore, the sensitivity analysis against illness occurrence were weighted to many zero-inflated data. The results of sensitivity analysis to the illness probability per serving were similar to the estimation results for the final concentration. In other words, it can be advocated that focusing on the correlation to the output that directly expresses "whether foodborne illness has occurred or not", such as the illness occurrence proposed in this study, is an appropriate method when the health of consumers is the primary

concern. However, this does not mean that sensitivity analysis to the concentration at the time of consumption is meaningless. The standards of laws and/or regulations are the number or concentration of bacteria. Sensitivity analysis to concentration is effective if standards have priority, and sensitivity analysis to output format such as “illness occurrence” is effective if food safety has priority.

Since illness occurrence is a direct expression of the occurrence of foodborne illness, the sensitivity analysis to illness occurrence may evaluate the association with risk better than the sensitivity analysis to final log pathogen concentrations at the time of consumption. Nevertheless, the values of correlation coefficients by sensitivity analysis to illness occurrence were very small and some factors were not stable. This could be due to the output type of illness occurrence and the small number of illness cases. Illness occurrence can only take the value 0 or 1. In addition, the very small frequency of illness scenarios (61 cases/10 billion) may make it difficult to estimate the correlation coefficient. The small the correlation values and the large standard deviation may make it difficult to compare the illness relevancies of food chain factors with high accuracy.

The estimation method proposed in this study, which focuses on the illness occurrence, is considered to be an intuitive and easy-to-understand output method. The output style clearly indicates the number of cases of foodborne illness. In addition, since the definition of foodborne illness outbreak is clear, traceback of the scenario in which foodborne illness occurred is possible. This is effective in showing what factors cause foodborne illness, like this study. Additionally, by set the iteration number of simulation as the number of produced (or consumed) samples, it would be possible to estimate the range of variation in the number of foodborne illness incidents, which has so far been estimated only as an average value. This would be useful not only for governments that want to assess the risk to consumers, but also for food producing companies by estimating the risk on the number of

each food product. The spaghetti plot (Fig. 7-1) and barcode charts (Figs. 7-2, 7-3, 7-5 and 7-6) were used to visually show which sections and which factors could cause foodborne illness. This is a useful method, for example, for determining shelf life. If a barcode chart of the distribution was made by adding the time until consumption after pasteurization as shown in Fig. 7-8, the shelf life longer than 4 days could have a higher risk. From the same point of view, it may be useful to select storage conditions and heating targets (although the illness comes from not only time but storage temperature). In addition, as in the sensitivity analysis, it is possible to indicate which CCPs should be focused on for control of pathogens. Not only for Listeria, but also for other pathogens, the relevance analysis of the barcode chart can be useful for setting processing and distribution conditions based on the hurdle theory. However, it should be noted that the barcode chart visualizes only a part of the risk, and the risk of foodborne illness will not be zero even if the food is managed under conditions that do not include the illness barcode. As an application of sensitivity analysis onto illness occurrence, setting up ideal food chain conditions that do not cause foodborne illness might be realized and the information from the sensitivity analysis can reduce costs by estimating the occurrence of foodborne illness and optimizing it using machine learning and other methods.

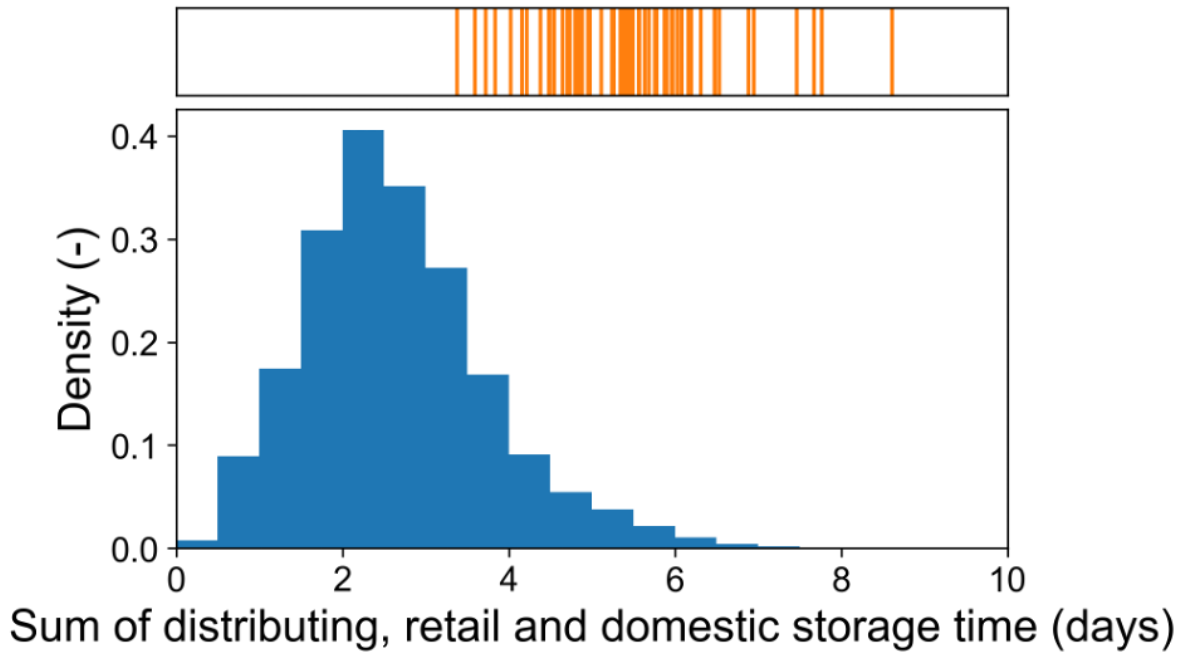


Fig. 7-8. The distribution (blue) of the post pasteurization time (sum of the storage time of distributing, retail and domestic), and its location in scenarios with illness (orange bars). The scale and x-axis grid of the above orange barcode chart is same as that of the below blue distribution.

While the output of Illness occurrence has brought a variety of information, it also has its disadvantages. The method requires a huge amount of computation and time. The simulation of 10 billion iterations in this study required one month of computation time. One of the disadvantages of the estimation method focusing on the illness occurrence is that it requires a corresponding amount of computation time to simulate a food with a huge consumption volume such as pasteurized milk. If it is necessary to simulate consumption more than 10 billion times, more time or a higher specification computer will be needed. However, with the remarkable rapid progress in computer performance, this problem would be solved in the near future.

The drastic increase in the risk of foodborne illness due to inadequate pasteurization and household storage, shown by the spaghetti plot (Fig. 7-1) and the barcode chart (Fig. 7-3), is not a new result and is generally well known. In this study, the QMRA clearly indicated

the importance of each of them so that we could compare the correlations of factors. In general, food producers such as pasteurized milk focus most of their management efforts on pasteurization. However, as shown in this study, what really matters most relevant time-temperature condition is the storage conditions in home by consumers after shipment. Most food chains causing listeriosis are stored in conditions above 10ºC, which does not meet the requirements for foods requiring cold storage. Improvements in input conditions of the QMRA simulation might be necessary. Since the data source of home storage conditions used in this study was for a single country (Greece), it does not show the distribution of home storage conditions in other countries or in the whole world. And since this study references information regarding storage conditions and consumption from Europe and North America, the scenario is a chimera-like simulation of the food chain around the world. In addition, it may be a weak point that the random numbers for each factor in this study were generated independently. The food stored in the home for a long time or the food with an obvious rotten smell tends not to be consumed, but this simulation assumes that milk in any condition will be consumed. Therefore, the number of foodborne illnesses may have been overestimated than that of the actual numbers of outbreak. In addition, there are some conditions in the present QMRA, such as the heating condition target, where the scenarios are evenly distributed. The distribution of target temperature of thermal processing should be estimated based on the actual consumption amount of milk. Considering these improvements would allow to realize a more accurate QMRA.

In this study, 10 billion iterations of QMRA simulations were performed to estimate the relevant factors in the food chain that cause listeriosis from pasteurized milk, and sensitivity analysis was performed. The order of the correlations for foodborne illness occurrence and the order of the correlations for the logarithmic concentration of pathogens at the time of consumption were different. Furthermore, the sensitivity analysis for illness

occurrence was preferable when estimating the importance for foodborne illness risk. However, it is difficult to assert what is the most important factor for the outbreak of foodborne illness, because it requires a huge amount of calculation and the estimated correlation values may not be stable. In conclusion, this study clearly demonstrated that the cause of foodborne illness is not only primary one factor but the effect of combination of plural important factors.

7.5. References

Asselt, E., & Zwietering, M. (2006). A systematic approach to determine global thermal inactivation parameters for various food pathogens. *International Journal of Food Microbiology*, *107*(1), 73–82. http://doi.org/10.1016/j.ijfoodmicro.2005.08.014

Barker, G. C., & Goméz-Tomé, N. (2013). A Risk Assessment Model for Enterotoxigenic Staphylococcus aureus in Pasteurized Milk: A Potential Route to Source-Level Inference, 1–21. http://doi.org/10.1111/j.1539-6924.2011.01667.x

Besten, den, H. M. W., Aryani, D. C., Metselaar, K. I., & Zwietering, M. H. (2017). Microbial variability in growth and heat resistance of a pathogen and a spoiler: All variabilities are equal but some are more equal than others. *International Journal of Food Microbiology*, *240*, 24–31. http://doi.org/10.1016/j.ijfoodmicro.2016.04.025

Dalzini, E., Bernini, V., Bertasi, B., Daminelli, P., Losio, M.-N., & Varisco, G. (2016). Survey of prevalence and seasonal variability of Listeria monocytogenes in raw cow milk from Northern Italy. *Food Control*, *60*, 466–470. http://doi.org/10.1016/j.foodcont.2015.08.019

Dennis, S. B., Buchanan, R. L., & Miller, A. J. (2002). Microbial Risk Assessment: Achievements and Future Challenges, 1–5.

Food and Agriculture Organization/ World Health Organization. (2021). Risk assessment of *Listeria monocytogenes* in ready-to-eat foods (pp. 1–311).

Gelman, A. (2006). Prior distributions for variance parameters in hierarchical models (comment on article by Browne and Draper). *Bayesian Analysis*, *1*(3), 515–534. http://doi.org/10.1214/06-BA117A

Koutsoumanis, K., Pavlis, A., Nychas, G.-J. E., & Xanthiakos, K. (2010). Probabilistic Model for Listeria monocytogenes Growth during Distribution, Retail Storage, and Domestic Storage of Pasteurized Milk. *Applied and Environmental Microbiology*, *76*(7), 2181–2191. http://doi.org/10.1128/AEM.02430-09

Koyama, K., Hokunan, H., Hasegawa, M., Kawamura, S., & Koseki, S. (2016). Do bacterial cell numbers follow a theoretical Poisson distribution? Comparison of experimentally obtained numbers of single cells with random number generation via computer simulation. *Food Microbiology*, *60*, 49–53. http://doi.org/10.1016/j.fm.2016.05.019

Meyer-Broseta, S. P., Diot, A., Riviere, J., & Cerf, O. (2003). Estimation of low bacterial concentration: Listeria monocytogenes in raw milk. *International Journal of Food Microbiology*, *80*(1), 1–15. http://doi.org/10.1016/S0168-1605(02)00117-4

Nauta, M. J. (2001). A modular process risk model structure for quantitative microbiological risk assessment and its application in an exposure assessment of Bacillus cereus in a

REPFED. Rijksinstituut voor Volksgezondheid en Milieu RIVM.

Polson, N. G., & Scott, J. G. (2012). On the Half-Cauchy Prior for a Global Scale Parameter. *Bayesian Analysis*, *7*(4), 887–902. http://doi.org/10.1214/12-BA730

Pouillot, R., Hoelzer, K., Chen, Y., & Dennis, S. B. (2015). *Listeria monocytogenes* Dose Response Revisited-Incorporating Adjustments for Variability in Strain Virulence and Host Susceptibility, 1–19. http://doi.org/10.1111/risa.12235

Servello, V., Hill, A. R., & Lencki, R. W. (2004). Towards an Optimum Mixing Protocol for On-Farm Bulk Milk Sampling. *Journal of Dairy Science*, *87*(9), 2846–2853. http://doi.org/10.3168/jds.S0022-0302(04)73413-X

U.S. Food and Drug Administration. (2003). Quantitative Assessment of the Relative Risk to Public Health from Foodborne Listeria monocytogenes Among Selected Categories of Ready-to-Eat Foods, 1–301.

World Health Organization. (2015). *WHO ESTIMATES OF THE GLOBAL BURDEN OF FOODBORNE DISEASES* (pp. 1–265).

Zwietering, M. H., Garre, A., Wiedmann, M., Robert L Buchanan. (2021). All food processes have a residual risk, some are small, some very small and some are extremely small: zero risk does not exist. *Current Opinion in Food Science*, *39*, 83–92. http://doi.org/10.1016/j.cofs.2020.12.017

Zwietering, M. H., Wijtzes, T., Rombouts, F. M., & Riet, K. V. (1993). A decision support system for prediction of microbial spoilage in foods. *Journal of Industrial Microbiology*, *12*(3-5), 324–329. http://doi.org/https://doi.org/10.1007/BF01584209

7.6. Supplementary materials

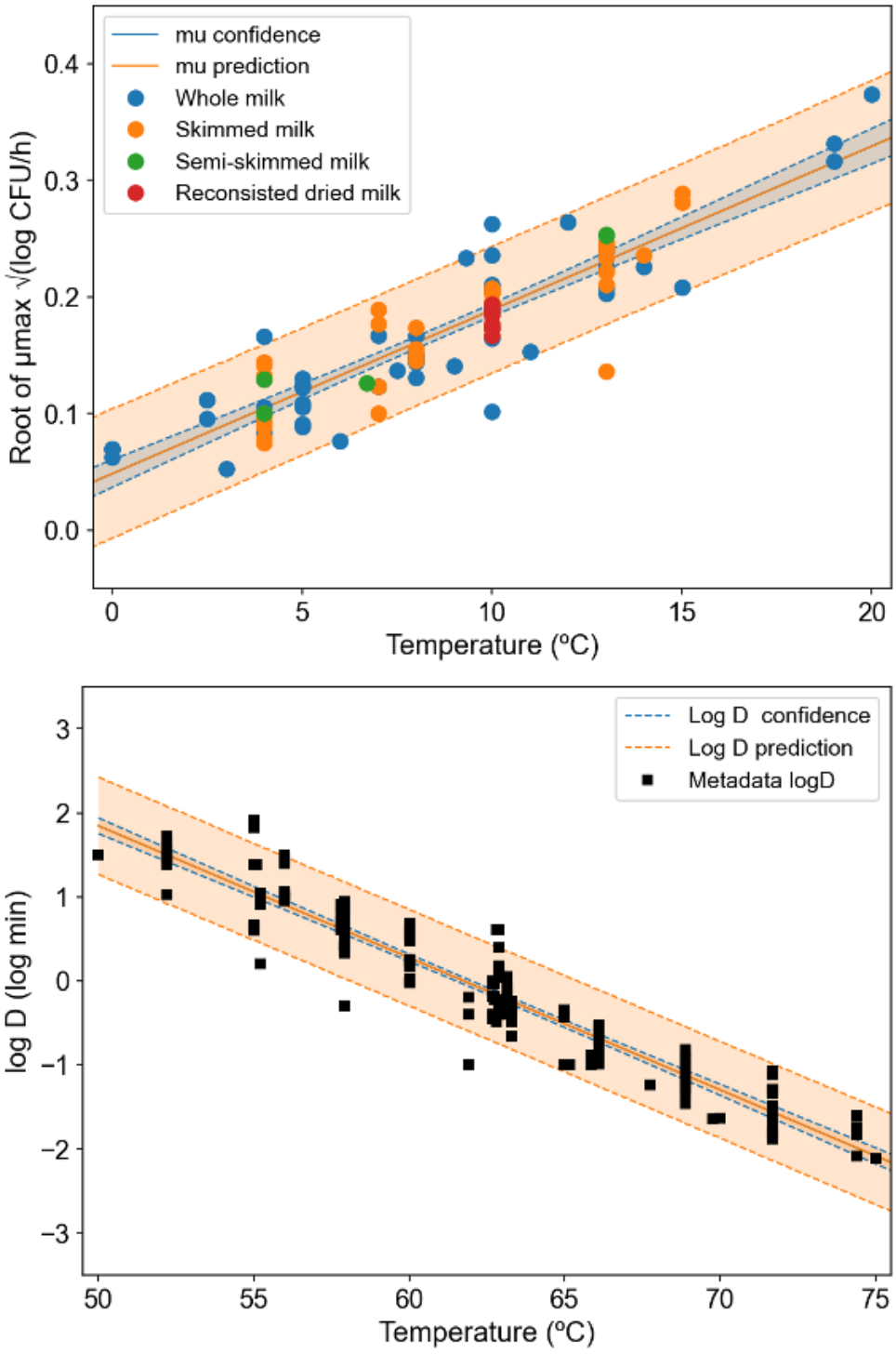


Fig. 7-S1. The metadata and the developed Bayesian model for the growth rate of *L. monocytogenes* in milk and the D-values of *L. monocytogenes* by pasteurization.

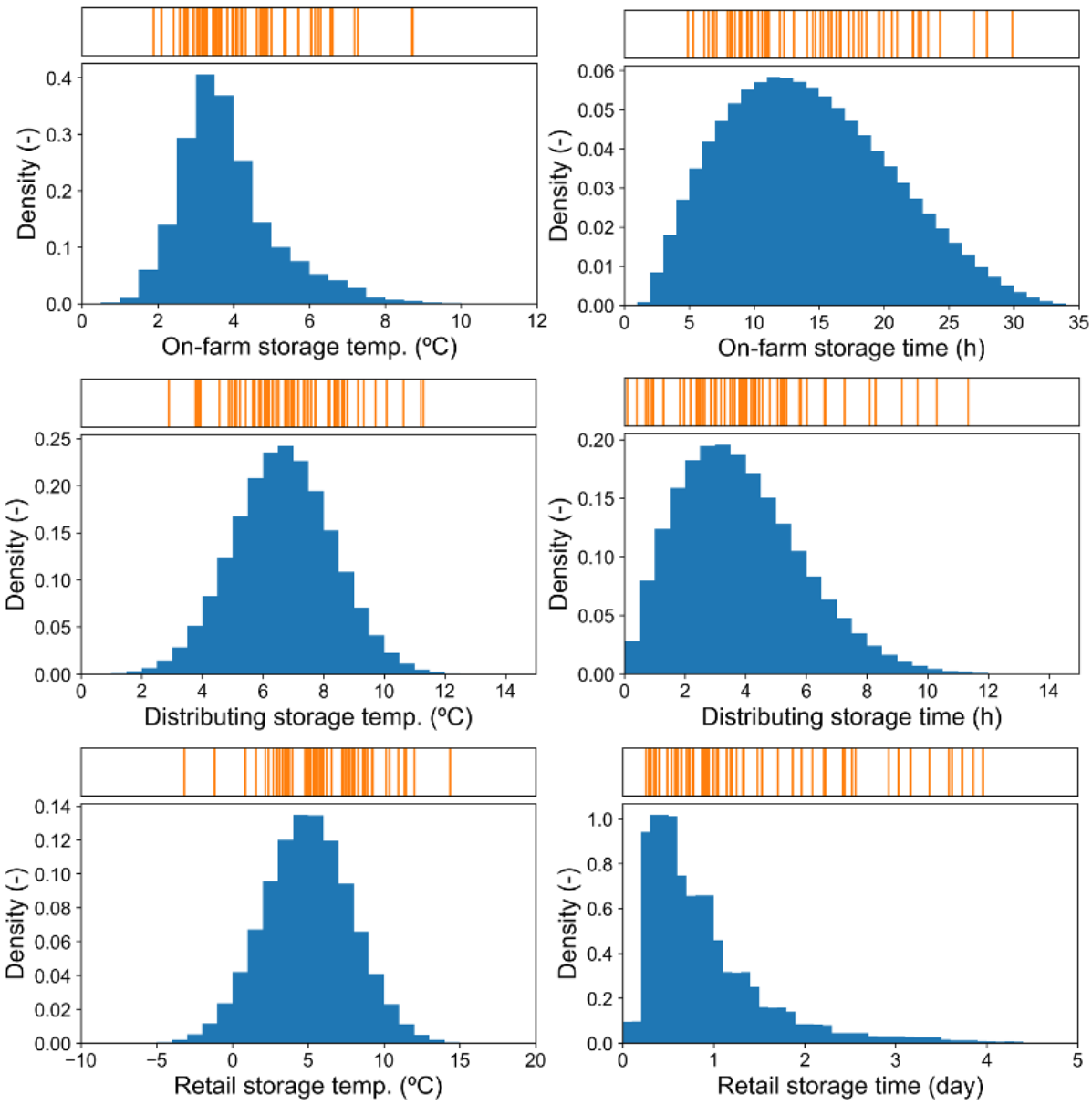


Fig. 7-S2. The distribution (blue) of the time-temperature conditions on farm, on distributing, on retail, and its location in scenarios with illness (orange bars). The scale and x-axis grid of the above orange barcode chart is same as that of the below blue distribution.

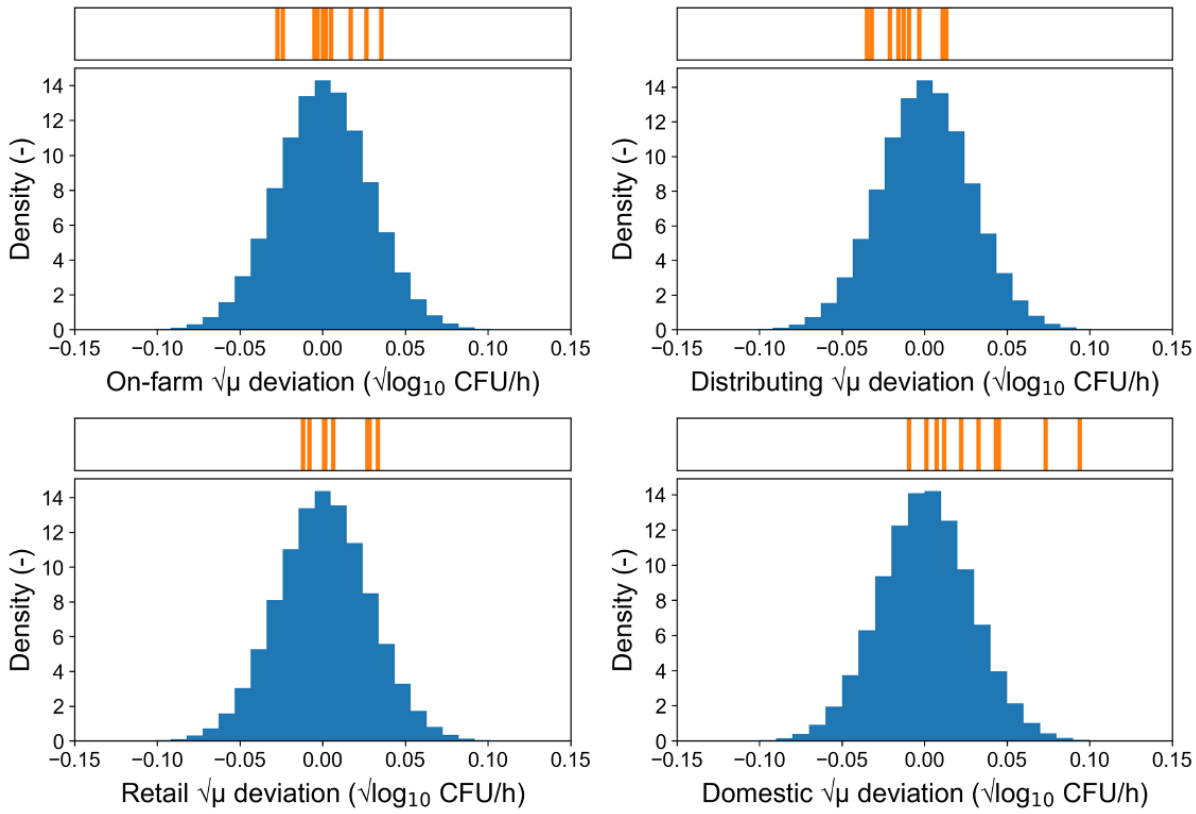


Fig. 7-S2. The distribution (blue) of the root growth rates on farm, on distributing, on retail, on domestic storage, and its location in scenarios with illness (orange bars). The scale and x-axis grid of the above orange barcode chart is same as that of the below blue distribution.

Chapter 8 General Discussion

8.1. Advantages and perspective of this study

In Chapters 2 to 4, variability in bacterial reduction (inactivation) behavior during thermal processing was described by using a probabilistic mathematical model. Chapters 5 and 6 indicated the differences in dose-response relationships between different conditions, such as food type and age, based on the digestive system. In Chapter 7, the importance of post-processing storage conditions (especially storage in home) was demonstrated by both the QMRA simulations and by the advanced output method of the simulation. The methods for expressing variability in exposure assessment and risk characterization, where mathematical approaches are important in QMRA, and methods for analyzing QMRA estimation results were developed in the present thesis. These developed procedures have enabled us to perform more realistic QMRA simulations and to increase the amount of information that can be extracted from QMRA. These results will greatly contribute to future progress in QMRA and predictive microbiology.

There are advantages to having developed different methods for evaluating different goals in each chapter. The essence of the prediction models in Chapters 2, 3, and 4, which represent the bactericidal behavior in food, is the combination of mathematical methods that constitute the prediction models. The bootstrap method was used to represent parameter variability of the predictive model, MCMC was used to represent the pure variability of the phenomenon, and a dynamic model using differential equations was used to represent the microbial response to a non-stationary (dynamic) environmental condition. These combinations are the most important point. to Describing the bacterial reduction behavior is only one example using these methods. These combinations of mathematical methods could be applied not only to reduction behavior but also to growth behavior during storage. The

deterministic dynamic prediction models have been proposed for bacterial growth behavior in non-stationary environments (Baranyi and Roberts, 1994). In addition, a stochastic model to explain the growth behavior in steady state has already been proposed by our research group (Koyama et al., 2021a). By combining these methods, we will be able to develop dynamic and probabilistic prediction models.

The developed dose-response models based on KEDRF in Chapters 5 and 6 have also a potential for development of other dose-response models. Both studies incorporate combinations of the methods that have never supposed to estimate dose-response relationships before. More detailed data on the digestive system in human body would allow for more reliable predictions. Probabilistic approaches, such as those developed in Chapters 2, 3, and 4, could also be applied to the KEDRF. The risk characterization part of the QMRA simulation in Chapter 7 used a simple dose-response model. As KEDRF becomes more generalized, exposure assessment in QMRA may include assessment of bacterial behavior in the digestive system based on KEDRF. Since the dose-response relationship was found to be highly dependent on the physical property of food ingested, it may become less common to use one dose-response model for one pathogen regardless of pathogen vehicle.

8.2. Further perspectives of predictive microbiology and QMRA

Research on QMRA and predictive microbiology for food has evolved over the last two decades. This thesis was also conducted to contribute to the development of this field, but there is still potential for further development. There has been a great interest in research to describe bacterial strain variability, such as some of the studies related to this thesis that used hierarchical Bayesian models to take into account for strain differences (Garre et al., 2020; Koyama et al., 2021b). One of the main advantages of these methods is that they would be able to predict the characteristics of unknown strains from the several dozen strains

sampled. As revealed in Chapter 7, pathogen characteristics such as thermotolerance and pathogenicity of bacteria are strongly related to the occurrence of foodborne illness.

Current models for expressing strain variability are based on statistical methods. However, bacterial species is only an artificially defined category. There is no evidence for the assumption that features follow one probabilistic distribution within a species. The essence of biological traits such as thermostability and pathogenicity lies in the proteins and environmental response systems that bacteria possess. These essential information are stored in the genome information. If biological features of bacteria can be estimated based on genomic information, it will be possible to apply them to QMRA. Although the application of genomic information and other omics to QMRA has currently been proposed (Besten et al., 2018; Njage et al., 2020), specific methods have not yet been established at this stage. The field of research on QMRA based on genomic information is expected to evolve significantly in the near future.

There is another major challenge in QMRA and predictive microbiology. The challenge is the complexity of real food. Unlike culture media that contain only components that are convenient for microbial experiment, real foods have complex physical properties and components. The differences in bacterial behavior due to the food type can only be defined by actual measurements at this moment in 2021. In other words, a large number of experiments are required to predict bacterial behavior for each target food. In addition, various food additives have been added to food products to prevent the growth of microorganisms in recent years, which is making the prediction of microbial behavior in food more complicated. The implementation of QMRA would be easier and more efficient if the differences in microbial behavior due to food type could also be predicted.

QMRA provides us with a variety of information, but its implementation requires a variety of information and a huge amount of data. Therefore, only a few governmental

agencies and a few food producers who have sufficient research resources are currently conducting QMRA. However, QMRA should be implemented for all food products to ensure the safety of foods being offered. The implementation of QMRA is not only to protect the consumers' health, but may also provide important information for compliance with international safety standards and optimization of processing procedures. I would strongly argue that reducing the hurdles for implementation of QMRA for various food and producers is a mission of the relevant researchers.

8.3. Summary

Control of microbial risk has become an extremely important issue among food production to consumption. Although the effectiveness of quantitative microbial risk assessment has been established for the evaluation and control of microbial risk, most of predictive models do not take into account the variability and uncertainty of bacterial behavior, which plays an important role in risk assessment. This doctoral thesis summarizes the results of studies on the development and validation of novel effective microbial behavior prediction models using probabilistic or stochastic method for quantitative microbial risk assessment.

In chapter 2, changes in the survival probability of *S. enterica* populations during thermal processing were represented by a cumulative gamma distribution. The required heating time estimated by the cumulative gamma distribution was shorter than that estimated by the conventional kinetic method. While the conventional method could overestimate the required heating time, the probabilistic estimation method enables to ensure the food safety and allow the relaxation of heating conditions. This is an important finding as one of the new methods for setting the target heating time.

In chapter 3, a Monte Carlo model was created from the survival kinetics data of *B. simplex* spores to describe the heterogeneity of the spore inactivation behavior. The developed model was compared and validated with observed data. The estimation results successfully predicted the observed changes in the survival probability of the spores and the changes in the distribution of the surviving spore counts. These results are novel findings that will contribute to design of processing conditions for risk criteria and improvement of the accuracy of risk assessment models.

In chapter 4, a dynamic and stochastic predictive model was developed to describe the heterogeneity of spore inactivation behavior during non-isothermal processing. The results of comparison of observed and predicted behavior on three non-isothermal conditions showed that the model successfully represented the heterogeneity in the survival spore counts. The developed dynamic and stochastic predictive model would allow to select an appropriate thermal condition to ensure microbial food safety and to reduce thermal effect to food quality.

In chapter 5, invasion behavior of intestinal epithelial cells by *C. jejuni* was investigated, and a predictive model of the invading *C. jejuni* counts was developed to reveal the infection behavior for the development of a new dose-response model. *C. jejuni* was co-cultured with monolayer-cultured intestinal cells, and the invading *C. jejuni* counts in the intestinal cells was observed. The invasion behavior of *C. jejuni* into the intestinal cells was successfully described by a differential equation model.

In chapter 6, The dose-response relationship of *C. jejuni* was estimated by developing and integrating a predictive model based on the food digestion process and pathogen infection behavior. The results of comparison with epidemiological dose-response relationships illustrated that the predicted range successfully represented the reported actual

values. Furthermore, host age and food type demonstrated higher importance than bacterial acid resistance and other factors, which leads to new insights for QMRA.

In chapter 7, QMRA of listeriosis by consumption of pasteurized milk in the Netherland was conducted for clarifying the cause of illness occurrence. The results of sensitivity analysis of 10 billion simulations illustrated that pathogenicity had the greatest relevance to the illness occurrence, which is different from the commonly analyzed results of sensitivity analysis of consumed log concentrations of pathogen. This result indicates that the conventional method may lead to results that differ from the true importance, and that a method directly describing the illness occurrence is more appropriate.

The developed predictive models and analysis procedures provide valuable contributions to quantitative microbial risk assessment frameworks, which needs to treat the number of bacterial cells and death/survival probability of bacterial populations as probability distributions.

8.4. References

Baranyi, J., Roberts, T.A., 1994. A dynamic approach to predicting bacterial growth in food. International Journal of Food Microbiology 23, 277–294. doi:10.1016/0168-1605(94)90157-0

Besten, den, H.M.W., Amézquita, A., Bover-Cid, S., Dagnas, S., Ellouze, M., Guillou, S., Nychas, G., OMahony, C., Perez-Rodriguez, F., Membré, J.M., 2018. Next generation of microbiological risk assessment: Potential of omics data for exposure assessment. International Journal of Food Microbiology 287, 18–27. doi:10.1016/j.ijfoodmicro.2017.10.006

Garre, A., Zwietering, M.H., Besten, den, H.M.W., 2020. Multilevel modelling as a tool to include variability and uncertainty in quantitative microbiology and risk assessment. Thermal inactivation of Listeria monocytogenes as proof of concept. Food Research International 137, 109374. doi:10.1016/j.foodres.2020.109374

Koyama, K., Hiura, S., Abe, H., Koseki, S., 2021a. Application of growth rate from kinetic model to calculate stochastic growth of a bacteria population at low contamination level. Journal of Theoretical Biology 525, 110758. doi:10.1016/j.jtbi.2021.110758

Koyama, K., Ranta, J., Takeoka, K., Abe, H., Koseki, S., 2021b. Evaluation of Strain Variability in Inactivation of Campylobacter jejuni in Simulated Gastric Fluid by Using Hierarchical Bayesian Modeling. Appl. Environ. Microbiol. 87, e0091821. doi:10.1128/AEM.00918-21

Njage, P.M.K., Leekitcharoenphon, P., Hansen, L.T., Hendriksen, R.S., Faes, C., Aerts, M.,

Hald, T., 2020. Quantitative Microbial Risk Assessment Based on Whole Genome Sequencing Data: Case of Listeria monocytogenes. Microorganisms 2020, Vol. 8, Page 1772 8, 1772. doi:10.3390/microorganisms8111772

Advances in predictive modeling for bacterial behaviors from food processing to human consumption: application to quantitative microbial risk assessment

March 2022

Hiroki Abe

Laboratory of Agricultural and Food Process Engineering
Frontiers in Production Science
Graduate School of Agricultural Science, Hokkaido University
Kita-9, Nishi-9, Kita-ku, Sapporo, Hokkaido, Japan
Tel. and Fax.: +81-11-706-2552